Oxoselenates(IV) of the Trivalent Rare-Earth Elements and Some Derivatives

Von der Fakultät Chemie der Universität Stuttgart
zur Erlangung der Würde eines Doktors der
Naturwissenschaften (Dr. rer. nat.) genehmigte Abhandlung

vorgelegt von

Joseph Wontcheu
aus Bafang (Kamerun)

Hauptberichter:	Prof. Dr. Thomas Schleid
Mitberichter:	Prof. Dr. Paul Keller
weiterer Prüfer:	Prof. Dr. Klaus Müller
Prüfungsvorsitzender:	Prof. Dr. Gerd Becker

Tag der mündlichen Prüfung: 23. April 2004

Institut für Anorganische Chemie der Universität Stuttgart

2004

Pledge

I certify that the present dissertation entitled:
"Oxoselenates(IV) of the Trivalent Rare-Earth Elements and Some Derivatives" was carried out without any unlawful devices. I did not use any other than the described literature sources or technical devices. This work has never been submitted before in this or similar form to any other university and has not been used for any examination.

Joseph Wontcheu

Acknowledgements

I would like to express my profound gratitude to Prof. Dr. Thomas Schleid for giving me opportunity to do this work in his laboratory and who, despite his charged work programme, accepted to supervise this dissertation.

I am also greatly indebted to:
Prof. Dr. Paul Keller
Prof. Dr. Klaus Müller
Prof. Dr. Gerd Becker, for the examination.

I would also like to thank: Christof Schneck for always giving me very new literature data during the course of this work, Dipl. Chem. Sabine Strobel, Dr. Hagen Grossholz, Dr. Steffen F. Meier for their continuous encouragements, friendliness, care and company and whose comments were very helpful.

I also thank Sumati Panicker-Otto for correcting the English language.

My gratitudes also go to Dr. Falk Lissner, Dr. Helge Müller Bunz, Dr. Ingo Hartenbach for the single crystal measurement.

I also wish to thank Prof. Dr. Emmanuel Ngameni, Dr. Ketcha Joseph Mbadcam, Dr. Paul Mingo Ghogomu (University of Yaounde I), for their advice and support in my application for the scholarship.

I appreciate and thank all Doctorates students of our research group, whose long experience in the laboratory was of great relief for me.

My heart-felt thanks go to my friend Mambe Fotsing Clarisse, whose moral support, generosity, advice, encouragement and permanent contact contributed emensely to the realisation of this work.

Finally I'm grateful to Flaubert Mbeunkui who kept me company and with whom I shared more time in Stuttgart.

Table of contents

1 Introduction 7

2 Generalities on the working methods 10

2.1 Use of apparatuses 10
2.1.1 Argon glove-box 10
2.1.2 Inert gas and vacuum equipment 11
2.2 Structure investigations by means of X-ray diffraction 12
2.2.1 Powder diffractometer 12
2.2.2 Single crystal investigations 13
2.2.2.1 Rotation and oscillation photographs 13
2.2.2.2 The *Weissenberg* camera 14
2.2.2.3 The IPDS (Image Plate Diffraction System) single crystal diffractometer 15
2.2.2.4 The CCD (Charge Coupled Device) single crystal diffractometer 16
2.2.3 Structure solution and refinement 17
2.3 Synthesis methods 19
2.3.1 Chemicals used 19
2.3.2 Reaction guidance 20
2.3.3 Devices and computer programs 21

3 Oxoselenates(IV) of the trivalent rare-earth elements 23

3.1 Prefaces and synthesis methods 23
3.2 Structure description of the hexagonal $Sc_2[SeO_3]_3$ 25
3.2.1 Structural data for the hexagonal $Sc_2[SeO_3]_3$ 30
3.3 Structure description of the orthorhombic $Ce_2[SeO_3]_3$ 33
3.3.1 Structural data for the orthorhombic $Ce_2[SeO_3]_3$ 36
3.4 Structure description of the monoclinic $Pr_2[SeO_3]_3$ 39
3.4.1 Structural data for the monoclinic $Pr_2[SeO_3]_3$ 43
3.5 Structure description of the triclinic $M_2[SeO_3]_3$ (M = Y, Sm – Ho, Tm – Lu) 50
3.5.1 Structural data for the triclinic $M_2[SeO_3]_3$ (M = Y; Sm – Ho, Tm – Lu) 56

4 Oxide oxoselenates(IV) of the trivalent rare-earth elements 73

4.1 Prefaces and synthesis methods 73
4.2 Structure description of $M_2O[SeO_3]_2$ (M = Sm – Tm) 74

4.3 Structural data for $M_2O[SeO_3]_2$ (M = Sm – Tm) 80

5 Oxyhalide oxoselenates(IV) of the trivalent rare-earth elements 87
5.1 Compounds of the formula $M_3O_2Cl[SeO_3]_2$ (M = Tb, Dy, Er) 88
5.1.1 Synthesis of $M_3O_2Cl[SeO_3]_2$ (M = Tb, Dy, Er) 88
5.1.2 Structure description of the orthorhombic $M_3O_2Cl[SeO_3]_2$ (M = Tb, Dy) 89
5.1.3 Structure description of the monoclinic $M_3O_2Cl[SeO_3]_2$ (M = Er) 90
5.1.4 Structural analogies 91
5.1.5 Structural data for $M_3O_2Cl[SeO_3]_2$ (M = Tb, Dy, Er) 97
5.2 Compounds of the formula $M_4O_3Cl_2[SeO_3]_2$ 102
5.2.1 Synthesis of $M_4O_3Cl_2[SeO_3]_2$ (M = Er, Yb) 102
5.2.2 Structure description of $M_4O_3Cl_2[SeO_3]_2$ (M = Er, Yb) 103
5.2.3 Structural data for $M_4O_3Cl_2[SeO_3]_2$ (M = Er, Yb) 109
5.3 Structure of $Gd_5O_4Br_3[SeO_3]_2$ and $Tb_5O_4Cl_3[SeO_3]_2$ 120
5.3.1 Synthesis of $Gd_5O_4Br_3[SeO_3]_2$ and $Tb_5O_4Cl_3[SeO_3]_2$ 120
5.3.2 Structure description of $Gd_5O_4Br_3[SeO_3]_2$ and $Tb_5O_4Cl_3[SeO_3]_2$ 120
5.3.3 Structural data for $Gd_5O_4Br_3[SeO_3]_2$ and $Tb_5O_4Cl_3[SeO_3]_2$ 125
5.4 Structure of $M_9O_8Br_3[SeO_3]_4$ (M = La, Pr) and $M_9O_8Cl_3[SeO_3]_4$ (M = Pr, Nd, Sm, Gd) 130
5.4.1 Synthesis methods 130
5.4.2 Structure description 131
5.4.3 Structural data 137

6 An alkali metal oxoselenate(IV) of a trivalent rare-earth element: $Li_3Lu_5[SeO_3]_9$ 152
6.1 Synthesis of $Li_3Lu_5[SeO_3]_9$ 152
6.2 Structure description of $Li_3Lu_5[SeO_3]_9$ 152
6.3 Structural data for $Li_3Lu_5[SeO_3]_9$ 157

7 An alkali metal halide oxoselenate(IV) of a trivalent rare-earth element: $CsTmCl_2[SeO_3]$ 166
7.1 Synthesis of $CsTmCl_2[SeO_3]$ 166
7.2 Structure description of $CsTmCl_2[SeO_3]$ 166
7.3 Structural data for $CsTmCl_2[SeO_3]$ 171

8 An alkali metal oxyhalide oxoselenate(IV) of a trivalent rare-earth element:

$CsEu_4O_3Cl_3[SeO_3]_2$ **174**
8.1 Synthesis of $CsEu_4O_3Cl_3[SeO_3]_2$ 174
8.2 Structure description of $CsEu_4O_3Cl_3[SeO_3]_2$ 174
8.3 Structural data for $CsEu_4O_3Cl_3[SeO_3]_2$ 180
9 Summary and outlook **185**
9.1 Results 185
9.1.1 Oxoselenates(IV) of the trivalent rare-earth elements 186
9.1.1.1 The hexagonal $Sc_2[SeO_3]_3$ 186
9.1.1.2 The orthorhombic $Ce_2[SeO_3]_3$ 186
9.1.1.3 The monoclinic $Pr_2[SeO_3]_3$ 187
9.1.1.4 The triclinic $M_2[SeO_3]_3$ (M = Y; Sm – Lu) 187
9.1.2 Oxide oxoselenates(IV) of the trivalent rare-earth elements 188
9.1.3 Oxide halide oxoselenates(IV) of the trivalent rare-earth elements 189
9.1.3.1 Compounds of the formula $M_3O_2Cl[SeO_3]_2$ (M = Tb, Dy, Er) 190
9.1.3.2 Compounds of the formula $M_4O_3Cl_2[SeO_3]_2$ (M = Er, Yb) 190
9.1.3.3 Structure of $Gd_5O_4Br_3[SeO_3]_2$ and $Tb_5O_4Cl_3[SeO_3]_2$ 191
9.1.3.4 Structure of $M_9O_8Br_3[SeO_3]_4$ (M = La, Pr) and $M_9O_8Cl_3[SeO_3]_4$ (M = Pr, Nd, Sm, Gd) 191
9.1.4 An alkali metal oxoselenate(IV) of a trivalent rare-earth-element: $Li_3Lu_5[SeO_3]_9$ 192
9.1.5 An alkali metal halide oxoselenate(IV) of a trivalent rare-earth-element: $CsTmCl_2[SeO_3]$ 193
9.1.6 An alkali metal oxide halide oxoselenate(IV) of a trivalent rare-earth-element: $CsEu_4O_3Cl_3[SeO_3]_2$ 193
9.2 Outlook 194

10 Zusammenfassung und Ausblick **195**
10.1 Ergebnisse 195
10.1.1 Oxoselenate(IV) der dreiwertigen Selten-Erd-Elemente 196
10.1.1.1 Das hexagonale $Sc_2[SeO_3]_3$ 196
10.1.1.2 Das orthorhombische $Ce_2[SeO_3]_3$ 197
10.1.1.3 Das monokline $Pr_2[SeO_3]_3$ 197
10.1.1.4 Das trikline $M_2[SeO_3]_3$ (M = Y, Sm – Lu) 198
10.1.2 Oxid-Oxoselenate(IV) der dreiwertigen Selten-Erd-Elemente 199
10.1.3 Oxidhalogenid-Oxoselenate(IV) der dreiwertigen Selten-Erd-Elemente 200
10.1.3.1 Verbindungen der Formel $M_3O_2Cl[SeO_3]_2$ (M = Tb, Dy, Er) 200

10.1.3.2 Verbindungen der Formel $M_4O_3Cl_2[SeO_3]_2$ (M = Er, Yb) 201
10.1.3.3 Struktur von $Gd_5O_4Br_3[SeO_3]_2$ und $Tb_5O_4Cl_3[SeO_3]_2$ 202
10.1.3.4 Struktur von $M_9O_8Br_3[SeO_3]_4$ (M = La, Pr) und $M_9O_8Cl_3[SeO_3]_4$ (M = Pr, Nd, Sm, Gd) 203
10.1.4 Ein Alkalimetall-Oxoselenate(IV) mit dreiwertigem Selten-Erd-Element: $Li_5Lu_5[SeO_3]_9$ 204
10.1.5 Ein Alkalimetall-Halogenide-Oxoselenate(IV) mit dreiwertigem Selten-Erd-Element: $CsTmCl_2[SeO_3]$ 204
10.1.6 Ein Alkalimetall-Oxihalogenide-Oxoselenate(IV) mit dreiwertigem Selten-Erd-Element: $CsEu_4O_3Cl_3[SeO_3]_2$ 205
10.2 Ausblick 206
11 References 207
Curriculum Vitae 212

1 Introduction

Since the discovery of rare-earth oxoselenates(IV) (selenites) by *Berzelius* in 1818 [1], considerable efforts have been made to gain and characterize in an aqueous solution new rare-earth hydrated selenites and hydrogenselenites. Of particular interest was the family of hydrogenselenites $MH[SeO_3]_2 \cdot n\ H_2O$ and unusual corresponding mixed-valence selenates(IV)/selenates(VI) $M[HSeO_3][SeO_4] \cdot n\ H_2O$ (M = rare-earth element) which have been known for some time [2 – 15]. Then again, anhydrous and non-hydrogenselenates of trivalent lanthanides were synthesized by many authors a few years ago. Namely compounds with the structural formula $M_2[SeO_3]_3$ (M = La, Nd, Er) which have been described as containing ψ^1-tetrahedral $[SeO_3]^{2-}$ groups and their structure strongly influenced by the steriochemically "*lone pair*" of electron at the Se^{4+} cations. Since the La compound crystallized with the orthorhombic system (Pnma) [16, 17], $Nd_2[SeO_3]_3$ was monoclinic ($P2_1/n$) [18] whereas $Er_2[SeO_3]_3$ was triclinic ($P\bar{1}$) [19]. By means of phase diagram supported by thermal analysis (DTA), thermogravimetric (TGA), differential scanning calorimetric (DSC) and IR spectroscopy, *Oppermann* and co-workers [20 – 24], *Gosponidov et al.* [25 – 28] as well as *De Pedro et al.* [29, 30] had suggested the presence of similar $M_2[SeO_3]_3$ phase obtained as homogeneous powder in the temperature range of 550 – 650°C. Up to this temperature their decompose losing SeO_2 due to the high stability of the oxidation state IV for the selenium, leading to the formation of phases with the composition $M_2Se_2O_7$ obtained at the temperature of about 800°C. Details concerning crystals structure of the latter remind unknown until now despite *Giester* [31], *Jones et al.* [32] succeeded in isolating similar compounds with trivalent transition metals, to be precise $Fe_2Se_2O_7$ and $Au_2Se_2O_7$ (according to $Fe_2O[SeO_3]_2$ and $Au_2O[SeO_3]_2$ due to the presence of a ψ^1-tetrahedral $[SeO_3]^{2-}$ units with additional oxygen atoms which are not coordinated to any selenium atom). A phase with the same situation in the homologous M_2O_3/TeO_2 system has also been described very recently for the oxotellurate(IV) $Pr_2O[TeO_3]_2$ as adopting the *pyrochlore*-type crystal structure [33] without stereochemical activity of the lone-pair at Te^{4+}.

During the last ten years, many works have been done in order to characterize anhydrous halide oxoselenates(IV) of trivalent lanthanide. In this way *Wickleder* and co-workers elucidated the structure of some fluoride oxoselenates for instance $M_3F[SeO_3]_4$ (M = Nd, Sm, Gd, Dy) crystallizing with the acentric space group $P6_3mc$ [19, 34] as well as $LaF[SeO_3]$ (monoclinic; $P2_1/c$) [16], these being the first rare-earth halides oxoselenates(IV) although a

chloride oxoselenate of trivalent bismuth $BiCl[SeO_3]$ had been pointed out before by *Berdonosov et al.* [35]. The formation of acentric fluoride oxoselenates(IV) encouraged corresponding authors to investigate also chlorides. Thus they have successfully synthesized as single crystals the first rare-earth chloride oxoselenates(IV) explicitely $NdCl[SeO_3]$, $ErCl[SeO_3]$ and $HoCl[SeO_3]$ which crystallized orthorhombically in the space group Pnma [36]. These results then came to confirm investigations made by *Oppermann et al.* which had reported the presence of three compounds $SmClSeO_3$, $SmClSe_2O_5$ and $SmClSe_3O_7$ from the phase diagram of the system $SmOCl/SeO_2$ [37].

In the crystal chemistry of the above-mentioned oxoselenates(IV), excepted those of $Fe_2O[SeO_3]_2$, $Au_2O[SeO_3]_2$ and $Pr_2O[TeO_3]_2$, descriptions of cations as central atoms and anions as ligands are given. However, *Krivovichev et al.* have analyzed very recently some transition metals oxoselenates(IV) on the basis of anion coordinations. This is particularly suitable in the description of compounds such as $Cu_9O_2Cl_6[SeO_3]_4$ and $Cu_5O_2Cl_2[SeO_3]_2$ which contain "additional" oxygen atoms, *i.e.* atoms not included into the usual $[SeO_3]^{2-}$ complex anions. The "additional" oxygen atoms have a tetrahedral coordination environment of metal atoms, therefore being centers in $[OCu_4]^{6+}$ cationic complexes. Relatively high bond strength in oxocentered tetrahedra allows authors to suggest their selection as independent structural subunits in those compounds [38, 39]. Furthermore, oxocentered $[OM_4]$-tetrahedral units (M = transition metal or rare-earth element) are well known in metal-organic compounds as polynuclear metal complexes with so-called μ_4-bridging oxygen atoms. Their structures have been subjected to extensive investigations because of their interesting magnetic properties due to the metal-metal interaction within the $[OM_4]$ tetrahedra [40, 41].

In addition to oxoselenates(IV) and halide oxoselenates(IV) of trivalent lanthanide, oxide oxoselenates(IV) and oxyhalide oxoselenates(IV) of trivalent or divalent transition metals and obviously the above-mentioned hydrated and hydrogenselenates, many efforts have been undertaken in order to synthesize mixed metal phases containing both lanthanides and alkali or transition metals. But their amount is quite limited to date although *Effenberger* described a number of mixed transition metals oxoselenates(IV) with main group elements for example $BaCu[SeO_3]_2$ and $SrCu[SeO_3]_2$ [42], $Sr_2Cu[SeO_3]_3$ [43], $PbCu_2[SeO_3]_3$ [44] and $Bi_2Cu[SeO_3]_4$ [45]. The presence of both heavier lanthanoids and another metal in anhydrous oxoselenates(IV) has been studied less extensively, the only compounds stated in the literature being $NaY[SeO_3]_2$ and $NaLa[SeO_3]_2$ [46], as well as $La_2Cu[SeO_3]$ (isostructural with $Bi_2Cu[SeO_3]_4$) [47]. In the same approach the combination of magnetic activities of d- and f-metals in the same oxoselenates(IV) compounds has interested *Wickleder* during the last two

years, those compounds are of fundamental interest in solid-state chemistry and materials science, besides they have the potential for useful physical properties. Novel mixed rare-earth and transition metals chloride oxoselenates(IV) have afterwards been synthesized and structurally characterized, to be exact $CuGdCl[SeO_3]_2$, $MnNdCl[SeO_3]_2$, $CoNd_{10}Cl_8[SeO_3]_{12}$ and $NiNd_{10}Cl_8[SeO_3]_{12}$ [48] for these reasons.

The free *non*-binding electron pairs ("*lone pair*") at the Se^{4+} cations always observed in those compounds, materials containing high coordinated trivalent rare-earth cations (Sc^{3+}, Y^{3+}; La^{3+} – Nd^{3+}, Sm^{3+} – Lu^{3+}) in combination with $[SeO_3]^{2-}$ groups and additional oxygen not coordinated to any selenium atom but forming $[OM_4]$ tetrahedra (M = rare-earth elements) as well as additional halide anions may be an excellent combination in the search for novel asymmetric structures. Such materials could have useful non-linear optical properties with potential applications in electro-optical devices. Furthermore, the oxoanion $[SeO_3]^{2-}$ holding a stereochemically active lone pair of electrons may have a tendency for aligning in the solid state to end up polar structures. This feature increases a number of important physical properties including second harmonic generation (SHG) and ferroelectric behaviour [49 – 51]. On the other hand, $[SeO_3]^{2-}$ anions can provide several advantages in that they could be both better donor ligands for metals (*vide infra*) and could be thermally very robust. Thus, their structures seem to be of interest and we are now exploring in our laboratory the solid-state chemistry of such compounds. It is the aim of this work, which contains three main parts. While the first one concerns generalities on the working methods, the second offers the process for single crystals syntheses and therefore the precondition for their structure determination and description, which the third one extensively deals with.

2 Generalities on the working methods

2.1 Use of apparatuses

2.1.1 Argon glove-box

The compounds we use must be of very great purity, and do not have to be in contact with air or moisture, the use of an argon glove-box (fig. 1.1.1, Fa. Braun, Garching) then simplifies working under exclusion of humidity (H_2O) and substantially atmosphere gases (especially O_2 and N_2). Inside the box, there are chemicals we need for our experiments and a balance with a uncertainty of 0.0001 g. Others necessaries for working inside the box (cupel, spatula, glass ampoules etc…) are carried on in some plate. All are introduced into an air-lock system (see figure). After air evacuation, weighings are made. This apparatus includes on its principal face three gloves and one pedal allowing the pressure control inside the box. The argon atmosphere is led by a regeneration cycle and is cleaned and rolled over at the same time. This is permanently supervised by an atmosphere controlling device (for H_2O and O_2).
In addition, the argon glove-box is very useful for preparation of air unstable compounds or for selection of single crystals, which are moisture and air sensitive.

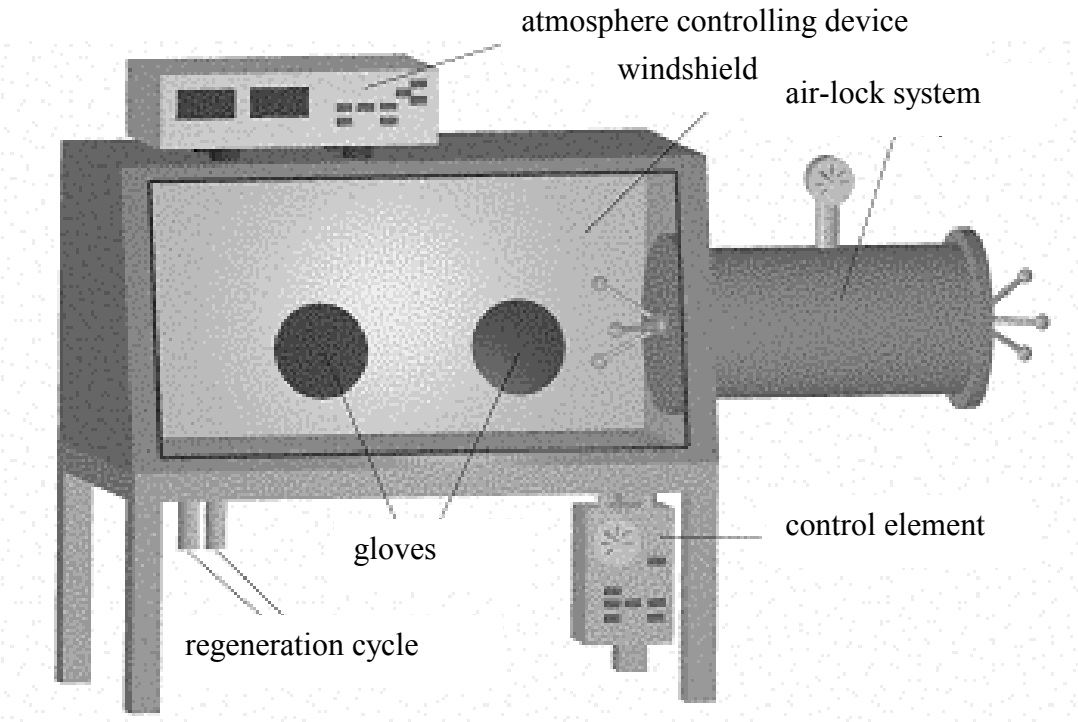

Fig. 2.1.1: Argon glove-box equipment (Labmaster MB 130, Fa. M. BRAUN, Garching)

2.1.2 Inert gas and vacuum equipment

After the loading processeses in the glove box, the silica tubes containing our reactants are charged with argon. In order to insure vacuum and to reduce argon pressure dominant in the reactions containers, it is necessary to evacuate them. For that operation, we need a vacuum equipment (fig. 2.1.2). It consists of a turbo-molecular pump with upstream rotary vane pump; a vacuum connected at it outlet side and an inert gas system out of glass. Its employment allows to evacuate our reactions containers up to residual pressure of about 10^{-5} – 10^{-6} mbar. Besides, a purifying flow control valve makes the supply of a defined inert gas stream possible and thus adjusting certain pressures, that should be desired and/or necessary.

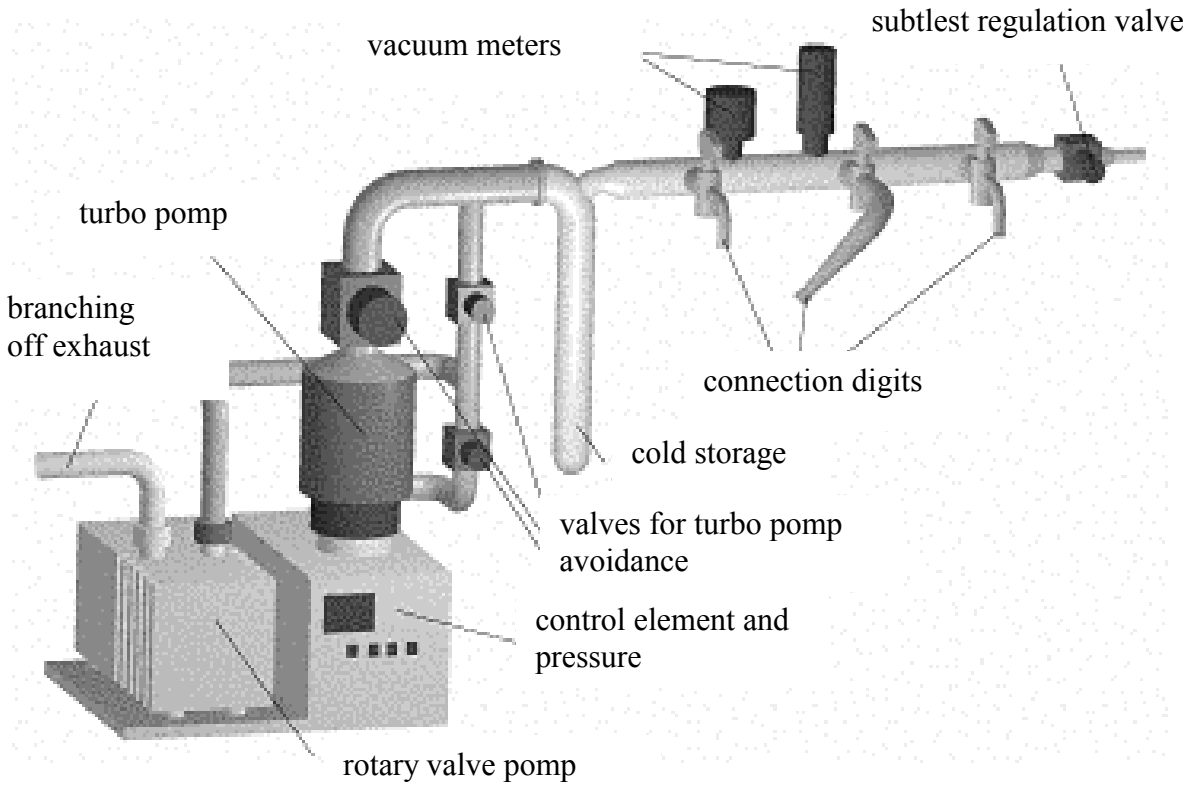

Fig. 2.1.2: Inert gas and vacuum equipment

2.2 Structure investigations by means of X-ray diffraction

2.2.1 Powder diffractometer

The sample is generally plane (extend the powder on a plane which is used as a support), and is irradiated by an incidental beam slightly divergent (fig. 2.2.1). One carries out the beam reflection by more significant quantity of matter, which produces more intense reflected beams easier to detect. However, the considered beam is focused on the meter slit input when the normal of the plate bisect the angle formed with the axis of the meter and the incidental beam. The sample must twist through θ degrees if the meter turns of 2θ. This rotation called θ–2θ movements is significant for two circles diffractometer (one for the sample and one for the meter). The powder diffractometer recordings are graphics where measured intensities radiations are carried according to the position of the meter. With its precision and its facility for using, the two circles diffractometer despite a high cost is most useful than Debye-Scherrer method. The photographic method keep nevertheless all its power in very weak diffraction lines detection, detection some time difficult to the diffractometer view the short time of the meter during a moving of 2θ. This method is a perfect identification one for materials, which are difficult to bring to the state of single crystal. The powder diffractogram are of a complexity in such a way that it is not possible for two different substances to have identical spectra.

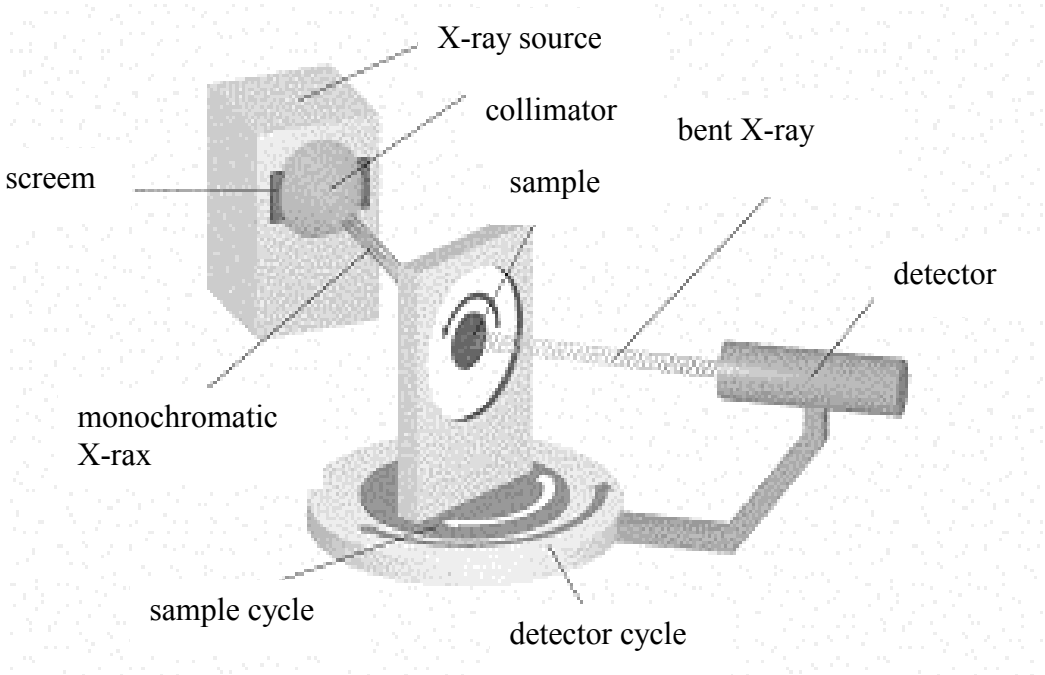

Fig. 2.2.1: Powder diffractometer

2.2.2 Single crystal investigations

2.2.2.1 Rotation and oscillation photographs

For the first evaluation of the crystals qualities, the preparation of the swivelling accommodation should be done. For this, a single crystal must be patched up in a mark tube and placed at the head of a goniometer, which is adjusted before X-ray beam and must rotate around any of its principal crystallographic axis, which is also a zone axis. The diffracted rays are received by a sheet of film held against the inner surface of a fixed, cylindrical shell that is concentric with the crystal rotation axis. After exposure the film is developed, fixed, and washed, revealing the diffraction pattern in the form of characteristic layers lines (n = 0, 1, 2, ….), stretching perpendicular to the axis of rotation. This predicates about the crystal quality, for example whether the preparation is really present single crystal or not. With good quality single crystal, reflection form straight lines parallel to the beam axis. The distance between two of them situated in both side of the zero level allows having an idea about the first unit cell system. From such an adjust swivelling manner accommodation, first information about the measured single crystal is received, thus for example about the symmetry of the axis or about the lattice straight-line dimension. The latter can occur, by measuring or by calculation of the length I according to the following formula:

$$I = \frac{n.\lambda}{sin\left[arctan\left(\frac{y}{d}\right)\right]}$$

(with I = Intensity period (axis length) (pm), d = the true film radius (mm), y = distance on the film, in the same units, from the zero-layer line to the *n*th-layer line, λ = wavelength (pm), n = reflexes diffraction order)

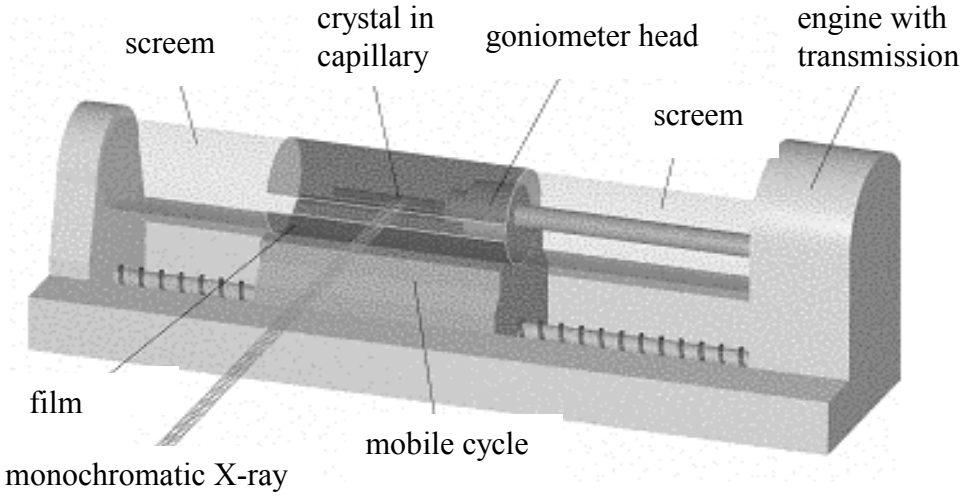

Fig. 2.2.2.1: The *Weissenberg* camera

2.2.2.2 The *Weissenberg* camera

The Weissenberg process is geometrically more nearly related to the rotation method, and shares its ability to explore a large part of reciprocal space. After the turning crystal accommodation, the same equipment is used immediately for *Weissenberg* technique (fig. 2.2.2.1). With the help of the swivelling accommodation, the crystal can be adjusted now so that a real lattice straight line appears exactly parallel or a reciprocal network level perpendicularly to the appropriate goniometer axis. Each line on the film thus corresponds to a reciprocal network level of the crystal (fig. 2.2.2.2). By mean of two screens all reflexes are faded out except those on the preferential line. From translation of the film at about 2°/mm, coupling with the turning of the crystal, results the typical diffraction patterns of a reciprocal atomic plane. An undistorted representation can then be designed, by transferring the individuals reflexes (with help of *Buerger*- or *Weissenberg*-triangle) to polar coordinates papers. The lengths and both remaining axis and angles are therefore inferred. By finding possible systematic extinctions, the determination of the crystal system and the *Laue*-symmetry are also possible.

The calculation of the length axis from *Weissemberg*-method follows the equation below:

$$I = \frac{n.\lambda}{sin(2d_n)}$$

(with I = Intensity period (axis length) (pm), n = number of intensity period (1, 2,…..), λ = wavelength (pm) and d_n = distance between n reflexes from the zero line (mm).

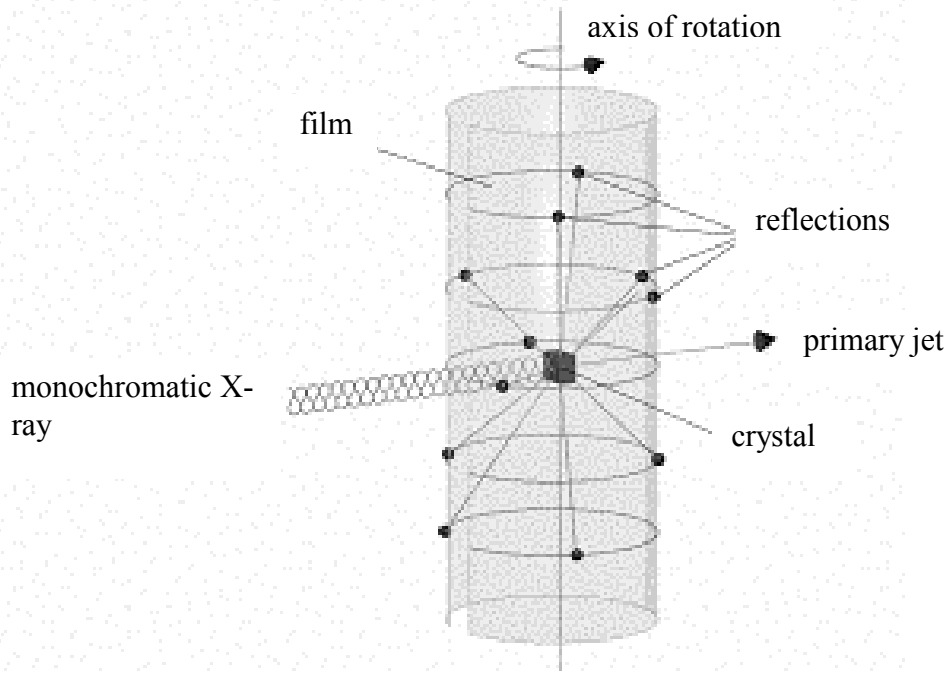

Fig. 2.2.2.2: Emergence of lines with a turning crystal accommodation

2.2.2.3 The IPDS (Image Plate Diffraction System) single crystal diffractometer

In order to enter the reflecting power of all crystal network levels, it must be swivelling during the measurement in all three space directions. The device prerequisites for this are carried out in a four circle diffractometer whose operation mode is based on geometry principle (CAD: κ-geometry). By combination of goniometer and detector, many of desired reflexes can be determined within a layer at the same time. The Imaging Plate Diffraction System (IPDS) is a single-crystal diffractometer (fig. 2.2.2.3). The measurement of the diffraction takes place via exposure of a fluorescence disk, which is read off after exposing with a laser, coated with Eu^+ doped BaFCl, scanned, and deleted afterwards again. With this technique, intermediate and foreign reflexes are always considered and can false the elementary cell suggestions. However, during the subsequent reflexes integration with the correct cell, these are neglected likewise. The great disadvantage of IPDS is the empirical absorption correction use for solving the crystal structure, because it is not possible to measure the intensities of individual reflexes in different orientation. Problems occur here particularly with crystal, which contains strongly absorbing items. With the use of program such as HABITUS [52] or X-SHAPE [53], this lack can however be balanced.

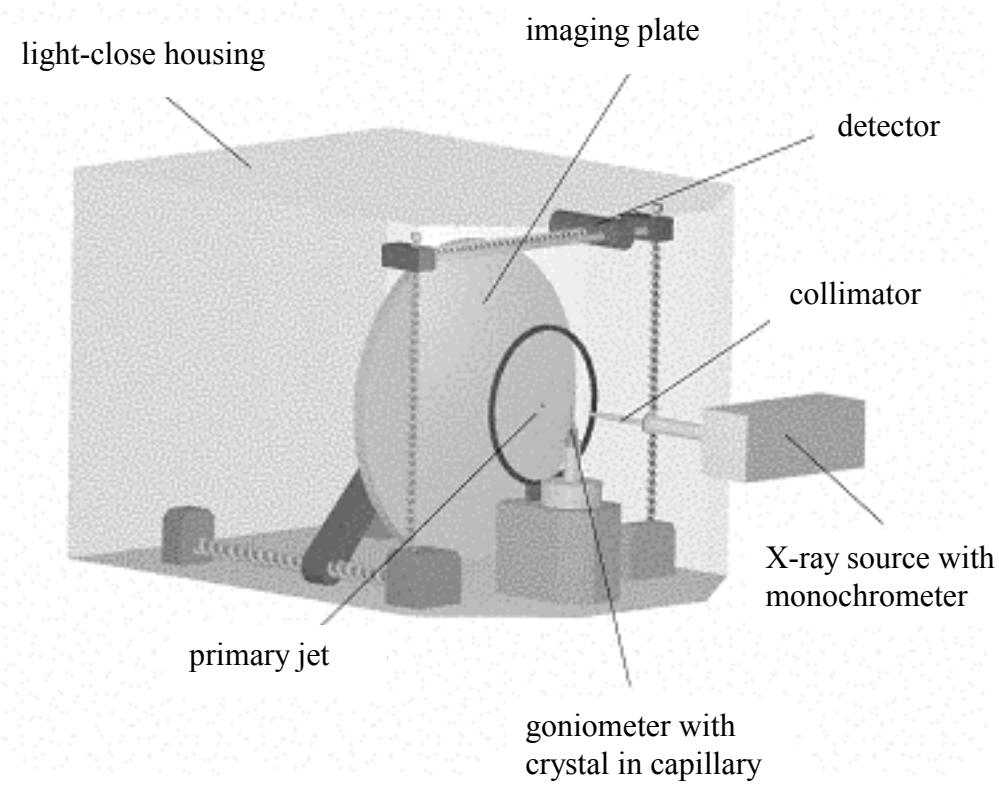

Fig. 2.2.2.3: IPDS (Image Plate Diffraction System) diffractometer equipment

2.2.2.4 The CCD (Charge Coupled Device) single crystal diffractometer

The Nonius-CCD (fig. 2.2.2.4) is a two dimensional detector allowing the measurement of several tasks of diffraction: an instantaneous browsing of a broad area of the reciprocal space of the crystal is thus possible. The detector does not need to move for seeking the peaks of diffraction, and the movement of the crystal are reduced. During the measurement, the crystal must, nevertheless rotate for allowing number of network reciprocal node to cross EWALD sphere. In practise, only rotations around φ-axis (if $\kappa = 0$) or ω-axis (if $\kappa \neq 0$) are realized. Because of the knowing crystal dimension and the divergence of the incidental crystal beam, the reciprocal network node has known volume. To each diffraction image, will be associated a low amplitude of rotation (1 or 2°) to avoid superposition of diffraction tasks corresponding to different nodes. Images are collected in two iterations in order to deminish disturbing effects of cosmic radiation. In this kind of diffractometer, the distance between X-ray source beam and crystal remind constant, and the one between the crystal and the detector is adjustable (adjustment of the detector resolution). The diffracted photons X arriving on the detector are converted to electronic signal. The detector is cooled between –40 and –80°, this allowed deminishing the thermal electronic noises. With instantaneous observation of a broad reciprocal space, the CCD diffratometer is a toll privileged for structural phase transitions study. The realization of some diffraction images lets to visualize immediately the structural changes. Particularly, it allows to easily identifying satellite lines, characteristics of superstructures or incommensurable phases.

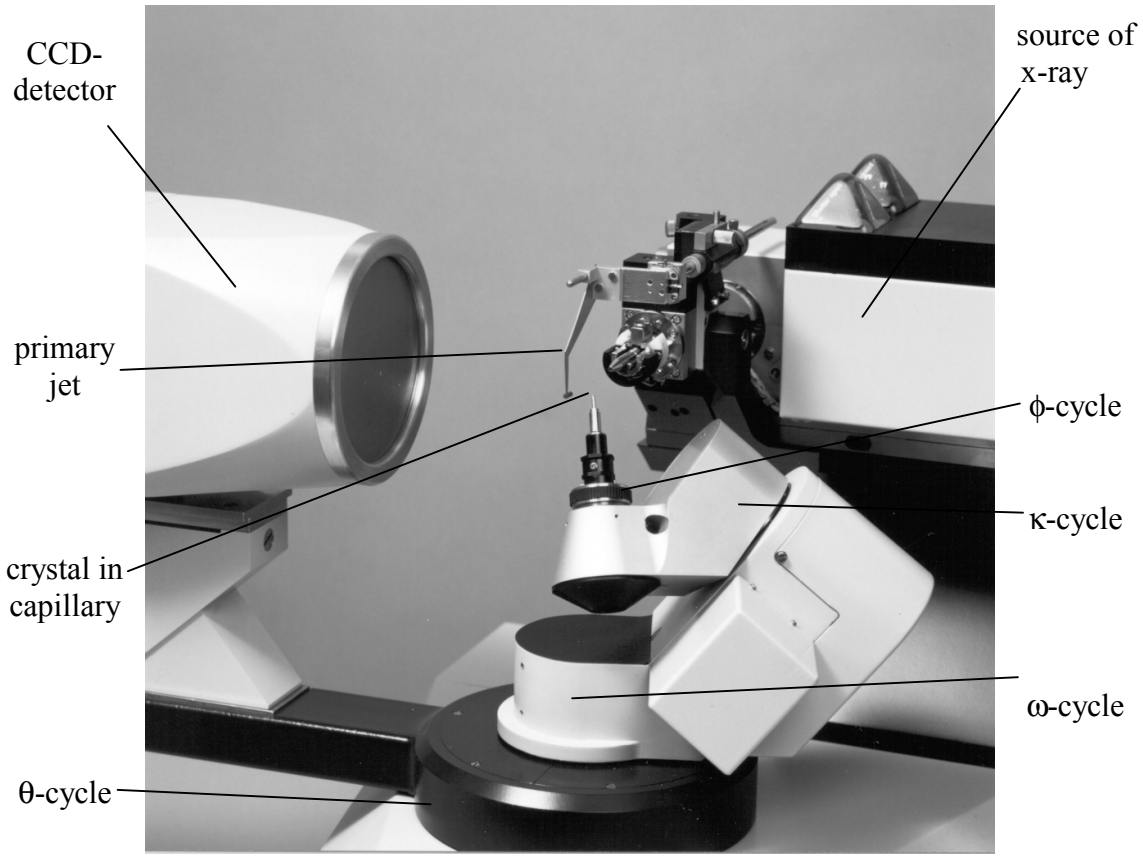

Fig. 2.2.2.4: The CCD (Coupling Charge Device) single crystal diffractometer

2.2.3 Structure solution and refinement

After above information about unit cell, crystal system, space group and peaks intensities, it is necessary to known the position of different atoms in the unit cell and therefore built a structural model of the compound. With the help of computer program SHELXS-86 [54], one have the possibility to use either "Patterson-Syntheses" [55] or "Direct-Methods" [55] for localizing atoms in the unit cell. Those methods are problematic when the structure contains only some heavy atoms against many light ones. With the help of difference Fourier-syntheses, the maximal residual electron density is localized, thus allowing having information about the remaining atoms position in the unit cell (SHELX-76 [56]). When a suitable structure model is found, the computer program SHELXL-93 [57] bases on the "least-squares" method is utilized for optimization, firstly with isotropic temperature factor for all atoms followed by refinement with anisotropic temperature factor for all of them. To estimate

good qualities data, intern residual value (R_{int}) must be calculated with the use of computer program SHELX-93 and SHELX-97 [58]. This value is defined as follows:

$$R_{int} = \frac{\sum_{i=1}^{n} \left| F_o^2 - \overline{F_o^2} \right|}{\sum_{i=1}^{n} F_o^2}$$

with n: number of measured reflections,

F_o^2 : square of the structure amplitude observed,

$\overline{F_o^2}$: average square of the symmetry equivalent of the structure amplitude and

$$R_\sigma = \frac{\sum_{i=1}^{n} \sigma\left(F_o^2\right)}{\sum_{i=1}^{n} F_o^2}$$

with $\sigma\left(F_o^2\right)$: standard deviation of the observed reflections.

Over the agreement of crystallographic data and the structural model, different factors of qualities are calculated. From SHELXL-93 or SHELXL-97 the minimized directly value is wR_2 which incorporates the reflection weights and is defined as follows:

$$wR_2 = \sqrt{\frac{\sum_{i=1}^{n} w\left(F_o^2 - F_c^2\right)^2}{\sum_{i=1}^{n} w\left(F_o^2\right)^2}}$$

with F_c^2: square of the structure amplitude calculated

w : priority factor,

this factor is defined by :

$$w = \frac{1}{\sigma^2\left(F_o^2\right) + \left(aP\right)^2 - bp}$$

with $P = 1/3(F_o^2 + 2F_c^2)$ as well as a and b from the refinement determined sizes.

Besides the received value of wR_2 there is also in this work the conventional unweighted index R-value (R_1), defined as follows:

$$R_1 = \frac{\sum_{i=1}^{n} \left| |F_0| - |F_c| \right|}{\sum_{i=1}^{n} |F_o|}$$

and is not from the square of the structure amplitude, but only from (non observable) amounts rests. The advantages of calculating and quoting this index together with wR_2 are that it

provides a comparison with older work, it is generally considerably smaller than wR_2 for F^2 refinements, and it is relatively insensitive to change in the weighting scheme, which dramatically alter wR_2. Another quality criterion for the structural model is the "factor of quality" ("Goodness of Fit", GOOF): it is a useful index often output by least squares refinement programs or a measure of the degree to which the found distribution of differences between $|F_o|$ and $|F_c|$ fits the distribution expected from the weights used in the refinement.

$$GOOF = S = \sqrt{\frac{\sum_{i=1}^{n} w\left(F_o^2 - F_c^2\right)^2}{n - p}}$$

with p as the number of refined parameters and n number of reflections. The degree of the structure parameters agreement is related to the difference n – p. If these weights are correct, which implies that the errors in the data are strictly random and correctly estimated and if the model properly represents the structure that gives rise to the data, this value must be around 1.0.

2.3 Synthesis methods

2.3.1 Chemicals used

Chemicals used for all reaction are quoted in table 2.3.1. They are available as commercial products at the specified companies and were used without further pre-treatment. Promethium is a radioactive element; it is neither accessible nor handy in our institute and is to be excluded therefore from the further discussion.

Table 2.3.1: List of chemicals used

Substance	Purity	Supplier
Ce, Pr, Tb powder	99.9%	CHEMPUR, Karlsruhe
Lanthanide oxides M_2O_3 (M = La, Nd, Sm – Gd, Dy – Lu, Sc, Y as well as CeO_2, Pr_6O_{11}, Tb_4O_7	99.9%	CHEMPUR, Karlsruhe
Lanthanide trichlorides MCl_3 (M = La – Lu)	99.9%	CHEMPUR, Karlsruhe
Lanthanide tribromides MBr_3 (M = La – Lu)	99.9%	CHEMPUR, Karlsruhe
Selenium dioxide SeO_2	99.9%	CHEMPUR, Karlsruhe
Cesium chloride *CsCl*	99.9%	CHEMPUR, Karlsruhe
Lithium chloride *LiBr*	99.9%	CHEMPUR, Karlsruhe
Cesium bromide *CsBr*	99.9%	CHEMPUR, Karlsruhe
Argon gas *Ar*	99.998%	Messer-Griesheim, Krefeld

2.3.2 Reaction guidance

Due to its melting point up to 1100°C, its very cheapest cost, the facility with which it can be used, silica glass is the best material utilized as container for all our reaction. It is stable for the long period we need to carry out the reaction (seven days) and the temperature range in which they are done (800 – 850°C). However, it sometime reacts with our educts to form lanthanide oxosilicate but this is seldom feasible. For the production of silica glass tubes, silica glass pipe (diameter of about 12 mm, external thickness of the walls (≡ 1.5 mm) is cut down to appropriate length. With the help of a detonating gas burner, one of its side is melted and finally closed. At the open end a cross section is set for the connection to the vacuum pump and at the distance of about 12 – 15 cm from the closed side, a very frayed section is

done in such a manner that after filling it with our educts in glove-box and evacuation with vacuum equipment, it will be easy to close the tube with a single gas oxygen burner. The tube with its contain is then put in a furnace with a precaution that reagents and flux must not be dispersed everywhere inside the tube.

2.3.3 Devices and computer programs

The devices and computer programs needed for update this work are arranged in the table 2.3.3.a and 2.3.3.b and are available in the research group of Prof. Dr. Thomas Schleid (the latters as license versions, if necessarily). Computations have been made with our personal computer in the group.

Table 2.3.3.a: Devices used

Apparatus	**Model**	**Manufacturers**
Microscope	SZ 40	OLYMPUS (Hamburg)
Glove box	LabMaster MB130 and MB 150-G-I	M. BRAUN (Garching)
Powder diffractometer	STADI-P	STOE (Darmstadt)
Weissenberg camera	WB- Goniometer 100	HUBER (Rimsting)
Single crystal diffractometer	IPDS	STOE (Darmstadt)
Single crystal diffractometer	κ-CCD	NONIUS, Delft (NL)

Table 2.3.3.b: Computer programs used

Programs	Fonction	Ref.
Win Xpow 1.03	Program for accommodation, analysis and simulation of powder diffractograms	[59]
X-RED	Program for space group regulation and numerical absorption correction (based on X-SHAPE)	[60]
X-SHAPE	Program for numerical absorption correction (IPDS and CCD data)	[53]
X-STEP	Surface work which use SHELXS-86 and SHELXL-93	[61]
SHELX-76	Program for crystal structure determination	[56]
SHELXS-86	Program for crystal structure solution	[54]
SHELXL-93	Program for crystal structure refinement	[57]
SHELXL-97	Advancement of SHELXS-86 and SHELXL-93	[58]
MAPLE 4.0	Program for calculation of linkage distances and angles, effective coordination numbers, and lattice energies	[62]
DIAMOND 2.0	Program for graphics, coordination polyhedra and crystal structure representation	[63]

3 Oxoselenates(IV) of the trivalent rare-earth elements

3.1 Prefaces and synthesis methods

Structural information about anhydrous rare-earth compounds in combination with complex anions $[SeO_3]^{2-}$ are seldom. However, structures of the composition $M_2[SeO_3]_3$ (M = rare-earth element) have been mentioned previously. They were prepared either by thermal decomposition of selenite hydrates [64 – 69], acidic selenite [70 – 72] or by fusing M_2O_3 and SeO_2 [20 – 22, 24], but these methods did not lead to single crystals so that only powder diffraction data are available. Recently many authors reported on the synthesis and crystal structure of $M_2[SeO_3]_3$ (M = La, Nd, Er) [16 – 19]. The latter three compounds were the first anhydrous rare-earth oxoselenates(IV) which were structurally characterized thus far. While the lanthanum compound crystallizes in an orthorhombic system (space group Pnma), Er compound crystallizes triclinic (space group $P\bar{1}$) and finally $Nd_2[SeO_3]_3$ crystallizes in the monoclinic system ($P2_1/n$). Their structure are strongly influenced by the free *non*-binding electron pairs ("*lone pair*") at the Se^{4+} cations and the $[SeO_3]^{2-}$ species lead to pyramidal coordination. A similar phase $Bi_2[SeO_3]_3$ was obtained by sintering of stoichiometric mixtures of Bi_2O_3 and SeO_2 at 623° K, single crystals were then prepared by chemical transport reaction using $BiBr_3$ or Br_2. The X-ray single crystal investigation also revealed the $P2_1/n$ space group of the monoclinic system for this bismuth oxoselenate(IV) [71].

We have extended in this work the crystal chemistry of such compounds for all lanthanides elements by synthesizing via direct solid-state reaction corresponding single crystals. Therefore this structural compound class is completely known. Single-crystalline phases of $M_2[SeO_3]_3$ (M = Sc, Y, Sm – Ho, Tm – Lu) were grown from a mixture of M_2O_3 and SeO_2 handled under inert atmosphere of argon glove box (additional $CeCl_3$, $PrCl_3$, $TbCl_3$, Ce, Pr and Tb were used in the case of CeO_2, Pr_6O_{11} and Tb_4O_7). The starting materials were placed in a quartz glass tube evacuated to 10^{-3} mbar, torch-sealed and heated at 830°C for seven days. The furnace was cooled down slowly (0.1°C/min) up to 400°C and finally switched down to room temperature. CsCl (melting point 646°C) or CsBr (melting point 636°C [72]) were added to the educts as fluxing reagent. After washing with distilled water in order to dissolve the excess of flux, suitable single crystals, big needle-shaped were selected for the X-ray measurement (see parts 2.2 – 2.5 for X-ray data collection). The reaction scheme for single crystal synthesis were as follows for lanthanides sesqui-oxides as well as for CeO_2 and

the mixed valences compounds Pr_6O_{11} and Tb_4O_7. As well, the use of LiBr as flux in the case of $Lu_2[SeO_3]_3$ also leads to $Li_3Lu_5[SeO_3]_9$ single-crystalline phase (paragraph 6).

$$M_2O_3 + 3\ SeO_2 \longrightarrow M_2[SeO_3]_3\ (M = Sc, Y, Sm - Gd, Dy, Ho, Tm - Lu) \qquad (1)$$

$$3\ CeO_2 + 3\ SeO_2 + Ce + CeCl_3 \longrightarrow Ce_2[SeO_3]_3 + 3\ CeOCl \qquad (2)$$

$$3\ Pr_6O_{11} + 27\ SeO_2 + 4\ Pr + 2\ PrCl_3 \longrightarrow 9\ Pr_2[SeO_3]_3 + 6\ PrOCl \qquad (3)$$

$$3\ Tb_4O_7 + 9\ SeO_2 + 2\ Tb + 4\ TbCl_3 \longrightarrow 3\ Tb_2[SeO_3]_3 + 12\ TbOCl \qquad (4)$$

Single crystals were obtained as green rod for praseodymium, pink rod for holmium and colourless rod for the residual rare-earth elements and are of very good quality as can testified by the comparison of an experimental powder diffractogram with the theoretical one in the case of thulium (diagram 3.1).

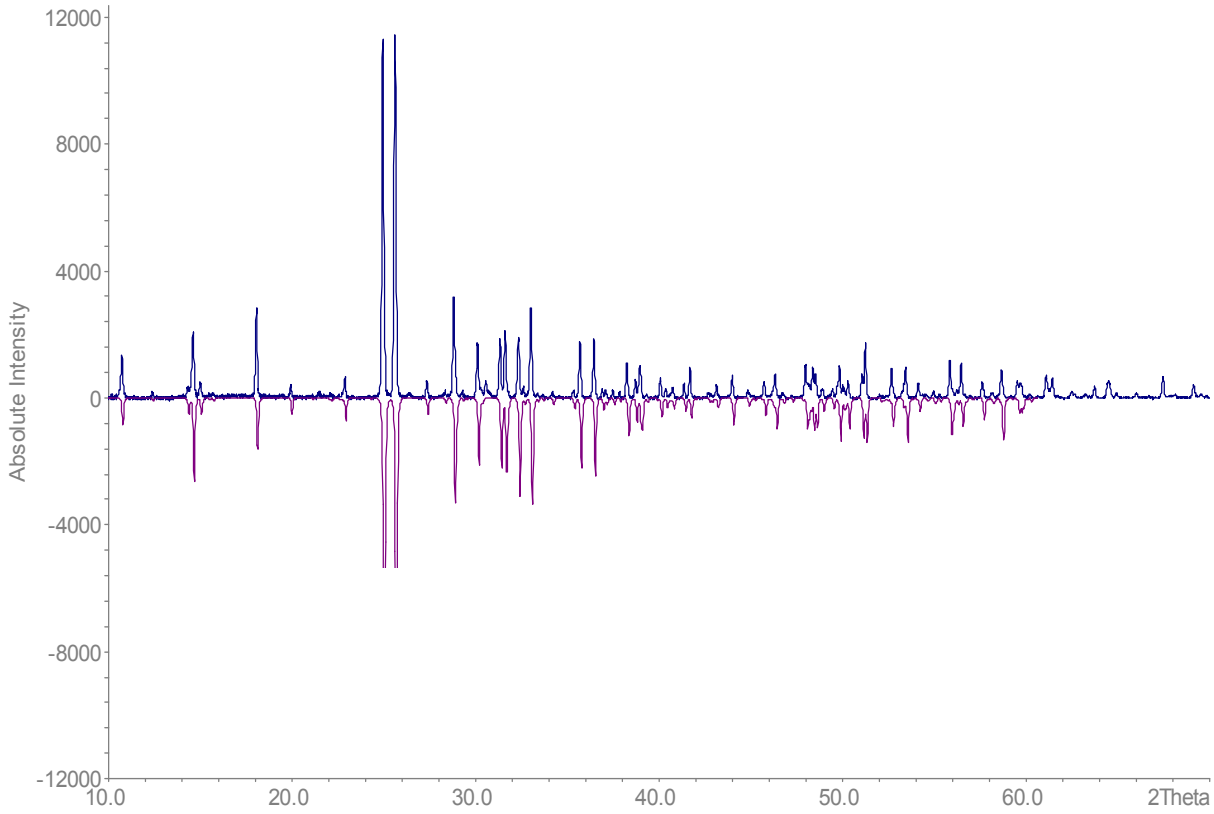

Diagram 3.1: Comparison of the measured $Tm_2[SeO_3]_3$ powder diffractogram (*above*) with the theoretical one (*below* as negative intensities)

3.2 Structure description of the hexagonal $Sc_2[SeO_3]_3$

Contrary to the three crystal systems (monoclinic, orthorhombic and triclinic) adopted by the other anhydrous rare-earth(III) oxoselenates(IV) known up to date, $Sc_2[SeO_3]_3$ crystallizes hexagonally and contains only a single crystallographical Sc^{3+} cation and a single anionic $[SeO_3]^{2-}$ group likewise. Scandium resides in an irregular sixfold coordination of oxygen atoms with distances d(Sc–O) between 202 and 220 pm (table 3.2.1.d). The coordination figure is best described as trigonal antiprism and six $[SeO_3]^{2-}$ groups are grafted onto the coordination sphere via commons vertices. The Sc–O distances can be divided into two groups, three short (201.9 pm) and three longer (219.8 pm) ones on opposite faces of the *quasi*-octahedron leading to a rather distorted polyhedron of coordination (fig. 3.2.a, *left* and table 3.2.1.d for the O–Sc–O bridging angles). Although being quite small compared with analogous rare-earth(III) oxoselenates(IV) $M_2[SeO_3]_3$ (M = La; Nd, Er) [16 – 19] they agree very well with those in other scandium compounds with sulfur or selenium containing discrete complex oxochalcogenate anions such as $Sc_2[SeO_4]_3 \cdot 5H_2O$ [70], $Sc[HSeO_3]_3$ [74], $Sc_2[SeO_4]_3$ [75], $(NH_4)_3Sc[SeO_4]_3$ [76] and $Na_3Sc[SO_4]_3 \cdot 2H_2O$ [77]. Two ScO_6 octahedra share one of their triangular face (O1,O1,O1) to form dimeric Sc_2O_9 groups similar to the M_2O_9 (M = Al, Ga) one in $Al_2(HPO_3)_3$- and $Ga_2(HPO_3)_3$-type structure [78] and this common face is a perfect symmetry plane in this structure (fig. 3.2.a, *right* and fig. 3.2.d). The triangular faces defined by the terminal O atoms in adjacent ScO_6 polyhedra are oriented in the same directions. The distortion among Sc_2O_9 manifests itself as a squeezing of the O1–Sc–O1 bond angles to values of 74.19°, coupled with small Sc–O1–Sc bridging angles of 91.7° (3×) (fig. 3.2.a, *right*). This complies well with the corresponding angles in the two phosphites $M_2(HPO_3)_3$ (M = Al, Ga) which were found to be 76.1° (M = Al) and 74.4° (M = Ga) for O2–M–O2 angles, 89.3° (M = Al) and 91.3° (M = Ga) for the M–O2–M ones.

The presence of double octahedra in $Sc_2[SeO_3]_3$ may be interpreted as a tendency to form stable $[Sc_2O_9]^{12-}$ ionic groups. One might expect that the stability of these ionic groups is due to covalent interactions between the Sc atoms across the shared face. Interestingly, the geometrical interaction criterion of *Cotton* and *Ucko* (1972) [79], supported by *Chabot* and *Parthé* (1978) [80] does not indicate an attractive interaction between Sc. In table 3.2.1.d, the interatomic distances and angles in the $[Sc_2O_9]^{12-}$ double octahedra are given using *Cotton* and *Ucko* notation. Figure 3.2.b illustrates this notation in detail. In the ideal case the filled double octahedra are built up of two regular octahedra with X atoms at their centres, and consequently: $90° - \alpha' = 0°$, $\beta - 70.53° = 0°$.

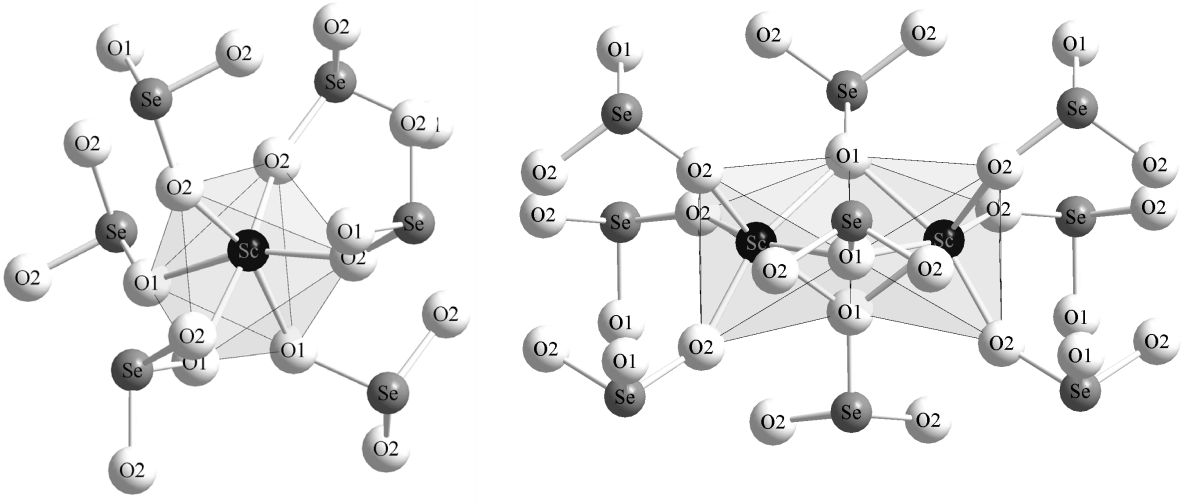

Fig. 3.2.a: Local environment of scandium indicating six $[SeO_3]^{2-}$ groups attached to the $[ScO_6]$ octahedral (*left*) and $[Sc_2O_9]$ dimer exhibiting the triangular face (O1,O1, O1) for the connectivity and the nine attached $[SeO_3]^{2-}$ groups (*right*)

In $Sc_2[SeO_3]_3$, the $[Sc_2O_9]^{12-}$ ions are geometrically alike: the angular deviations with respect to the undistorted double octahedra are positive (15.81° for 90° – α′ and 21.17 for β – 70.53°). Those values attest the stability of the $[Sc_2O_9]^{12-}$ groups and prove less contractive or repulsive forces between Sc–Sc within the $[Sc_2O_9]^{12-}$ groups.

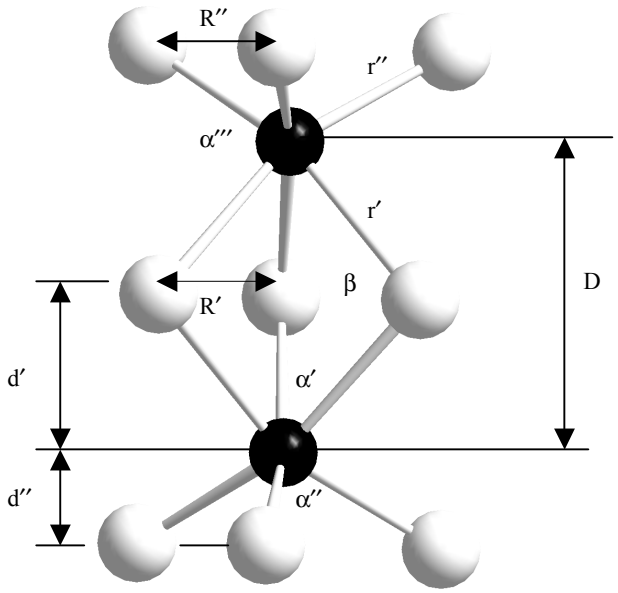

Fig. 3.2.b: Notation of distances and angles in the $[Sc_2O_9]^{12-}$ double octahedra after *Cotton* and *Ucko* (1972)

The dimers are linked into a three-dimensional framework by means of selenate(IV) groups, which share their three O atoms with three separate dimers units exactly as the M_2O_9 units and the phosphite groups in $Al_2(HPO_3)_3$ and $Ga_2(HPO_3)_3$ (fig. 3.2.c and fig. 3.2.d). This occurs such as to produce columns of alternating dimmer-selenate(IV) linkages that are joined to form hexagonal channels (of approximate dimensions 447.4 pm (6×), 402.5 pm (6×) and 601.8 pm (3×) measured atom-to-atom) parallel to the (001) plane (fig. 3.2.c). These tunnels are probably associated with the stereochemically active lone pairs on the selenium(IV) and do not represent space accessible by other chemical species as the ones in $Al_2(HPO_3)_3$ and $Ga_2(HPO_3)_3$ which were lined by the phosphite protons. In this compound the $[SeO_3]^{2-}$ groups adopts their characteristic pyramidal coordination (d(Se–O) = 166 – 170 pm), with the Se^{4+} *lone-pair* electrons presumably occupying the fourth tetrahedral vertex. The O–Se–O bond angles show a few distortions (values of 100° for the O2–Se–O1 angle (2×) versus 103° for the O2–Se–O2 one) but lie well within the range observed for the other anhydrous rare-earth(III) oxoselenates(IV) $M_2[SeO_3]_3$ (M = La, Nd, Er) [16 – 19] and their anionic derivatives such as $M_3F[SeO_3]_4$ (M = Nd, Sm, Gd, Dy) [34], MCl]SeO_3] (M = Nd, Ho, Er) [36]. Furthermore, four cations (Sc^{3+} terminal) complete the coordination sphere about the trigonal pyramidal $[Se(O1)(O2)_2]^{2-}$ anion (fig. 3.2.e) and the distance between the central cation of the pyramidal (Se^{4+}) and the plane containing O1, O2, O2 is about 74.7 pm. With its Sc_2O_9–selenate(IV)–Sc_2O_9 linking unit, the structure of $Sc_2[SeO_3]_3$ is closely related to $Al_2(HPO_3)_3$ and $Ga_2(HPO_3)_3$, the differences among them being accounted for by the presence of the proton within channels for the latter and by the lone pair electron replacing the phosphite proton in the $[SeO_3]^{2-}$ groups. Similar influence of the lone-pair effect has been observed for $M_2[SeO_3]_3$ (M = La, Nd, Er) [16 – 19] and $M_3F[SeO_3]_4$ (M = Nd, Sm, Gd, Dy) [34] where rectangular, respectively hexagonal, channels incorporating free electrons of the selenium(IV) are exhibited. If one regards the complex $[SeO_3]^{2-}$ anions as dianionic spheres (Z^{2-}), the crystal structure of $Sc_2[SeO_3]_3$ (≡ Sc_2Z_3) represents a cation-deficient NiAs-type (hexagonal, $P6_3/mmc$) [81] arrangement with 1/3 of the cations missing in an ordered fashion (see fig. 3.2.f). Unlike for the pair $Sc_2[SO_4]_3$ [82] / Lu_2S_3 [83] there is *no* basic corundum-type (α-Al_2O_3: trigonal, $R\bar{3}c$) [84] structure present, however, since the cation vacancies do not show a R-centred distribution over a trigonal unit cell and Z^{2-} is not coordinated tetrahedrally by the M^{3+} cations. For the present structure, the Sc_2Z_3 organization offers an octahedral coordination of Z^{2-} for Sc^{3+} (d(Sc···Se) = 350 pm (3×) and 356 pm (3×), CN = 6), but an off-plane trapezium-shaped one of Sc^{3+} for Z^{2-} (d(Se···Sc) = 350 pm (2×) and 356 pm (2×), CN

= 4) with a distance of Z^{2-} from the center of gravity for the plane of the four Sc^{3+} cations of 176 pm instead. If another Sc^{3+} cation would show up in the origin of the unit cell (*2b*: 0, 0, 0 and 0, 0, ½) at a distance of 301 pm (6×) apart from Z^{2-} (≡ Se), an almost perfect NiAs-type structure would result with octahedrally coordinated cations and trigonal prismatically coordinated anions (see fig. 3.2.f).

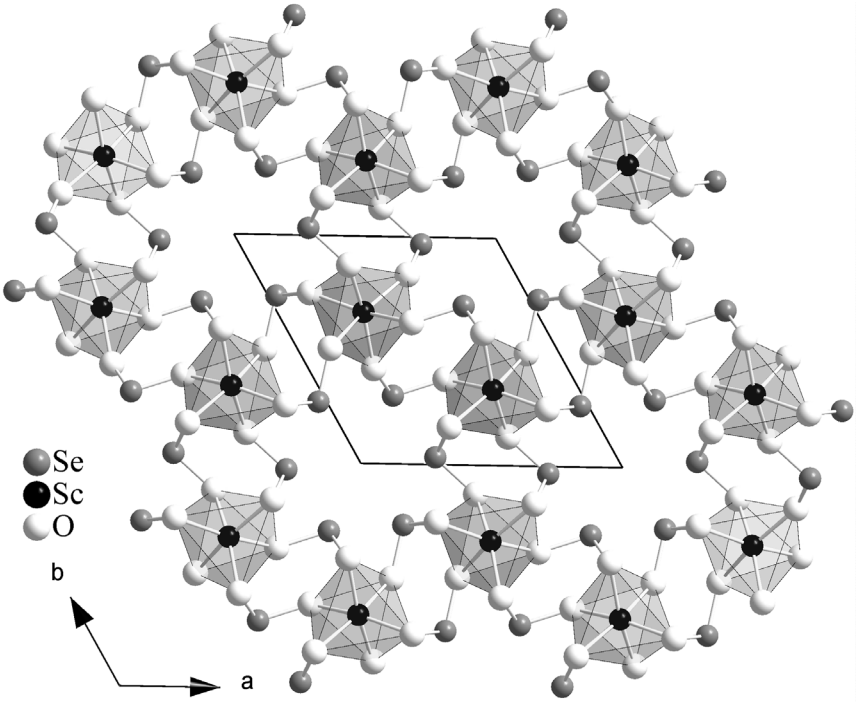

Fig. 3.2.c: The crystal structure of $Sc_2[SeO_3]_3$ emphasizing its hexagonal empty channel and the connectivity of the $[Sc_2O_9]$ dimer for the three dimensional framework

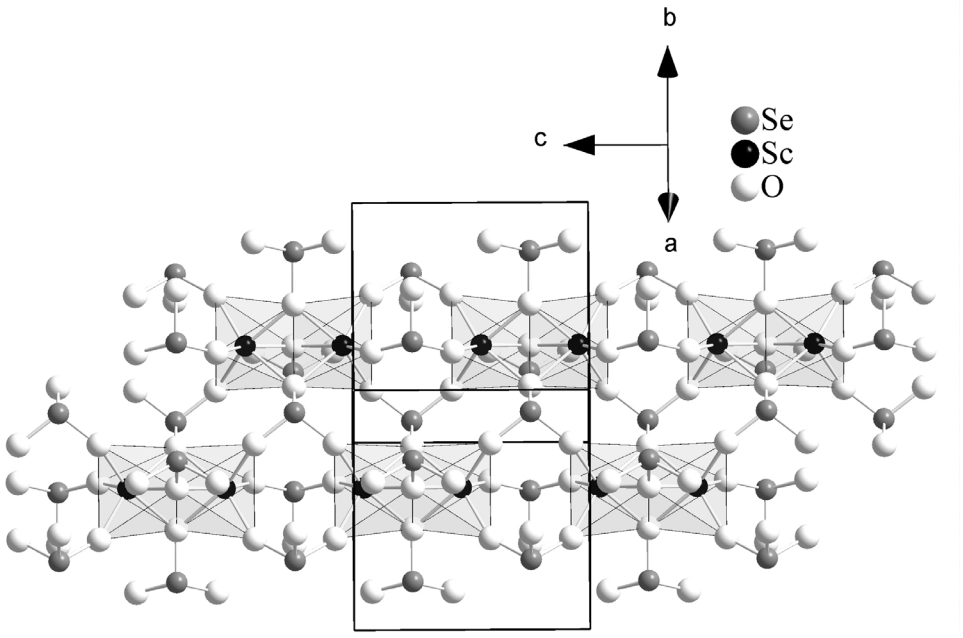

Fig. 3.2.d: Connectivity of the $[Sc_2O_9]$ dimer viewed along the [001] direction

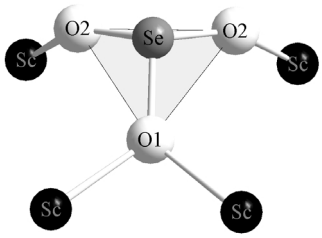

Fig. 3.2.e: Coordination sphere of four terminal Sc^{3+} cations about the trigonal pyramidal $[Se(O1)(O2)_2]^{2-}$ anion

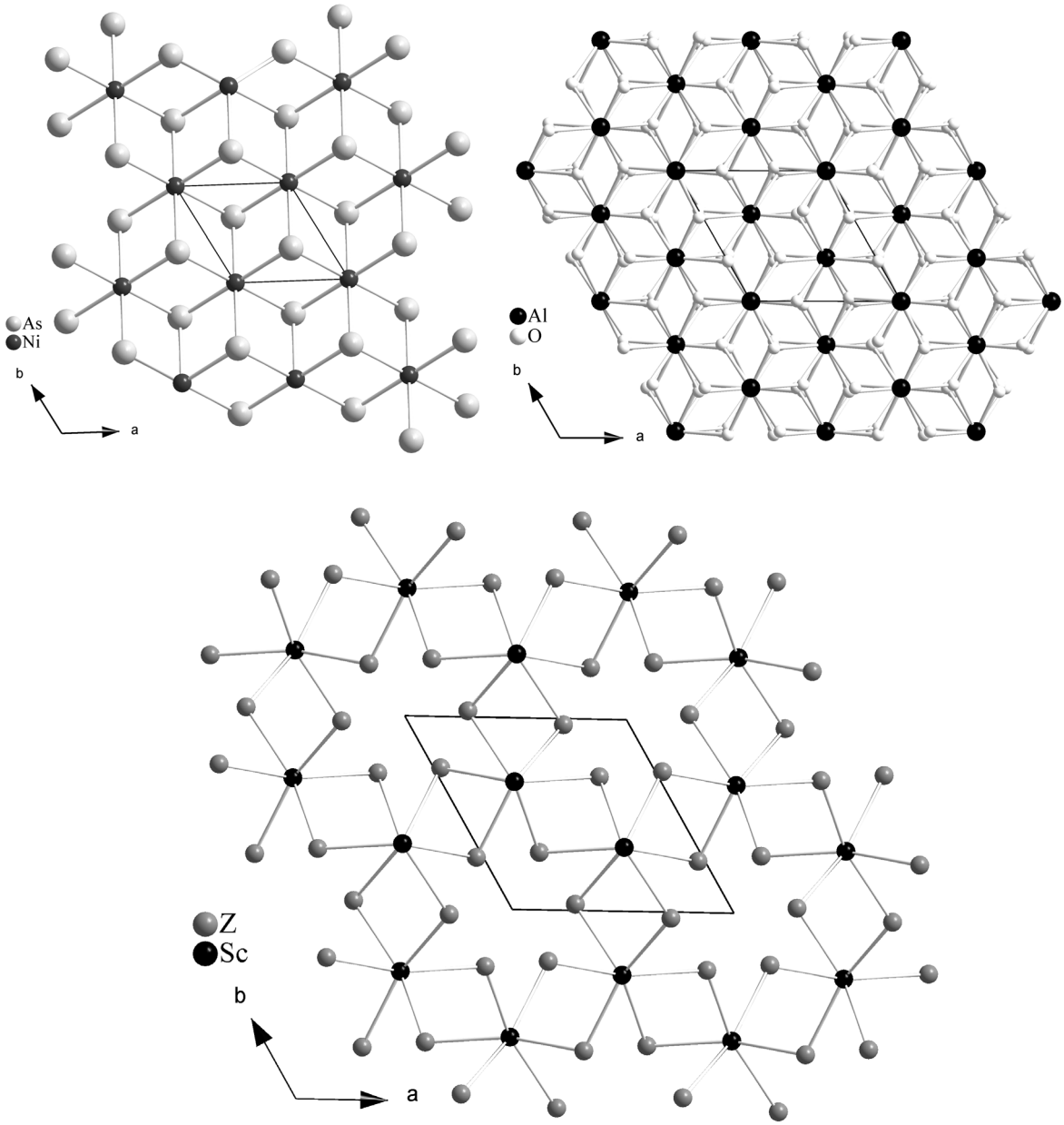

Fig. 3.2.f: Comparison of the crystal structure of NiAs (*above left*) and α-Al_2O_3 (*above right*) with the one of $Sc_2[SeO_3]_3$ represented only in its Sc_2Z_3 form (*below*)

3.2.1 Structural data for the hexagonal $Sc_2[SeO_3]_3$

Table 3.2.1.a: Crystallographic data for $Sc_2[SeO_3]_3$ and their determination

Formula		$Sc_2[SeO_3]_3$
Crystal system and space group		hexagonal, $P6_3/m$ (No. 176)
Formula unit per unit cell (Z)		2
Unit cell parameters:	a =	814.28(5) pm
	c =	764.56(4) pm
	c/a =	0.939
Calculated density (D_x / g · cm^3)		3.561
Molar volume (V_m / cm^3 · mol^{-1})		132.213
Diffractometer, radiation		κ-CCD (Fa. Nonius); Mo-K_α: λ = 71.07 pm
$2\theta_{max.}$		54.9
Index range	$\pm h_{max}$ / $\pm k_{max}$ / $\pm l_{max}$ =	10 / 10 / 9
F(000)		432.0
Absorption coefficient (μ)		14.00 mm^{-1}
Absorption correction		Numerical, after crystal shape optimization with the program X-SHAPE [53]
Other data corrections		background, polarization, *Lorentz* factors
Collected reflections		5113
Unique reflections		364
R_{int} / R_σ		0.062 / 0.025
Reflections with $\|F_o\| \geq 4\sigma\|F_o\|$		339
Structure solution and refinement		Program system SHELX-97 [58]
Scattering factors		International Tables, Vol. C [85]
R_1 / R_1 with $\|F_o\| \geq 4\sigma\|F_o\|$		0.034 / 0.028
wR_2 / Goodness of fit (GooF)		0.059 / 1.15
Extinction (g·10^{4-})		74(14)
Residual electron density (ρ / e$^-$ · 10^6 pm)		max. 0.70 min. –0.52

Table 3.2.1.b: Atomic coordinates for $Sc_2[SeO_3]_3$

Atom	Wyckoff Position	x / a	y / b	z / c
Sc	4f	1/3	2/3	0.0440(2)
Se	6h	0.30016(8)	0.03220(8)	1/4
O1	6h	0.1272(6)	0.5040(6)	1/4
O2	12i	0.4185(4)	0.1664(4)	0.796(4)

Table 3.2.1.c: Anisotropic thermal displacement parameters[b)] (U_{ij}/pm^2) for $Sc_2[SeO_3]_3$

Atom	U_{11}	U_{22}	U_{33}	U_{23}	U_{13}	U_{12}
Sc	211(5)	211(5)	127(6)	0	$= U_{23}$	106(2)
Se	185(3)	218(4)	177(3)	0	$= U_{23}$	96(3)
O1	257(22)	216(20)	119(18)	0	$= U_{23}$	114(18)
O2	301(16)	291(16)	259(15)	98(13)	76(13)	152(14)

[b)] defined as temperature factor according to: $\exp[-2\pi^2(a^{*2}h^2U_{11} + b^{*2}k^2U_{22} + c^{*2}l^2U_{33} + 2b^*c^*klU_{23} + 2a^*c^*hlU_{13} + 2a^*b^*hkU_{12})]$

Table 3.2.1.d: Selected internuclear distances (d/pm) and angles (∢/deg) in $Sc_2[SeO_3]_3$

Sc – $(O2)_t$	(r″)	201.9 (3×)	O2 – Se – O1		100.9 (2×)
– $(O1)_{br}$	(r′)	219.7 (3×)	O2 – Se – O2		103.1 (1×)
Se – O2		166.3 (2×)	$(O1)_{br}$ – Sc – $(O1)_{br}$	(α′)	74.2 (3×)
– O1		169.8 (1×)	$(O2)_t$ – Sc – $(O2)_t$	(α″)	99.9 (3×)
			$(O1)_{br}$ – Sc – $(O2)_t$	(α‴)	87.9 (3×)
$(O1)_{br}$ – $(O1)_{br}$	(R′)	264.8 (3×)	Sc – $(O1)_{br}$ – Sc	(β)	91.7 (3×)
$(O2)_t$ – $(O2)_t$	(R″)	308.8 (3×)			

$(O1)_{br}$ denotes bridging O1 atoms and $(O2)_t$ denotes terminal O2 atoms in the $[Sc_2O_9]^{12-}$ double octahedra only.

Table 3.2.1.e: Motifs of mutual adjunction in $Sc_2[SeO_3]_3$

	O1	O2	CN
Sc	3 / 2	3 / 1	6
Se	1 / 1	2 / 1	3
CN	3	2	

3.3 Structure description of the orthorhombic $Ce_2[SeO_3]_3$

$Ce_2[SeO_3]_3$ is isostructural to $La_2[SeO_3]_3$ described independently by *Harrison* [17] and *Wickleder* [16]. It crystallizes orthorhombically (space group: Pnma) thus confirming the result obtained by *Krügermann* from X-ray powder diffractometry [19]. Its crystal structure contains a single crystallographically Ce^{3+} cation only but two different anions $[SeO_3]^{2-}$ groups. The cerium cation adopts an irregular tenfold coordination (fig. 3.3.a) with (Ce–O) distances ranging from 244 to 280 pm. The two distinct selenium(IV) species are coordinated by three oxygen atoms each in a one-sided pyramidal configuration, a characteristic consequent of the stereochemical non-binding activity of lone-pair electrons at the selenium(IV) central atoms. Individual and mean Se–O bond distances (d(Se–O) = 167 – 171 pm) and O–Se–O angles (∢(O–Se–O) = 94 – 104°) are in accordance with the geometries found in many other oxoselenate(IV) compounds or with averages values cited in the literature [1–16]. The partially strong bond angles deviations within the $[SeO_3]^{2-}$ groups (94 – 104°) from ideal tetrahedra angles can not probably be attributed to the "lone-pair" effect alone, but also to the high coordination of both types of $[SeO_3]^{2-}$ anions. In fact four and five Ce^{3+} cations (terminal and edge-spanning) constitute the coordination around the $[(Se1)O_3]^{2-}$ and $[(Se2)O_3]^{2-}$ groups, respectively (fig. 3.3.b).

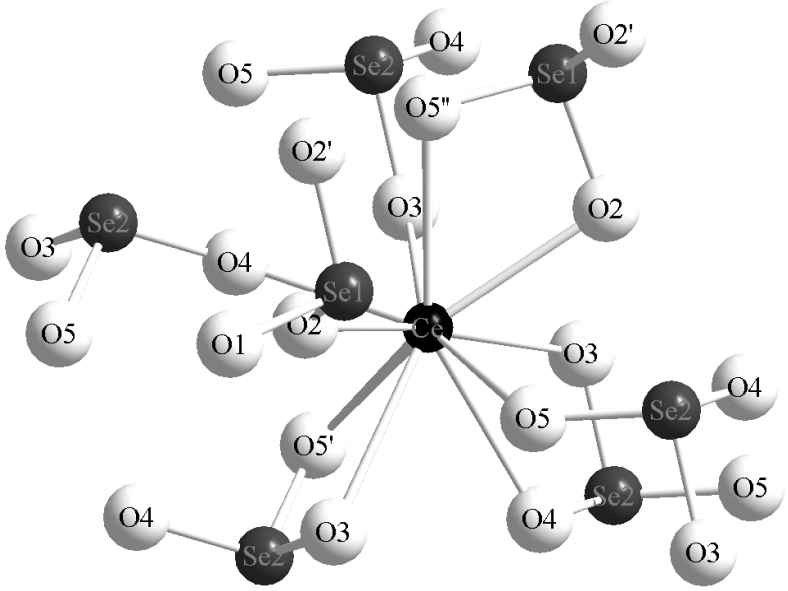

Fig. 3.3.a: Ce^{3+} cation in $Ce_2[SeO_3]_3$ coordinated by seven $[SeO_3]^{2-}$ anions, four as mono- and three are bidentate (chelating) ligands

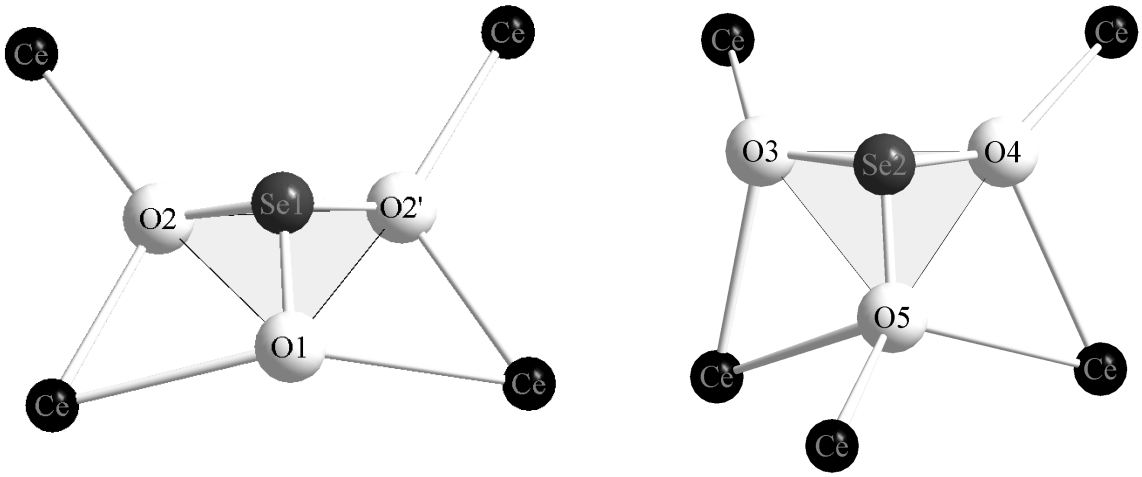

Fig. 3.3.b: Coordination of Ce^{3+} about the $[(Se1)O_3]^{2-}$ (*left*) and $[(Se2)O_3]^{2-}$ (*right*) units in $Ce_2[SeO_3]_3$

The connectivity among $[CeO_{10}]$ polyhedra results in infinite sheets of face- (O5, O2 and O3) and edge-sharing (O3 and O4) units propagating normal to [001]. The $[(Se1)O_3]^{2-}$ group is closely related to these layers and the $[(Se2)O_3]^{2-}$ group serves to fuse adjacent layers into a three-dimensional network. Further linkage between the metal-oxygen double sheets is achieved by a shared corner, (O1) via a Ce–(O1)(Se1)–Ce bond. Consequently, particularly protracted Ce–O1 contacts (280 pm) are observed for all $[CeO_{10}]$ polyhedra. Seven $[SeO_3]^{2-}$ anions (two $[(Se1)O_3]^{2-}$ and five $[(Se2)O_3]^{2-}$ groups) are grafted onto the $[CeO_{10}]$ polyhedra via either common edges or vertices. In chelating and bridging between Ce^{3+} centers they create the fundamental framework structure shown in Figure 3.3.c. This kind of connectivity between $[CeO_{10}]$ polyhedra and the $[SeO_3]^{2-}$ groups complies well with similar ones observed for tenfold coordinated M^{3+} cations (*e.g.* M = La, Nd) in the crystal structures of $La_2[SeO_3]_3$ [16, 17], $Nd[HSeO_3][SeO_4] \cdot H_2O$ [6] and $La[HSeO_3][SeO_3]$ [9]. By viewing $Ce_2[SeO_3]_3$ structure down [010] (fig. 3.3.c), it appears to be infinite tunnels of six-membered rings with approximate diameters of 412 pm (2×), 431 pm (2×) and 566 pm (2×) measured atom-to-atom (Se···Se) space width enough to incorporate the free electron pairs of the Se^{4+} cations. The corresponding ones in the prototypical $La_2[SeO_3]_3$-type structure are approximately 360 × 550 pm [17, 19].

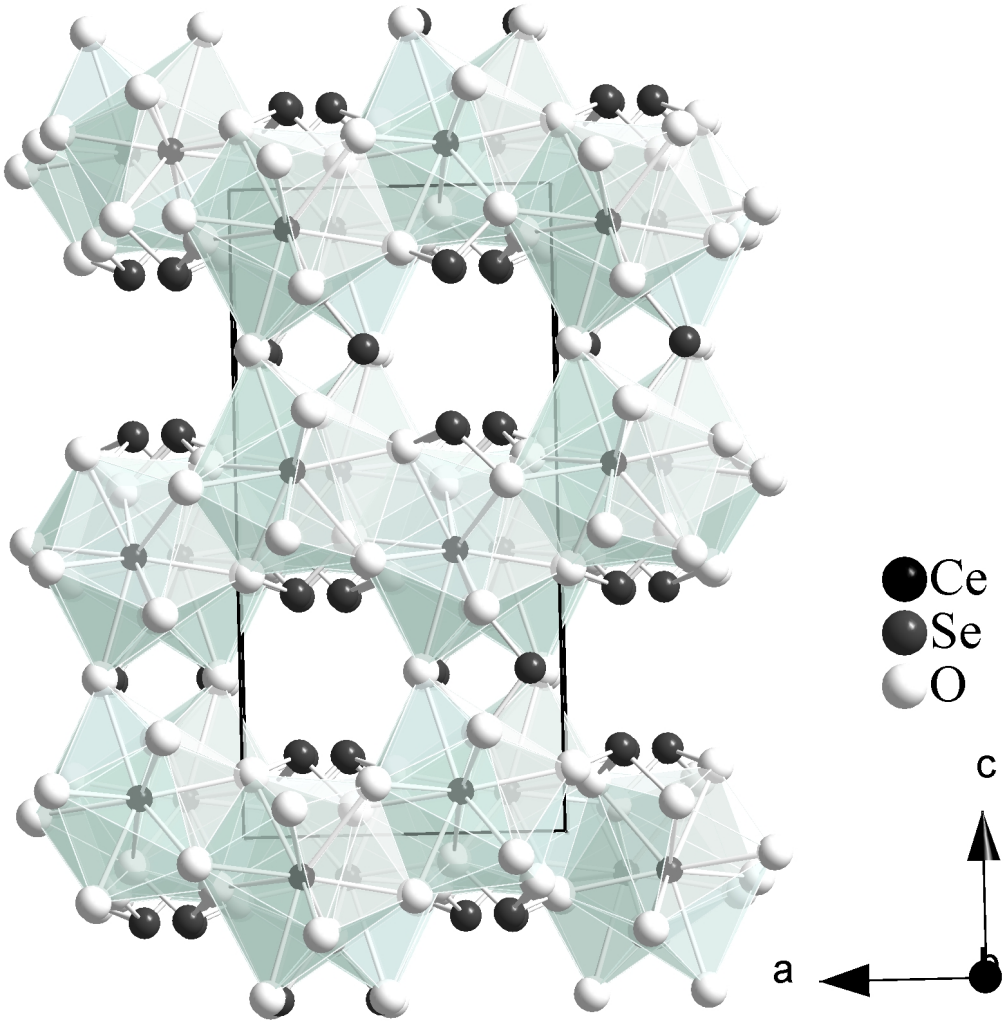

Fig. 3.3.c: Packing diagram of $Ce_2[SeO_3]_3$ viewed down [010] showing a double net-shaped sheet of condensed $[CeO_{10}]$ polyhedra with adjacent $[SeO_3]^{2-}$ groups

3.3.1 Structural dada for the orthorhombic $Ce_2[SeO_3]_3$

Table 3.3.1.a: Crystallographic data for $Ce_2[SeO_3]_3$ and their determination

Formula		$Ce_2[SeO_3]_3$
Crystal system and space group		orthorhombic, Pnma (No. 62)
Formula unit per unit cell (Z)		4
Unit cell parameters:	a =	839.23(5) pm
	b =	1421.12(9) pm
	c =	704.58(4) pm
Calculated density (D_x / g · cm^3)		5.226
Molar volume (V_m / cm^3 · mol^{-1})		126.530
Diffractometer, radiation		κ-CCD (Fa. Nonius); Mo-K_α: λ = 71.07 pm
$2\theta_{max.}$		55.1
Index range	$\pm h_{max}$ / $\pm k_{max}$ / $\pm l_{max}$ =	10 / 18 / 9
F(000)		1160.0
Absorption coefficient (μ)		23.72 mm^{-1}
Absorption correction		Numerical, after crystal shape optimization with the program X-SHAPE [53]
Other data corrections		background, polarization, *Lorentz* factors
Collected reflections		10206
Unique reflections		1009
R_{int} / R_σ		0.065 / 0.031
Reflections with $\|F_o\| \geq 4\sigma\|F_o\|$		900
Structure solution and refinement		Program system SHELX-97 [58]
Scattering factors		International Tables, Vol. C [85]
R_1 / R_1 with $\|F_o\| \geq 4\sigma\|F_o\|$		0.029 / 0.022
wR_2 / Goodness of fit (GooF)		0.037 / 1.11
Extinction (g)		0.00490(13)
Residual electron density		max. 0.80
(ρ / e$^-$ · 10^6 pm)		min. –0.78

Table 3.3.1.b: Atomic coordinates for $Ce_2[SeO_3]_3$

Atoms	Wyckoff Position	x / a	y / b	z / c
Ce	8d	0.19803(3)	0.43645(2)	0.17983(4)
Se1	4c	0.45545(7)	1/4	0.40755(9)
Se2	8d	0.04737(5)	0.12535(3)	0.67953(7)
O1	4c	0.1536(5)	1/4	0.0652(7)
O2	8d	0.4424(4)	0.1549(2)	0.2616(5)
O3	8d	0.3813(4)	0.0775(2)	0.9107(5)
O4	8d	0.1979(4)	0.0966(2)	0.5316(5)
O5	8d	0.0725(4)	0.0407(2)	0.8502(5)

Table 3.3.1.c: Anisotropic thermal displacement parameters[b)] (U_{ij}/pm^2) for $Ce_2[SeO_3]_3$

Atoms	U_{11}	U_{22}	U_{33}	U_{23}	U_{13}	U_{12}
Ce	124(1)	162(1)	132(1)	7(1)	2(1)	2(1)
Se1	145(3)	143(3)	164(3)	0	9(3)	0
Se2	147(2)	130(2)	142(2)	–1(2)	6(2)	–4(2)
O1	150(23)	276(24)	286(30)	0	53(22)	0
O2	183(17)	174(15)	210(18)	–61(14)	–4(14)	5(14)
O3	155(18)	356(19)	168(19)	–45(15)	47(14)	–59(14)
O4	126(15)	298(16)	180(18)	8(15)	42(15)	–22(13)
O5	140(15)	230(16)	191(19)	92(14)	19(13)	–2(13)

[b)] defined as temperature factor according to: $\exp[-2\pi^2(a^{*2}h^2U_{11} + b^{*2}k^2U_{22} + c^{*2}l^2U_{33} + 2b^*c^*klU_{23} + 2a^*c^*hlU_{13} + 2a^*b^*hkU_{12})]$

Table 3.3.1.d: Selected internuclear distances (d/pm) and angles (∢/deg) in $Ce_2[SeO_3]_3$

	d / pm		d / pm
Ce – O3	244.9	Se1 – O1	167.4
– O2	249.5	– O2	170.1 (2×)
– O4	252.3		
– O2′	254.2		
– O5	257.1	Se2 – O3	167.6
– O4′	265.2	– O4	169.0
– O3′	266.6	– O5	171.4
– O5′	271.0		
– O5″	271.9		
– O1	279.5		
	∢ / grd		∢ / grd
O1 – Se1 – O2	97.7 (2×)	O3 – Se2 – O5	94.8
O2 – Se1 – O2′	105.1	O4 – Se2 – O5	99.9
		O3 – Se2 – O4	106.9

Table 3.3.1.e: Motifs of mutual adjunction in $Ce_2[SeO_3]_3$

	O1	O2	O3	O4	O5	CN
Ce	1 / 0	2 / 2	2 / 1	2 / 1	3 / 1	10
Se1	1 / 1	2 / 1	0 / 0	0 / 0	0 / 0	3
Se2	0 / 0	0 / 0	1 / 1	1 / 1	1 / 1	3
CN	2	4	3	3	4	

3.4 Structure description of the monoclinic $Pr_2[SeO_3]_3$

$Pr_2[SeO_3]_3$ crystallizes isostructural to $Nd_2[SeO_3]_3$ [18] in the monoclinic space group $P2_1/n$ with twelve formula units per unit cell. The six crystallographically distinct Pr^{3+} cations are nine- and tenfold coordinated to oxygen atoms with Pr–O distances ranging from 231 to 313 pm (see table 3.4.1.d). The coordination polyhedra about Pr1 and Pr4 can be described as distorted capped square antiprisms (CN = 9) while Pr2 and Pr3 reside in an irregular capped square prismatic vicinity (CN = 9). The $[(Pr5)O_{10}]$ polyhedra exhibit distorted bicapped square antiprismatic (CN = 10) shape and the $[(Pr6)O_{10}]$ shows a trigonal prism capped by four oxygen occupying almost the equatorial plane of the coordination figure (CN = 10). Five $[SeO_3]^{2-}$ anions vertex-sharing and two as edge-spanning ones are grafted onto each polyhedron as mono- or bidentate ligands (fig. 3.4.a). If one takes into account Pr···Se contacts up to 400 pm and regards the complex $[SeO_3]^{2-}$ anions only as dianionic spheres (Z^{2-}), it appears that all Pr^{3+} cations are sevenfold coordinated by Z^{2-} anions in the shape of distorted capped trigonal prisms. From this point of view, these $[PrZ_7]$ polyhedra resemble the $[(M1)Se_7]$ ones in the U-type crystal structure of M_2Se_3 (M = Sm, Tb) [86]. However, the Pr_2Z_3 organization offers no closer relationship with this latter.

The structure contains nine discrete pyramidal oxoselenate(IV) units $[SeO_3]^{2-}$ which apart from $[(Se2)O_3]^{2-}$ adopt both bridging and chelating/bridging binding modes, and serve to link four or five praseodymium moieties and thereby create the three-dimensional network observed in this compound. Their coordination spheres can be written as follows: three Pr^{3+} terminal and two Pr^{3+} edge-spanning each about $[(Se4)O_3]^{2-}$, $[(Se5)O_3]^{2-}$, $[(Se7)O_3]^{2-}$ and $[(Se8)O_3]^{2-}$; four Pr^{3+} terminal against one Pr^{3+} edge-spanning for $[(Se3)O_3]^{2-}$ and $[(Se6)O_3]^{2-}$ groups whereas two Pr^{3+} terminal and two Pr^{3+} edge-spanning coordinate the $[(Se1)O_3]^{2-}$ and $[(Se9)O_3]^{2-}$ groups. Lastly four Pr^{3+} all terminal are present around the $[(Se2)O_3]^{2-}$ anion (Fig. 2.4.b). There are few distortions in the $[SeO_3E]^{2-}$ ψ^1-tetrahedra as they include d(Se–O) = 164 – 172 pm, $\sphericalangle$(O–Se–O) = 94 – 107°, displacement of the selenium atoms from their O–O–O plane = 74 – 82) (*E* = lone pair at Se) but these are well in the range observed for other oxoselenate(IV) compounds (see 3.3). When the structure of $Pr_2[SeO_3]_3$ is viewed down [101] direction, it has strong aspects of a two-dimensional double layer-type structure formed by $[PrO_9]$ and $[PrO_{10}]$ polyhedra. Within these layers, the polyhedra are linked either via edges or faces and two adjacent layers are joined by O1–O25 edges of the $[(Pr5)O_{10}]$ and $[(Pr6)O_{10}]$

polyhedra. The resulting framework is rectangular channels along [101] sandwiched between different sheets (fig. 3.4.c). The smallest metal-metal contacts within channels are very close to 435 pm for Pr···Pr and to 365 pm for Se···Se.

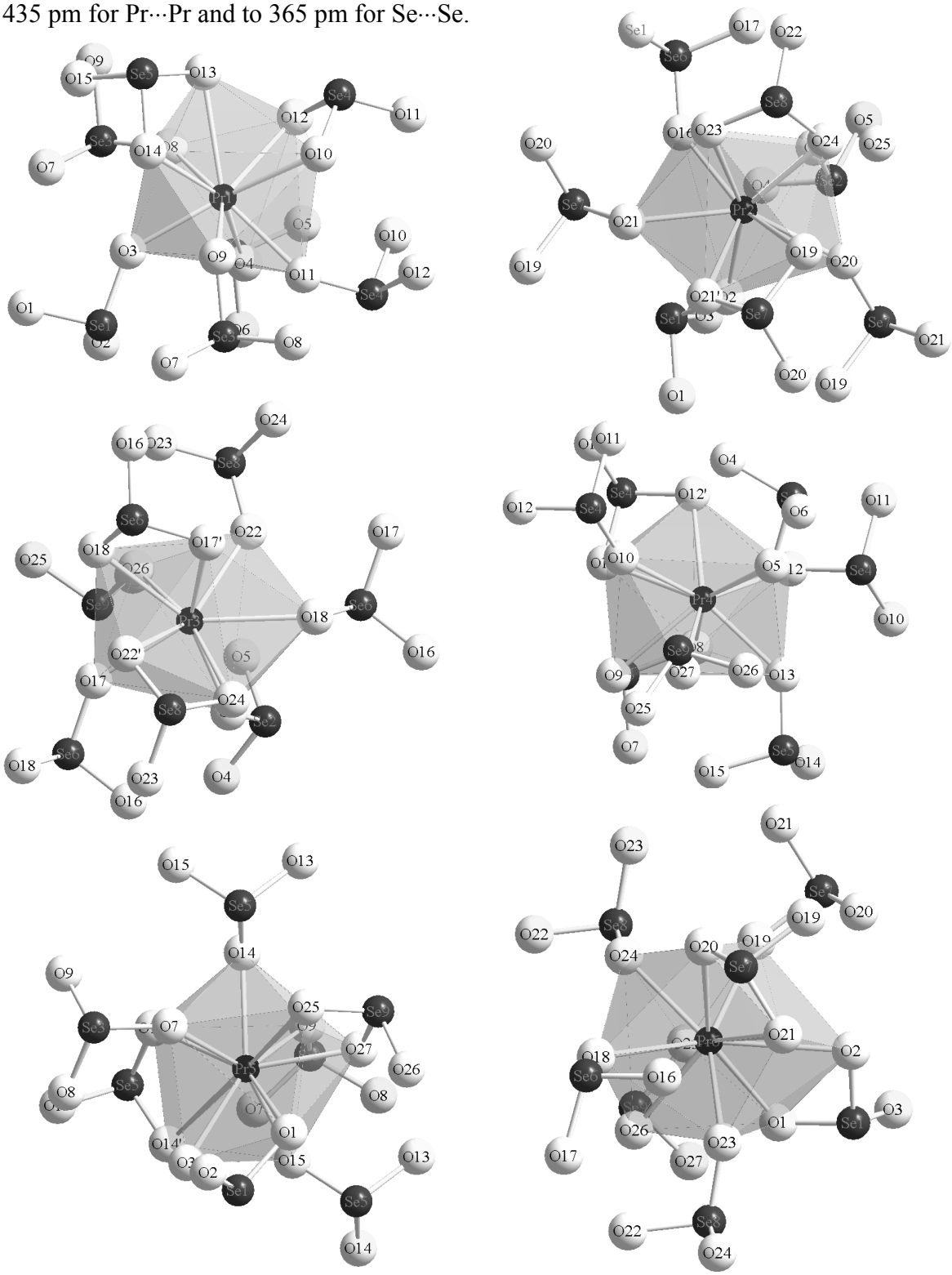

Fig. 3.4.a: Coordination about the six independent Pr^{3+} cations in $Pr_2[SeO_3]_3$ showing $[SeO_3]^{2-}$ anions as mono- and bidentate (chelating) ligands

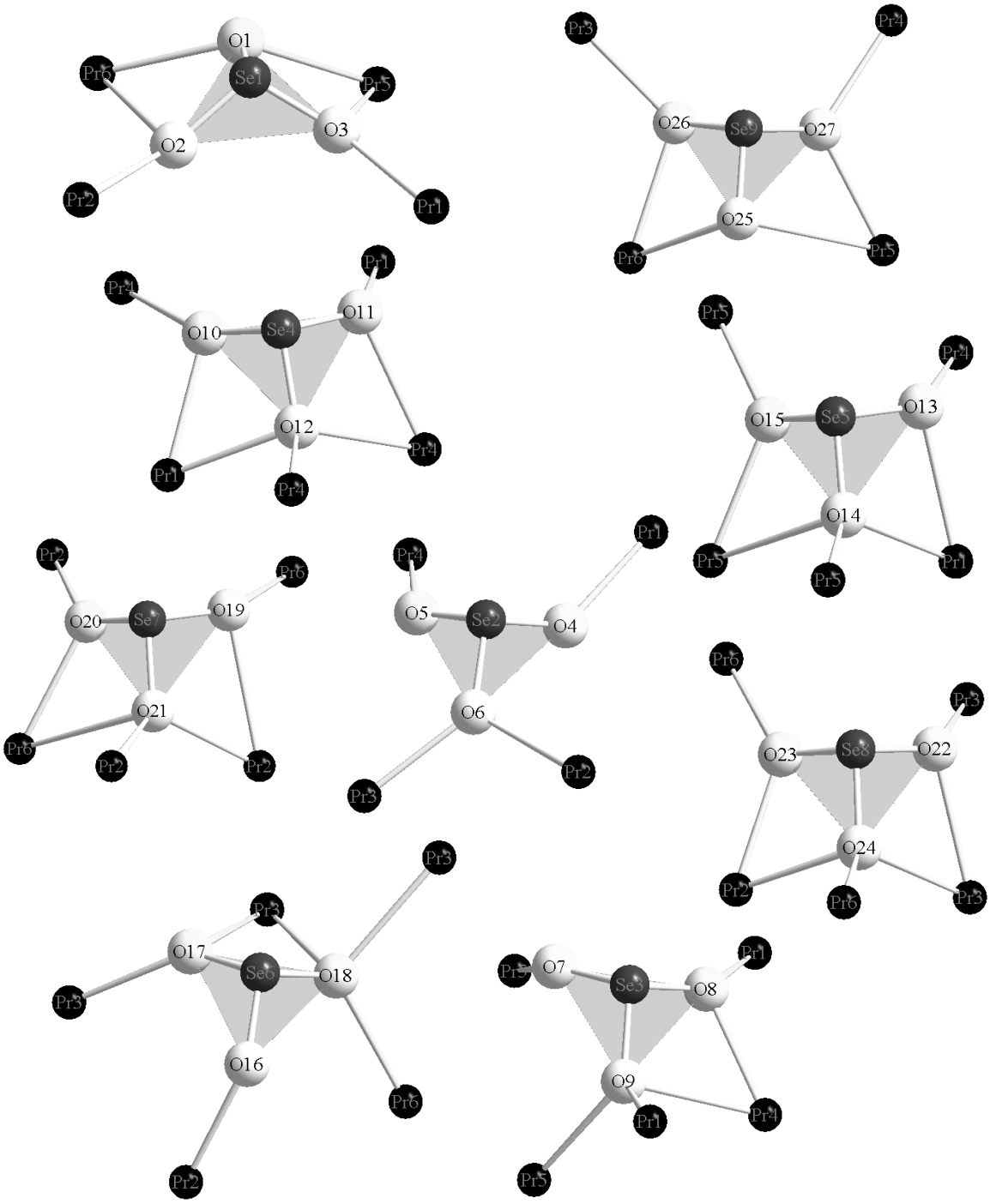

Fig. 3.4.b: Cationic coordination of Pr^{3+} about the nine independent $[SeO_3]^{2-}$ anions in $Pr_2[SeO_3]_3$

The stabilization of the structure is further ensured *via* $[(Se1)O_3]^{2-}$, $[(Se2)O_3]^{2-}$ and $[(Se9)O_3]^{2-}$ groups which are located within the layers and bonded to them through Pr–O–Se–O–Pr contacts. The six residual $[SeO_3]^{2-}$ groups are included within layers and positioned such that different channels are lined by the free electron pair at the Se^{4+} cations (fig. 3.4.c).

The monoclinic crystal structure of the present compound is therefore related in many respects to the $Bi_2[SeO_3]_3$-type structure (monoclinic, $P2_1/n$ (no. 14), a = 1349.1(1) pm, b = 467.5(1) pm, c = 1496.1(1) pm, β = 115.64(4)°), where $[(Bi1)O_6]$ and $[(Bi2)O_6]$ polyhedra are corner-linked leading to $[Bi_2O_9]^{12-}$ layers including both $[(Se1)O_3]^{2-}$ and $[(Se3)O_3]^{2-}$ groups and bonded each other by $[(Se2)O_3]^{2-}$ groups via Bi1–O4–Se2–O3–Bi2 contacts [71]. But there are no O···O contacts between two adjacent $[Bi_2O_9]^{12-}$ layers as observed in $Pr_2[SeO_3]_3$. This organization pattern also complies rather well with that one exhibited in the orthorhombic $La_2[SeO_3]_3$-type structure (paragraph 3.3 for $Ce_2[SeO_3]_3$ and [16, 17]). In fact, the projections in figure 3.3.c ($Ce_2[SeO_3]_3$) and figure 3.4.c ($Pr_2[SeO_3]_3$) reveal an almost identical stacking mode of the type ···A B A B ·· (hexagonal closest packet) for the metal-oxygen double layers and therefore clarifies the structure analogy of both compounds impressively.

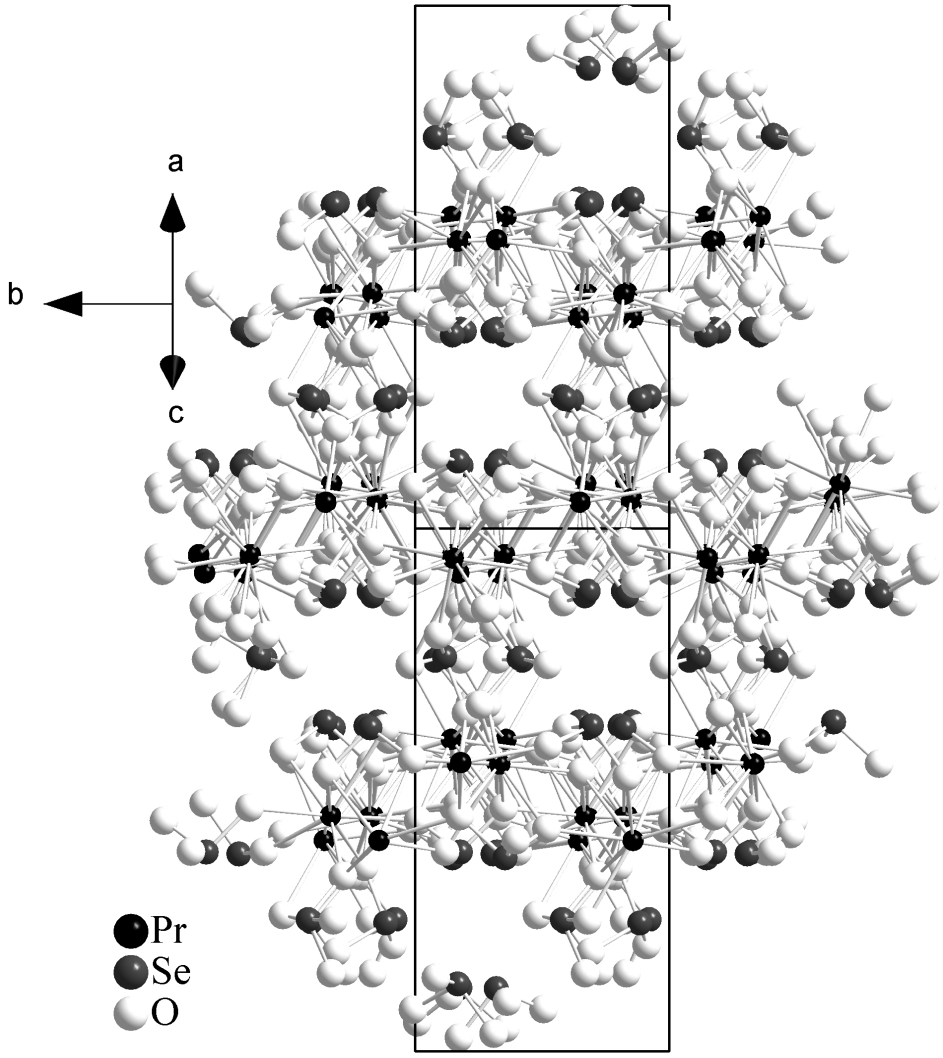

Fig. 3.4.c: Extended view of the $Pr_2[SeO_3]_3$ structure illustrating the connectivity among $[PrO_9]$ and $[PrO_{10}]$ polyhedra via $[SeO_3]^{2-}$ anions

3.4.1 Structural data for the monoclinic $Pr_2[SeO_3]_3$

Table 3.4.1.a: Crystallographic data for $Pr_2[SeO_3]_3$ and their determination

Formula		$Pr_2[SeO_3]_3$
Crystal system and space group		monoclinic, $P2_1/n$ (No. 14)
Formula unit per unit cell (Z)		12
Unit cell parameters:	a =	1683.76(9) pm
	b =	703.38(4) pm
	c =	2167.19(12) pm
	β =	102.063(7) °
Calculated density (D_x / g · cm^3)		5.246
Molar volume (V_m / cm^3 · mol^{-1})		123.338
Diffractometer, radiation		κ-CCD (Fa. Nonius); Mo-K_α: λ = 71.07 pm
$2\theta_{max.}$		55.0
Index range	$\pm h_{max}$ / $\pm k_{max}$ / $\pm l_{max}$ =	21 / 9 / 28
F(000)		3504.0
Absorption coefficient (μ)		24.51 mm^{-1}
Absorption correction		Numerical, after crystal shape optimization with the program X-SHAPE [53]
Other data corrections		background, polarization, *Lorentz* factors
Collected reflections		45269
Unique reflections		5763
R_{int} / R_σ		0.097 / 0.049
Reflections with $\|F_o\| \geq 4\sigma\|F_o\|$		4911
Structure solution and refinement		Program system SHELX-97 [58]
Scattering factors		International Tables, Vol. C [85]
R_1 / R_1 with $\|F_o\| \geq 4\sigma\|F_o\|$		0.067 / 0.055
wR_2 / Goodness of fit (GooF)		0.127 / 1.127
Extinction (g)		0.00007(2)
Residual electron density		max. 4.09
(ρ / e$^-$ · 10^6 pm)		min. –2.83

Table 3.4.1.b: Atomic coordinates for $Pr_2[SeO_3]_3$

Atoms	Wyckoff Position	x / a	y / b	z / c
Pr1	4e	0.13728(5)	0.3518(1)	0.08721(4)
Pr2	4e	0.39858(5)	0.3327(1)	0.94789(4)
Pr3	4e	0.23500(5)	0.1795(1)	0.78715(4)
Pr4	4e	0.46775(5)	0.3506(1)	0.41083(4)
Pr5	4e	0.32283(5)	0.1718(1)	0.23801(4)
Pr6	4e	0.03980(5)	0.3577(1)	0.63658(4)
Se1	4e	0.36553(8)	0.4208(2)	0.11335(7)
Se2	4e	0.19588(8)	0.1164(2)	0.95063(7)
Se3	4e	0.26668(8)	0.3324(2)	0.39588(7)
Se4	4e	0.43409(8)	0.1808(2)	0.55389(7)
Se5	4e	0.10901(8)	0.1762(2)	0.23065(7)
Se6	4e	0.26036(8)	0.1943(2)	0.63801(7)
Se7	4e	0.10292(8)	0.1322(2)	0.48431(7)
Se8	4e	0.43064(8)	0.3544(2)	0.80057(7)
Se9	4e	0.03857(8)	0.4089(2)	0.79066(7)
O1	4e	0.4262(6)	0.3208(16)	0.1757(5)
O2	4e	0.3904(7)	0.2857(17)	0.0558(6)
O3	4e	0.2772(6)	0.3305(16)	0.1276(5)
O4	4e	0.1812(7)	0.3103(16)	0.9914(6)
O5	4e	0.1046(6)	0.0907(16)	0.9014(6)
O6	4e	0.2535(6)	0.2010(15)	0.8999(5)
O7	4e	0.1970(6)	0.4204(15)	0.3376(5)
O8	4e	0.1626(6)	0.0089(14)	0.0832(5)
O9	4e	0.3252(6)	0.1898(14)	0.3582(5)
O10	4e	0.0037(6)	0.4950(14)	0.9227(5)
O11	4e	0.3854(6)	0.1394(14)	0.4782(5)
O12	4e	0.0066(6)	0.1712(14)	0.0331(5)
O13	4e	0.0532(6)	0.1351(15)	0.1576(5)
O14	4e	0.1637(6)	0.3551(14)	0.2081(6)
O15	4e	0.1839(6)	0.0105(15)	0.2398(6)
O16	4e	0.1967(6)	0.0954(14)	0.5776(5)

Table 3.4.1.b: continued

Atoms	Wyckoff Position	x / a	y / b	z / c
O17	4e	0.2804(6)	0.0233(14)	0.6956(5)
O18	4e	0.1983(6)	0.3334(14)	0.6730(5)
O19	4e	0.0356(7)	0.3867(16)	0.4189(5)
O20	4e	0.0981(7)	0.4891(15)	0.5394(5)
O21	4e	0.0431(7)	0.1520(15)	0.5096(6)
O22	4e	0.3441(6)	0.3970(15)	0.7480(5)
O23	4e	0.0659(6)	0.0170(14)	0.6402(5)
O24	4e	0.3894(6)	0.1737(14)	0.8383(5)
O25	4e	0.0129(7)	0.4786(16)	0.2739(5)
O26	4e	0.0909(6)	0.2543(15)	0.7536(5)
O27	4e	0.4605(6)	0.2255(15)	0.3067(5)

Table 3.4.1.c: Anisotropic thermal displacement parameters[b] (U_{ij}/pm^2) for $Pr_2[SeO_3]_3$

Atoms	U_{11}	U_{22}	U_{33}	U_{23}	U_{13}	U_{12}
Pr1	102(3)	102(3)	99(3)	4(3)	20(3)	9(3)
Pr2	149(4)	102(4)	103(4)	4(4)	21(3)	−13(3)
Pr3	105(3)	109(4)	109(4)	−4(3)	14(3)	0(3)
Pr4	113(3)	87(3)	102(3)	−3(3)	26(3)	3(3)
Pr5	161(4)	103(4)	98(3)	−1(3)	9(3)	−16(3)
Pr6	134(4)	108(4)	133(4)	27(3)	16(3)	−2(3)
Se1	130(6)	121(6)	148(7)	20(5)	74(5)	14(5)
Se2	130(6)	145(7)	148(7)	14(5)	85(5)	1(5)
Se3	96(6)	105(6)	110(6)	9(5)	35(5)	5(5)
Se4	104(6)	86(6)	113(6)	8(5)	42(5)	12(5)
Se5	98(6)	85(6)	99(6)	6(5)	42(5)	6(5)
Se6	109(6)	115(6)	103(6)	9(5)	34(5)	1(5)
Se7	94(6)	126(6)	110(6)	−6(5)	32(5)	22(5)
Se8	89(6)	110(6)	109(6)	−10(5)	40(5)	2(5)
Se9	113(6)	122(6)	149(7)	−20(5)	79(5)	−20(5)

Table 3.4.1.c: continued

Atoms	U_{11}	U_{22}	U_{33}	U_{23}	U_{13}	U_{12}
O1	74(45)	436(72)	201(56)	97(51)	7(40)	–9(45)
O2	398(75)	389(75)	235(66)	–131(57)	215(57)	–69(60)
O3	123(49)	394(68)	183(54)	–41(49)	57(41)	–15(46)
O4	466(83)	176(55)	210(59)	–60(46)	185(57)	33(53)
O5	92(49)	361(68)	396(72)	–159(56)	–45(47)	–112(46)
O6	78(43)	305(60)	182(52)	5(45)	63(38)	–18(40)
O7	202(52)	241(56)	140(50)	110(43)	36(42)	–25(43)
O8	172(48)	78(44)	186(51)	40(38)	24(40)	–4(37)
O9	176(50)	167(50)	132(48)	–5(39)	60(39)	–25(39)
O10	218(52)	84(45)	159(49)	–46(38)	10(41)	–17(38)
O11	167(48)	153(49)	172(50)	–18(40)	61(40)	–20(39)
O12	134(47)	105(46)	192(52)	–12(38)	14(39)	–0(36)
O13	238(54)	182(52)	124(48)	0(40)	12(41)	55(42)
O14	137(46)	139(47)	122(46)	61(38)	24(37)	–42(37)
O15	89(46)	188(53)	332(64)	–20(46)	26(42)	–1(39)
O16	274(55)	109(47)	107(46)	–46(37)	74(41)	–42(40)
O17	217(54)	70(41)	174(53)	62(37)	2(42)	57(37)
O18	133(46)	137(47)	119(46)	–42(37)	19(37)	0(37)
O19	246(56)	269(58)	119(49)	–15(43)	–15(42)	74(46)
O20	317(61)	115(49)	200(55)	29(42)	–21(47)	–12(44)
O21	213(56)	161(55)	456(76)	124(51)	55(52)	–80(43)
O22	106(45)	187(51)	155(49)	16(40)	–27(38)	12(38)
O23	174(49)	119(47)	143(48)	44(38)	14(39)	6(38)
O24	92(43)	169(49)	131(46)	33(38)	23(36)	20(36)
O25	389(67)	168(55)	222(57)	104(45)	100(49)	19(48)
O26	159(48)	208(52)	143(49)	–80(41)	105(39)	–5(40)
O27	161(49)	222(53)	136(49)	–5(41)	66(39)	48(41)

[b] defined as temperature factor according to: $\exp[-2\pi^2(a^{*2}h^2U_{11} + b^{*2}k^2U_{22} + c^{*2}l^2U_{33} + 2b^*c^*klU_{23} + 2a^*c^*hlU_{13} + 2a^*b^*hkU_{12})]$

Table 3.4.1.d: Selected internuclear distances (d/pm) and angles (∢/deg) in $Pr_2[SeO_3]_3$

	d / pm		d / pm		d / pm
Pr1 – O3	234.0	Pr2 – O2	239.4	Pr3 – O6	240.3
– O4	236.3	– O16	243.8	– O22	242.9
– O11	245.9	– O20	243.9	– O26	244.1
– O8	246.0	– O23	248.4	– O17	247.5
– O14	256.4	– O21	252.2	– O17′	252.4
– O10	257.6	– O21′	255.1	– O24	260.5
– O12	260.0	– O24	260.2	– O18	265.3
– O9	267.8	– O6	261.7	– O22	266.4
– O13	275.1	– O19	295.2	– O18′	275.0
Pr4 – O5	239.2	Pr5 – O7	239.0	Pr6 – O19	238.2
– O27	240.2	– O15	244.4	– O23	244.1
– O13	247.6	– O27	250.8	– O24	253.3
– O8	249.0	– O14	250.9	– O25	257.1
– O10	251.2	– O9	260.0	– O1	257.7
– O12	256.1	– O3	260.8	– O26	260.6
– O12′	259.8	– O15′	260.9	– O18	262.6
– O11	266.8	– O1	263.4	– O20	266.9
– O9	268.4	– O14	292.3	– O2	292.8
		– O25	*314.0*	*– O21*	312.2
Se1 – O1	167.0	Se2 – O4	167.5	Se3 – O7	165.5
– O2	169.0	– O5	168.8	– O8	171.7
– O3	170.4	– O6	171.8	– O9	172.8
Se4 – O10	168.8	Se5 – O13	168.9	Se6 – O16	166.2
– O11	169.9	– O14	169.4	– O17	171.7
– O12	173.6	– O15	170.0	– O18	172.1
Se7 – O19	168.1	Se8 – O22	167.9	Se9 – O25	168.3
– O20	169.2	– O23	171.3	– O26	170.5
– O21	172.7	– O24	173.6	– O27	171.4

Table 3.4.1.d: continued

	∢ / grd		∢ / grd		∢ / grd
O1 – Se1 – O3	96.0	O5 – Se2 – O6	101.2	O8 – Se3 – O9	96.6
O1 – Se1 – O2	98.9	O4 – Se2 – O5	101.9	O7 – Se3 – O9	104.0
O2 – Se1 – O3	106.5	O4 – Se2 – O6	102.7	O7 – Se3 – O8	105.8
O11 – Se4 – O12	94.4	O13 – Se5 – O14	95.0	O17 – Se6 – O18	97.2
O10 – Se4 – O12	96.8	O14 – Se5 – O15	96.4	O16 – Se6 – O18	103.6
O10 – Se4 – O11	107.5	O13 – Se5 – O15	104.2	O16 – Se6 – O17	105.9
O19 – Se7 – O21	96.9	O22 – Se8 – O24	94.3	O25 – Se9 – O26	97.9
O20 – Se7 – O21	98.2	O23 – Se8 – O24	95.3	O25 – Se9 – O27	98.4
O19 – Se7 – O20	106.4	O22 – Se8 – O23	106.1	O26 – Se9 – O27	103.6

Table 3.4.1.e: Motifs of mutual adjunction in $Pr_2[SeO_3]_3$

	O1	O2	O3	O4	O5	O6	O7	O8	O9	O10	O11	O12	O13	O14
Pr1	0 / 0	0 / 0	1 / 1	1 / 1	0 / 0	0 / 0	0 / 0	1 / 1	1 / 1	1 / 1	1 / 1	1 / 1	1 / 1	1 / 1
Pr2	0 / 0	1 / 1	0 / 0	0 / 0	0 / 0	1 / 1	0 / 0	0 / 0	0 / 0	0 / 0	0 / 0	0 / 0	0 / 0	0 / 0
Pr3	0 / 0	0 / 0	0 / 0	0 / 0	0 / 0	1 / 1	0 / 0	0 / 0	0 / 0	0 / 0	0 / 0	0 / 0	0 / 0	0 / 0
Pr4	0 / 0	0 / 0	0 / 0	0 / 0	1 / 1	0 / 0	0 / 0	1 / 1	1 / 1	1 / 1	1 / 1	2 / 2	1 / 1	0 / 0
Pr5	1 / 1	0 / 0	1 / 1	0 / 0	0 / 0	0 / 0	1 / 1	0 / 0	1 / 1	0 / 0	0 / 0	0 / 0	0 / 0	2 / 1
Pr6	1 / 1	1 / 0	0 / 0	0 / 0	0 / 0	0 / 0	0 / 0	0 / 0	0 / 0	0 / 0	0 / 0	0 / 0	0 / 0	0 / 0
Se1	1 / 1	1 / 1	1 / 1	0 / 0	0 / 0	0 / 0	0 / 0	0 / 0	0 / 0	0 / 0	0 / 0	0 / 0	0 / 0	0 / 0
Se2	0 / 0	0 / 0	0 / 0	1 / 1	1 / 1	1 / 1	0 / 0	0 / 0	0 / 0	0 / 0	0 / 0	0 / 0	0 / 0	0 / 0
Se3	0 / 0	0 / 0	0 / 0	0 / 0	0 / 0	0 / 0	1 / 1	1 / 1	1 / 1	0 / 0	0 / 0	0 / 0	0 / 0	0 / 0
Se4	0 / 0	0 / 0	0 / 0	0 / 0	0 / 0	0 / 0	0 / 0	0 / 0	0 / 0	1 / 1	1 / 1	1 / 1	0 / 0	0 / 0
Se5	0 / 0	0 / 0	0 / 0	0 / 0	0 / 0	0 / 0	0 / 0	0 / 0	0 / 0	0 / 0	0 / 0	0 / 0	1 / 1	1 / 1
Se6	0 / 0	0 / 0	0 / 0	0 / 0	0 / 0	0 / 0	0 / 0	0 / 0	0 / 0	0 / 0	0 / 0	0 / 0	0 / 0	0 / 0
Se7	0 / 0	0 / 0	0 / 0	0 / 0	0 / 0	0 / 0	0 / 0	0 / 0	0 / 0	0 / 0	0 / 0	0 / 0	0 / 0	0 / 0
Se8	0 / 0	0 / 0	0 / 0	0 / 0	0 / 0	0 / 0	0 / 0	0 / 0	0 / 0	0 / 0	0 / 0	0 / 0	0 / 0	0 / 0
Se9	0 / 0	0 / 0	0 / 0	0 / 0	0 / 0	0 / 0	0 / 0	0 / 0	0 / 0	0 / 0	0 / 0	0 / 0	0 / 0	0 / 0
CN	3	2	3	2	2	3	2	3	4	3	3	4	3	3

Table 3.4.1.e: continued

	O15	O16	O17	O18	O19	O20	O21	O22	O23	O24	O25	O26	O27	CN
Pr1	0 / 0	0 / 0	0 / 0	0 / 0	0 / 0	0 / 0	0 / 0	0 / 0	0 / 0	0 / 0	0 / 0	0 / 0	0 / 0	9
Pr2	0 / 0	1 / 1	0 / 0	0 / 0	1 / 0	1 / 1	2 / 2	0 / 0	1 / 1	1 / 1	0 / 0	0 / 0	0 / 0	9
Pr3	0 / 0	0 / 0	2 / 2	2 / 2	0 / 0	0 / 0	0 / 0	2 / 2	0 / 0	1 / 1	0 / 0	1 / 1	0 / 0	9
Pr4	0 / 0	0 / 0	0 / 0	0 / 0	0 / 0	0 / 0	0 / 0	0 / 0	0 / 0	0 / 0	0 / 0	0 / 0	1 / 1	9
Pr5	2 / 2	0 / 0	0 / 0	0 / 0	0 / 0	0 / 0	0 / 0	0 / 0	0 / 0	0 / 0	1 / 0	0 / 0	1 / 1	10
Pr6	0 / 0	0 / 0	0 / 0	1 / 1	1 / 1	1 / 1	1 / 0	0 / 0	1 / 1	1 / 1	1 / 1	1 / 1	0 / 0	10
Se1	0 / 0	0 / 0	0 / 0	0 / 0	0 / 0	0 / 0	0 / 0	0 / 0	0 / 0	0 / 0	0 / 0	0 / 0	0 / 0	3
Se2	0 / 0	0 / 0	0 / 0	0 / 0	0 / 0	0 / 0	0 / 0	0 / 0	0 / 0	0 / 0	0 / 0	0 / 0	0 / 0	3
Se3	0 / 0	0 / 0	0 / 0	0 / 0	0 / 0	0 / 0	0 / 0	0 / 0	0 / 0	0 / 0	0 / 0	0 / 0	0 / 0	3
Se4	0 / 0	0 / 0	0 / 0	0 / 0	0 / 0	0 / 0	0 / 0	0 / 0	0 / 0	0 / 0	0 / 0	0 / 0	0 / 0	3
Se5	1 / 1	0 / 0	0 / 0	0 / 0	0 / 0	0 / 0	0 / 0	0 / 0	0 / 0	0 / 0	0 / 0	0 / 0	0 / 0	3
Se6	0 / 0	1 / 1	1 / 1	0 / 0	0 / 0	0 / 0	0 / 0	0 / 0	0 / 0	0 / 0	0 / 0	0 / 0	0 / 0	3
Se7	0 / 0	0 / 0	0 / 0	1 / 1	1 / 1	1 / 1	1 / 1	0 / 0	0 / 0	0 / 0	0 / 0	0 / 0	0 / 0	3
Se8	0 / 0	0 / 0	0 / 0	0 / 0	0 / 0	0 / 0	0 / 0	1 / 1	1 / 1	1 / 1	0 / 0	0 / 0	0 / 0	3
Se9	0 / 0	0 / 0	0 / 0	0 / 0	0 / 0	0 / 0	0 / 0	0 / 0	0 / 0	0 / 0	1 / 1	1 / 1	1 / 1	3
CN	3	2	3	3	2	3	3	3	3	4	2	3	3	

3.5 Structure description of the triclinic $Sm_2[SeO_3]_3$ and $M_2[SeO_3]_3$ (M = Y; Eu – Lu)

In paragraphs 3.2, 3.3 and 3.4 we have described the hexagonal, the orthorhombic as well as the monoclinic forms adopted by $Sc_2[SeO_3]_3$, $Ce_2[SeO_3]_3$ and $Pr_2[SeO_3]_3$, respectively. This class of compounds $M_2[SeO_3]_3$ is completed here for all lanthanides by the description of the triclinic erbium prototype of structure since the latter was already quoted in the literature for $Er_2[SeO_3]_3$ [18, 19]. According to the structure determinations (table 3.5.1.a), the ten investigated single crystals are isostructural and belong to this $Er_2[SeO_3]_3$-type structure. Their lattice constants are given in table 3.5.a and reflect perfectly what one can expect due to the "lanthanide contraction": the unit cell deminishes from $Eu_2[SeO_3]_3$ with a = 712.64, b = 812.85, c = 887.26 pm up to $Lu_2[SeO_3]_3$ with a = 690.22, b = 793.41, c = 911.52 pm. However, $Sm_2[SeO_3]_3$ presents a few differences in this observation but the values are not far deviated from the straight line in diagram 3.5.1 where lattice constants are plotted versus ionic radiis. The very close value of $r(Y^{3+})$ (115.9 pm) to $r(Ho^{3+})$ (115.5 pm) all for a coordination number of eight [87] also lead to close unit cell constants for $Y_2[SeO_3]_3$ and $Ho_2[SeO_3]_3$ (see diagram 3.5.1 and table 3.5.1.a). These oxoselenates(IV) of trivalent lanthanides are crystallizing in the triclinic structure type with the space group $P\bar{1}$ containing two formula units per units cell. While two inequivalent Sm^{3+} cations in eight-and nine-fold coordination are present in $Sm_2[SeO_3]_3$, the remainder elements of this series show hepta- and octa-coordinated M^{3+} cations (M = Y, Eu – Lu) only, but we ought to mention that there are three crystallographically independent $[SeO_3]^{2-}$ groups in both cases. The difference in the coordination being accounted for the different radiis among them. The $(Sm1)^{3+}$ and $(Sm2)^{3+}$ as well as the $(M1)^{3+}$ and $(M2)^{3+}$ coordination spheres are depicted in fig. 3.5.a and 3.5.b, respectively. While two $[SeO_3]^{2-}$ groups ($[(Se1)O_3]^{2-}$ and $[(Se2)O_3]^{2-}$) act as chelating ligands in the coordination of $(Sm1)^{3+}$ only the $[(Se1)O_3]^{2-}$ group is chelatingly observed about $(M1)^{3+}$ and its coordination sphere can thus be seen as distorted square antiprism on the one hand and as pentagonal bipyramid on the other hand. Oxygen atoms that coordinate $(Sm2)^{3+}$ belong to three $[(Se1)O_3]^{2-}$, two $[(Se2)O_3]^{2-}$ and two $[(Se3)O_3]^{2-}$ against three $[(Se1)O_3]^{2-}$, two $[(Se2)O_3]^{2-}$ but only one $[(Se3)O_3]^{2-}$ in the case of the $(M2)^{3+}$ cations. Nevertheless two of them are in both cases attached as chelating ligands (1× $[(Se2)O_3]^{2-}$, 1× $[(Se3)O_3]^{2-}$) and the remainder in a monodentate way. For those compounds, $[(Sm1)O_8]$ and $[(Sm2)O_9]$ units as well as $[(M1)O_7]$ and $[(M2)O_8]$ polyhedra share opposite edges and are further linked by

$[(Se1)O_3]^{2-}$ and $[(Se2)O_3]^{2-}$ to zigzag chains along [100]. The M^{3+}–M^{3+} contacts in that direction are 399 and 401 pm for Eu, through 391 and 394 pm for Ho up to 385 and 388 pm for Lu. Of course, this reveals what the lanthanide contraction demands and what has been already anticipated by comparison of the lattice constants. The corresponding distances were found to be 390 and 394 for Y, 382 and 404 pm for the special case of $Sm_2[SeO_3]_3$.

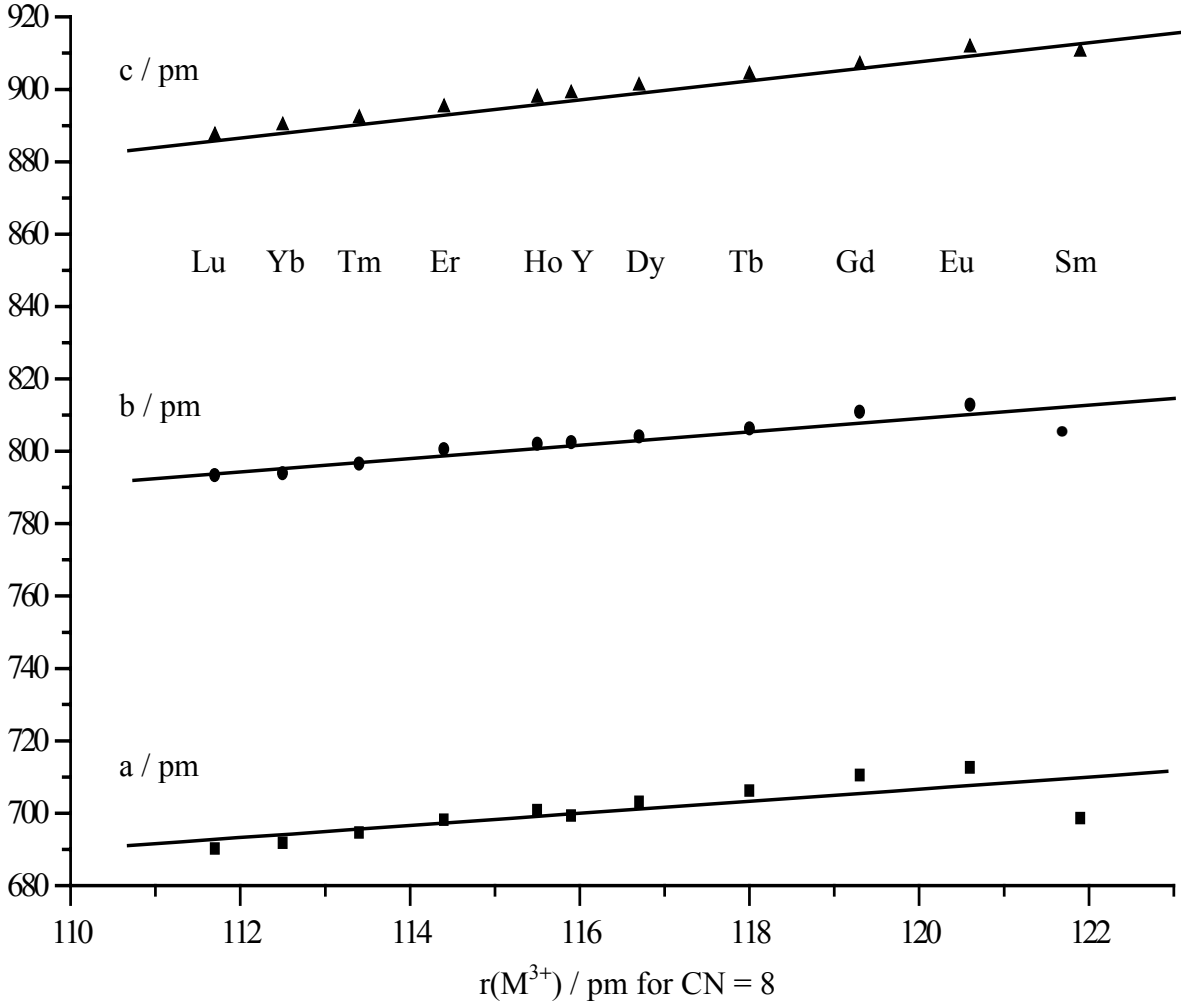

Diagram 3.5.1: Unit cell constants of rare-earth(III) oxoselenates(IV) $M_2[SeO_3]_3$ (M = Y; Sm – Lu) versus rare-earth(III) ionic radiis [87]

Further linkage of the zigzag chains occurs via $[(Se3)O_3]^{2-}$ groups leading to rectangular channels in the $[01\bar{1}]$ direction (fig. 3.5.c and 3.5.d). The average M^{3+}–M^{3+} contacts in [010] direction are 571 pm for Eu through 567 pm for Ho up to 563 pm for Lu. Once more those contacts display as 565 and 659 pm for the samarium compound. Aforesaid tunnels incorporate free electrons pairs "*lone pairs*" of the selenium atoms and therefore the second

main structural feature of those compounds comes up. Three independent Se^{4+} cations exhibit the usual pyramidal geometry with an observed stereochemically active lone-pair of electrons (d(Se–O) = 164 –175 pm, average ∢(O–Se–O) = 99.5°, table 3.5.1.d).

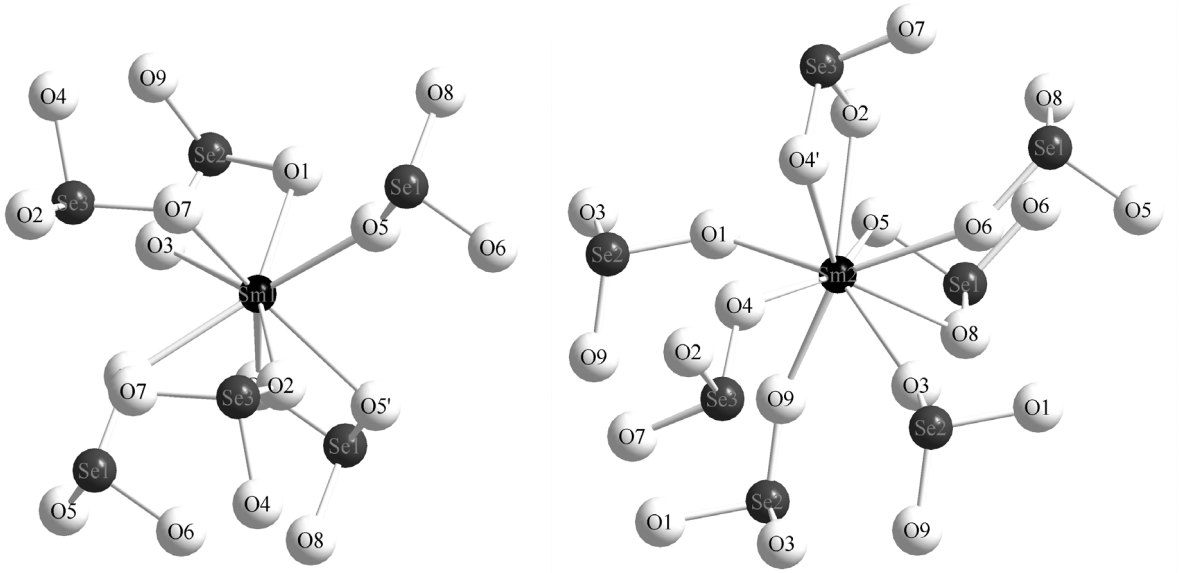

Fig. 3.5.a: Coordination of $(Sm1)^{3+}$ and $(Sm2)^{3+}$ in the crystal structure of $Sm_2[SeO_3]_3$, both ions are surrounded by six and seven $[SeO_3]^{2-}$ groups, respectively

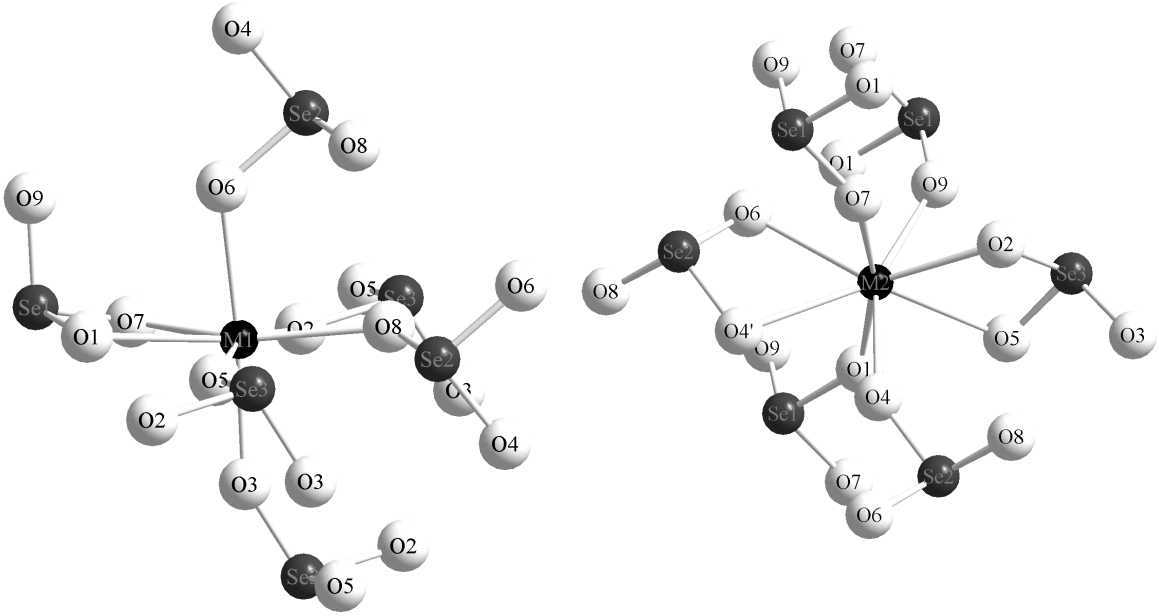

Fig. 3.5.b: Coordination of six $[SeO_3]^{2-}$ groups about $(M1)^{3+}$ and $(M2)^{3+}$ in the crystal structure of $M_2[SeO_3]_3$ (M = Y; Eu – Ho, Tm – Lu)

These values compare satisfactorily well with the average geometrical corresponding parameters in paragraphs 3.2, 3.3 and 3.4 and with a large number of oxoselenate(IV)- and hydrogenoxoselenate(IV) species [88, 89]. The shortest Se–O distances observed always correspond to monodentate oxygen ligands thus showing the strong attachment of the $[SeO_3]^{2-}$ groups grafted to polyhedral units by a monodentate way. The pyramidal $[SeO_3]^{2-}$ anions show different cationic vicinity. One M^{3+} is edge-spanning and three other ones are all terminal for the coordination about the $[SeO_3]^{2-}$ groups in $M_2[SeO_3]_3$ (M = Y; Eu – Lu) whereas two Sm^{3+} edge-spanning and three Sm^{3+} terminal are observed around the $[(Se1)O_3]^{2-}$ units in $Sm_2[SeO_3]_3$ (fig. 3.5.e and 3.5.f). Despite the diversities within coordination polyhedra in $Sm_2[SeO_3]_3$ (CN = 8, 9) and $M_2[SeO_3]_3$ (M = Y; Eu – Lu) (CN = 7, 8) as well as the differences observed for their units cells constants, their main structural features remind the same and consist of rectangular channels arising from chains of edge-connected chairs of $[(Sm1)O_8]$ and $[(Sm2)O_9]$, respectively $[(M1)O_7]$ and $[(M2)O_8]$ polyhedra (fig. 3.5.c and 3.5.d).

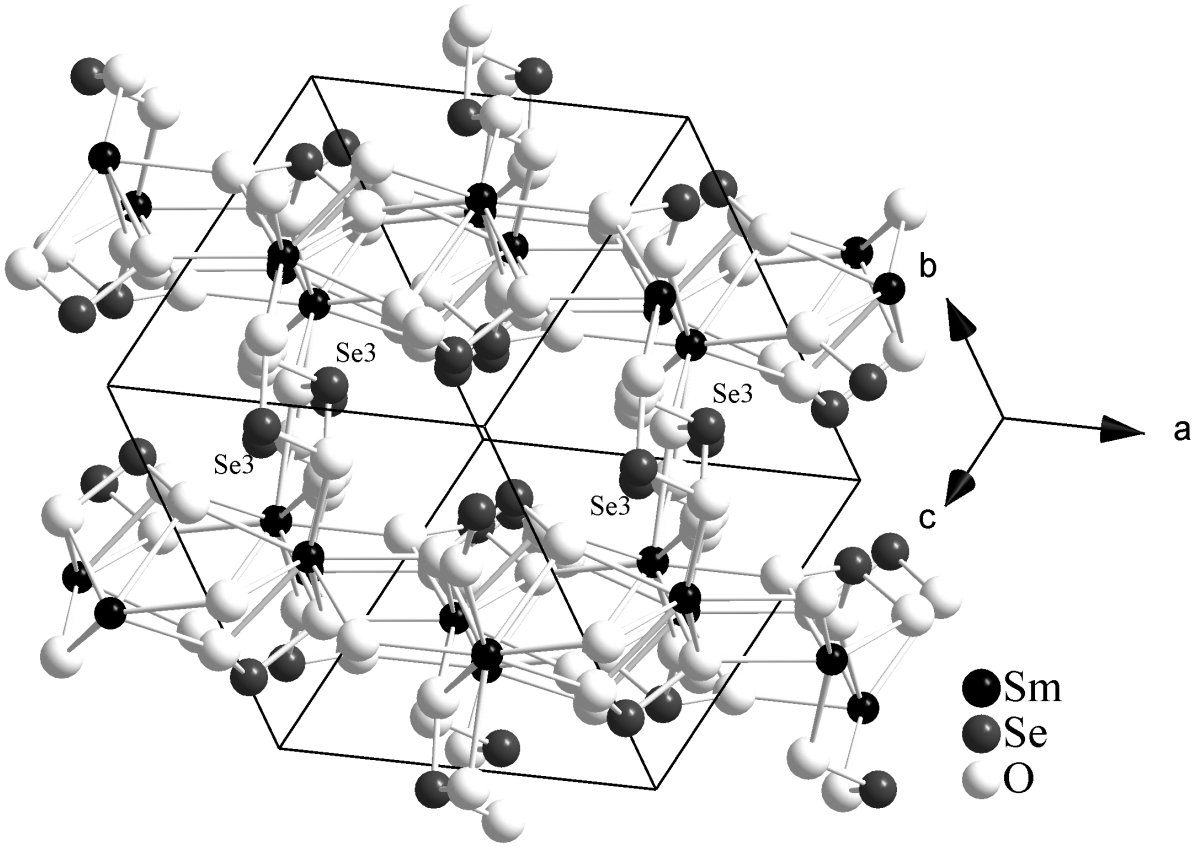

Fig. 3.5.c: Crystal structure of $Sm_2[SeO_3]_3$ viewed along [011] exhibiting the linkage of Sm^{3+} polyhedra and its rectangular "lone-pair" channels

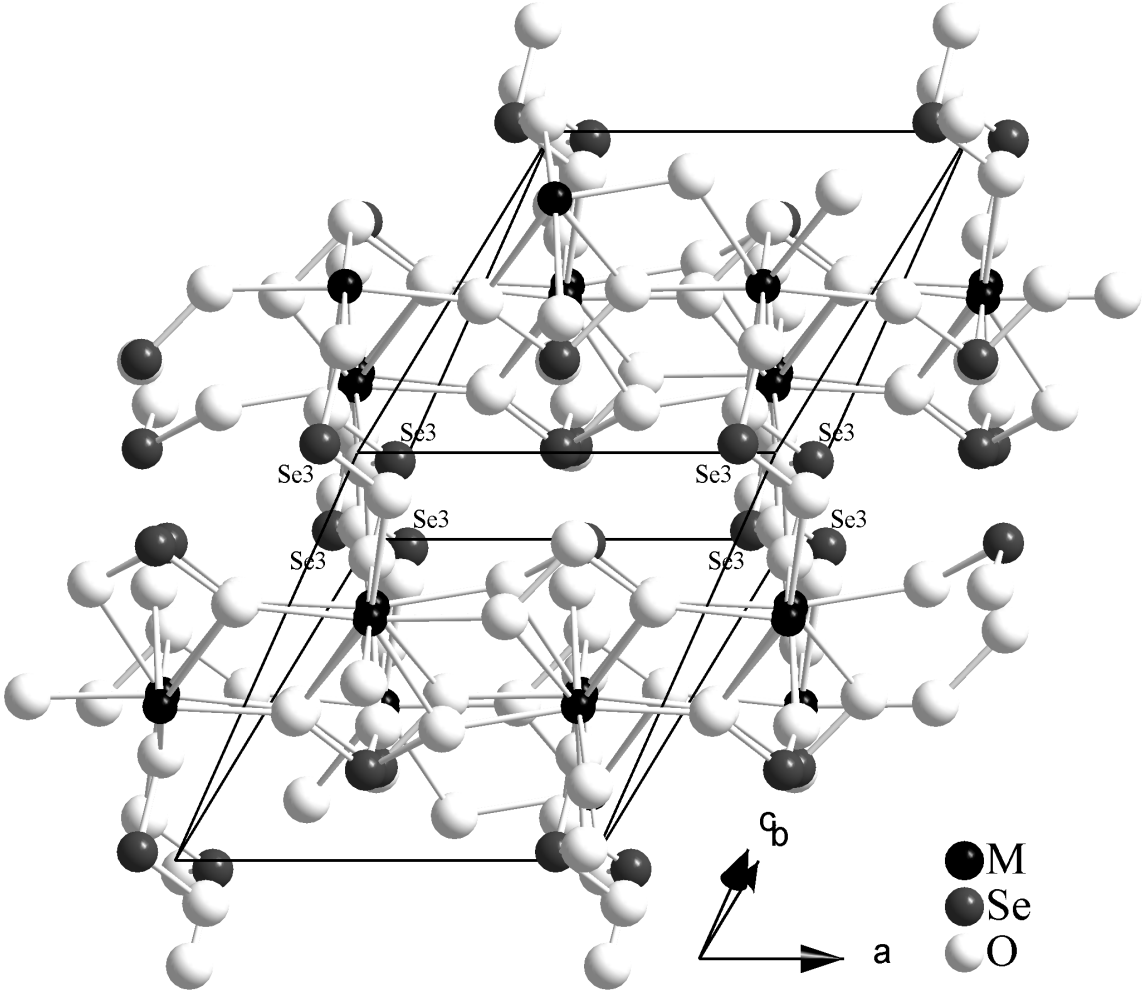

Fig. 3.5.d: Crystal structure of $M_2[SeO_3]_3$ (M = Y; Eu – Ho, Tm – Lu) viewed along [01 $\bar{1}$] exhibiting the linkage of M^{3+} polyhedra and the rectangular "lone-pair" channel

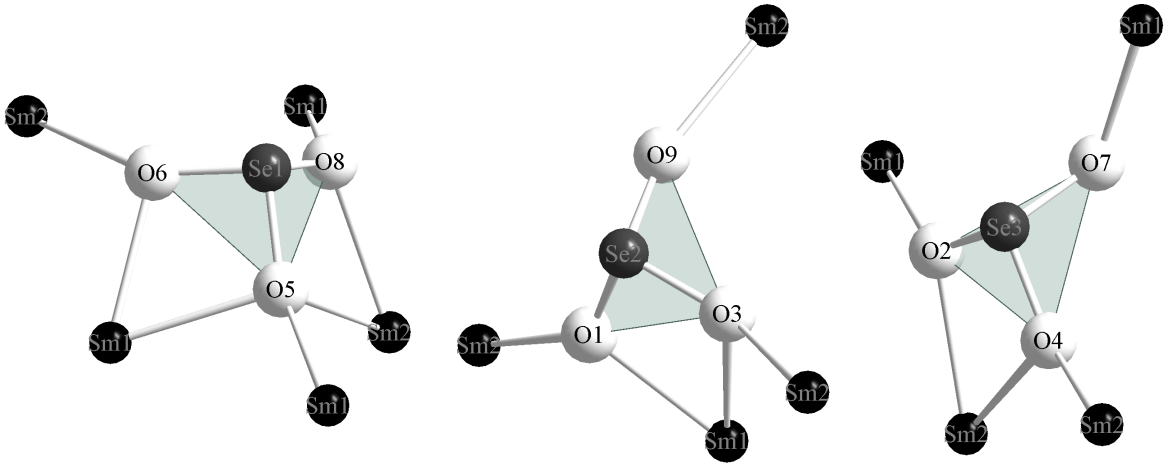

Fig. 3.5.e: Cationic vicinities of Sm^{3+} cations about the $[SeO_3]^{2-}$ units in $Sm_2[SeO_3]_3$

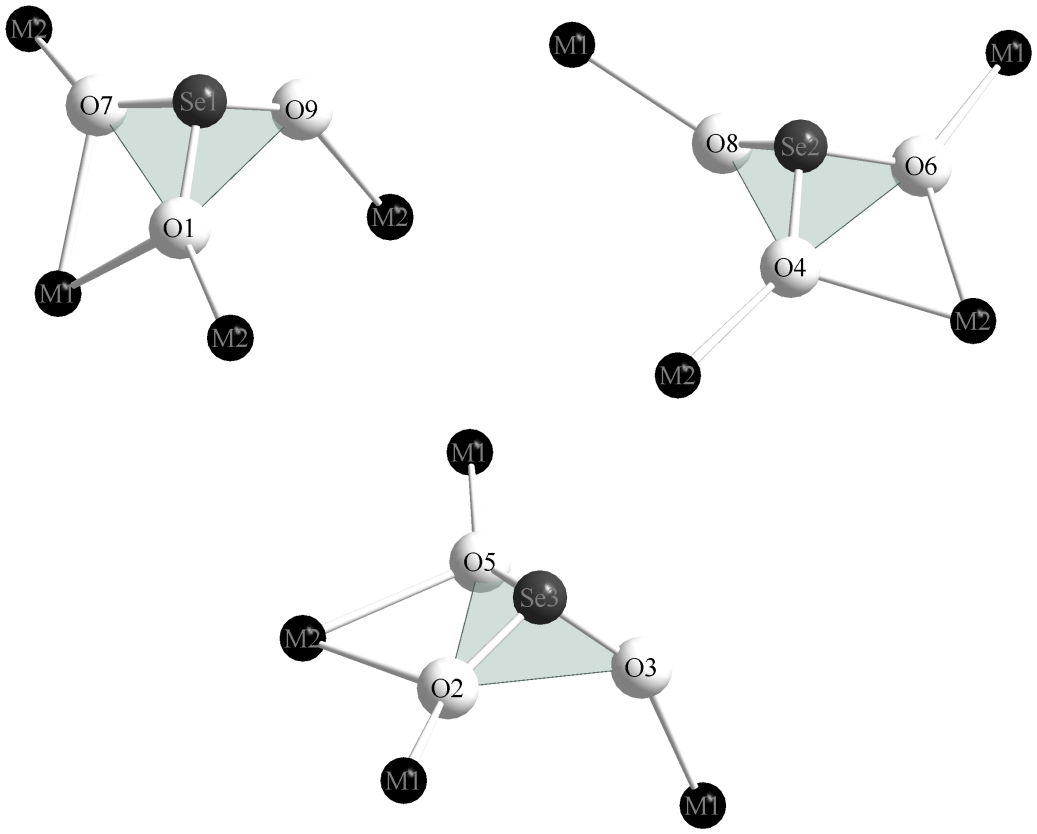

Fig. 3.5.f: Cationic coordination of M^{3+} cations about the three crystallographically independent $[SeO_3]^{2-}$ units in $M_2[SeO_3]_3$ (M = Y; Eu – Lu)

3.5.1 Structural data for $M_2[SeO_3]_3$ (M = Y; Sm – Lu)

Table 3.5.1.a: Crystallographic data for $M_2[SeO_3]_3$ and their determination

M		Y	Sm	Eu	Gd
Crystal system and space group			triclinic, $P\bar{1}$ (No. 2)		
Formula unit per unit cell (Z)			2		
Unit cell parameters:	a / pm =	699.34(5)	698.60(10)	712.64(4)	710.52(5)
	b / pm =	802.49(6)	789.60(2)	812.85(4)	810.87(7)
	c / pm =	898.82(8)	910.34(2)	911.52(6)	906.73(8)
	α / ° =	71.332(3)	96.693(10)	71.372(2)	71.364(4)
	β / ° =	69.916(3)	104.64(10)	70.075(2)	70.168(4)
	γ / ° =	65.770(4)	115.87(10)	65.652(2)	65.747(4)
Calculated density (D_x / g · cm^3)		4.392	5.363	5.142	5.272
Molar volume (V_m / cm^3 · mol^{-1})		127.26	127.17	126.34	125.99
Diffractometer, radiation		κ-CCD (Fa. Nonius); Mo-K_α: λ = 71.07 pm			
$2\theta_{max.}$		55.7	54.9	54.9	55.5
Index ranges: $\pm h_{max}$ / $\pm k_{max}$ / $\pm l_{max}$		9 / 10 / 11	9 / 10 / 11	9 / 10 / 11	9 / 10 / 11
F(000)		504.0	596.0	600.0	604.0
Absorption coefficients (μ / mm^{-1})		26.62	26.74	26.42	27.50
Absorption correction		Numerical, after crystal shape optimization with the program X-SHAPE [53]			
Other data corrections		background, polarization, *Lorentz* factors			
Collected reflections		12614	3674	9881	13218
Unique reflections		1945	1933	2016	2013
R_{int} / R_σ		0.115 / 0.060	0.029 / 0.040	0.151 / 0.086	0.150 / 0.087
Reflections with $\|F_o\| \geq 4\sigma\|F_o\|$		1697	1651	1521	1422
Structure solution and refinement			Program system SHELX-97 [58]		
Scattering factors			International Tables, Vol. C [85]		
R_1 / R_1 with $\|F_o\| \geq 4\sigma\|F_o\|$		0.114 / 0.105	0.037 / 0.029	0.123 / 0.104	0.138 / 0.108
wR_2 / Goodness of fit (GooF)		0.272 / 1.193	0.067 / 1.131	0.294 / 1.154	0.305 / 1.142
Extinction (g)		0.0037(4)	0.0056(3)	0.0054(5)	0.0058(6)
Residual electron	max.	6.78	2.46	14.87	12.73
density (ρ / e$^-$ 10^6 pm)	min.	–2.19	–1.59	–4.28	–4.51

Table 3.5.1.a: Continued

M		Tb	Dy	Ho	Tm
Crystal system and space group			triclinic, $P\bar{1}$ (No. 2)		
Formula unit per unit cell (Z)			2		
Unit cell parameters:	a / pm =	706.20(3)	703.08(1)	700.79(3)	694.61(3)
	b / pm =	806.29(4)	804.10(2)	802.04(4)	796.58(4)
	c / pm =	904.06(5)	900.96(1)	897.69(4)	891.96(5)
	α / ° =	71.476(2)	71.383(1)	71.370(2)	71.480(2)
	β / ° =	70.084(2)	70.095(1)	70.098(2)	70.223(2)
	γ / ° =	65.896(2)	65.903(1)	65.935(2)	65.964(2)
Calculated density (D_x / g cm^3)		5.370	5.484	5.574	5.755
Molar volume (V_m / cm^3 mol^{-1})		125.97	125.63	124.97	124.65
Diffractometer, radiation			κ-CCD (Fa. Nonius); Mo-K_α: λ = 71.07 pm		
$2\theta_{max.}$		54.9	70.0	55.3	55.1
Index ranges:	$\pm h_{max}$ / $\pm k_{max}$ / $\pm l_{max}$	9 / 10 / 11	11 / 12 / 14	9 / 10 / 11	9 / 10 / 11
F(000)		608.0	612.0	616.0	624.0
Absorption coefficients (μ / mm^{-1})		28,89	30.14	31.46	34.44
Absorption correction		Numerical, after crystal shape optimization with the program X-SHAPE [53]			
Other data corrections		background, polarization, *Lorentz* factors			
Collected reflections		12716	20026	12838	11683
Unique reflections		1959	3759	1943	1903
R_{int} / R_σ		0.068 / 0.040	0.074 / 0.054	0.074 / 0.040	0.110 / 0.057
Reflections with $\|F_o\| \geq 4\sigma\|F_o\|$		1680	3051	1776	1691
Structure solution and refinement			Program system SHELX-97 [58]		
Scattering factors			International Tables, Vol. C [85]		
R_1 / R_1 with $\|F_o\| \geq 4\sigma\|F_o\|$		0.057 / 0.049	0.067 / 0.054	0.058 / 0.055	0.099 / 0.094
wR_2 / Goodness of fit (GooF)		0.135 / 1.062	0.160 / 1.055	0.152 / 1.106	0.277 / 1.244
Extinction (g)		0.0020(3)	0.0019(4)	0.0023(5)	0.0035(4)
Residual electron	max.	6.72	10.64	8.42	17.28
density (ρ / e$^-$ 10^6 pm)	min.	–2.75	–4.42	–2.57	–4.92

Table 3.5.1.a: Continued

M		Yb	Lu
Crystal system and Space group		triclinic, $P\bar{1}$ (No. 2)	
Formula unit per unit cell (Z)		2	
Unit cell parameters:	a / pm =	691.79(1)	690.22(2)
	b / pm =	793.93(1)	793.81(2)
	c / pm =	890.01(2)	887.26(2)
	α / ° =	71.455(1)	71.413(1)
	β / ° =	70.293(1)	70.235(1)
	γ / ° =	66.038(1)	65.985(1)
Calculated density (D_x / g cm^3)		5.873	5.944
Molar volume (V_m / cm^3 mol^{-1})		123.96	123.67
Diffractometer, radiation		κ-CCD (Fa. Nonius); Mo-K_α: λ = 71.07 pm	
$2\theta_{max.}$		59.8	60.1
Index ranges:	$\pm h_{max}$ / $\pm k_{max}$ / $\pm l_{max}$	9 / 11 / 12	9 / 11 / 12
F(000)		628.0	632.0
Absorption coefficients (μ / mm^{-1})		35.91	37.43
Absorption correction		Numerical, after crystal shape optimization with the program X-SHAPE [53]	
Other data corrections		background, polarization, *Lorentz* factors	
Collected reflections		11608	19427
Unique reflections		2371	2387
R_{int} / R_σ		0.065 / 0.044	0.143 / 0.066
Reflections with $\|F_o\| \geq 4\sigma\|F_o\|$		2183	1973
Structure solution and refinement		Program system SHELX-97 [58]	
Scattering factors		International Tables, Vol. C [85]	
R_1 / R_1 with $\|F_o\| \geq 4\sigma\|F_o\|$		0.036 / 0.032	0.092 / 0.080
wR_2 / Goodness of fit (GooF)		0.094 / 1.108	0.235 / 1.077
Extinction (g)		0.0125(6)	0.0016(4)
Residual electron density		max. 3.49	max. 15.62
(ρ / e$^-$ 10^6 pm)		min. –3.55	min. –4.99

Table 3.5.1.b: Atomic coordinates for $M_2[SeO_3]_3$ (M = Y; Sm –Lu)

Atoms	Wyckoff Position	x / a	y / b	z / c
Y1	2i	0.2404(3)	0.7363(3)	0.7995(2)
Y2	2i	0.8332(3)	0.7295(3)	0.5899(2)
Se1	2i	0.3883(3)	0.7556(3)	0.4155(3)
Se2	2i	0.6460(3)	0.7529(3)	0.9656(3)
Se3	2i	0.9283(4)	0.7750(3)	0.1989(3)
O1	2i	0.1607(24)	0.7453(22)	0.5607(16)
O2	2i	0.5602(24)	0.6967(21)	0.8324(18)
O3	2i	0.6684(26)	0.5674(20)	0.1171(17)
O4	2i	0.8615(28)	0.9420(19)	0.3051(18)
O5	2i	0.9064(24)	0.7112(20)	0.8504(18)
O6	2i	0.3447(26)	0.9807(20)	0.3458(21)
O7	2i	0.0155(29)	0.5923(21)	0.3520(19)
O8	2i	0.5332(26)	0.7049(20)	0.5539(19)
O9	2i	0.1459(27)	0.7958(22)	0.0522(19)
Sm1	2i	0.53911(7)	0.31071(6)	0.87203(5)
Sm2	2i	0.97638(7)	0.34946(6)	0.67709(5)
Se1	2i	0.9536(1)	0.7666(1)	0.96275(9)
Se2	2i	0.3462(1)	0.2202(1)	0.48881(9)
Se3	2i	0.3702(1)	0.8236(1)	0.74349(9)
O1	2i	0.2807(10)	0.3120(9)	0.6388(6)
O2	2i	0.3459(11)	0.6639(9)	0.8559(7)
O3	2i	0.5716(10)	0.2163(9)	0.6142(7)
O4	2i	0.1245(10)	0.6654(9)	0.5941(6)
O5	2i	0.7564(10)	0.6601(9)	0.0537(7)
O6	2i	0.8667(10)	0.5638(9)	0.8250(7)
O7	2i	0.3060(10)	0.9804(9)	0.8341(7)
O8	2i	0.1758(10)	0.7884(9)	0.1065(7)
O9	2i	0.1578(11)	0.9876(9)	0.4142(7)

Table 3.5.1.b: Continued

Atoms	Wyckoff Position	x / a	y / b	z / c
Eu1	2i	0.2397(2)	0.7357(2)	0.8017(2)
Eu2	2i	0.8320(2)	0.7334(2)	0.5884(1)
Se1	2i	0.3897(4)	0.7527(3)	0.4169(3)
Se2	2i	0.6471(4)	0.7549(3)	0.9646(3)
Se3	2i	0.9265(4)	0.7739(3)	0.2010(3)
O1	2i	0.1590(25)	0.7418(21)	0.5625(18)
O2	2i	0.5606(27)	0.7008(20)	0.8353(20)
O3	2i	0.9018(29)	0.7215(20)	0.8484(22)
O4	2i	0.5335(27)	0.7104(25)	0.5553(20)
O5	2i	0.8552(28)	0.9415(22)	0.3062(20)
O6	2i	0.0162(27)	0.5930(21)	0.3462(19)
O7	2i	0.6693(28)	0.5718(26)	0.1155(21)
O8	2i	0.1430(28)	0.7916(24)	0.0608(21)
O9	2i	0.3484(29)	0.9735(22)	0.3414(23)
Gd1	2i	0.2404(2)	0.7356(2)	0.8009(2)
Gd2	2i	0.8324(2)	0.7328(2)	0.5886(2)
Se1	2i	0.3894(4)	0.7538(4)	0.4161(3)
Se2	2i	0.6469(5)	0.7545(3)	0.9650(3)
Se3	2i	0.9275(5)	0.7745(4)	0.1999(3)
O1	2i	0.1557(31)	0.7426(26)	0.5644(19)
O2	2i	0.9045(32)	0.7253(22)	0.8453(22)
O3	2i	0.5567(31)	0.6986(22)	0.8378(23)
O4	2i	0.0156(31)	0.5940(28)	0.3454(21)
O5	2i	0.5330(27)	0.7117(26)	0.5570(22)
O6	2i	0.8654(33)	0.9340(27)	0.3025(23)
O7	2i	0.6693(34)	0.5721(30)	0.1206(22)
O8	2i	0.3482(32)	0.9778(23)	0.3402(23)
O9	2i	0.1402(29)	0.7950(23)	0.0594(24)

Table 3.5.1.b: Continued

Atoms	Wyckoff Position	x / a	y / b	z / c
Tb1	2i	0.24026(8)	0.73598(7)	0.80020(6)
Tb2	2i	0.83229(8)	0.73188(7)	0.58895(6)
Se1	2i	0.3886(2)	0.7544(2)	0.4153(1)
Se2	2i	0.9284(2)	0.7739(2)	0.1996(1)
Se3	2i	0.6468(2)	0.7536(1)	0.9652(1)
O1	2i	0.1584(12)	0.7450(11)	0.5622(8)
O2	2i	0.5646(12)	0.6996(10)	0.8345(9)
O3	2i	0.6688(13)	0.5696(11)	0.1162(9)
O4	2i	0.0160(13)	0.5937(11)	0.3485(10)
O5	2i	0.9028(13)	0.7190(10)	0.8497(10)
O6	2i	0.8601(12)	0.9410(10)	0.3052(9)
O7	2i	0.5333(12)	0.7058(11)	0.5542(9)
O8	2i	0.1444(13)	0.7929(11)	0.0582(10)
O9	2i	0.3450(14)	0.9802(10)	0.3454(10)
Dy1	2i	0.24019(6)	0.73601(5)	0.80004(4)
Dy2	2i	0.83284(6)	0.73084(5)	0.58914(4)
Se1	2i	0.3882(1)	0.7555(1)	0.4151(1)
Se2	2i	0.9280(1)	0.7747(1)	0.1991(1)
Se3	2i	0.6467(1)	0.7533(1)	0.9651(1)
O1	2i	0.1584(11)	0.7472(9)	0.5614(7)
O2	2i	0.5638(9)	0.7006(8)	0.8340(7)
O3	2i	0.6673(10)	0.5687(9)	0.1171(7)
O4	2i	0.8598(10)	0.9418(8)	0.3042(7)
O5	2i	0.9029(10)	0.7183(9)	0.8502(8)
O6	2i	0.0166(10)	0.5949(9)	0.3474(7)
O7	2i	0.5335(10)	0.7070(9)	0.5542(7)
O8	2i	0.3461(11)	0.9816(8)	0.3434(7)
O9	2i	0.1470(10)	0.0566(8)	0.0566(8)

Table 3.5.1.b: Continued

Atoms	Wyckoff Position	x / a	y / b	z / c
Ho1	2i	0.24086(8)	0.73597(7)	0.79914(7)
Ho2	2i	0.83287(9)	0.73020(7)	0.58922(7)
Se1	2i	0.3875(2)	0.7559(2)	0.4142(2)
Se2	2i	0.9286(2)	0.7751(2)	0.1985(2)
Se3	2i	0.6465(2)	0.7528(2)	0.9654(2)
O1	2i	0.1578(14)	0.7445(14)	0.5626(10)
O2	2i	0.9046(14)	0.7183(12)	0.8493(11)
O3	2i	0.5643(14)	0.6968(12)	0.8331(11)
O4	2i	0.8602(14)	0.9405(11)	0.3066(10)
O5	2i	0.6687(15)	0.5692(13)	0.1179(11)
O6	2i	0.0168(15)	0.5938(12)	0.3493(11)
O7	2i	0.5326(14)	0.7055(13)	0.5542(10)
O8	2i	0.3429(16)	0.9845(12)	0.3450(11)
O9	2i	0.1472(15)	0.7918(13)	0.0556(12)
Tm1	2i	0.2408(1)	0.7358(1)	0.7985(1)
Tm2	2i	0.8328(1)	0.7286(1)	0.5898(1)
Se1	2i	0.3854(3)	0.7574(3)	0.4137(3)
Se2	2i	0.9296(3)	0.7760(3)	0.1977(3)
Se3	2i	0.6455(3)	0.7523(3)	0.9656(2)
O1	2i	0.1537(21)	0.7438(19)	0.5640(15)
O2	2i	0.9050(21)	0.7147(17)	0.8515(18)
O3	2i	0.5640(23)	0.6949(21)	0.8312(16)
O4	2i	0.0185(21)	0.5930(16)	03509(16)
O5	2i	0.6669(21)	0.5683(18)	0.1192(17)
O6	2i	0.8601(19)	0.9461(16)	0.3041(17)
O7	2i	0.5305(23)	0.7054(23)	0.5551(17)
O8	2i	0.1518(22)	0.7913(19)	0.0533(17)
O9	2i	0.3410(24)	0.9885(17)	0.3442(18)

Table 3.5.1.b: Continued

Atoms	Wyckoff Position	x / a	y / b	z / c
Yb1	2i	0.24108(4)	0.73560(4)	0.79852(4)
Yb2	2i	0.83300(5)	0.72770(4)	0.58997(4)
Se1	2i	0.3851(1)	0.7582(1)	0.41352(9)
Se2	2i	0.9289(1)	0.7766(1)	0.19703(9)
Se3	2i	0.6459(1)	0.7515(1)	0.96602(9)
O1	2i	0.1558(8)	0.7461(8)	0.5639(7)
O2	2i	0.0184(9)	0.5944(7)	0.3503(7)
O3	2i	0.8610(9)	0.9453(7)	0.3036(7)
O4	2i	0.5656(8)	0.6948(8)	0.8330(7)
O5	2i	0.6667(9)	0.5672(7)	0.1204(7)
O6	2i	0.9075(8)	0.7120(8)	0.8519(7)
O7	2i	0.5348(8)	0.7041(8)	0.5530(7)
O8	2i	0.1525(9)	0.7927(8)	0.0519(7)
O9	2i	0.3413(9)	0.9868(7)	0.3463(8)
Lu1	2i	0.2417(1)	0.73583(9)	0.79760(8)
Lu2	2i	0.8334(1)	0.72721(9)	0.59026(9)
Se1	2i	0.3857(3)	0.7590(2)	0.4121(2)
Se2	2i	0.9289(3)	0.7770(2)	0.1968(2)
Se3	2i	0.6451(3)	0.7511(2)	0.9666(2)
O1	2i	0.1551(19)	0.7414(16)	0.5664(14)
O2	2i	0.5647(20)	0.6999(18)	0.8298(16)
O3	2i	0.9094(19)	0.7154(17)	0.8472(17)
O4	2i	0.5317(18)	0.7038(18)	0.5559(15)
O5	2i	0.8634(19)	0.9448(15)	0.3042(14)
O6	2i	0.6624(20)	0.5704(16)	0.1235(15)
O7	2i	0.0170(18)	0.5950(16)	0.3503(14)
O8	2i	0.3425(20)	0.9863(16)	0.3458(17)
O9	2i	0.1529(20)	0.7902(19)	0.0537(17)

Table 3.5.1.c: Anisotropic thermal displacement parameters[b] (U_{ij}/pm^2) for $M_2[SeO_3]_3$ (M = Y; Sm – Lu)

Atoms	U_{11}	U_{22}	U_{33}	U_{23}	U_{13}	U_{12}
Y1	298(11)	186(10)	232(10)	7(7)	–74(8)	–95(8)
Y2	303(11)	173(9)	245(10)	10(7)	–72(8)	–93(8)
Se1	318(11)	183(10)	236(11)	5(7)	–55(8)	–111(8)
Se2	306(11)	145(9)	245(10)	26(7)	–66(8)	–104(7)
Se3	351(12)	234(10)	265(11)	–15(8)	–70(8)	–127(9)
O1	311(75)	407(87)	101(62)	54(57)	–70(54)	–152(66)
O2	305(76)	293(76)	265(75)	–87(60)	–19(59)	–156(62)
O3	434(88)	215(71)	165(68)	71(54)	–60(61)	–136(64)
O4	524(97)	139(64)	241(74)	–35(55)	–154(68)	–49(62)
O5	278(72)	212(69)	286(76)	157(57)	–49(59)	–173(58)
O6	344(83)	170(68)	390(88)	27(61)	–67(68)	–84(60)
O7	514(99)	195(72)	269(79)	–33(59)	–45(70)	–122(68)
O8	392(86)	199(69)	264(76)	79(57)	–151(65)	–40(61)
O9	379(86)	283(79)	287(81)	–124(64)	65(66)	–110(67)
Sm1	98(2)	121(2)	104(2)	13(2)	36(2)	53(2)
Sm2	98(2)	123(2)	99(2)	18(2)	34(2)	57(2)
Se1	109(4)	105(4)	111(4)	30(3)	44(3)	59(3)
Se2	112(4)	128(4)	104(4)	9(3)	31(3)	59(3)
Se3	122(4)	108(4)	120(4)	6(3)	48(3)	31(3)
O1	119(28)	156(30)	114(27)	–40(23)	7(22)	85(25)
O2	226(33)	195(32)	130(29)	55(25)	65(25)	113(28)
O3	132(29)	257(34)	173(29)	5(25)	42(24)	147(27)
O4	127(29)	161(30)	50(25)	–26(22)	–26(22)	1(24)
O5	139(30)	159(31)	204(31)	31(25)	109(25)	52(26)
O6	180(31)	184(32)	100(28)	–36(24)	66(24)	18(26)
O7	180(31)	183(32)	149(29)	17(24)	65(24)	84(27)
O8	126(29)	234(34)	139(28)	41(25)	34(23)	98(27)
O9	168(31)	82(30)	229(33)	–66(24)	–23(26)	21(25)

Table 3.5.1.c: continued

Atoms	U_{11}	U_{22}	U_{33}	U_{23}	U_{13}	U_{12}
Eu1	212(7)	150(7)	190(7)	–30(5)	–47(5)	–58(5)
Eu2	208(7)	144(7)	183(7)	–26(5)	–51(5)	–53(5)
Se1	225(12)	140(12)	170(12)	–35(9)	–28(9)	–63(9)
Se2	215(13)	150(11)	175(12)	–41(9)	–44(9)	–50(9)
Se3	257(13)	218(13)	226(13)	–73(10)	–65(10)	–78(10)
O1	257(84)	188(79)	25(63)	–46(59)	8(60)	–11(65)
O2	332(91)	92(71)	192(84)	6(62)	–83(70)	–92(65)
O3	397(103)	60(72)	276(99)	–26(70)	–21(81)	69(68)
O4	245(87)	331(97)	132(83)	–45(72)	–22(67)	–49(72)
O5	345(94)	159(78)	168(84)	–73(66)	–30(69)	–88(69)
O6	368(96)	102(72)	105(75)	2(59)	–114(68)	–8(66)
O7	319(98)	309(99)	207(92)	–73(76)	–20(74)	–126(79)
O8	317(98)	276(93)	214(94)	–65(75)	42(74)	–170(80)
O9	434(105)	83(75)	249(94)	49(68)	–66(80)	–40(71)
Gd1	337(8)	208(8)	251(8)	25(5)	–85(6)	–114(6)
Gd2	320(8)	199(8)	266(8)	15(5)	–81(6)	–102(6)
Se1	364(15)	220(14)	241(13)	14(10)	–73(11)	–131(12)
Se2	362(15)	195(13)	245(13)	7(10)	–85(11)	–114(11)
Se3	374(15)	246(14)	310(15)	–16(11)	–113(11)	–109(12)
O1	546(117)	369(107)	45(74)	–28(70)	–135(75)	–71(93)
O2	626(129)	77(79)	322(102)	49(75)	–347(98)	67(82)
O3	480(115)	115(83)	378(109)	–38(76)	6(87)	–150(81)
O4	432(112)	398(116)	162(86)	21(81)	–33(78)	–99(93)
O5	213(84)	320(101)	290(98)	12(79)	–49(73)	13(74)
O6	517(123)	392(116)	297(106)	–37(89)	–58(88)	–216(100)
O7	615(135)	397(118)	208(95)	45(83)	–15(89)	–286(105)
O8	613(126)	105(85)	219(90)	90(70)	–68(86)	10(84)
O9	342(99)	141(84)	443(117)	–24(79)	–31(83)	–104(76)

Table 3.5.1.c: continued

Atoms	U_{11}	U_{22}	U_{33}	U_{23}	U_{13}	U_{12}
Tb1	169(3)	153(3)	138(3)	−14(2)	−36(2)	−59(2)
Tb2	159(3)	151(3)	147(3)	−14(2)	−33(2)	−57(2)
Se1	183(6)	159(6)	121(5)	−20(4)	−26(4)	−67(4)
Se2	223(6)	181(6)	157(6)	−37(4)	−52(4)	−63(5)
Se3	181(6)	147(5)	146(5)	−24(4)	−33(4)	−59(4)
O1	146(39)	328(44)	34(33)	−60(30)	−21(29)	−125(35)
O2	224(39)	199(39)	200(41)	−35(32)	−41(31)	−109(33)
O3	337(45)	156(39)	167(41)	−15(31)	−102(33)	−18(34)
O4	305(44)	191(39)	180(41)	−2(32)	−51(34)	−65(35)
O5	250(42)	241(42)	222(44)	−39(36)	−69(34)	−71(35)
O6	240(39)	166(37)	194(42)	−62(32)	−29(31)	−43(32)
O7	201(38)	266(42)	163(40)	−4(33)	−70(32)	−62(33)
O8	260(42)	247(41)	165(42)	−50(34)	18(32)	−64(35)
O9	404(48)	119(38)	198(42)	16(32)	−8(37)	−40(35)
Dy1	135(2)	120(2)	109(2)	−25(2)	−27(1)	−47(1)
Dy2	126(2)	121(2)	117(2)	−16(1)	−24(1)	−46(1)
Se1	151(4)	127(3)	102(3)	−25(3)	−16(3)	−56(3)
Se2	191(4)	153(4)	121(4)	−30(3)	−42(3)	−59(3)
Se3	146(4)	112(3)	115(3)	−23(3)	−24(3)	−42(3)
O1	182(27)	277(31)	88(25)	−37(22)	−19(21)	−109(23)
O2	168(26)	232(29)	113(26)	−57(22)	−6(20)	−103(22)
O3	281(31)	160(27)	106(26)	−10(20)	−55(23)	−71(23)
O4	272(30)	105(24)	103(26)	−9(19)	−31(22)	−54(21)
O5	167(28)	213(30)	230(32)	−32(25)	−81(24)	−36(22)
O6	302(33)	187(28)	87(25)	−16(21)	−46(23)	−76(24)
O7	192(28)	281(32)	120(27)	24(23)	−52(22)	−102(24)
O8	354(34)	134(26)	113(27)	12(21)	−26(24)	−67(23)
O9	210(29)	204(28)	123(27)	−68(22)	62(22)	−51(22)

Table 3.5.1.c: continued

Atoms	U_{11}	U_{22}	U_{33}	U_{23}	U_{13}	U_{12}
Ho1	173(4)	127(3)	145(4)	2(2)	–44(2)	–49(2)
Ho2	171(4)	128(3)	154(4)	–1(2)	–42(2)	–50(2)
Se1	189(6)	138(6)	138(6)	–8(4)	–36(5)	–63(5)
Se2	213(6)	159(6)	168(6)	–26(5)	–55(5)	–58(5)
Se3	188(6)	123(6)	146(6)	–10(4)	–44(5)	–46(4)
O1	224(42)	348(51)	88(39)	–83(36)	–12(33)	–97(38)
O2	231(44)	216(45)	236(48)	–45(38)	–94(38)	–41(36)
O3	234(43)	199(42)	209(46)	–39(36)	–24(35)	–100(35)
O4	303(45)	118(38)	141(41)	–54(32)	–7(34)	–68(34)
O5	335(50)	189(46)	190(46)	–12(35)	–112(38)	–61(38)
O6	277(46)	161(42)	172(43)	3(34)	–69(36)	–34(36)
O7	183(41)	333(50)	116(41)	34(37)	–46(34)	–96(37)
O8	421(53)	94(40)	171(44)	64(33)	–9(40)	–94(37)
O9	282(47)	209(45)	199(48)	17(37)	5(38)	–86(38)
Tm1	190(7)	120(6)	156(6)	–10(4)	–44(4)	–33(4)
Tm2	187(6)	122(6)	176(6)	–18(4)	–46(4)	–31(4)
Se1	196(10)	136(10)	149(10)	–19(7)	–33(8)	–52(7)
Se2	230(11)	154(10)	184(10)	–37(8)	–65(8)	–42(7)
Se3	208(10)	116(9)	158(10)	–29(7)	–44(8)	–33(7)
O1	233(64)	260(68)	17(55)	–2(49)	–49(48)	–18(52)
O2	227(65)	100(57)	263(78)	–17(55)	–76(58)	25(48)
O3	293(70)	443(88)	105(64)	–187(61)	95(53)	–222(65)
O4	264(65)	55(53)	163(63)	–8(46)	–69(53)	–16(46)
O5	276(67)	98(58)	253(73)	–68(50)	–99(57)	–35(49)
O6	165(25)	145(45)	165(43)	4(37)	–67(37)	–35(34)
O7	301(73)	491(93)	106(66)	135(65)	–129(60)	–190(68)
O8	275(70)	232(67)	124(66)	–25(54)	106(54)	–119(56)
O9	427(76)	96(60)	188(71)	41(50)	–56(61)	–46(52)

Table 3.5.1.c: continued

Atoms	U_{11}	U_{22}	U_{33}	U_{23}	U_{13}	U_{12}
Yb1	89(2)	97(2)	92(2)	–19(1)	–18(1)	–35(1)
Yb2	85(2)	101(2)	103(2)	–23(1)	–15(1)	–35(1)
Se1	103(3)	109(3)	79(3)	–26(3)	–5(3)	–44(3)
Se2	126(3)	116(3)	97(3)	–33(3)	–26(3)	–45(3)
Se3	95(3)	95(3)	88(3)	–24(3)	–15(3)	–34(3)
O1	106(23)	219(27)	137(26)	–55(22)	–14(20)	–81(21)
O2	215(26)	84(23)	118(25)	–19(19)	–46(21)	–11(20)
O3	180(25)	100(23)	147(26)	–29(20)	–22(21)	–29(20)
O4	120(23)	213(27)	115(25)	–75(21)	–22(19)	–62(20)
O5	217(27)	96(24)	151(27)	–10(20)	–62(22)	–32(20)
O6	110(23)	220(27)	163(28)	–51(22)	2(20)	–74(21)
O7	106(23)	235(28)	140(26)	–18(22)	–62(20)	–49(21)
O8	172(25)	234(28)	104(26)	–58(22)	34(21)	–106(22)
O9	273(29)	96(24)	202(30)	5(21)	–40(24)	–45(21)
Lu1	153(4)	132(4)	128(4)	–16(3)	–30(3)	–48(3)
Lu2	154(4)	135(4)	140(4)	–20(3)	–31(3)	–48(3)
Se1	167(8)	142(8)	121(8)	–26(6)	–21(6)	–63(6)
Se2	199(8)	168(8)	146(8)	–34(6)	–54(6)	–63(6)
Se3	162(8)	122(8)	127(8)	–23(6)	–27(6)	–51(6)
O1	226(57)	164(54)	51(49)	–67(42)	4(42)	–15(44)
O2	213(58)	271(64)	232(66)	–169(54)	–55(51)	–102(50)
O3	170(56)	212(62)	318(77)	–100(56)	–98(46)	–57(47)
O4	192(56)	281(65)	129(57)	84(49)	–58(45)	–107(50)
O5	281(60)	104(51)	114(54)	–15(42)	–78(47)	–22(44)
O6	289(63)	64(50)	156(58)	37(42)	–30(43)	–42(44)
O7	196(55)	88(50)	116(54)	21(42)	–30(43)	46(41)
O8	291(63)	133(54)	221(66)	–22(49)	–39(51)	–11(46)
O9	222(61)	313(69)	173(63)	–74(53)	121(49)	–169(53)

[b] defined as temperature factor according to: $\exp[-2\pi^2(a^{*2}h^2U_{11} + b^{*2}k^2U_{22} + c^{*2}l^2U_{33} + 2b^*c^*klU_{23} + 2a^*c^*hlU_{13} + 2a^*b^*hkU_{12})]$

Table 3.5.1.d: Selected internuclear distances (d/pm) and angles (∢/deg) in $M_2[SeO_3]_3$ (M = Y; Sm – Lu)

$M_2[SeO_3]_3$	Y d / pm	Sm d / pm	Eu d / pm	Gd d / pm	Tb d / pm
M1 – O3	218.9	231.8	224.3	223.7	221.6
– O2	223.6	235.7	230.0	226.9	230.4
– O5	228.7	241.2	234.3	231.4	232.4
– O8	230.2	241.9	236.2	235.3	233.6
– O6	233.5	242.0	237.7	239.5	236.0
– O1	236.9	247.4	241.8	241.4	238.4
– O7	244.1	247.5	249.1	246.4	246.7
– O5′		258.1			
M2 – O1	226.6	236.0	228.9	226.4	227.5
– O9	229.8	236.4	233.6	231.9	230.3
– O7	231.0	237.3	237.2	234.6	233.6
– O4	232.2	242.4	237.2	237.1	235.2
– O2	237.7	252.7	243.9	246.2	239.7
– O4′	242.8	253.9	251.0	250.1	246.7
– O5	251.2	259.7	254.8	252.6	253.3
– O6	257.6	261.1	258.2	257.9	257.7
– O3		271.1			
Se1 – O9	164.3	167.5	164.1	166.2	165.9
– O1	169.0	168.5	174.1	176.2	172.6
– O7	171.6	173.7	175.3	176.4	173.5
Se2 – O8	165.9	164.8	166.7	168.2	165.0
– O4	171.1	171.0	172.0	174.5	170.2
– O6	174.9	172.4	173.6	173.8	171.3

Table 3.5.1.d: continued

$M_2[SeO_3]_3$	Y d / pm	Sm d / pm	Eu d / pm	Gd d / pm	Tb d / pm
Se3 – O3	166.5	168.7	166.0	164.3	166.1
– O2	171.0	169.4	169.7	166.3	171.0
– O5	172.2	170.6	172.2	168.8	171.0

Table 3.5.1.d: Continued

$M_2[SeO_3]_3$	Dy d / pm	Ho d / pm	Tm d / pm	Yb d / pm	Lu d / pm
M1 – O3	220.1	220.0	217.7	216.0	218.0
– O2	228.9	227.2	224.1	224.7	223.5
– O5	231.4	230.0	228.2	226.7	224.8
– O8	232.0	230.7	228.2	227.2	227.8
– O6	234.5	235.0	229.4	229.3	229.2
– O1	237.4	236.0	234.2	232.3	230.6
– O7	245.8	244.0	240.9	243.0	238.8
M2 – O1	227.1	225.4	221.2	222.7	220.4
– O9	230.2	227.4	224.3	224.7	225.2
– O7	232.1	232.3	229.4	228.3	228.9
– O4	234.5	232.7	230.9	229.1	229.0
– O2	238.7	237.6	234.9	234.6	231.8
– O4′	246.2	244.2	241.6	240.9	239.9
– O5	252.6	251.6	251.0	250.8	247.2
– O6	258.0	255.3	258.2	258.0	257.1
Se1 – O9	165.9	166.8	167.7	165.1	164.1
– O1	171.3	171.9	172.2	171.1	172.9
– O7	173.2	172.8	172.8	172.1	173.6

Table 3.5.1.d: Continued

$M_2[SeO_3]_3$	Dy d / pm	Ho d / pm	Tm d / pm	Yb d / pm	Lu d / pm
Se2 – O8	166.1	165.2	166.3	166.9	165.3
– O4	169.2	170.5	171.6	170.6	170.4
– O6	170.6	170.6	171.7	171.0	170.6
Se3 – O3	166.2	165.4	165.3	165.4	164.6
– O2	170.3	171.1	170.0	170.2	170.3
– O5	170.4	171.9	172.8	170.5	173.0

Table 3.5.1.d: Continued

$M_2[SeO_3]_3$	Y ∢ / grd	Sm ∢ / grd	Eu ∢ / grd	Gd ∢ / grd	Tb ∢ / grd
O1 – Se1 – O8	87.4	96.3	88.6	89.7	90.6
O6 – Se1 – O1	103.9	104.8	101.2	100.7	101.2
O8 – Se1 – O6	104.2	105.8	105.5	105.4	103.8
O5 – Se2 – O2	94.1	96.7	95.8	94.3	96.5
O3 – Se2 – O5	102.6	103.5	104.0	104.4	105.1
O2 – Se2 – O2	103.7	108.1	104.5	105.7	106.1
O7 – Se3 – O4	93.9	94.5	95.3	99.5	98.6
O9 – Se3 – O4	105.2	103.6	105.1	104.3	104.0
O7 – Se3 – O9	107.7	104.0	105.5	106.2	104.2

Table 3.5.1.d: Continued

$M_2[SeO_3]_3$	Dy ∢ / grd	Ho ∢ / grd	Tm ∢ / grd	Yb ∢ / grd	Lu ∢ / grd
O1 – Se1 – O8	87.7	88.7	89.6	88.5	99.9
O6 – Se1 – O1	101.2	101.2	101.4	101.3	101.4
O8 – Se1 – O6	104.0	103.9	104.5	103.9	105.1
O5 – Se2 – O2	95.4	96.4	97.5	98.4	97.2
O3 – Se2 – O5	105.1	105.8	105.8	105.7	105.3
O2 – Se2 – O2	105.6	106.1	106.0	105.8	105.7
O7 – Se3 – O4	93.9	95.4	97.3	94.3	95.1
O9 – Se3 – O4	104.1	104.0	103.5	103.2	105.4
O7 – Se3 – O9	104.3	104.3	104.3	104.5	106.7

Table 3.5.1.e: Motifs of mutual adjunction in $M_2[SeO_3]_3$ (M = Y; Sm – Lu)

	O1	O2	O3	O4	O5	O6	O7	O8	O9	CN
Sm1	1 / 1	1 / 1	1 / 1	0 / 0	2 / 2	1 / 1	1 / 1	1 / 1	0 / 1	8
Sm2	1 / 1	1 / 1	1 / 1	2 / 2	1 / 1	1 / 1	0 / 0	1 / 1	1 / 1	9
Se1	0 / 0	0 / 0	0 / 0	0 / 0	1 / 1	1 / 1	0 / 0	1 / 1	0 / 0	3
Se2	1 / 1	0 / 0	1 / 1	0 / 0	0 / 0	0 / 0	0 / 0	0 / 0	1 / 1	3
Se3	0 / 0	1 / 1	0 / 0	1 / 1	0 / 0	0 / 0	1 / 1	0 / 0	0 / 1	3
CN	3	3	3	3	3	3	2	3	4	
	O1	O2	O3	O4	O5	O6	O7	O8	O9	CN
M1	1 / 1	1 / 1	1 / 1	1 / 1	1 / 1	0 / 0	0 / 0	1 / 1	1 / 1	7
M2	1 / 1	1 / 1	0 / 0	1 / 1	1 / 1	1 / 1	2 / 2	1 / 0	0 / 0	8
Se1	1 / 1	0 / 0	0 / 0	0 / 0	0 / 0	1 / 1	0 / 0	1 / 1	0 / 0	3
Se2	0 / 0	1 / 1	1 / 1	0 / 0	1 / 1	0 / 0	0 / 0	0 / 0	0 / 0	3
Se3	0 / 0	0 / 0	0 / 0	1 / 1	0 / 0	0 / 0	1 / 1	0 / 0	1 / 1	3
CN	3	3	2	3	3	2	3	2	2	

4 Oxide oxoselenates(IV) of the trivalent rare-earth elements

4.1 Prefaces and synthesis methods

Among different other formula types *(e.g.* M_2SeO_5, $M_2Se_{1.5}O_6$, $M_2Se_3O_9$, $M_2Se_{3.5}O_{10}$ and $M_2Se_4O_{11}$ [6, 10, 30, 90 – 92]) the existence of phases with the composition $M_2Se_2O_7$ in the phase diagrams of the systems M_2O_3/SeO_2 (M = rare-earth element) has been pointed out by many authors a moment ago [93 – 95]. In spite of some arguments over their thermodynamic stability [21 – 26], thermogravimetric studies, supported by IR and X-ray powder diffraction measurements, verified this beyond doubt. Although these $M_2Se_2O_7$-type compounds have been often obtained at temperatures of about 800°C, details concerning their crystal structure were not available so far. The unambiguous presence of discrete anionic selenite units ($[SeO_3]^{2-}$) suggested their formulation as rare-earth(III) oxide oxoselenate(IV) with lonesome O^{2-} anions which are not bonded to any selenium atom according to $M_2O[SeO_3]_2$. A phase with a similar situation in the homologous M_2O_3/TeO_2 system has already been described recently for the oxotellurate(IV) $Pr_2Te_2O_7$ [33] as adopting the *pyrochlore*-type crystal structure (cubic, space group: $Fd\bar{3}m$) according to $Pr_2O(TeO_3)_2$. In this case, the non-tellurium bonded oxide anions form a three-dimensional network $^3_\infty\{[OPr_{4/2}]^{4+}\}$ of vertex-shared $[OPr_4]^{10+}$ tetrahedra with *anti-cristobalite*-type topology which interpenetrates a complementary network $^3_\infty\{([TeO_{6/2}]^{2-})_2\}$ of vertex-shared $[TeO_6]^{8-}$ octahedra with the *pyrochlore*-type pattern. The missing stereochemical effect of the non-binding "lone-pair" electrons at the Te^{4+} cations was nevertheless surprising, but yet impossible to transfer to the analogous oxochalcogenates(IV) $M_2Se_2O_7$ with the lighter homologue selenium. Among transition metal elements, phases also containing additional O^{2-} anions and $[SeO_3]^{2-}$ units have been identified in the last decade, namely $Fe_2O(SeO_3)_2$ [31], $Au_2O(SeO_3)_2$ [32], $Mn^{II}Mn^{III}O(SeO_3)_3$ [95], $Cu_2O(SeO_3)$-I and $Cu_2O(SeO_3)$-II [96], $Cu_4O(SeO_3)_3$-I and $Cu_4O(SeO_3)_3$-II [96]. The coordination number of the oxo-oxygen atoms in these compounds are 3, 2, 3 and 4, respectively, and no close structural relationships exist among them. Very recently, a simple method to synthesize $Tb_2Se_2O_7$ as single-crystalline material and its (one-dimensional) structural solution as $Tb_2O[SeO_3]_2$ in terms of a description emphasizing infinite strands of *trans*-edge sharing oxygen-centered terbium tetrahedra and "lone pair" channels as a result of the stereochemical activity of the non-binding electrons of the discrete

oxoselenate(IV) entities was reported [97]. This is therefore extended in this work to other lanthanide elements so that many rare-earth oxide oxoselenates(IV) with the formula $M_2O[SeO_3]_2$ (M = Sm – Tm) are characterized as isostructural to $Tb_2O[SeO_3]_2$.

It was possible to synthesize $M_2Se_2O_7$ from stoichiometric mixtures (molar ratio: 2:1:2) of M_2O_3, MBr_3 and SeO_2 handled under the inert argon atmosphere of a glove box in the presence of an excess of CsBr as flux. Terbium powder was additionally used for the mixed-valent Tb_4O_7 oxide. The reaction schemes are depicted below.

$$3\ Tb_4O_7 + 14\ SeO_2 + 2\ Tb \longrightarrow 7\ Tb_2O[SeO_3]_2 \qquad (5)$$

$$2\ M_2O_3 + MBr_3 + 2\ SeO_2 \longrightarrow M_2O[SeO_3]_2 + 3\ MOBr\ (M = Sm – Gd, Dy – Tm) \qquad (6)$$

The starting materials were mixed, thoroughly ground together and filled into silica vessels. Those glass tubes were evacuated and torch-sealed under vacuum (10^{-3} mbar) before they were heated up to 850°C for seven days. With a decreasing temperature rate of 0.1°C/min the subsequent cooling proceeded slowly until 500°C and the furnace was then just turned off to allow the sample to cool down to room temperature. The best results in terms of growing needle-shaped single crystals, which turned out to be insensitive to water and air, were obtained this way. Certain percentages of MOBr were always detectable as by-products. A suitable single crystal of $M_2Se_2O_7$ (≡ $M_2O[SeO_3]_2$; M = Sm – Tm) was selected and mounted on a κ-CCD diffractometer (Nonius, Delft/NL). A primitive tetragonal unit cell was determined for all those compounds and the data analysis indicated $P4_2/ncm$ as correct space group. Crystal data and details of the data collection are given in part 4.2.1. Direct methods and difference-*Fourier* cycling were then used to locate the different light atoms in the unit cell. Positional and anisotropic thermal displacement parameters obtained from the final full-matrix least-squares refinements, important internuclear distances and angles and finally the motifs of mutual adjunction in the $M_2O[SeO_3]_2$ series are also outlined in section 4.2.1.

4.2 Structure description of $M_2O[SeO_3]_2$ (M = Sm – Tm)

The tetragonal crystal structure of $M_2Se_2O_7$ (space group: $P4_2/ncm$) contains only a single crystallographic site for the M^{3+} cations *(8h,* site symmetry: *..2).* From Sm^{3+} ($r(Sm^{3+})$ = 121.9 pm) up to the small Tm^{3+} ($r(Tm^{3+})$ = 113.4 pm), the coordination polyhedra are very similar

and can be regarded as a square antiprism with M–O distances ranging from 229 – 260 pm for Sm through 224 – 253 pm for Dy up to 221 – 249 pm for Tm (fig. 4.2.a and table 4.2.1.d). Figure 3.2.a *(left)* displays the connectivity of these [MO_8] polyhedra among each other, showing that the *ipso*-polyhedron shares common oxygen edges (one O1–O1, four O1–O3 and one O2–O2) with six neighbouring ones with rather short non-bonding M–M distances varying from 385 pm for the light samarium through 367 pm for the dysprosium up to 362 pm for the heavy thulium compound. From this point of view the behaviour resembles the interconnection of the cube-like [PrO_8] polyhedra in $Pr_2Te_2O_7$ [33]. Furthermore, six trigonal non-planar $[SeO_3]^{2-}$ groups belong to each [MO_8] antiprism (fig. 4.2.a, *right)* and coordinate the central cation via six vertices exclusively.

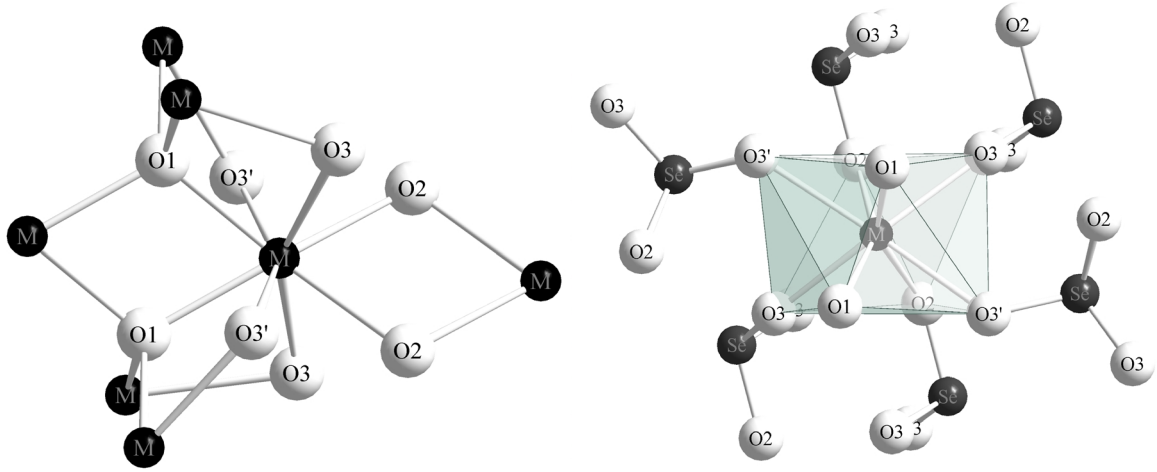

Fig. 4.2.a: Oxygen coordination about M^{3+} showing that six edges of the square antiprism (CN = 8) are bridging a central polyhedron with their six neighbouring ones (*left*) and coordination polyhedron about M^{3+} with six terminal $[SeO_3]^{2-}$ groups and two $(O1)^{2-}$ anions (*right*) in the crystal structure of $M_2O[SeO_3]_2$ (M = Sm – Tm)

Again short but non-bonding M–Se distances (364 – 390 pm) occur. The coordination about the selenium atoms is ψ^1-tetrahedral ($[SeO_3E]^{2-}$; *E*: *non*-binding electron pair, "*lone pair*") with Se–O distances ranging from 169 to 172 pm and angles ($\sphericalangle$(O–Se–O)) within a 102 – 106° span. The isolated trigonal non-planar $[SeO_3]^{2-}$ anions (distance from Se to the O2–O3-O3 plane: 72 pm) exhibit almost C_{3v} symmetry (site symmetry of Se in *8i: ..m)* and are surrounded by six M^{3+} cations each (fig. 4.2.b, *left)*. Whereas six oxygen atoms (O2 and O3) of the M^{3+} coordination sphere belong to six terminal $[SeO_3]^{2-}$ anions, comparable to those observed in the *buetschliite*-type minerals ($K_2Ca[SeO_3]_2$ [98, 99], $K_2Mg[SeO_3]_2$ [100],

$K_2Co[SeO_3]_2$ and $K_2Mn[SeO_3]_2$ [101]), the remaining two (O1) are not bonded to selenium at all. Their coordination sphere actually consists of four M^{3+} cations arranged as tetrahedron with O–M distances in the range of 221 – 230 pm (4×), M–M edge-lengths of 362 – 385 pm (6×) and ∢(M–O1–M) angles between 109 and 110° for the eight aforesaid compounds (see table 4.2.1.d and figure 4.2.b, *right).*

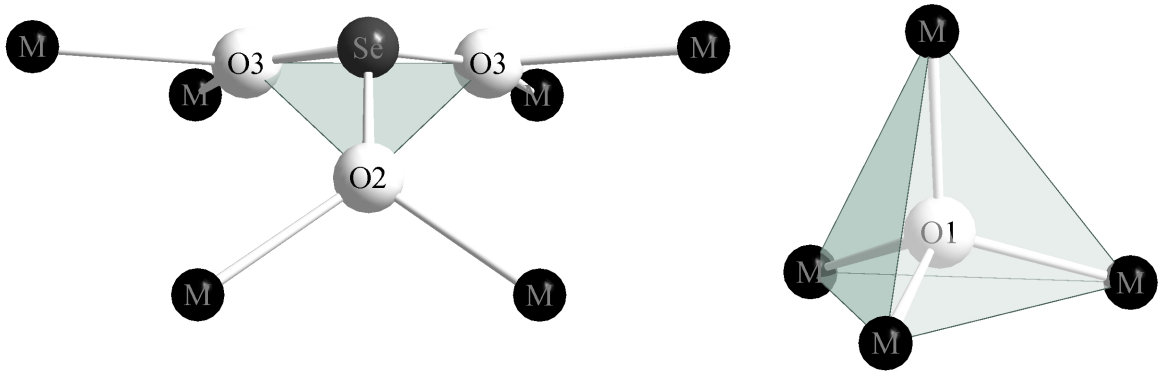

Fig. 4.2.b: Coordination sphere of six terminal M^{3+} cations about the trigonal pyramidal $[Se(O2)(O3)_2]^{2-}$ anion (*left*) and tetrahedron of four M^{3+} cations about an $(O1)^{2-}$ anions (*right*) in $M_2O[SeO_3]_2$ (M = Sm – Tm)

These $[OM_4]^{10+}$ tetrahedra (site symmetry of O1 in *4b:* $\bar{4}$*..)* form infinite one-dimensional $^1_\infty\{[OM_{4/2}]^{4+}\}$ chains along [001] by sharing *trans*-oriented edges (fig. 4.2.c, *above)* which are packed such that a central strand is quadratically surrounded in (001) projection by four close chains at a distance of $a/\sqrt{2}$ and another square of four more of them which are rotated by 45° and further apart by a factor of $\sqrt{2}$ (≡ value of the a axis; see figure 4.2.c, *below).* The $^1_\infty\{[OM_2]^{4+}\}$ chains exhibit two tetrahedra within the identity period and no rotation of anion-centered tetrahedra about axes normal to the extension of the chain is observed. The O–M distances within the $[OM_4]$ tetrahedra units decrease from 229 pm (4×) (M = Sm) through 226 pm (4×) (M = Tb) up to 222 pm (4×) (M = Tm). Consequently, the unit cell constants shrink (2.5% for the a-axis and 2.3% for the c-axis) from the Sm to the Tm compound. In the same way, the M–M edge-lengths deminish from 374.5 pm (6×) for the large samarium via 369.3 pm (6×) for terbium up to 361.8 pm (6×) for the smaller thulium. This contraction phenomenon is shown best in diagram 4.2.1 where the $M_2O[SeO_3]_2$ (M = Sm – Tm) lattice constants versus the M^{3+} radiis are plotted. Of course this reveals what the "lanthanide

contraction" demands. Additionnally, a comparison of the c/a ratios reveals an expected trend: these are almost constant for the eight investigated compounds (table 4.3.1.a).

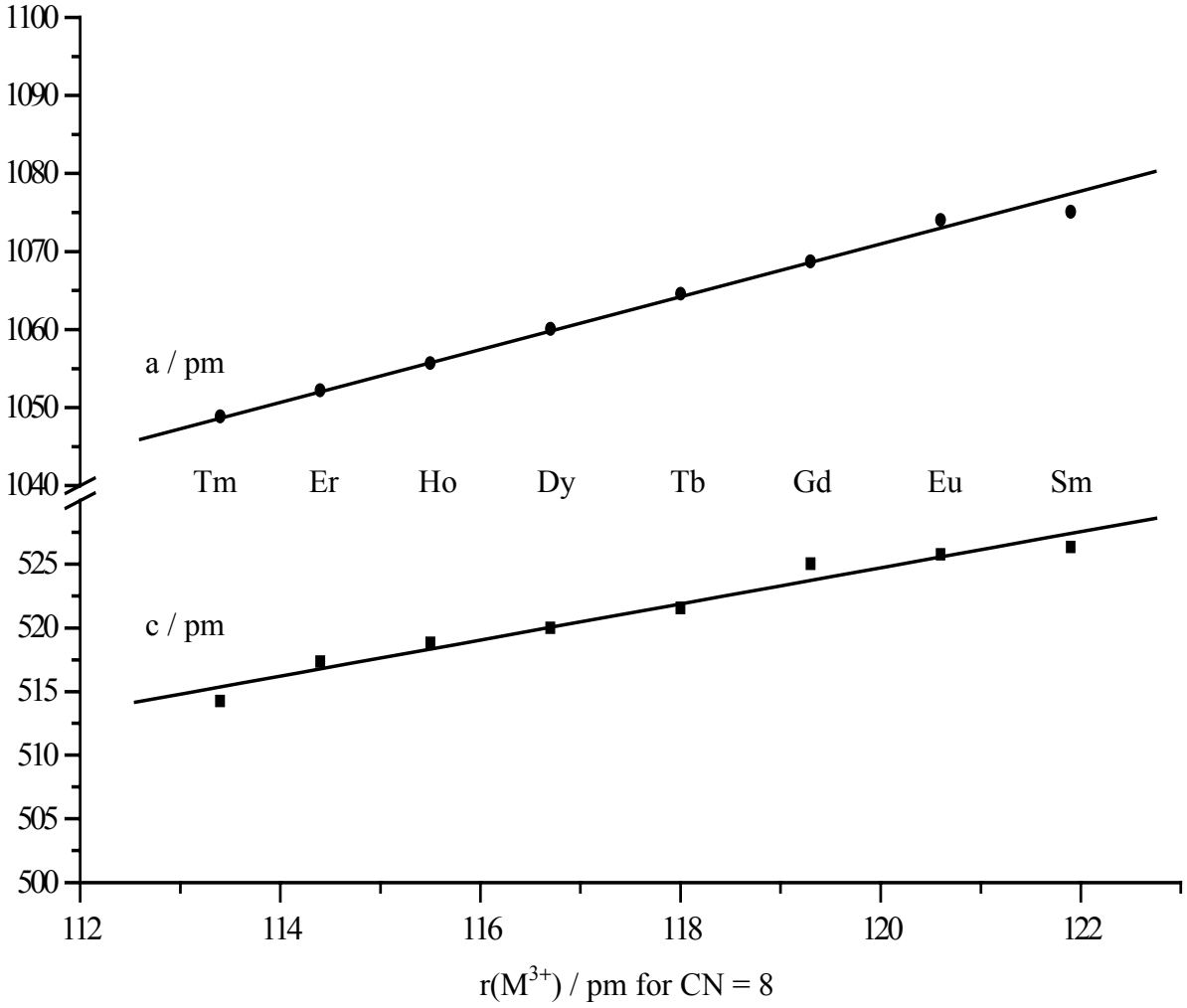

Diagram 4.2.1: Lattice constants of rare-earth(III) oxides oxoselenates(IV) $M_2O[SeO_3]_2$ (M = Sm – Tm) versus rare-earth(III) ionic radiis [87]

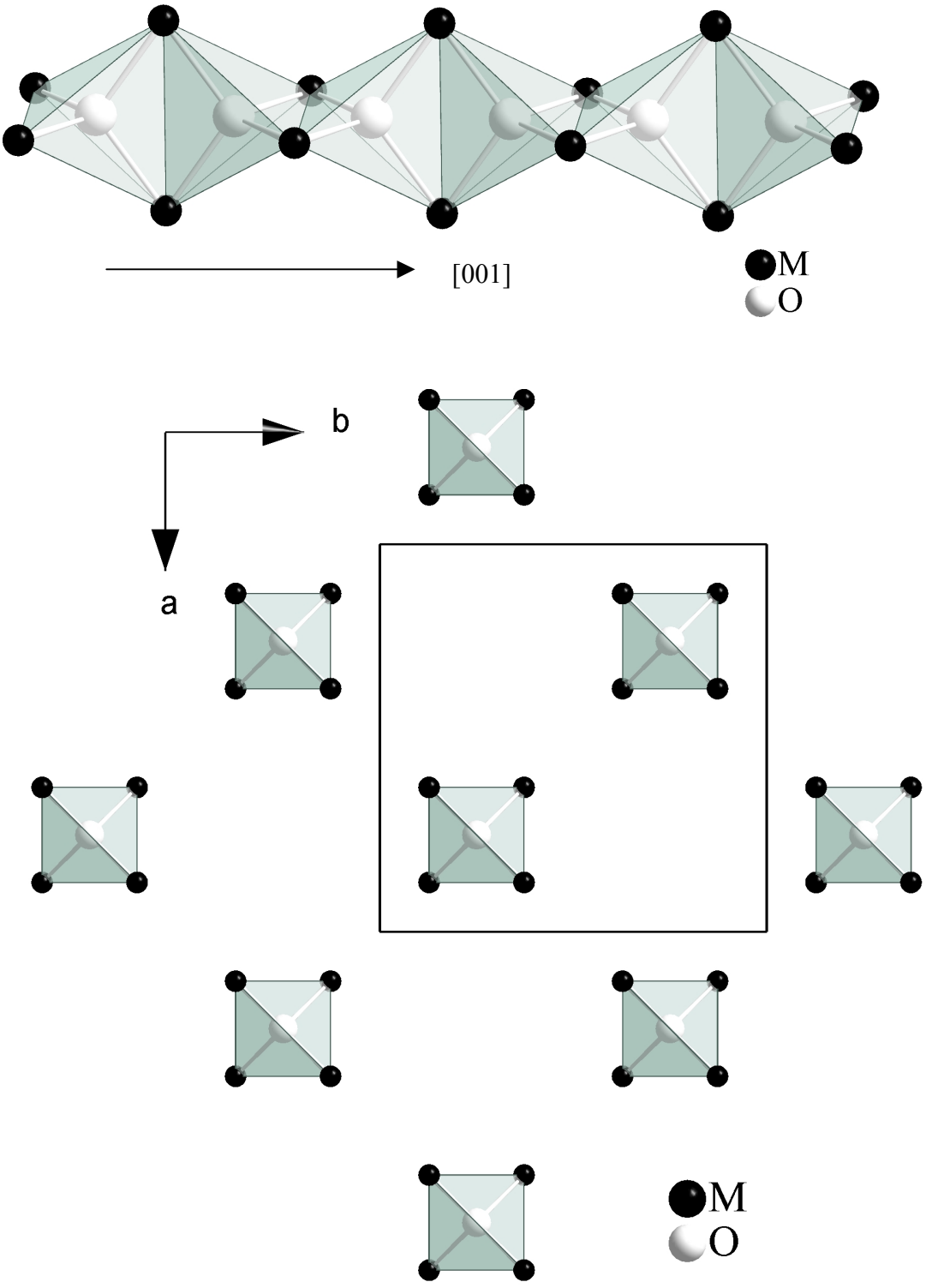

Fig. 4.2.c: $^{1}_{\infty}\{[OM_{4/2}]^{4+}\}$ chain of *trans*-edge connected $[(O1)M_4]$ tetrahedra along [001] (*above*) and quadratic rod-packing of these strands in (001) projection (*below*) in $M_2O[SeO_3]_2$ (M = Sm – Tm)

Because of the regularities of all observed distances (see table 4.3.1.d), no distortion is found among the $[OM_4]$ tetrahedra and even the $^{1}_{\infty}\{[OM_{4/2}]^{4+}\}$ chains in the eight investigated compounds. Charge balance and three-dimensional interconnection of this particular rod-packing occurs via discrete trigonal $[SeO_3]^{2-}$ pyramids. Each motif of the chain is thus surrounded by eight $[SeO_3]^{2-}$ groups to form the complex anionic chain $^{1}_{\infty}\{(OM_{4/2})[SeO_3]_{8/2}\}^{4-}$. Due to the ψ^1-tetrahedral shape of the $[SeO_3]^{2-}$ anions, the whole crystal structure gets strongly influenced by the stereochemical "lone-pair" activity of these groups. This provides the second main structural feature of $M_2Se_2O_7$ ($\equiv M_2O[SeO_3]_2$) series: empty channels along [001] obviously occupied by the non-binding "lone-pair" electrons at the Se^{4+} cations of the $[SeO_3]^{2-}$ units (fig. 4.2.d). Remarkably enough, the $\bar{4}$ symmetry of the $^{1}_{\infty}\{[OM_{4/2}]^{4+}\}$ chains is thereby perfectly repeated by these "lone-pair" channels.

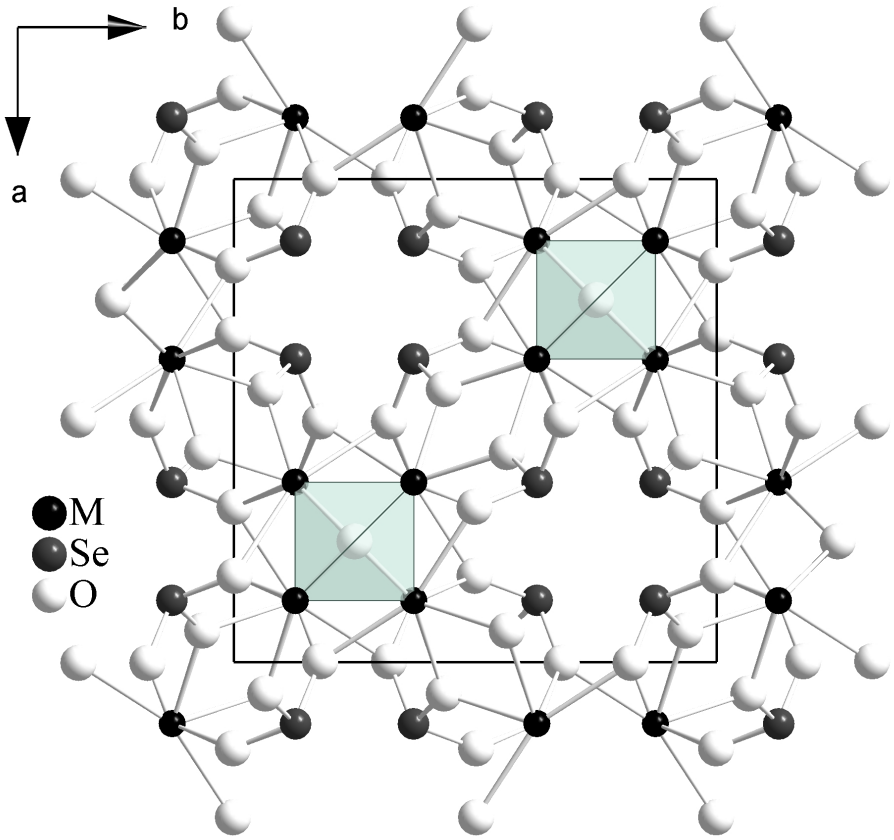

Fig. 4.2.d: Presentation of the whole crystal structure of $M_2O[SeO_3]_2$ as (001) projection emphasizing the $^{1}_{\infty}\{[OM_{4/2}]^{4+}\}$ strands and the "*lone-pair*" channels along [001] formed by the stereochemical active *non*-binding electron pairs at the Se^{4+} cations

4.3 Structural data for $M_2O[SeO_3]_2$ (M = Sm – Tm)

Table 4.3.1.a: Crystallographic data for $M_2O[SeO_3]_2$ (M = Sm – Tm)

M		Sm	Eu	Gd	Tb
Crystal system and Space group		tetragonal, $P4_2/ncm$ (no. 138)			
Formula unit per unit cell (Z)		4			
Unit cell parameters:	a / pm =	1075.07(15)	1074.05(7)	1068.73(6)	1064.57(8)
	c / pm =	526.35(7)	525.77(3)	525.03(2)	521.56(4)
	c/a =	0.490	0.490	0.491	0.490
Calculated density (D_x / g · cm^3)		6.230	6.284	6.473	6.605
Molar volume (V_m / cm^3 · mol^{-1})		89.532(4)	89.321(5)	88.999(3)	88.989(8)
Diffractometer, radiation		κ-CCD (Fa. Nonius); Mo-K_α: λ = 71.07 pm			
$2\theta_{max.}$		55.0	55.1	55.0	54.9
Index ranges:	$\pm h_{max} = \pm k_{max} / \pm l_{max}$ =	13 / 6	13 / 6	13 / 6	13 / 6
F(000)		992	1000	1008	1016
Absorption coefficients (μ / mm^{-1})		31.07	32.48	34.05	36.03
Absorption correction		Numerical, after crystal shape optimization with the program X-SHAPE [53]			
Other data corrections		background, polarization, *Lorentz* factors			
Collected reflections		5525	5759	7893	7331
Unique reflections		378	377	371	369
R_{int}		0.118	0.063	0.078	0.079
R_σ		0.048	0.024	0.028	0.025
Reflections with $\|F_o\| \geq 4\sigma\|F_o\|$		303	338	317	311
Structure solution and refinement		Program system SHELX-97 [58]			
Scattering factors		International Tables, Vol. C [85]			
R_1		0.088	0.034	0.052	0.036
R_1 with $\|F_o\| \geq 4\sigma\|F_o\|$		0.066	0.028	0.040	0.024
wR_2		0.161	0.074	0.078	0.045
Goodness of fit (GooF)		1.249	1.155	1.280	1.100
Extinction (g)		0.0023(3)	0.0014(3)	0.0019(1)	0.0012(1)
Residual electron density	max.	1.88	1.31	1.61	0.75
(ρ / e$^-$ 10^6 pm)	min.	–1.58	–1.41	–1.23	–0.93

Table 4.3.1.a: continued

M		Dy	Ho	Er	Tm
Crystal system and Space group		tetragonal, $P4_2/ncm$ (no. 138)			
Formula unit per unit cell (Z)		4			
Unit cell parameters:	a / pm =	1060.07(4)	1055.70(3)	1052.20(6)	1048.87(5)
	c / pm =	520.00(2)	518.80(1)	517.35(2)	514.25(4)
	c/a =	0.490	0.491	0.491	0.490
Calculated density (D_x / g · cm^3)		6.762	6.890	7.009	7.136
Molar volume (V_m / cm^3 · mol^{-1})		88.675(2)	87.996(2)	87.654(8)	87.213(5)
Diffractometer, radiation		κ-CCD (Fa. Nonius); Mo-K_α: λ = 71.07 pm			
$2\theta_{max.}$		54.9	60.0	54.9	55.0
Index range	$\pm h_{max} = \pm k_{max} / \pm l_{max}$ =	13 / 6	14 / 7	13 / 6	13 / 6
F(000)		1024	1032	1040	1048
Absorption coefficients (μ / mm^{-1})		37.82	39.74	41.80	44.01
Absorption correction		Numerical, after crystal shape optimization with the program X-SHAPE [53]			
Other data corrections		background, polarization, *Lorentz* factors			
Collected reflections		6948	10030	6421	7222
Unique reflections		365	455	359	353
R_{int}		0.097	0.070	0.128	0.077
R_σ		0.029	0.024	0.039	0.026
Reflections with $\|F_o\| \geq 4\sigma\|F_o\|$		320	411	315	309
Structure solution and refinement		Program system SHELX-97 [58]			
Scattering factors		International Tables, Vol. C [85]			
R_1		0.048	0.070	0.047	0.052
R_1 with $\|F_o\| \geq 4\sigma\|F_o\|$		0.040	0.032	0.039	0.039
wR_2		0.087	0.070	0.107	0.066
Goodness of fit (GooF)		1.258	1.296	1.220	1.260
Extinction (g)		0.0307(5)	0.0288(6)	0.0013(5)	0.0013(4)
Residual electron density	max.	2.17	2.30	2.79	1.11
(ρ / e$^-$ 10^6 pm)	min.	–3.48	–2.99	–1.81	–1.32

Table 4.3.1.b: Atomic coordinates for $M_2O[SeO_3]_2$ (M = Sm – Tm)

Atoms	Wyckoff Position	x / a	y / b	z / c
Sm	8h	0.62667(6)	–x / a	0
Se	8i	0.8720(1)	x / a	0.9655(4)
O1	4b	3/4	1/4	3/4
O2	8i	0.934(1)	x / a	0.694(3)
O3	16j	0.9996(9)	0.678(1)	0.123(2)
Eu	8h	0.62687(2)	–x / a	0
Se	8i	0.87200(5)	x / a	0.9458(2)
O1	4b	3/4	1/4	3/4
O2	8i	0.9999(4)	x / a	0.1252(8)
O3	16j	0.9346(4)	0.5654(4)	0.695(1)
Gd	8h	0.62709(3)	–x / a	0
Se	8i	0.87192(7)	x / a	0.9670(3)
O1	4b	3/4	1/4	3/4
O2	8i	0.9348(5)	x / a	0.694(1)
O3	16j	0.0002(5)	0.6779(6)	0.124(1)
Tb	8h	0.12738(2)	–x / a	0
Se	8i	0.12798(5)	x / a	0.5352(1)
O1	4b	3/4	1/4	3/4
O2	8i	0.0645(4)	x / a	0.8082(9)
O3	16j	0.0011(4)	0.6788(4)	0.1253(8)
Dy	8h	0.62758(3)	–x / a	0
Se	8i	0.87204(7)	x / a	0.9647(4)
O1	4b	3/4	1/4	3/4
O2	8i	0.9360(5)	x / a	0.692(1)
O3	16j	0.0015(5)	0.6788(5)	0.125(1)

Table 4.3.1.b: continued

Atoms	Wyckoff Position	x / a	y / b	z / c
Ho	8h	0.62781(2)	–x / a	0
Se	8i	0.87200(5)	x / a	0.9649(3)
O1	4b	3/4	1/4	3/4
O2	8i	0.9361(3)	x / a	0.692(1)
O3	16j	0.0017(3)	0.67963)	0.1274(7)
Er	8h	0.62804(3)	–x / a	0
Se	8i	0.87192(8)	x / a	0.9643(4)
O1	4b	3/4	1/4	3/4
O2	8i	0.9354(6)	x / a	0.691(2)
O3	16j	0.0024(6)	0.6795(6)	0.128(1)
Tm	8h	0.12804(4)	–x / a	0
Se	8i	0.12781(9)	x / a	0.5347(3)
O1	4b	3/4	1/4	3/4
O2	8i	0.0647(8)	x / a	0.809(2)
O3	16j	0.9972(7)	0.1796(8)	0.372(1)

Table 4.3.1.c: Anisotropic thermal displacement parameters[b)] (U_{ij}/pm^2) for $M_2O[SeO_3]_2$ (M = Sm – Tm)

Atoms	U_{11}	U_{22}	U_{33}	U_{23}	U_{13}	U_{12}
Sm	172(8)	= U_{11}	176(8)	16(4)	= U_{23}	26(5)
Se	128(9)	= U_{11}	178(11)	26(6)	= U_{23}	36(9)
O1	225(64)	= U_{11}	153(103)	0	0	0
O2	250(54)	= U_{11}	113(73)	117(45)	= U_{23}	–113(67)
O3	255(63)	236(61)	195(55)	23(45)	–18(47)	45(48)
Eu	112(3)	= U_{11}	100(3)	3(1)	= U_{23}	14(2)
Se	96(4)	= U_{11}	117(4)	–7(2)	= U_{23}	7(3)
O1	127(21)	= U_{11}	80(37)	0	0	0
O2	201(22)	= U_{11}	133(29)	–35(17)	= U_{23}	–9(23)
O3	182(18)	161(21)	167(22)	–29(18)	–25(17)	–4(16)
Gd	105(3)	= U_{11}	105(4)	6(2)	= U_{23}	14(3)
Se	78(4)	= U_{11}	121(5)	12(3)	= U_{23}	8(6)
O1	114(31)	= U_{11}	94(49)	0	0	0
O2	159(27)	= U_{11}	93(37)	19(22)	= U_{23}	–21(35)
O3	206(34)	148(32)	151(29)	7(24)	17(24)	–31(26)
Tb	110(2)	= U_{11}	134(2)	–7(1)	= U_{23}	14(2)
Se	82(3)	= U_{11}	160(4)	15(2)	= U_{23}	–9(4)
O1	174(22)	= U_{11}	60(34)	0	0	0
O2	169(18)	= U_{11}	106(27)	33(16)	= U_{23}	7(25)
O3	231(25)	156(23)	170(22)	26(17)	–24(18)	–11(18)
Dy	108(4)	= U_{11}	98(4)	4(1)	= U_{23}	13(2)
Se	91(6)	= U_{11}	114(6)	13(3)	= U_{23}	–1(5)
O1	155(31)	= U_{11}	47(48)	0	0	0
O2	171(25)	= U_{11}	123(39)	12(21)	= U_{23}	20(31)
O3	227(30)	126(27)	118(28)	9(22)	–36(22)	–12(22)

Table 4.3.1.c: continued

Atoms	U_{11}	U_{22}	U_{33}	U_{23}	U_{13}	U_{12}
Ho	91(2)	= U_{11}	74(3)	2(1)	= U_{23}	11(1)
Se	78(4)	= U_{11}	95(4)	9(2)	= U_{23}	6(3)
O1	112(19)	= U_{11}	39(33)	0	0	0
O2	138(15)	= U_{11}	85(23)	23(14)	= U_{23}	–9(20)
O3	169(19)	109(17)	125(18)	5(14)	–34(14)	21(15)
Er	142(4)	= U_{11}	78(5)	3(1)	= U_{23}	9(2)
Se	138(6)	= U_{11}	94(7)	11(3)	= U_{23}	4(5)
O1	93(32)	= U_{11}	102(58)	0	0	0
O2	195(28)	= U_{11}	83(39)	18(23)	= U_{23}	36(36)
O3	220(33)	199(32)	103(30)	–23(26)	–21(24)	43(27)
Tm	129(3)	= U_{11}	122(4)	–10(2)	= U_{23}	13(3)
Se	90(4)	= U_{11}	150(7)	22(4)	= U_{23}	–10(7)
O1	148(40)	= U_{11}	141(70)	0	0	0
O2	218(36)	= U_{11}	52(50)	2(32)	= U_{23}	18(46)
O3	211(45)	183(42)	160(42)	14(33)	–24(34)	–15(32)

[b] defined as temperature factor according to: $\exp[-2\pi^2(a^{*2}h^2U_{11} + b^{*2}k^2U_{22} + c^{*2}l^2U_{33} + 2b^*c^*klU_{23} + 2a^*c^*hlU_{13} + 2a^*b^*hkU_{12})]$

Table 4.3.1.d: Selected internuclear distances (d/pm) and angles (∢/deg) in for $M_2O[SeO_3]_2$ (M = Sm – Tm)

$M_2O[SeO_3]_2$	Sm	Eu	Gd	Tb	Dy	Ho	Er	Tm
	d / pm	d / pm	d / pm	d / pm	d / pm	d / pm	d / pm	d / pm
M – O1 (2×)	229.1	228.6	227.5	226.0	224.9	223.8	222.9	221.9
– O2 (2×)	240.1	239.8	238.8	237.1	236.2	235.5	235.1	234.4
– O3 (2×)	247.0	245.9	245.7	243.4	242.4	241.0	239.5	238.4
– O3′ (2×)	259.1	258.5	257.0	254.8	253.5	251.9	250.8	249.5
O1 – M (4×)	229.1	228.6	227.5	226.0	224.9	223.8	222.9	221.9
Se – O3 (2×)	169.0	169.7	168.8	169.8	169.5	169.8	170.2	169.3
– O2 (1×)	171.1	171.3	171.4	171.5	171.1	170.8	170.3	169.4
	∢ / grd	∢ / grd	∢ / grd	∢ / grd	∢ / grd	∢ / grd	∢ / grd	∢ / grd
M – O1 – M (4×)	109.3	109.3	109.4	109.4	109.4	109.2	109.1	109.2
M – O1 – M' (2×)	109.9	109.8	109.5	109.5	109.5	109.6	109.7	109.6
O2 – Se – O3 (2×)	102.5	102.5	102.3	102.5	102.3	102.7	102.9	102.7
O3 – Se – O3 (1×)	105.7	105.6	105.7	105.8	105.8	105.7	105.3	105.6

Table 4.3.1.e: Motifs of mutual adjunction in $M_2O[SeO_3]_2$ (M = Sm – Tm)

	O1	O2	O3	CN
M	2 / 4	2 / 2	4 / 2	8
Se	0 / 0	1 / 1	2 / 1	3
CN	4	3	3	

5 Oxyhalide oxoselenates(IV) of the trivalent rare-earth elements

The structure of $M_3F[SeO_3]_4$ (M = Nd, Sm, Gd, Dy) [34] and $MCl[SeO_3]$ (M = Nd, Er, Ho) [36] have been reported in the recent literature, these being the only examples of anhydrous and non-hydrogenated halide oxoselenates(IV) of trivalent lanthanides obtained as single crystals. *Oppermann* and co-workers [37] revealed very recently by means of powder diffraction supported by IR spectroscopy the presence of three compounds in the system $SmOCl/SeO_2$, namely $SmClSeO_3$, $SmClSe_2O_5$, and $SmClSe_3O_7$, but their crystal structures are not elucidated. Concerning oxyhalide oxoselenates(IV), the chemistry of such systems has not been widely studied with only two known oxide compounds of copper(II) and selenium(IV), $Cu_9O_2Cl_6[SeO_3]_4$ and $Cu_5O_2Cl_2[SeO_3]_2$ [40, 41], the *francisite* mineral $Cu_3BiO_2X[SeO_3]_2$ (X = Cl, Br and I) [102] and its erbium analogue $Cu_3ErO_2Cl[SeO_3]_2$ [103] which seem to be the only oxyhalide oxoselenate(IV) containing a rare-earth element known up to the beginning of this present work. The structure of the latter compounds contains empty channels occupied by the stereochemically active lone pair of electrons at the selenium atoms. In fact, the work done in our laboratories have led to the synthesis and characterization of many novel structural types of anhydrous rare-earth oxyhalide oxoselenates(IV). The main concern regarding these compounds is that their crystal structures are quite complicated with the stereochemical lone pair effect on selenium(IV) which is assumed to act as chemical scissors for rare-earth elements and the lonesome anions O^{2-}: additional oxygen atoms, which are not bonded with selenium, but have tetrahedral coordination to rare-earth atoms forming oxocentered tetrahedral units $[OM_4]$ (M = rare-earth element). The M–O bonds are almost always shorter and stronger than M–OSe bonds. This makes reasonable consideration of homometallic $[OM_4]^{10+}$ tetrahedra as independent structural subunits in this class of compounds. The $[OM_4]$ tetrahedra, with edges or edges *and* vertices sharing produces a large variety of structural motifs, $[O_nM_m]$ (m, n are integers and n < m). Both chloride and bromide used in this part have led to isostructural compounds with comparable coordination for the two different halides.

5.1 Compounds of the formula $M_3O_2Cl[SeO_3]_2$ (M = Tb, Dy, Er)

5.1.1 Synthesis of $M_3O_2Cl[SeO_3]_2$

M_2O_3, MOCl and SeO_2 (molar ratio 1:1:2; M = Dy, Er) were inserted into an evacuated sealed silica tube and heated together at 850°C for seven days. CsCl was added to the educts as flux. After this period, the furnace was cooled down slowly with about 0.1°C/min to 500°C and then switched off. The products obtained were water and air stable, consisted of fine needle-shaped single crystals showing the typical colour of the rare-earth cation (Dy: colourless, Er: pink) and were attached to the surface of amorphous, fine-grained aggregates. For $Tb_3O_2Cl[SeO_3]_2$, a stoechiometric mixture of Tb_4O_7, Tb, $TbCl_3$ and SeO_2 (molar ratio 12:8:7:42) was used. The reaction schemes are described below.

$$M_2O_3 + MOCl + 2\ SeO_2 \longrightarrow M_3O_2Cl[SeO_3]_2 \qquad (7)$$

$$12\ Tb_4O_7 + 8\ Tb + 7\ TbCl_3 + 42\ SeO_2 \longrightarrow 21\ Tb_3O_2Cl[SeO_3]_2 \qquad (8)$$

Crystallographic data from the X-ray measurements, atom coordinates, temperature factors, selected interatomic distances and angles as well as motifs of the mutual adjunction are outlined in tables 5.1.5.a – 5.1.5.e.

MOCl was prepared according to the method used by *Caro* [104], *Haeuseler* [105] and *Wendlandt* [106] for preparation and thermal decomposition of the heavier rare-earth metal chloride hydrates. It so happens that a mixture of lanthanide oxide with hydrochloric acid (0.5 g M_2O_3 + 50 ml concentrated HCl solution) is evapourated to dryness, the residue which consists of $MCl_3 \cdot nH_2O$ (M = rare-earth element and n is six for all lanthanoids except for lanthanum, cerium and praseodymium which form heptahydrates [104 – 106]) is then put in an agate crucible and introduced into a furnace initially at room temperature. On increasing the temperature (0.1°C/min), these compounds decompose to form the metal oxyhalides in the temperature range 360 to 450°C [105, 106]. A slow stream of air was passed through the furnace during the pyrolysis. Having reached the end temperature, the furnace was just turned off to allow the sample to cool down to room temperature, now without an air stream any more.

5.1.2 Structure description of the orthorhombic $M_3O_2Cl[SeO_3]_2$ (M = Tb, Dy)

The rare-earth oxychloride oxoselenates(IV) $M_3O_2Cl[SeO_3]_2$ (M = Tb, Dy) crystallize in the orthorhombic crystal system with the space group Pnma. After X-ray analysis, the two crystallographically independent M^{3+} cations have the following anionic environment: M1 is surrounded by six O^{2-} and two Cl^- with the shape of a bicapped trigonal antiprism, the plane containing the two chloride anions and the central atom (*4c*, site symmetry: ·*m*·) being a perfect symmetry plane for this coordination. The eight anions around M2 (seven O^{2-} and one Cl^-) build up a distorted square antiprism. The M–O bond lengths between 220 and 274 pm for the Tb–O or 219 and 272 pm for the Dy–O bonds correlate well with those in the ternary compounds $M_2O[SeO_3]_2$ (M = Tb, Dy; paragraph 4.3). The corresponding distances and angles are summarized in table 5.1.5.d. Two trigonal non-planar $[SeO_3]^{2-}$ groups belong to the $[(M1)O_6Cl_2]$ polyhedron while five take care for the $[(M2)O_7Cl]$ one and coordinate both central cations only via vertices (fig. 5.1.2.a). The coordination about the selenium atom is ψ^1-terahedral ($[SeO_3E]^{2-}$; *E*: *non*-binding electron pair, "*lone pair*") with Se–O distances ranging between 167 – 172 pm and angles ∢(O–Se–O) within a 101 – 104° span. The isolated non-planar $[SeO_3]^{2-}$ group shows an almost C_{3v} symmetry with a displacement of the selenium atom from the O4–O2–O3 plane of 73.7 pm for Tb and 74.2 pm for Dy (table 4.1.5.d).

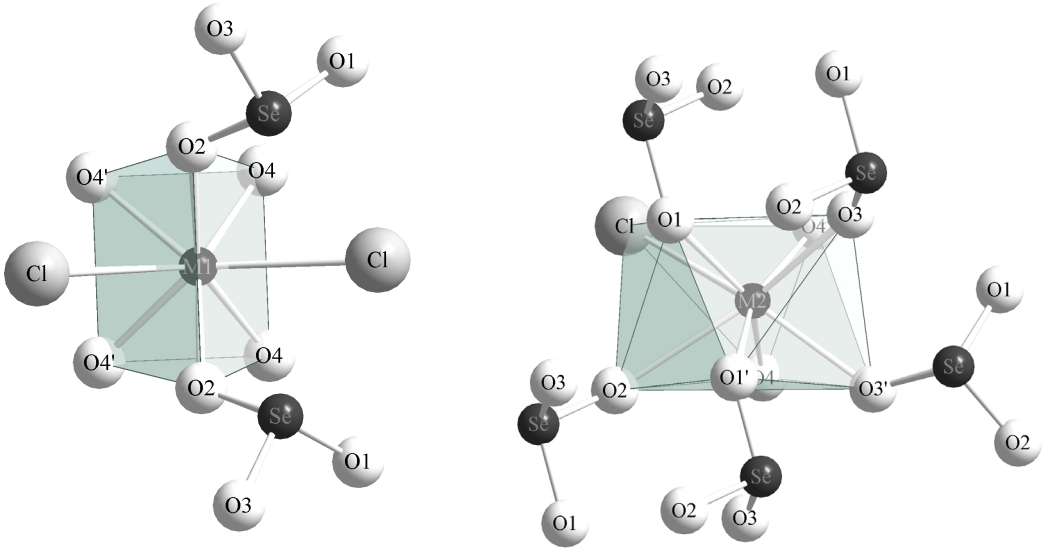

Fig. 5.1.2.a: Coordination around the $(M1)^{3+}$ and $(M2)^{3+}$ cations with their two and five attached $[SeO_3]^{2-}$ groups in $M_3O_2Cl[SeO_3]_2$ (M = Tb, Dy)

5.1.3 Structure description of the monoclinic $Er_3O_2Cl[SeO_3]_2$

In contrast to $M_3O_2Cl[SeO_3]_2$ (M = Tb, Dy), $Er_3O_2Cl[SeO_3]_2$ is non-isostructural and crystallizes monoclinic in the space group C2/c (a = 1498.23(6), b = 1102.03(5), c = 547.95(3) pm, β = 105.515(2)°, Z = 4). Its structure also contains two crystallographically different Er^{3+} cations in eight- and sevenfold coordination respectively. The $[(Er1)O_6Cl_2]$ polyhedron is best described as bicapped trigonal prism with d(Er1–O) ranging between 233 and 260 pm, d(Er1–Cl) = 305 pm (2×) and perfectly emphasize the symmetry elements of the C2/c space group. The $[(Er2)O_6Cl]$ units build up a distorted capped trigonal antiprism with d(Er2–O) = 217 – 238 pm and d(Er2–Cl) = 296 pm (fig. 5.1.3.a). Above mentioned Er–O-bond lengths correlate well with the analogous ones in the ternary $Er_2O[SeO_3]_2$ (paragraph 4.3). Alternatively, with values of 295 and 305 pm, the Er–Cl-bond lengths are very close to those in the tetragonal ErOCl (d(Er–Cl) = 304 and 305 pm, PbFCl-type structure) [107]. Two oxygen atoms of the $[(Er1)O_6Cl_2]$ polyhedra belong to two selenate groups simultaneously as four of the six oxygen atoms of the $[(Er2)O_6Cl]$ units are donated by four $[SeO_3]^{2-}$ anions in a monodentate way. The trigonal pyramidal $[SeO_3]^{2-}$ unit is characterized by d(Se–O) = 165 – 172 pm and angles ∢(O–Se–O) within a 100 – 104° span resulting in a displacement of the selenium atom from the O1–O2–O3 plane of 73.8 pm (table 5.1.5.d).

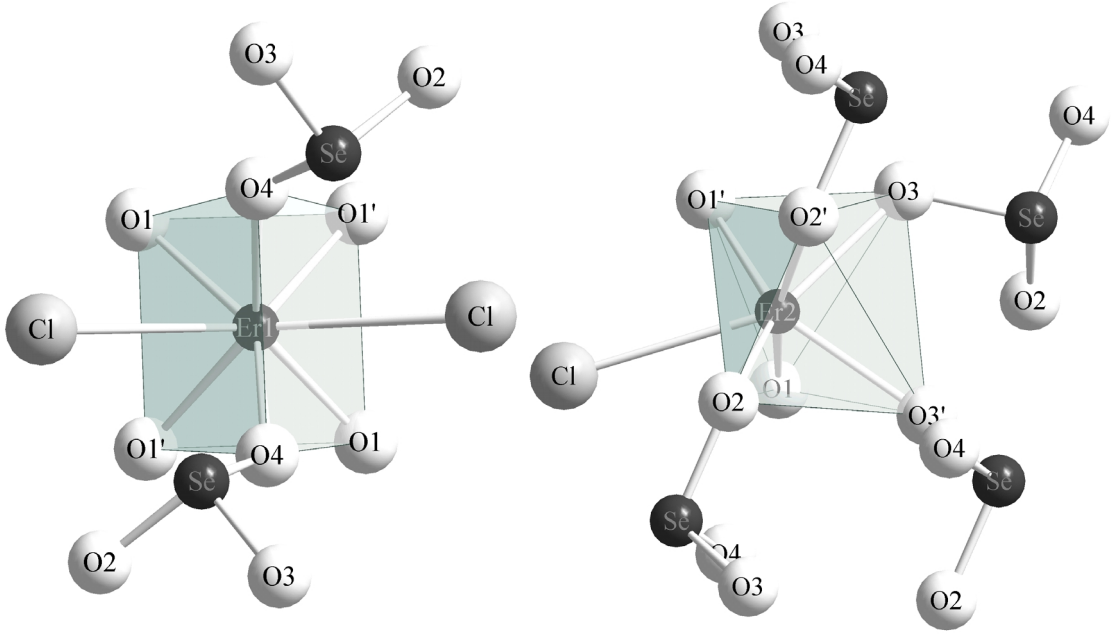

Fig. 5.1.3.a: Coordination around the $(Er1)^{3+}$ and $(Er2)^{3+}$ cations with their two and four attached $[SeO_3]^{2-}$ groups in $Er_3O_2Cl[SeO_3]_2$

5.1.4 Structural analogies

The crystal structures of $M_3O_2Cl[SeO_3]_2$ (M = Tb, Dy) and $Er_3O_2Cl[SeO_3]_2$ comprise one-dimensional strands $^1_\infty\{[(M1)_{3/3}(M2)_{2/1}O_{4/2}]^{5+}\}$ ($\equiv {}^1_\infty\{[O_2M_3]^{5+}\}$) along [100] formed by two parallel chains $^1_\infty\{[OM_{4/2}]^{4+}\}$ of *trans*-edge connected $[OM_4]$ tetrahedra (d(O–M) = 218 – 231 pm) which share an extra edge per chain link. The chains pattern is repeated after two double tetrahedra in that direction (fig. 5.1.4.a, *above*). Within these strands, each $[OM_4]$ unit shares three edges with neighbouring ones leading to more or less distorted tetrahedra. By this point of view, all tetrahedra forming chains are topologically equivalent. The M–M contacts of the bridging edges are shorter than all others in the three compounds: 361.5 pm (2×) and 356.9 pm (1×) for terbium, 359.1 pm (2×) and 355,2 pm (1×) for dysprosium and 351.9 pm (2×) and 355.5 pm (1×) for erbium, while the M–M contacts non-shared edges of the $[OM_4]$ units are always somewhat larger: 366.6, 372.6, 388.9 pm for terbium; 364.9, 371.2, 382.2 pm for dysprosium and 361.2, 377.0, 386.0 pm for erbium. Consequently, their corresponding opposite M–O–M-bond angles exhibit small (average of 105.4° for the three compounds) and respectively large values (average of 114.3°) more or less deviating from the ideal value of 109.5° for all M atoms considered. The possible repulsive forces between close M–M pairs of the bridging edges are therefore compensated by elongated M–M contacts for the non-shared edges and large M–O–M angles leading to double chains where $[OM_4]$ tetrahedra are firmly related. Each central strand is surrounded in (100) or (001) projection by four close ones which are rotated by 45° similar to the single chains observed in the $M_2O[SeO_3]_2$-type structure (fig. 5.1.4.a, *middle* and *below*). Interestingly, one $^1_\infty\{[O_2Er_{6/2}]^{5+}\}$ double strand is located at the center of the monoclinic unit cell, so that the four closest ones are positioned on the four vertices of the latter. By translating the monoclinic unit cell according to ¼ along *a* and *b* axis, both structures are quite similar in (001) and (100) projection.

The lower coordination number of the $(Er2)^{3+}$ cation (CN = 7) in $Er_3O_2Cl[SeO_3]_2$ compared to that of $(M2)^{3+}$ (CN = 8) in $M_3O_2Cl[SeO_3]_2$ (M = Tb, Dy) leads also to a decreasing coordination number of the $[SeO_3E]^{2-}$ units. Their coordination sphere actually being consisted of five terminal Er^{3+} in the case of $Er_3O_2Cl[SeO_3]_2$ against six terminal M^{3+} for $M_3O_2Cl[SeO_3]_2$ is thus reduced (fig. 5.1.4.b). This can also explain the difference in their crystal system. Similar effects were revealed in the structures of $ErClSeO_3$ and $NdClSeO_3$ where the $[SeO_3]^{2-}$ groups are connected to four Er^{3+} but five Nd^{3+}, respectively, leading to the non-isotypism of the two compounds [36].

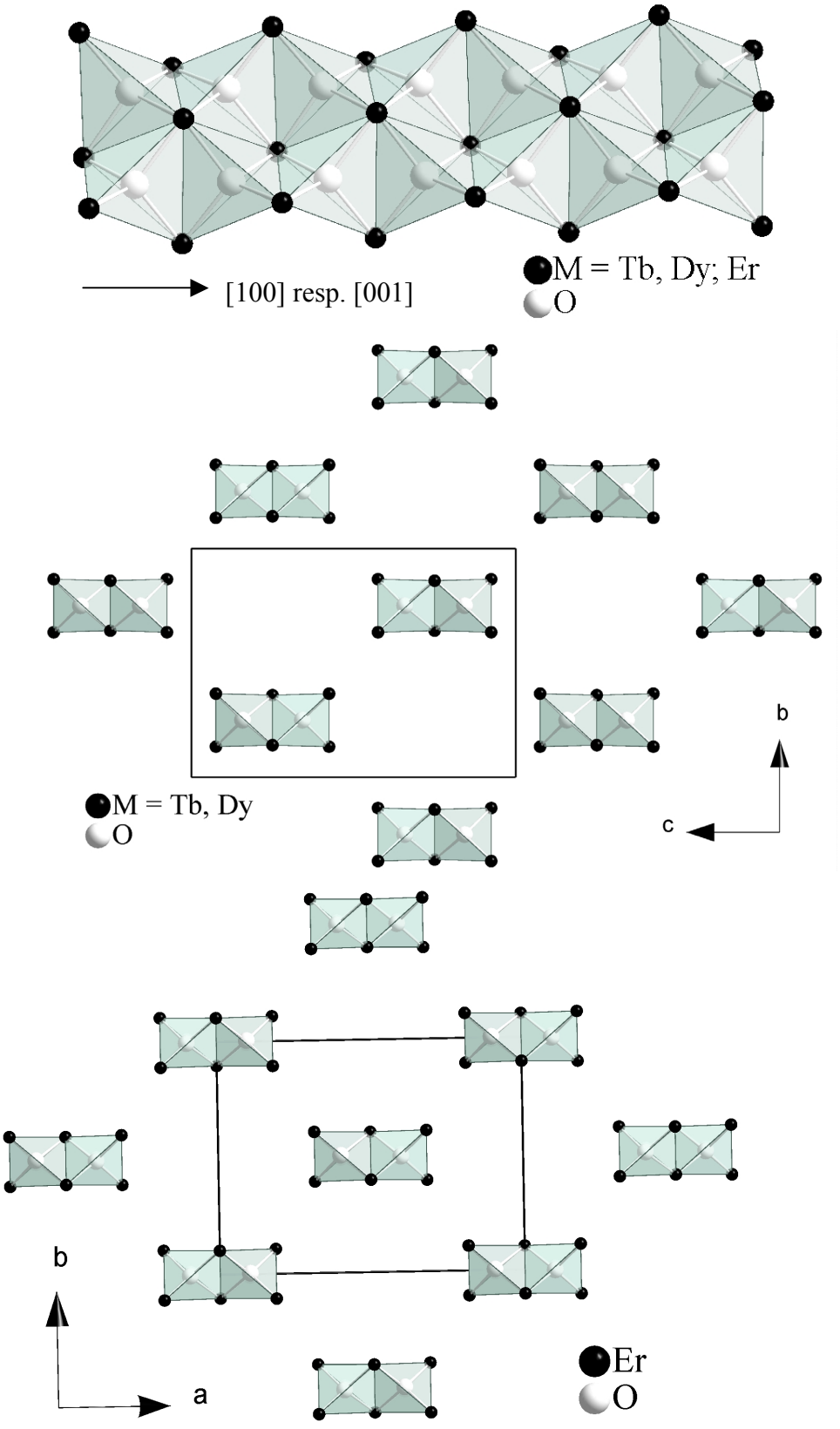

Fig. 5.1.4.a: $^{1}_{\infty}\{[O_2M_{6/2}]^{5+}\}$ or $^{1}_{\infty}\{[O_2Er_{6/2}]^{5+}\}$ chain of edge-connected $[OM_4]$ tetrahedra (*above*) and quadratic rod-packing of these strands in (100) projection for Tb and Dy (*middle*) and in (001) projection for Er (*below*)

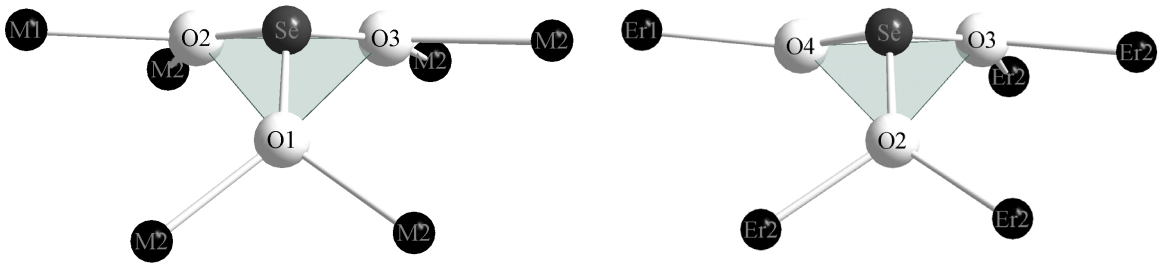

Fig. 5.1.4.b: Coordination sphere of six M^{3+} (*left*) and five Er^{3+} (*right*) cations about the trigonal pyramidal $[SeO_3]^{2-}$ anions in $M_3O_2Cl[SeO_3]_2$ (M = Tb, Dy) and $Er_3O_2Cl[SeO_3]_2$

Nevertheless, one-dimensional strands $^{1}_{\infty}\{[(M1)_{3/3}(M2)_{2/1}O_{4/2}]^{5+}\}$ (≡ $^{1}_{\infty}\{[O_2M_3]^{5+}\}$) (M = Tb, Dy; Er) along [100] formed by two parallel chains $^{1}_{\infty}\{[OM_{4/2}]^{4+}\}$ of *trans*-edge connected $[OM_4]$ tetrahedra and lone-pairs channels are observed as main structural features in both cases. These double chains arrange like a hexagonal closest packing of rods and are bordered by Cl^- and $[SeO_3]^{2-}$ anions in a 1:2-molar ratio. Together, the $[SeO_3]^{2-}$ groups and the $^{1}_{\infty}\{[O_2M_3]^{5+}\}$ double strands form a complex anionic chain $^{1}_{\infty}\{[O_2M_3][SeO_3]_4\}^{3-}$ decorated by two Cl^- anions at both sides. The non-binding "lone-pair" electrons at the Se^{4+} cations in the three compounds reside in *pseudo*-hexagonal empty channels running throughout the structure (fig. 5.1.4.c) along [100] between four cationic $^{1}_{\infty}\{[O_2M_3]^{5+}\}$ strands as in the copper mineral *francisite* ($Cu_3BiO_2Cl[SeO_3]_2$) [102] and its synthetic analogue $Cu_3ErO_2Cl[SeO_3]_2$ [103], thus providing the second main structural feature of those compounds. Two diametrically opposite Cl^- anions are involved within the six-membered rings contrary to the tetragonal ones observed in $M_2O[SeO_3]_2$ which were built up only by Se^{4+} cations. Average distances between the "lone-pair" channel forming particles (four Se^{4+} and two diametrically adjacent Cl^-) like 380 (2×) 462 pm (2×) and 598 (2×) for d(Se–Se) as well as 337 (4×) and 477 pm (4×) for d(Cl–Se), finally 616 pm (1×) for d(Cl–Cl) attest for the large width of the tube. As the cavities are lined only by free electron pairs of Se^{4+} cations and Cl^- anions, the compounds are highly stable in water, so they could have potential as an ion-exchange material. Related channels with about 663 pm in diameter and incorporating the lone pairs of the $[SeO_3]^{2-}$ groups were detected in some fluoride selenites by *Wickleder* and co-workers with the particularity that only selenium atoms were involved in the tunnel formation [34].

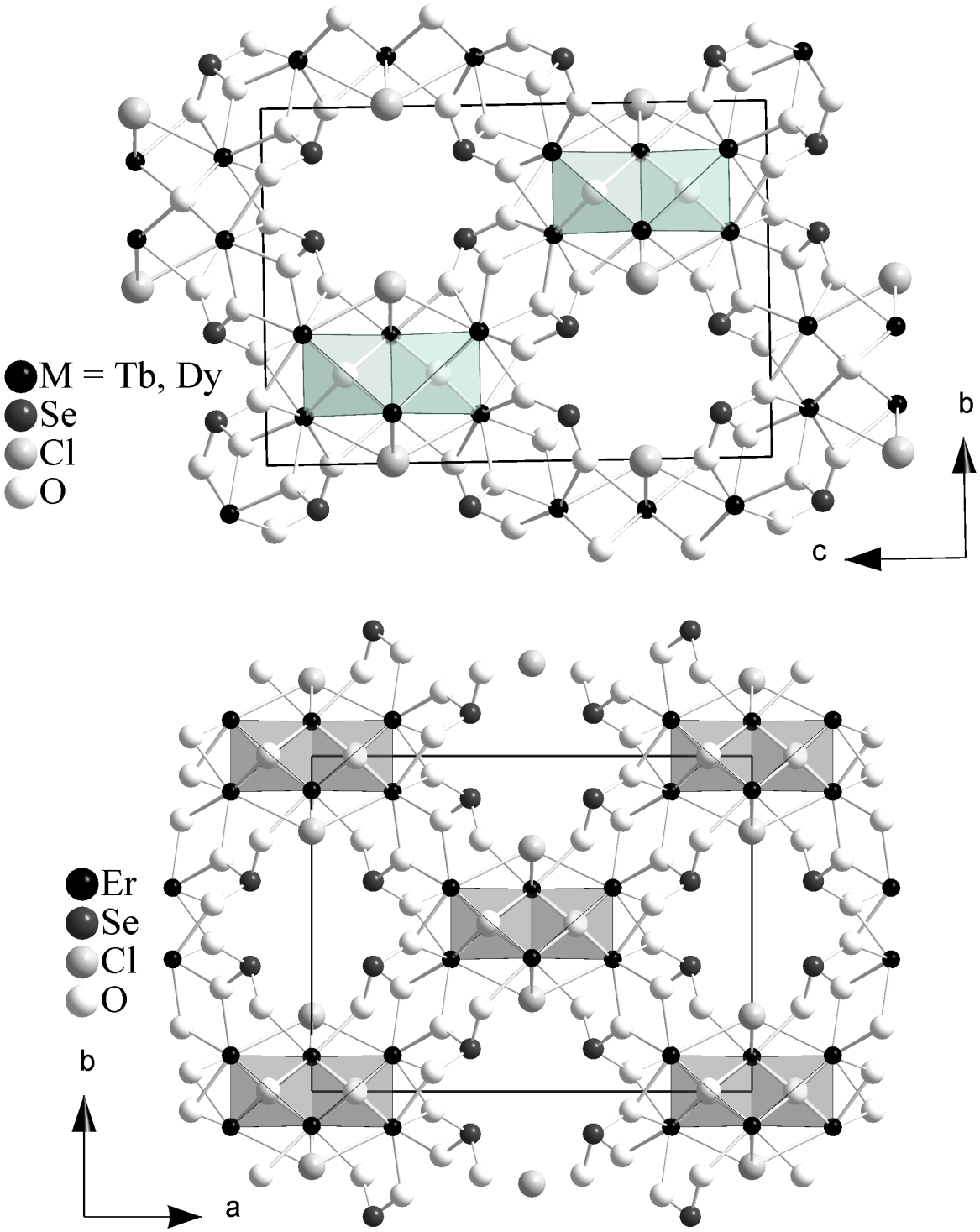

Fig. 5.1.4.c: Presentation of the whole crystal structure of $M_3O_2Cl[SeO_3]_2$ (M = Tb, Dy) as (100) projection (*above*) and $Er_3O_2Cl[SeO_3]_2$ as (001) projection (*below*) emphasizing the $^{1}_{\infty}\{[O_2M_3]^{5+}\}$ strands and the "*lone-pair*" channels formed by the stereochemical active *non*-binding electron pairs at the Se^{4+} cations and the Cl^{-} anions

Viewed down on the (010) plane, the structural diversity of the aforesaid compounds can be expressed only in the stacking mode of consecutive $^{1}_{\infty}\{[O_2M_3]^{5+}\}$ chains. In $M_3O_2Cl[SeO_3]_2$ (M = Tb, Dy) repeated $^{1}_{\infty}\{[O_2M_3]^{5+}\}$ strands are stacked without displacement underlining the mirror plane of the Pnma space group, contrary to the corresponding ones in $Er_3O_2Cl[SeO_3]_2$ where some considerable displacement of closest chains along [001] direction occurs (fig. 5.1.4.d). However, no rotation of anion-centered tetrahedra about axes normal to the extension of the double chain is observed in both cases. Their structural analogy can also be expressed by a group-subgroup diagram. The two involved space groups (P $2_1/n$ $2_1/m$ $2_1/a$ for $Tb_3O_2Cl[SeO_3]_2$) and (C 1 2/c 1 for $Er_3O_2Cl[SeO_3]_2$) are related to each other by their common non-isomorphic subgroup $P2_1/c$. The **a**-, **b**- and **c**-directions of $Tb_3O_2Cl[SeO_3]_2$ correspond to the **c**-, **a**- and **b**-directions of $Er_3O_2Cl[SeO_3]_2$. By the loss of two screw axes and two mirror planes, the transformation of the coordinate system and the unit cells for $Tb_3O_2Cl[SeO_3]_2$ into the setting of $Er_3O_2Cl[SeO_3]_2$ is possible. Additionally, if the row of 2-fold axes at x = 0 in the monoclinic space group C2/c is replaced by a mirror plane, the orthorhombic space group Pnma can be obtained. The electrostatic lattice energies of the two compounds are calculated using MAPLE [62]. The energies of the orthorhombic and the monoclinic structure are much alike: 47607 kJ/mol for $Tb_3O_2Cl[SeO_3]_2$ *vs*. 47884 kJ/mol for $Er_3O_2Cl[SeO_3]_2$. For this reason one should expect that monoclinic and orthorhombic domains can coexist within one crystal leading to a more or less disordered structure during a possible phase transition.

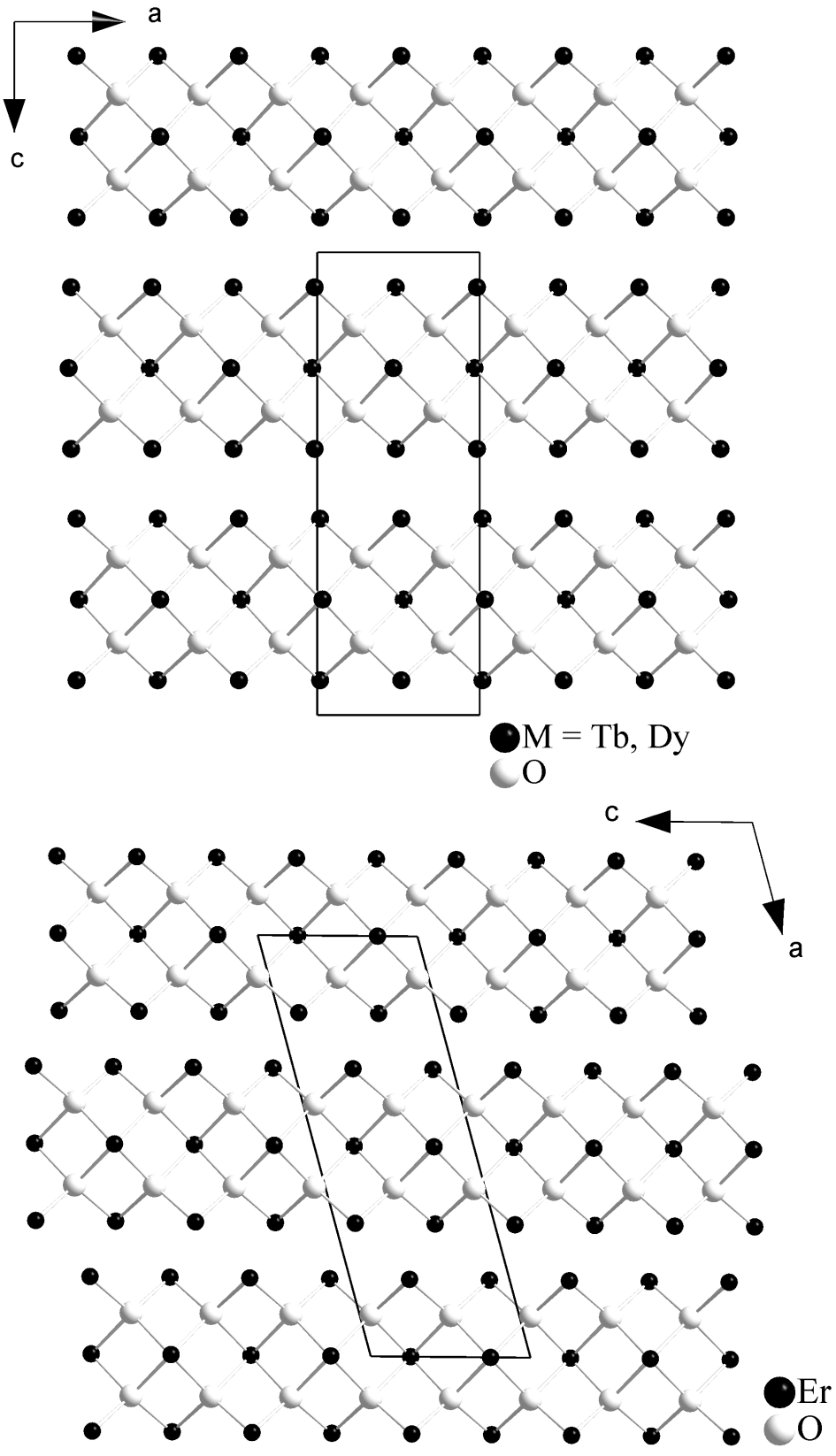

Fig. 5.1.4.d: Schematic [010] projection of $M_3O_2Cl[SeO_3]_2$ (M = Tb, Dy) (*above*) and $Er_3O_2Cl[SeO_3]_2$ (*below*) showing the stacking mode of the $^{1}_{\infty}\{[O_2M_3]^{5+}\}$ double strands

5.1.5 Structural data for $M_3O_2Cl[SeO_3]_2$ (M = Tb, Dy; Er)

Table 5.1.5.a: Crystallographic data for $M_3O_2Cl[SeO_3]_2$ (M = Tb, Dy; Er)

$M_3O_2Cl[SeO_3]_2$		Tb	Dy	Er
Crystal system		orthorhombic		monoclinic
Space group		Pnma (No. 62)		C2/c (No. 15)
Formula unit per unit cell (Z)		4		
Unit cell parameters:	a / pm =	535.16(4)	533.81(2)	1498.23(6)
	b / pm =	1530.51(9)	1521.04(7)	1102.03(5)
	c / pm =	1081.72(7)	1076.56(4)	547.95(3)
	β / ° =	90	90	105.515(2)
Calculated density (D_x / g cm^3)		5.984	6.146	6.272
Molar volume (V_m / cm^3 mol^{-1})		133.410	133.210(3)	131.264(3)
Diffractometer. radiation		κ-CCD (Fa. Nonius); Mo-K_α: λ = 71.07 pm		
$2\theta_{max.}$		55.0		
Index range	$\pm h_{max}$ / $\pm k_{max}$ / $\pm l_{max}$ =	6 / 14 / 19	6 / 13 / 19	19 / 14 / 7
F(000)		1376	1388	1412
Absorption coefficients (μ / mm^{-1})		32.22	34.03	37.29
Absorption correction		Numerical, after crystal shape optimization with the program X-SHAPE [53]		
Other data corrections		background, polarization, *Lorentz* factors		
Collected reflections		13256	11703	8441
Unique reflections		1049	1031	927
R_{int} / R_σ		0.074 / 0.030	0.075 / 0.034	0.116 / 0.054
Reflections with $\|F_o\| \geq 4\sigma\|F_o\|$		865	834	654
Structure solution and refinement		Program system SHELX-97 [58]		
Scattering factors		International Tables, Vol. C [85]		
R_1 / R_1 with $\|F_o\| \geq 4\sigma\|F_o\|$		0.0459 / 0.0317	0.058 / 0.041	0.074 / 0.043
wR_2 / Goodness of fit (GooF)		0.0652 / 1.098	0.093 / 1.186	0.097 / 1.047
Extinction (g)		0.00054(5)	0.00063(4)	0.00041(2)
Residual electron density	max.	1.22	1.76	1.56
(ρ / e$^-$ 10^6 pm)	min.	–1.17	–3.13	–2.45

Table 5.1.5.b: Atomic coordinates for $M_3O_2Cl[SeO_3]_2$ (M = Tb, Dy; Er)

Atoms	Wyckoff Position	x / a	y / b	z / c
Tb1	4c	0.03173(9)	1/4	0.35927(5)
Tb2	8d	0.01691(6)	0.07541(2)	0.13413(4)
Cl	4c	0.0771(5)	1/4	0.0062(2)
Se	8d	0.0484(1)	0.59915(5)	0.37442(7)
O1	8d	0.1116(9)	0.1291(3)	0.4995(5)
O2	8d	0.3867(9)	0.5123(3)	0.1826(5)
O3	8d	0.3047(9)	0.5492(3)	0.4392(5)
O4	8d	0.2737(9)	0.1572(3)	0.2506(5)
Dy1	4c	0.0316(1)	1/4	0.35880(6)
Dy2	8d	0.01691(9)	0.07536(3)	0.13444(4)
Cl	4c	0.0803(6)	1/4	0.0054(3)
Se	8d	0.0479(2)	0.59944(7)	0.37418(9)
O1	8d	0.1159(13)	0.1295(5)	0.5001(7)
O2	8d	0.3874(12)	0.5127(5)	0.1832(6)
O3	8d	0.3053(12)	0.5498(5)	0.4400(6)
O4	8d	0.2731(12)	0.1567(4)	0.2495(6)
Er1	4e	0	0.89730(8)	1/4
Er2	8f	0.81618(4)	0.10683(6)	0.1273(1)
Cl	4e	0	0.2246(5)	1/4
Se	8f	0.86030(9)	0.3734(1)	0.4859(3)
O1	8f	0.9003(6)	0.9952(9)	0.429(1)
O2	8f	0.7951(7)	0.3076(9)	0.210(2)
O3	8f	0.7746(6)	0.4409(9)	0.586(2)
O4	8f	0.8859(7)	0.2512(9)	0.670(2)

Table 5.1.5.c: Anisotropic thermal displacement parameters[b] (U_{ij}/pm^2) for $M_3O_2Cl[SeO_3]_2$ (M = Tb, Dy; Er)

Atoms	U_{11}	U_{22}	U_{33}	U_{23}	U_{13}	U_{12}
Tb1	92(3)	90(3)	100(3)	0	0(2)	0
Tb2	114(2)	104(2)	114(2)	–26(1)	5(1)	0
Cl	163(13	171(14)	176(14)	0	–33(10)	0
Se	124(4)	88(4)	126(4)	–5(3)	–15(3)	11(3)
O1	181(26)	100(27)	234(30)	81(23)	–25(24)	–45(22)
O2	177(27)	182(30)	151(30)	23(23)	–25(24)	–8(23)
O3	120(26)	241(33)	136(30)	31(23)	–25(24)	46(22)
O4	83(23)	95(26)	104(27)	9(21)	19(19)	58(19)
Dy1	85(3)	95(4)	106(4)	0	2(2)	0
Dy2	112(3)	111(3)	112(3)	–24(2)	4(2)	–6(2)
Cl	153(17)	196(21)	192(18)	0	–31(14)	0
Se	120(5)	99(6)	124(5)	–15(4)	–15(4)	8(4)
O1	165(35)	122(40)	229(39)	79(31)	–38(32)	–14(32)
O2	130(34)	201(42)	132(36)	30(30)	1(29)	6(31)
O3	56(33)	192(44)	168(38)	–3(31)	–43(27)	60(28)
O4	97(32)	47(34)	127(34)	16(27)	–3(25)	–18(27)
Er1	134(7)	142(7)	137(7)	0	29(5)	0
Er2	165(6)	144(6)	156(6)	–4(3)	37(4)	–26(3)
Cl	218(31)	187(31)	258(36)	0	78(27)	0
Se	139(9)	165(9)	183(11)	5(7)	42(8)	14(7)
O1	98(58)	213(70)	79(59)	72(48)	23(47)	75(45)
O2	196(63)	245(70)	131(65)	–125(57)	37(51)	–24(56)
O3	115(62)	189(71)	351(88)	–35(58)	55(58)	–34(51)
O4	282(74)	232(73)	146(71)	130(57)	7(57)	132(57)

[b] defined as temperature factor according to: $\exp[-2\pi^2(a^{*2}h^2U_{11} + b^{*2}k^2U_{22} + c^{*2}l^2U_{33} + 2b^*c^*klU_{23} + 2a^*c^*hlU_{13} + 2a^*b^*hkU_{12})]$

Table 5.1.5.d: Selected internuclear distances (d/pm) and angles (∢/deg) in $M_3O_2Cl[SeO_3]_2$ (M = Tb, Dy; Er)

$M_3O_2Cl[SeO_3]_2$		Tb	Dy	Er
		d / pm	d / pm	d / pm
M1 – O4	(2×)	225.3	225.0	226.8
– O4′	(2×)	231.0	229.7	230.7
– O1	(2×)	243.1	242.4	232.3
– Cl	(1×)	283.5	281.8	305.1
– Cl′	(1×)	326.1	327.4	305.1
M2 – O4	(1×)	219.5	218.7	217.3
– O4′	(1×)	224.6	222.1	218.3
– O3	(1×)	234.9	233.1	229.8
– O3′	(1×)	235.7	235.4	233.1
– O2	(1×)	244.8	244.6	238.8
– O2′	(1×)	249.4	247.5	239.6
– O1	(1×)	249.4	271.3	
– Cl	(1×)	302.6	301.7	295.5
Se – O1	(1×)	167.4	167.5	166.4
– O2	(1x)	170.2	169.0	169.7
– O3	(1x)	172.0	172.0	172.5
		∢ / grd	∢ / grd	∢ / grd
O1 – Se – O3		101.4	101.8	99.6
O2 – Se – O3		101.9	102.3	100.2
O1– Se – O2		104.4	104.1	103.3
M1 – O4 – M1		103.0	102.7	102.0
M2 – O4 – M1		106.8	106.4	103.2
M2′ – O4 – M1′		107.0	106.9	104.9
M2 – O4 – M2		111.3	111.7	112.1
M2″ – O4 – M1″		113.8	113.5	114.5
M2‴ – O4 – M1‴		114.8	115.5	120.3

Table 5.1.5.e: Motifs of mutual adjunction in $M_3O_2Cl[SeO_3]_2$ (M = Tb, Dy)

	Cl	O1	O2	O3	O4	CN
M1	2 / 2	2 / 1	0 / 0	0 / 0	4 / 2	8
M2	1 / 2	1 / 1	2 / 2	2 / 2	2 / 2	8
Se	0 / 0	1 / 1	1 / 1	1 / 1	0 / 0	3
CN	3	3	3	3	4	

Table 5.1.5.f: Motifs of mutual adjunction in $Er_3O_2Cl[SeO_3]_2$

	Cl	O1	O2	O3	O4	CN
Er1	2 / 2	2 / 1	0 / 0	0 / 0	4 / 2	8
Er2	1 / 2	1 / 1	2 / 2	2 / 2	1 / 2	7
Se	0 / 0	1 / 1	1 / 1	1 / 1	0 / 0	3
CN	3	3	3	3	4	

5.2 Compounds of the formula $M_4O_3Cl_2[SeO_3]_2$ (M = Er, Yb)

5.2.1 Synthesis of $M_4O_3Cl_2[SeO_3]_2$ (M = Er, Yb)

M_2O_3, MOCl, MCl_3 and SeO_2 as starting materials (molar ratio 3:1:1:4) were inserted into a quartz-glass tube. Evacuated and sealed under 10^{-3} mbar, the closed vessels were heated to 850°C for seven days, afterward cooled slowly (0.1°C/min) to 400°C and finally to the room temperature by turning off the furnace. The following phases $M_4O_3Cl_2[SeO_3]_2$ were observed when CsCl was added to the reactants as flux. The reaction pathway is showed below and MOCl was prepared as in paragraph 5.1.1.

$$3\ M_2O_3 + MOCl + MCl_3 + 4\ SeO_2 \longrightarrow 2\ M_4O_3Cl_2[SeO_3]_2 \qquad (9)$$

The crystal data and relevant data concerning the measurement of X-ray intensities such like the final obtained structure parameters are summarized in part 5.2.3. The comparison of the experimental powder diffractogram with the theoretical one for $Yb_4O_3Cl_2[SeO_3]_2$ shows additional, but no sharp peaks probably due to fine impurities in our single-crystalline sample (diagram 5.2.1.a).

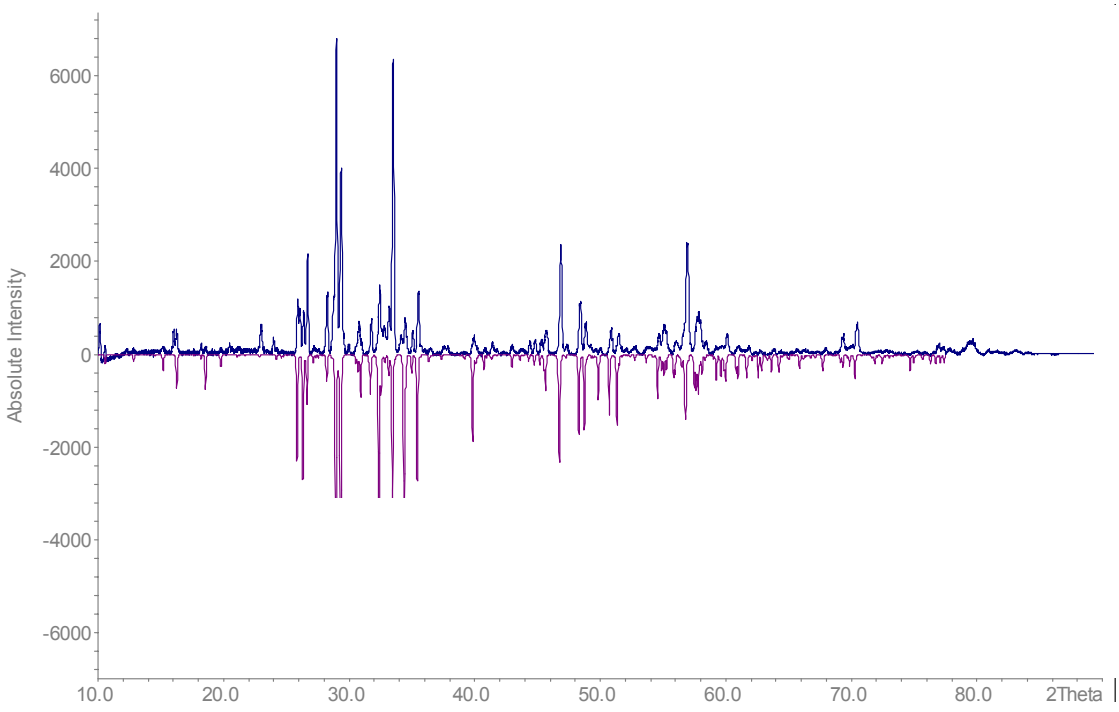

Diagram 5.2.1: Comparison of the measured powder diffractogram of $Yb_4O_3Cl_2[SeO_3]_2$ (*above*) with the theoretical one (*below*, as negative intensities)

5.2.2 Structure description of $M_4O_3Cl_2[SeO_3]_2$ (M = Er, Yb)

$M_4O_3Cl_2[SeO_3]_2$ (M = Er, Yb) crystallize in the triclinic system with the $P\bar{1}$ space group. The X-ray structure analysis shows eight different M^{3+} cations in seven- and eightfold coordination and four crystallographically independent anionic $[SeO_3]^{2-}$ groups. The latter exhibit a cationic vicinities of two M^{3+} edge-spanning each. Three terminal M^{3+} for the $[(Se1)O_3]^{2-}$, $[(Se2)O_3]^{2-}$, and $[(Se4)O_3]^{2-}$ anions against two edge-spanning and four terminal M^{3+} for the $[(Se3)O_3]^{2-}$ units complete the picture (fig. 5.2.2.a). The square prismatical vicinities of oxygen about $(M1)^{3+}$, $(M2)^{3+}$ and $(M3)^{3+}$ are quite regular despite further monodentate effects of $[(Se3)O_3]^{2-}$ for the $[(M1)O_8]$ and of $[(Se4)O_3]^{2-}$ for the $[(M2)O_8]$ polyhedra. Around $(M4)^{3+}$ and $(M5)^{3+}$ one chloride and seven oxygen particles build distorted square antiprismatic or prismatic coordination spheres, while the seven anions (five O^{2-} and two Cl^-) around $(M6)^{3+}$, $(M7)^{3+}$ and $(M8)^{3+}$ are arranged at the vertices of a trigonal prism capped by one Cl^- anion which resides approximately perpendicular to a rectangular face of the prism. The irregularities among the coordination spheres arise not only from two different type of ligands but also from the additional $[SeO_3]^{2-}$ groups coordinating the $[MO_7Cl]$ and $[MO_5Cl_2]$ polyhedra in a mono- or bidentate way (fig. 5.2.2.b and 5.2.2.b′).

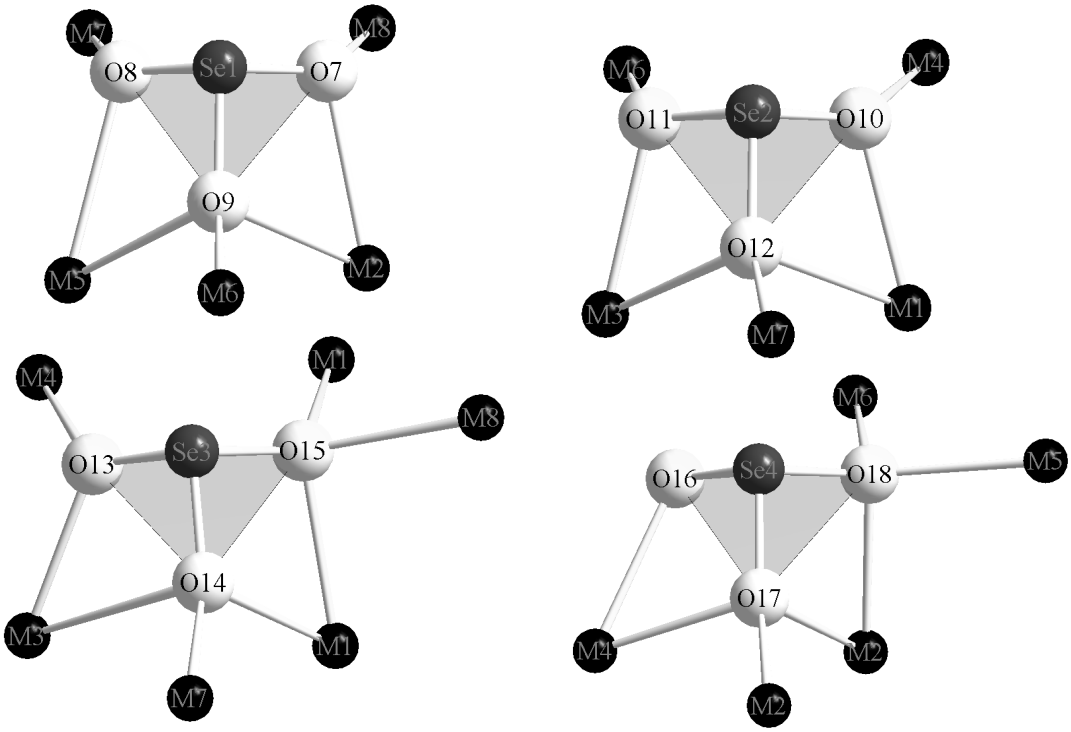

Fig. 5.2.2.a: Coordination sphere of five and six M^{3+} cations about the four independent trigonal pyramidal $[SeO_3]^{2-}$ anions in $M_4O_3Cl_2[SeO_3]_2$ (M = Er, Yb)

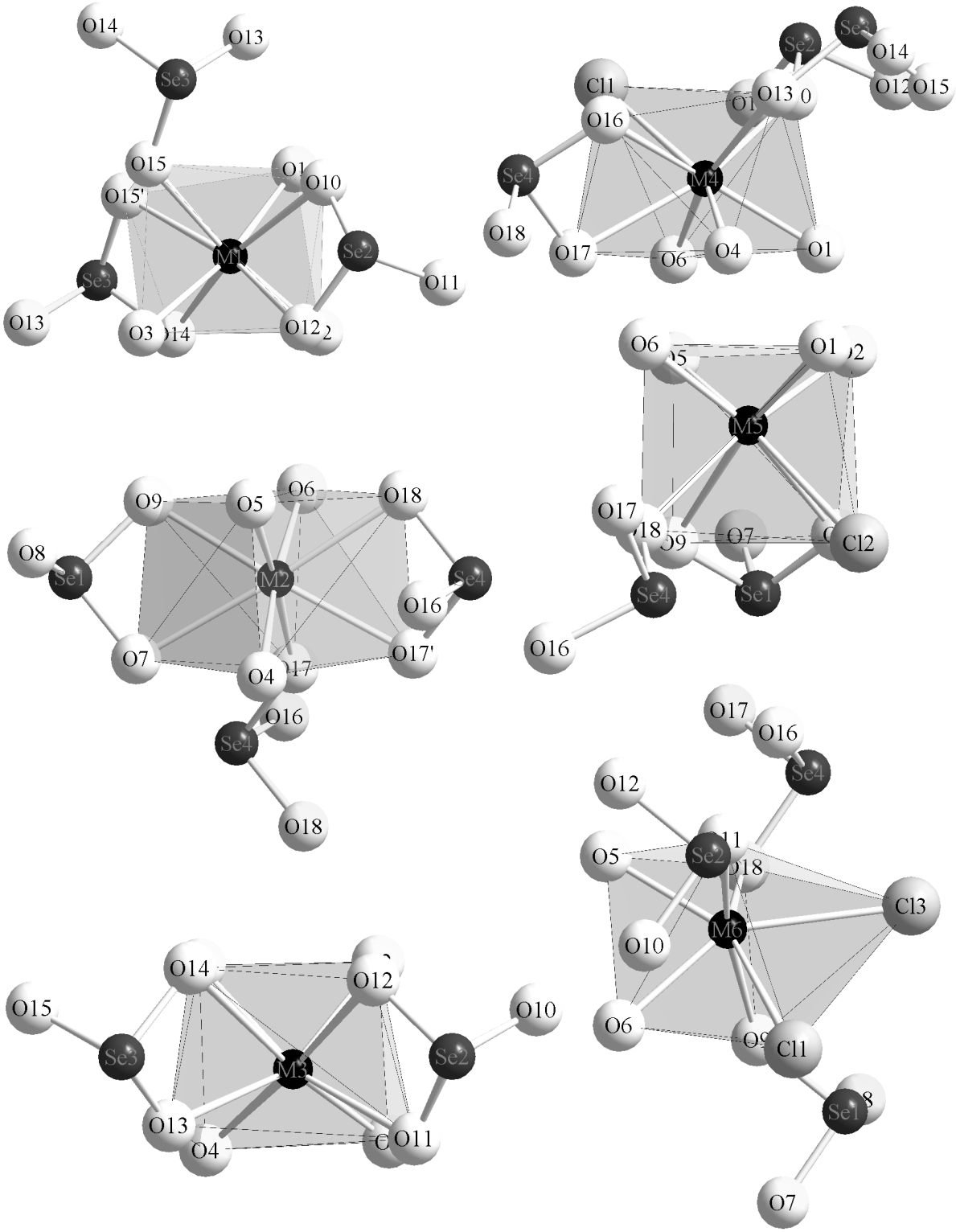

Fig. 5.2.2.b: Coordination of O^{2-}, Cl^{-} and $[SeO_3]^{2-}$ anions about the $(M1)^{3+}$ – $(M6)^{3+}$ cations in $M_4O_3Cl_2[SeO_3]_2$ (M = Er, Yb)

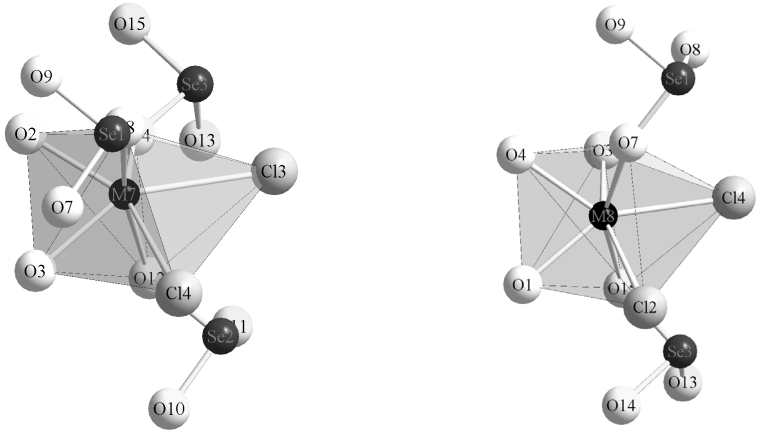

Fig. 5.2.2.b′: Coordination of O^{2-}, Cl^{-} and $[SeO_3]^{2-}$ anions about the $(M7)^{3+}$ and $(M8)^{3+}$ cations in $M_4O_3Cl_2[SeO_3]_2$ (M = Er, Yb)

The $[(M1)O_8]$ and $[(M3)O_8]$ polyhedra are joined by four common edges O1–O17 (299.2 pm, 2×) and O9–O5 (280.4 pm, 2×), to form four-membered rings resembling $[M_4O_{24}]^{36-}$ complex anions. These latter are condensed by two opposite edges, O7–O7 (266.5 pm, 2×), of the $[(M1)O_8]$ polyhedra so that infinite one-dimensional anionic chains like $^{1}_{\infty}\{[M_4O_{24}]^{36-}\}$ running along [100] are emerging (fig. 5.2.2.c). Further connectivity of the above-mentioned strands occurs via two other opposite edges O2–O6 (273.3 pm, 2×), with $[(M8)_2O_{14}]^{22-}$ units ($[(M2)_2O_{14}]^{22-}$ ≡ two $[(M2)O_8]$ double polyhedra) leading to layers illustrated like $^{2}_{\infty}\{[M_6O_{36}]^{54-}\}$ spreading parallel to a (011) projection. The M–M contacts within the layers are ranging between 350 and 410 pm (fig. 5.2.2.d).

Six out of the eighteen oxygen anions in the unit cell (O1 – O6) are tetracoordinated by M^{3+} cations only and we therefore consider $[OM_4]$ tetrahedra as independent structural subunits in those compounds. Firstly the oxocentered tetrahedra $[OM_4]$ are linked through M–M edges to form $[O_6M_{12}]^{24+}$ units which are further condensed via two *trans*-edges (M1–M3) and four vertices (two M5 and two M2) into a two-dimensional framework structure spreading parallel (011). This is suggestive of the pattern $^{2}_{\infty}\{[(M)^{i}_{4/1}(M)^{s}_{8/2}(O)_{6/1}]^{12+}\}$ (≡ $^{2}_{\infty}\{([O_3M_4]^{6+})_2\}$) according to *Niggli's* formalism (*i* denotes M atoms exclusively belonging to the same $[O_6M_{12}]^{24+}$ units and *s* the ones that are shared between a central $[O_6M_{12}]^{24+}$ unit and their neighbours; fig. 5.2.2.e). All tetrahedra contained in this layer are not crystallographically equivalent as the ones observed in the structure of $Cu_9O_2Cl_6[SeO_3]_4$ and $Cu_5O_2Cl_2[SeO_3]_2$ with their linear $^{1}_{\infty}\{[O_2Cu_6]^{8+}\}$ and $^{1}_{\infty}\{[O_2Cu_5]^{6+}\}$ chains, respectively [38, 39]. In the $[O_6M_{12}]^{24+}$ units forming the $^{2}_{\infty}\{([O_3M_4]^{6+})_2\}$ sheets, four out of the six tetrahedra involved (*i.e.* $[(O2)M_4]$, $[(O4)M_4]$, $[(O5)M_4]$, and $[(O6)M_4]$) share three edges and one vertex with

neighbouring ones while only two edges and one vertex sharing is observed in the case of [(O1)M_4] and [(O3)M_4] (fig. 5.2.2.e). The former are less distorted: they include O–M bond lengths in the range of 220 – 224 pm for Yb, and 220 – 226 pm for Er, whereas the latter are strongly distorted with O–M bond lengths ranging from 221 to 229 pm for Yb and from 220 to 232 pm for Er. These distortions are undeniably dictated by the topology of tetrahedral linkage. Analysis of the metal-metal contacts within the layers reveals the same trend as previously shown in paragraph 5.1.4 for the $M_3O_2Cl[SeO_3]_2$-type structure: shortening for the M–M contacts of the bridging edges (average value of 353 pm for the two compounds) against more elongated M–M contacts for the non-shared edges of [OM_4] tetrahedra (average value of 385 pm for both). By viewing the structure down the [100] direction, we ought to mention that different cationic $^{2}_{\infty}\{([O_3M_4]^{6+})_2\}$ sheets are bordered by $[SeO_3]^{2-}$ and Cl^- anions in a 3:4-molar ratio and the three-dimensional connectivity of the structure occurs only via M4–Cl1–M6 bonds, thus the task of the interlayer halide anions is to link adjacent sheets. Conversely the $[SeO_3]^{2-}$ units are positioned on the base of the [OM_4] tetrahedra so that their free electron pairs are always pointing away from the $^{2}_{\infty}\{([O_3M_4]^{6+})_2\}$ layers. But the M–M–M triangular face of the oxocentered tetrahedra and the O–O–O one of the $[SeO_3]^{2-}$ groups are not parallel oriented to each other, *i.e.* the O–O–O face of the $[SeO_3]^{2-}$ groups are not directly bonded to the M–M–M face of the [OM_4] tetrahedra (fig. 5.2.2.f). Therefore no face-to-face relationship between [OM_4] tetrahedra and $[SeO_3]^{2-}$ groups similar to the ones observed in the structure of $Cu_9O_2Cl_6[SeO_3]_4$ and $Cu_5O_2Cl_2[SeO_3]_2$ with their [OCu_4] tetrahedra and $[SeO_3]^{2-}$ pyramids can be discussed. The distances Se–Cl1 although not bonding are quite important (average of 325 pm, 2×) thus providing large voids for the free electron pairs carried by both the chloride anions and the selenium cations between two different $^{2}_{\infty}\{([O_3M_4]^{6+})_2\}$ layers.

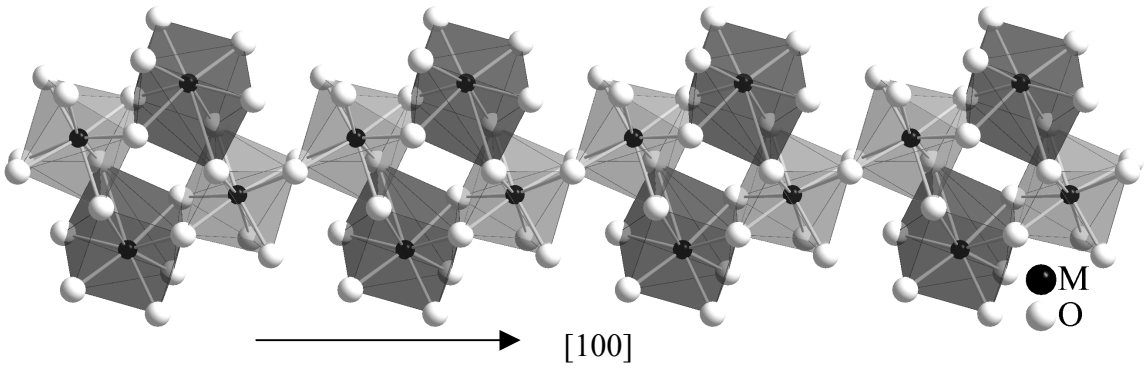

Fig. 5.2.2.c: $^{1}_{\infty}\{[M_4O_{24}]^{36-}\}$ infinite chains along the [100] direction in the crystal structure of $M_4O_3Cl_2[SeO_3]_2$ (M1: medium grey, M3: dark grey polyhedra)

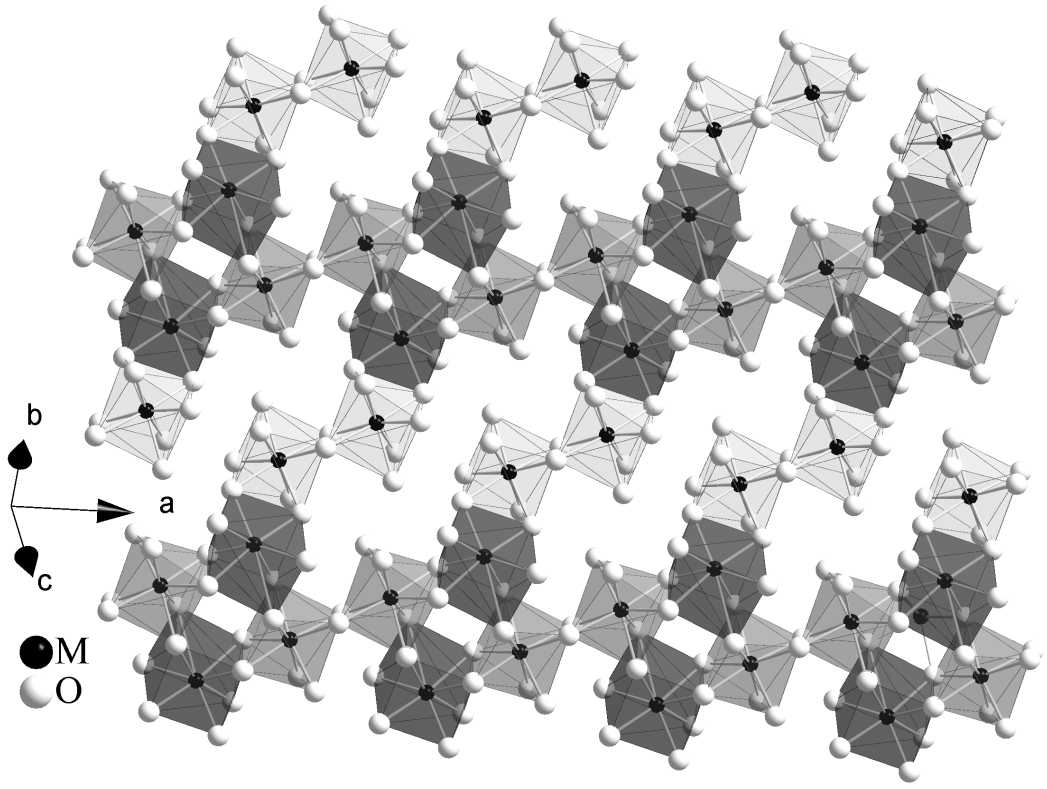

Fig. 5.2.2.d: The $^{2}_{\infty}\{[M_6O_{36}]^{54-}\}$ layers in $M_4O_3Cl_2[SeO_3]_2$ (M1, M2 and M3 with medium grey, dark grey and light grey polyhedra, respectively)

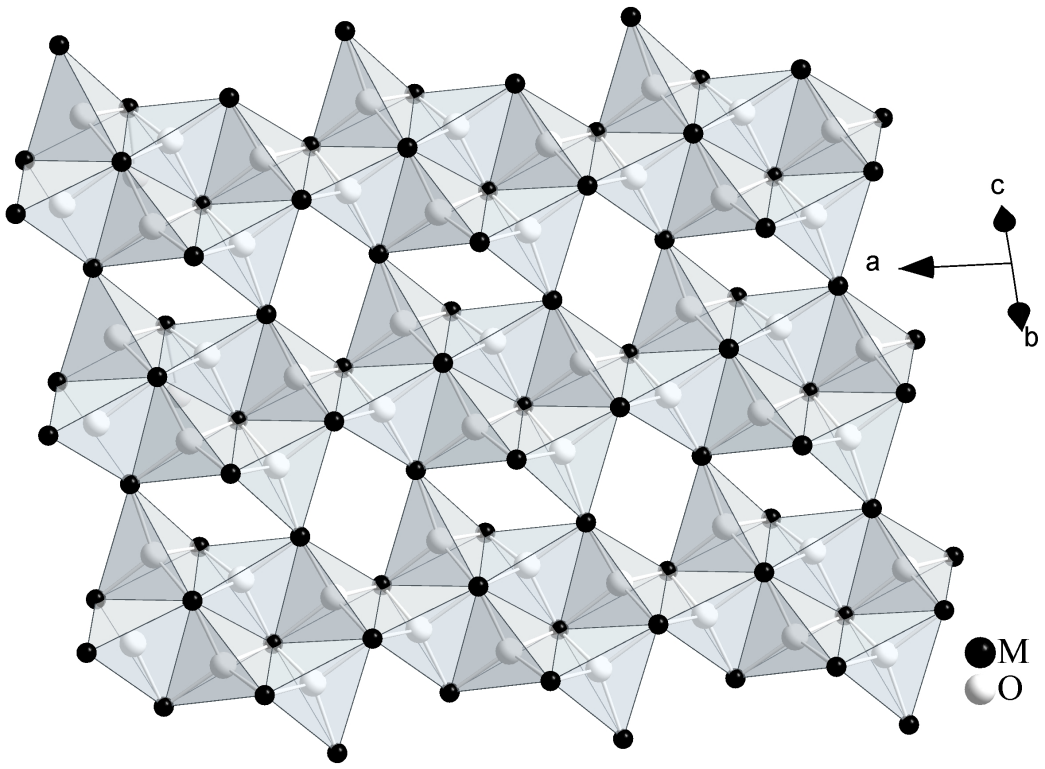

Fig. 5.2.2.e: The $^{2}_{\infty}\{([O_3M_4]^{6+})_2\}$ network in the structure of $M_4O_3Cl_2[SeO_3]_2$ (M = Er, Yb) emphasizing the connectivity among the $[OM_4]$ tetrahedra

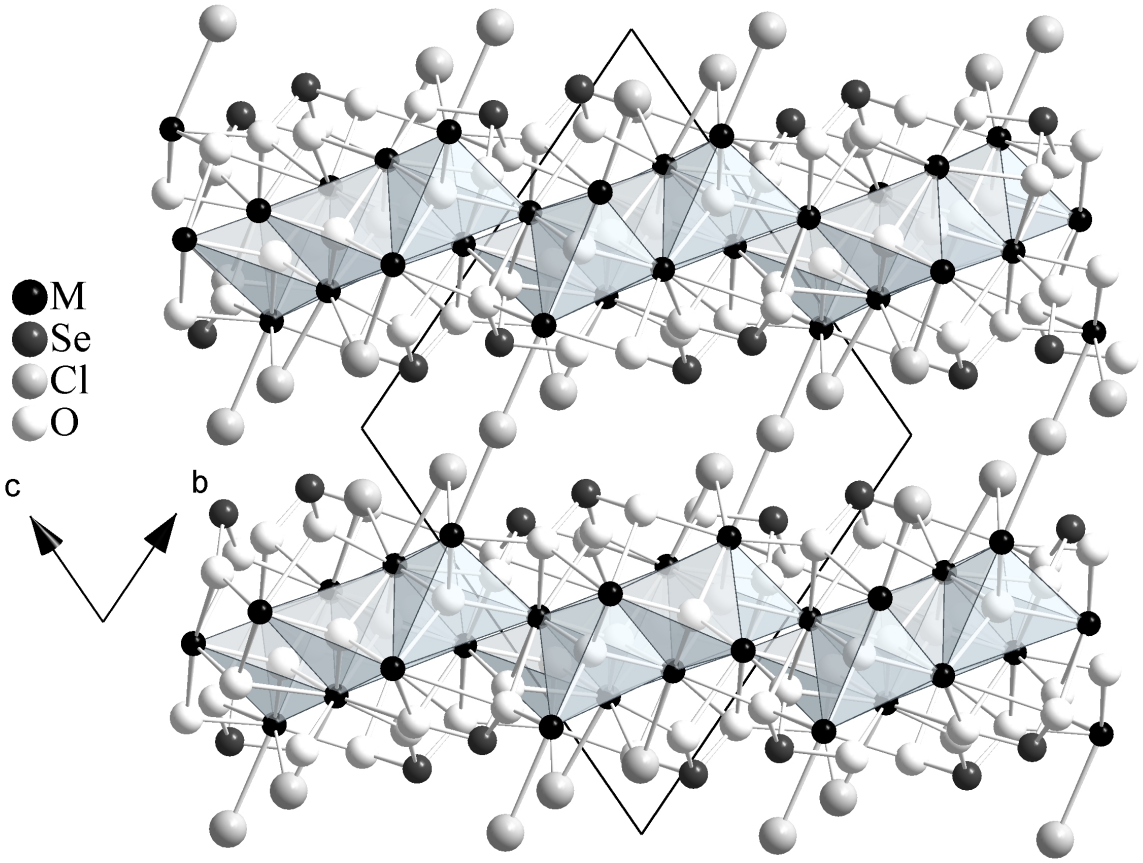

Fig. 5.2.2.f: Projection of the $M_4O_3Cl_2[SeO_3]_2$ structure (M = Er, Yb) onto the (100) plane showing the bridging role of Cl^- between adjacent $^2_\infty\{([O_3M_4]^{6+})_2\}$ layers

The twofold coordination around all Cl^- anions (fig. 5.2.2.g) in this structure is endued with an almost linear bridging angle for M6–Cl1–M4 with a value of 178.4° and d(Cl1–M4) = 284.4 pm, d(Cl1–M6) = 289.8 pm, whereas the M3–Cl2–M6, M4–Cl3–M1 and M2–Cl4–M3 triples are bent in shape with values of 82.5, 85.3 and 88.8°, respectively, for the angles.

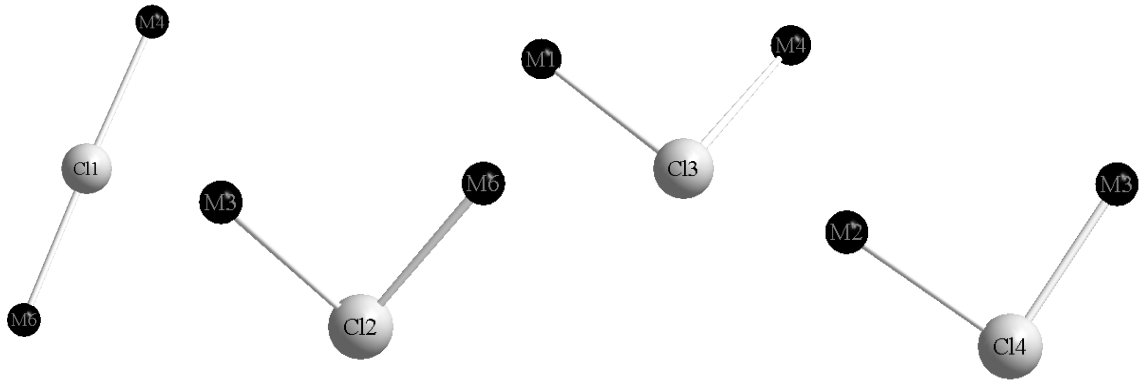

Fig. 5.2.2.g: Coordination of M^{3+} cations about the four Cl^- anions in $M_4O_3Cl_2[SeO_3]_2$

5.2.3 Structural data for $M_4O_3Cl_2[SeO_3]_2$ (M = Er, Yb)

Table 5.2.3.a: Crystallographic data for $M_4O_3Cl_2[SeO_3]_2$ (M = Er, Yb)

M		Er	Yb
Crystal system and space group		triclinic, $P\bar{1}$ (No. 2)	
Formula unit per unit cell (Z)		4	
Unit cell parameters:	a / pm =	861.64(2)	853.87(6)
	b / pm =	1170.56(3)	1145.92(8)
	c / pm =	1208.42(3)	1195.46(9)
	α / ° =	67.666(1)	68.132(7)
	β / ° =	77.833(1)	78.113(7)
	γ / ° =	85.270(1)	85.748(7)
Calculated density (D_x / g · cm^3)		6.279	6.659
Molar volume (V_m / cm^3 · mol^{-1})		160.843	159.951
Diffractometer, radiation		κ-CCD (Fa. Nonius); Mo-K_α: λ = 71.07 pm	
$2\theta_{max.}$		54.9	64.1
Index range:	$\pm h_{max}$ / $\pm k_{max}$ = $\pm l_{max}$ =	11 / 15	12 / 17
F(000)		1784	1816
Absorption coefficients (μ / mm^{-1})		37.26	42.28
Absorption correction		Numerical, after crystal shape optimization with the program X-SHAPE [53]	
Other data corrections		background, polarization, *Lorentz* factors	
Collected reflections		34373	55248
Unique reflections		5031	7376
R_{int} / R_σ		0.081 / 0.041	0.066 / 0.038
Reflections with $\|F_o\| \geq 4\sigma\|F_o\|$		4056	5660
Structure solution and refinement		Program system SHELX-97 [58]	
Scattering factors		International Tables, Vol. C [85]	
R_1 / R_1 with $\|F_o\| \geq 4\sigma\|F_o\|$		0.081 / 0.068	0.065 / 0.048
wR_2 / Goodness of fit (GooF)		0.220 / 1.087	0.129 / 1.070
Extinction (g)		0.00045(5)	0.00005(3)
Residual electron density (ρ / e$^-$ 10^6 pm)		max.12.17; min. –4.74	max. 6.51; min –5.85

Table 5.2.3.b: Atomic coordinates for $M_4O_3Cl_2[SeO_3]_2$ (M = Er, Yb)

Atoms	Wyckoff Position	x / a	y / b	z / c
Er1	2i	0.47692(8)	0.61811(6)	0.71831(6)
Er2	2i	0.12403(8)	0.73518(7)	0.85784(7)
Er3	2i	0.53373(8)	0.88524(7)	0.77497(7)
Er4	2i	0.07043(9)	0.46951(7)	0.79477(7)
Er5	2i	0.28157(8)	0.91400(7)	0.54846(7)
Er6	2i	0.92256(8)	0.02638(7)	0.70789(7)
Er7	2i	0.87158(8)	0.75528(7)	0.64942(7)
Er8	2i	0.28944(8)	0.41840(7)	0.03991(6)
Se1	2i	0.2311(2)	0.1774(2)	0.9783(2)
Se2	2i	0.2100(2)	0.6767(2)	0.4834(2)
Se3	2i	0.3237(2)	0.1688(2)	0.5984(2)
Se4	2i	0.6895(2)	0.3685(2)	0.8535(2)
O1	2i	0.6366(7)	0.2012(6)	0.2808(6)
O2	2i	0.9488(7)	0.1379(6)	0.3165(6)
O3	2i	0.2378(7)	0.0577(6)	0.3651(6)
O4	2i	0.3594(7)	0.2988(6)	0.2147(6)
O5	2i	0.0583(7)	0.3729(6)	0.1732(6)
O6	2i	0.7570(7)	0.4426(6)	0.1446(6)
O7	2i	0.3689(8)	0.1998(6)	0.0438(6)
O8	2i	0.0895(8)	0.0892(6)	0.1035(6)
O9	2i	0.1316(8)	0.3133(6)	0.9628(6)
O10	2i	0.6528(8)	0.2989(6)	0.4501(6)
O11	2i	0.9356(8)	0.4089(6)	0.3953(6)
O12	2i	0.1106(8)	0.8133(6)	0.4663(6)
O13	2i	0.3286(8)	0.2758(6)	0.4522(6)
O14	2i	0.1717(8)	0.0860(6)	0.6029(6)
O15	2i	0.4655(8)	0.0589(6)	0.5790(6)
O16	2i	0.2610(8)	0.5163(6)	0.2853(6)
O17	2i	0.4632(8)	0.5529(6	0.0849(6)
O18	2i	0.1741(8)	0.6146(6)	0.0684(6)

Table 5.2.3.b: continued

Atoms	Wyckoff Position	x / a	y / b	z / c
Cl1	2i	0.0035(3)	0.2478(2)	0.7521(2)
Cl2	2i	0.6169(4)	0.1036(3)	0.7968(3)
Cl3	2i	0.3878(3)	0.4075(3)	0.6818(3)
Cl4	2i	0.2573(4)	0.9177(4)	0.9164(4)
Yb1	2i	0.71933(4)	0.08618(3)	0.45088(3)
Yb2	2i	0.28834(4)	0.41895(3)	0.04075(3)
Yb3	2i	0.12852(4)	0.24683(3)	0.34941(3)
Yb4	2i	0.52461(4)	0.38544(3)	0.28054(3)
Yb5	2i	0.87433(4)	0.26410(3)	0.14267(3)
Yb6	2i	0.07030(4)	0.46426(3)	0.79647(3)
Yb7	2i	0.07627(4)	0.96989(3)	0.29337(3)
Yb8	2i	0.46409(4)	0.11282(3)	0.22751(3)
Se1	2i	0.22675(9)	0.17120(8)	0.97987(8)
Se2	2i	0.20624(9)	0.67110(8)	0.48438(8)
Se3	2i	0.32725(9	0.17354(8)	0.59836(8)
Se4	2i	0.31559(9)	0.63871(8)	0.14428(8)
O1	2i	0.6369(7)	0.2012(6)	0.2808(6)
O2	2i	0.9487(7)	0.1374(6)	0.3165(6)
O3	2i	0.2378(7)	0.0577(6)	0.3651(6)
O4	2i	0.3594(7)	0.2986(6)	0.2147(6)
O5	2i	0.0583(7)	0.3727(6)	0.1732(6)
O6	2i	0.7569(7)	0.4426(6)	0.1446(6)
O7	2i	0.3689(8)	0.1998(6)	0.0438(6)
O8	2i	0.0895(8)	0.0892(6)	0.1035(6)
O9	2i	0.1316(8)	0.3133(6)	0.9628(6)
O10	2i	0.6528(8)	0.2989(6)	0.4501(6)
O11	2i	0.9354(8)	0.4089(6)	0.3953(6)
O12	2i	0.1106(8)	0.8133(6)	0.4663(6)
O13	2i	0.3285(8)	0.2756(6)	0.4522(6)
O14	2i	0.1717(8)	0.0860(6)	0.6029(6)

Table 5.2.3.b: continued

Atoms	Wyckoff Position	x / a	y / b	z / c
O15	2i	0.4650(8)	0.0589(6)	0.5790(6)
O16	2i	0.2610(8)	0.5163(6)	0.2853(6)
O17	2i	0.4632(8)	0.5528(6	0.0842(6)
O18	2i	0.1741(8)	0.6143(6)	0.0680(6)
Cl1	2i	0.3766(3)	0.4074(2)	0.6894(2)
Cl2	2i	0.7378(3)	0.0857(2)	0.0869(2)
Cl3	2i	0.0021(3)	0.2481(2)	0.7524(2)
Cl4	2i	0.3766(3)	0.8969(2)	0.2089(2)

Table 5.2.3.c: Anisotropic thermal displacement parameters[b] (U_{ij}/pm^2) for $M_4O_3Cl_2[SeO_3]_2$ (M = Er, Yb)

Atoms	U_{11}	U_{22}	U_{33}	U_{23}	U_{13}	U_{12}
Er1	117(4)	122(4)	129(4)	–24(3)	–36(3)	–10(3)
Er2	106(4)	141(4)	137(4)	–37(3)	–40(3)	0(3)
Er3	113(4)	123(4)	145(4)	–35(3)	–39(3)	–6(3)
Er4	147(4)	120(4)	1129(4)	–22(3)	–40(3)	3(3)
Er5	106(4)	143(4)	130(4)	–31(3)	–41(3)	–6(3)
Er6	123(4)	114(4)	123(4)	–13(3)	–33(3)	–7(3)
Er7	100(4)	146(4)	137(4)	–41(3)	–33(3)	0(3)
Er8	107(4)	168(4)	14242)	–35(3)	–43(3)	–1(3)
Se1	179(8)	148(8)	140(8)	–46(6)	–55(6)	17(6)
Se2	138(8)	147(8)	144(8)	–54(6)	–45(6)	6(6)
Se3	147(8)	144(8)	221(9)	–75(7)	–43(6)	6(8)
Se4	166(8)	306(10)	274(10)	–174(8)	–75(7)	55(7)
Cl1*						
Cl2	38(13)	61(14)	99(15)	–53(12)	12(11)	–25(10)
Cl3*						
Cl4	74(15)	253(19)	265(20)	–174(16)	27(13)	–59(13)

*) isotropic calculated

Table 5.2.3.c: continued

Atoms	U_{11}	U_{22}	U_{33}	U_{23}	U_{13}	U_{12}
O1	262(61)	98(53)	122(55)	–43(44)	–32(46)	–10(44)
O2	224(57)	84(52)	134(56)	6(43)	–24(45)	–45(42)
O3	175(54)	63(27)	148(56)	–6(43)	–7(43)	–23(40)
O4	83(48)	59(48)	127(55)	–17(43)	–6(43)	–15(41)
O5	120(53)	106(52)	143(56)	–26(45)	–16(41)	17(40)
O6	197(58)	177(56)	208(63)	–96(52)	–21(45)	–44(45)
O7	232(58)	279(65)	230(65)	–78(51)	–151(45)	15(46)
O8	168(55)	194(61)	186(61)	–10(46)	34(48)	47(43)
O9	295(63)	128(54)	245(65)	–67(49)	–78(47)	–52(44)
O10	152(52)	170(58)	165(60)	–38(48)	26(47)	62(47)
O11	228(59)	179(58)	226(62)	11(48)	–116(50)	–22(42)
O12	257(61)	179(56)	360(74)	–77(55)	–55(45)	71(47)
O13	380(73)	199(60)	311(70)	–102(53)	–126(53)	–85(46)
O14	206(58)	189(59)	204(67)	51(53)	–33(52)	–86(53)
O15	380(73)	249(66)	216(68)	–140(56)	17(50)	54(48)
O16	206(58)	308(69)	295(70)	–121(57)	–176(54)	27(51)
O17	262(63)	308(65)	137(57)	–22(49)	–31(44)	–59(45)
O18	461(72)	328(72)	311(76)	–23(61)	–100(61)	–51(58)
Yb1	86(2)	102(2)	99(2)	–24(1)	–25(1)	7(1)
Yb2	86(2)	132(2)	108(2)	–26(1)	–32(1)	8(1)
Yb3	77(2)	103(2)	111(2)	–36(1)	–25(1)	3(1)
Yb4	87(2)	85(2)	107(2)	–23(1)	–28(1)	6(1)
Yb5	83(2)	100(2)	105(2)	–33(1)	–29(1)	–1(1)
Yb6	111(2)	81(2)	104(2)	–19(1)	–33(1)	7(1)
Yb7	90(2)	82(2)	94(2)	–14(1)	–27(1)	0(1)
Yb8	83(2)	83(2)	113(2)	–29(1)	–28(1)	–2(1)
Se1	161(4)	102(4)	98(4)	–37(3)	–45(3)	14(3)
Se2	128(4)	105(4)	98(4)	–40(3)	–30(3)	5(3)
Se3	105(4)	120(4)	174(5)	–57(3)	–21(3)	5(3)

Table 5.2.3.c: continued

Atoms	U_{11}	U_{22}	U_{33}	U_{23}	U_{13}	U_{12}
Se4	122(4)	303(5)	258(5)	−191(4)	−57(4)	53(4)
Cl1	203(11)	203(11)	319(14)	−153(10)	−26(10)	5(9)
Cl2	206(11)	322(14)	361(15)	−227(12)	8(10)	−17(10)
Cl3	205(12)	279(13)	315(14)	−189(11)	−60(11)	−2(10)
Cl4	162(10)	199(11)	289(13)	−152(10)	−2(9)	−7(8)
O1	55(25)	106(28)	106(28)	5(22)	−29(21)	−12(21)
O2	111(28)	83(28)	186(32)	−58(24)	−74(24)	6(22)
O3	160(30)	63(27)	106(29)	−2(22)	−27(23)	−23(22)
O4	93(26)	85(27)	106(28)	−35(22)	−39(22)	15(21)
O5	51(25)	81(27)	158(30)	−21(23)	−38(22)	7(20)
O6	116(28)	75(27)	120(29)	−32(22)	−40(23)	10(21)
O7	203(32)	169(32)	242(36)	−72(27)	−151(28)	−4(25)
O8	252(35)	183(34)	198(35)	−33(28)	−45(28)	−37(27)
O9	247(34)	119(30)	187(33)	−75(26)	−92(27)	36(25)
O10	197(32)	127(30)	249(36)	−83(27)	−79(27)	−15(24)
O11	181(32)	207(34)	133(32)	−8(26)	−3(25)	−40(26)
O12	194(31)	113(30)	145(31)	−29(24)	−61(25)	38(24)
O13	214(32)	139(31)	130(31)	12(25)	−56(25)	8(25)
O14	114(29)	208(34)	312(40)	−148(30)	47(27)	−88(25)
O15	101(27)	132(30)	191(33)	−51(25)	−17(24)	24(23)
O16	267(40)	167(33)	226(36)	10(28)	−109(31)	−17(30)
O17	66(26)	170(32)	245(35)	−112(27)	−24(24)	36(23)
O18	104(28)	194(33)	231(36)	−95(28)	−28(25)	−13(24)

[b] defined as temperature factor according to: $\exp[-2\pi^2(a^{*2}h^2U_{11} + b^{*2}k^2U_{22} + c^{*2}l^2U_{33} + 2b^*c^*klU_{23} + 2a^*c^*hlU_{13} + 2a^*b^*hkU_{12})]$

Table 5.2.3.d: Selected internuclear distances (d/pm) and angles (∢/deg) in $M_4O_3Cl_2[SeO_3]_2$ (M = Er, Yb)

Er				Yb			
	d / pm		d / pm		d / pm		d / pm
Er1 – O1	223.6	Er2 – O3	225.9	Yb1 – O1	219.6	Yb2 – O3	220.3
– O2	223.9	– O5	226.6	– O2	222.1	– O5	221.2
– O3	230.1	– O6	226.9	– O3	228.7	– O6	228.5
– O15	238.2	– O4	229.4	– O15	235.2	– O4	229.6
– O14	238.2	– O13	243.6	– O14	236.6	– O13	239.2
– O0	244.6	– O11	252.4	– O10	245.9	– O11	247.1
– O12	250.9	– O14	254.4	– O12	247.1	– O14	248.1
– O15′	256.9	– O7	265.4	– O15′	253.7	– O7	254.3
Er3 – O4	222.8	Er4 – O5	220.1	Yb3 – O4	223.3	Yb4 – O4	220.2
– O2	223.4	– O1	225.9	– O2	223.3	– O1	225.3
– O5	232.3	– O6	228.6	– O5	223.7	– O6	225.3
– O3	235.0	– O10	237.8	– O3	225.2	– O10	235.5
– O13	241.0	– O13	238.5	– O13	240.5	– O13	236.1
– O11	249.6	– O17	252.7	– O11	253.0	– O17	254.3
– O12	251.2	– O17	266.6	– O12	259.3	– O16	261.3
– O14	251.4	– Cl1	286.2	– O14	298.6	– Cl1	274.5
Er5 – O6	224.5	Er6 – O5	221.4	Yb5 – O6	221.6	Yb6 – O5	220.2
– O2	225.7	– O11	224.3	– O2	223.4	– O11	221.8
– O5	226.4	– O9	224.7	– O5	223.9	– O9	222.7
– O1	229.0	– O6	225.8	– O1	230.4	– O6	224.1
– O18	248.6	– O18	241.0	– O18	248.7	– O18	236.5
– O9	270.9	– Cl1	295.5	– O9	266.5	– Cl1	281.1
– O8	271.1	– Cl3	296.0	– O8	272.2	– Cl3	284.4
– Cl2	284.1			– Cl2	277.0		

Table 5.2.3.d: continued

Er				Yb			
	d / pm		d / pm		d / pm		d / pm
Er7 – O8	219.5	Er8 – O1	219.4	Yb7 – O8	215.4	Yb8 – O1	216.8
– O2	223.3	– O4	223.7	– O2	221.6	– O4	221.0
– O14	223.4	– O3	223.7	– O14	222.7	– O3	222.2
– O3	225.2	– O7	235.3	– O3	223.3	– O7	233.7
– O12	227.0	– O15	259.7	– O12	223.3	– O15	256.9
– Cl4	285.4	– Cl2	273.4	– Cl4	274.6	– Cl2	265.6
– Cl3	299.3	– Cl4	282.5	– Cl3	289.9	– Cl4	273.5
Se1 – O7	168.3	Se2 – O10	167.8	Se1 – O7	167.2	Se2 – O10	168.2
– O8	169.5	– O11	168.8	– O8	169.0	– O11	168.4
– O9	173.5	– O12	172.7	– O9	172.6	– O12	172.7
Se3 – O13	169.6	Se4 – O16	169.2	Se3 – O13	170.1	Se4 – O16	174.3
– O14	167.7	– O17	173.8	– O14	170.3	– O17	174.5
– O15	174.1	– O18	174.9	– O15	174.5	– O18	175.0
O1 – Er8	223.7	O2 – Er7	225.7	O1 – Yb8	216.8	O2 – Yb7	221.6
– Er1	225.2	– Er1	225.8	– Yb1	219.6	– Yb1	222.1
– Er4	229.4	– Er3	225.9	– Yb4	225.2	– Yb3	223.3
– Er5	230.1	– Er5	232.3	– Yb5	230.4	– Yb5	223.4
O3 – Er8	219.4	O4 – Er4	220.1	O3 – Yb8	222.2	O4 – Yb4	220.2
– Er7	223.6	– Er2	222.8	– Yb7	223.3	– Yb2	220.3
– Er1	228.6	– Er8	223.7	– Yb3	225.2	– Yb8	221.0
– Er2	229.0	– Er3	226.9	– Yb1	228.7	– Yb3	223.3
O5 – Er6	223.4	O6 – Er5	221.4	O5 – Yb6	220.2	O6 – Yb5	221.6
– Er2	223.9	– Er6	223.4	– Yb2	221.2	– Yb6	224.1
– Er3	224.5	– Er4	225.9	– Yb3	223.7	– Yb4	225.3
– Er5	226.6	– Er2	226.4	– Yb5	223.9	– Yb2	228.5

Table 5.2.3.d: continued

Er		Yb	
	∢ / grd		∢ / grd
O8 – Se1 – O9	93.5	O8 – Se1 – O9	93.8
O7 – Se1 – O9	95.3	O7 – Se1 – O9	94.4
O7 – Se1 – O8	103.1	O7 – Se1 – O8	102.6
O11 – Se2 – O12	93.5	O11 – Se2 – O12	92.9
O10 – Se2 – O12	94.4	O10 – Se2 – O12	94.1
O10 – Se2 – O11	104.1	O10 – Se2 – O11	103.9
O14 – Se3 – O15	92.4	O14 – Se3 – O15	91.5
O13 – Se3 – O14	95.1	O13 – Se3 – O14	94.8
O13 – Se3 – O15	103.9	O13 – Se3 – O15	103.4
O17 – Se4 – O18	93.1	O17 – Se4 – O18	93.4
O16 – Se4 – O17	94.2	O16 – Se4 – O17	94.7
O16 – Se4 – O18	99.8	O16 – Se4 – O18	99.0
Er1 – O1 – Er5	102.1	Yb1 – O1 – Yb5	102.3
Er4 – O1 – Er5	102.7	Yb4 – O1 – Yb5	102.5
Er8 – O1 – Er4	104.8	Yb8 – O1 – Yb4	104.9
Er1 – O1 – Er4	115.2	Yb1 – O1 – Yb4	114.6
Er8 – O1 – Er1	115.9	Yb8 – O1 – Yb1	115.8
Er8 – O1 – Er5	116.4	Yb8 – O1 – Yb5	116.3
Er1 – O2 – Er5	103.5	Yb1 – O2 – Yb5	103.8
Er3 – O2 – Er5	105.6	Yb3 – O2 – Yb5	105.5
Er7 – O2 – Er3	105.9	Yb7 – O2 – Yb3	106.1
Er7 – O2 – Er5	110.5	Yb7 – O2 – Yb5	111.2
Er7 – O2 – Er1	111.4	Yb7 – O2 – Yb1	111.9
Er1 – O2 – Er3	117.9	Yb1 – O2 – Yb3	118.2

Table 5.2.3.d: continued

Er		Yb	
	∢ / grd		∢ / grd
Er8 – O3 – Er3	101.2	Yb8 – O3 – Yb3	101.4
Er7 – O3 – Er3	104.3	Yb7 – O3 – Yb3	104.9
Er7 – O3 – Er1	107.5	Yb7 – O3 – Yb1	108.0
Er8 – O3 – Er7	108.0	Yb8 – O3 – Yb7	108.3
Er8 – O3 – Er1	111.4	Yb8 – O3 – Yb1	111.9
Er3 – O3 – Er1	119.6	Yb3 – O3 – Yb1	121.6
Er8 – O4 – Er3	101.9	Yb8 – O4 – Yb3	102.4
Er2 – O4 – Er3	103.8	Yb2 – O4 – Yb3	104.3
Er4 – O4 – Er8	105.1	Yb4 – O4 – Yb8	105.1
Er4 – O4 – Er3	110.9	Yb4 – O4 – Yb3	110.7
Er4 – O4 – Er2	114.8	Yb4 – O4 – Yb2	115.5
Er2 – O4 – Er8	119.1	Yb2 – O4 – Yb8	118.0
Er2 – O5 – Er3	103.5	Yb2 – O5 – Yb3	103.9
Er3 – O5 – Er5	104.9	Yb3 – O5 – Yb5	105.2
Er6 – O5 – Er5	104.7	Yb6 – O5 – Yb5	105.3
Er6 – O5 – Er3	107.9	Yb6 – O5 – Yb3	108.3
Er6 – O5 – Er2	113.9	Yb6 – O5 – Yb2	114.7
Er2 – O5 – Er5	116.8	Yb2 – O5 – Yb5	118.8
Er5 – O6 – Er7	103.7	Yb5 – O6 – Yb6	104.7
Er5 – O6 – Er4	105.4	Yb5 – O6 – Yb4	105.6
Er6 – O6 – Er2	106.3	Yb6 – O6 – Yb2	106.9
Er4 – O6 – Er2	110.7	Yb4 – O6 – Yb2	110.6
Er6 – O6 – Er4	113.6	Yb6 – O6 – Yb4	113.7
Er5 – O6 – Er2	115.8	Yb5 – O6 – Yb2	115.6

Table 5.2.3.e: Motifs of mutual adjunction in $M_4O_3Cl_2[SeO_3]_2$ (M = Er, Yb)

	Cl1	Cl2	Cl3	Cl4	O1	O2	O3	O4	O5	O6	O7	O8	O9
M1	0 / 0	0 / 0	0 / 0	0 / 0	1 / 1	1 / 1	1 / 1	0 / 0	0 / 0	0 / 0	0 / 0	0 / 0	0 / 0
M2	0 / 0	0 / 0	0 / 0	0 / 0	0 / 0	0 / 0	0 / 0	1 / 1	1 / 1	1 / 1	1 / 1	0 / 0	1 / 1
M3	0 / 0	0 / 0	0 / 0	0 / 0	0 / 0	1 / 1	1 / 1	1 / 1	1 / 1	0 / 0	0 / 0	0 / 0	0 / 0
M4	1 / 1	0 / 0	0 / 0	0 / 0	1 / 1	0 / 0	0 / 0	1 / 1	0 / 0	1 / 1	0 / 0	0 / 0	0 / 0
M5	0 / 0	1 / 1	0 / 0	0 / 0	1 / 1	1 / 1	0 / 0	0 / 0	1 / 1	1 / 1	0 / 0	1 / 0	1 / 1
M6	1 / 1	0 / 0	1 / 1	0 / 0	0 / 0	0 / 0	0 / 0	0 / 0	1 / 1	1 / 1	0 / 0	0 / 0	1 / 1
M7	0 / 0	0 / 0	1 / 1	1 / 1	0 / 0	1 / 1	1 / 1	0 / 0	0 / 0	0 / 0	0 / 0	1 / 1	0 / 0
M8	0 / 0	1 / 1	0 / 0	1 / 1	1 / 1	0 / 0	1 / 1	1 / 1	0 / 0	0 / 0	1 / 1	0 / 0	0 / 0
Se1	0 / 0	0 / 0	0 / 0	0 / 0	0 / 0	0 / 0	0 / 0	0 / 0	0 / 0	0 / 0	1 / 1	1 / 1	1 / 1
Se2	0 / 0	0 / 0	0 / 0	0 / 0	0 / 0	0 / 0	0 / 0	0 / 0	0 / 0	0 / 0	0 / 0	0 / 0	0 / 0
Se3	0 / 0	0 / 0	0 / 0	0 / 0	0 / 0	0 / 0	0 / 0	0 / 0	0 / 0	0 / 0	0 / 0	0 / 0	0 / 0
Se4	0 / 0	0 / 0	0 / 0	0 / 0	0 / 0	0 / 0	0 / 0	0 / 0	0 / 0	0 / 0	0 / 0	0 / 0	0 / 0
CN	2	2	2	2	4	4	4	4	4	4	3	2	4

Table 5.2.3.e: continued

	O10	O11	O12	O13	O14	O15	O16	O17	O18	CN
M1	1 / 1	0 / 0	1 / 1	0 / 0	1 / 1	2 / 2	0 / 0	0 / 0	0 / 0	8
M2	0 / 0	0 / 0	0 / 0	0 / 0	0 / 0	0 / 0	0 / 0	2 / 2	1 / 1	8
M3	0 / 0	1 / 1	1 / 1	1 / 1	0 / 0+1	0 / 0	0 / 0	0 / 0	0 / 0	7+1
M4	1 / 1	0 / 0	0 / 0	1 / 1	0 / 0	0 / 0	1 / 1	1 / 1	0 / 0	8
M5	0 / 0	0 / 0	0 / 0	0 / 0	0 / 0	0 / 0	0 / 0	0 / 0	1 / 1	8
M6	0 / 0	1 / 1	0 / 0	0 / 0	0 / 0	0 / 0	0 / 0	0 / 0	1 / 1	7
M7	0 / 0	0 / 0	1 / 1	0 / 0	1 / 1	0 / 0	0 / 0	0 / 0	0 / 0	7
M8	0 / 0	0 / 0	0 / 0	0 / 0	0 / 0	1 / 1	0 / 0	0 / 0	0 / 0	7
Se1	0 / 0	0 / 0	0 / 0	0 / 0	0 / 0	0 / 0	0 / 0	0 / 0	0 / 0	3
Se2	1 / 1	1 / 1	1 / 1	0 / 0	0 / 0	0 / 0	0 / 0	0 / 0	0 / 0	3
Se3	0 / 0	0 / 0	0 / 0	1 /1	1 / 1	1 / 1	0 / 0	0 / 0	0 / 0	3
Se4	0 / 0	0 / 0	0 / 0	0 / 0	0 / 0	0 / 0	1 / 1	1 / 1	1 / 1	3
CN	3	3	4	3	3	4	2	4	4	

5.3 Structure of $Gd_5O_4Br_3[SeO_3]_2$ and $Tb_5O_4Cl_3[SeO_3]_2$

5.3.1 Synthesis of $Gd_5O_4Br_3[SeO_3]_2$ and $Tb_5O_4Cl_3[SeO_3]_2$

Homogeneous powders of $Gd_5O_4Br_3[SeO_3]_2$ and $Tb_5O_4Cl_3[SeO_3]_2$ were obtained starting from the mixtures 3 Gd_2O_3 / 3 GdOBr / $GdBr_3$ / 4 SeO_2 and 9 Tb_4O_7 / 21 TbOCl / 7 $TbCl_3$ / 28 SeO_2 / 6 Tb, respectively, corresponding to the reactions schemes:

$$3\ Gd_2O_3 + 3\ GdOBr + GdBr_3 + 4\ SeO_2 \longrightarrow 2\ Gd_5O_4Br_3[SeO_3]_2 \qquad (10)$$

$$9\ Tb_4O_7 + 21\ TbOCl + 7\ TbCl_3 + 28\ SeO_2 + 6\ Tb \longrightarrow 14\ Tb_5O_4Cl_3[SeO_3]_2 \qquad (11)$$

The mixtures were housed into quartz-glass tubes, which were sealed under primary vacuum and then heated at 830°C for seven days. Single crystals could be obtained after this thermal treatment followed by slow cooling (0.1°C/min) to 400°C when excess of molten CsBr or CsCl were added to the reactants as flux. Plate-like crystals suitable for single crystal X-ray diffraction studies were isolated from the bulk materials. The synthesis of GdOBr and TbOCl has been described elsewhere in this work (paragraph 5.1.1). The set of physical and crystallographic characteristics obtained from κ-CCD single crystal diffractemeter data, final atomic coordinates, anisotropic thermal displacement parameters as well as selected interatomic distances and angles and the motifs of the mutual adjunction are listed in paragraph 5.3.3.

5.3.2 Structure description of $Gd_5O_4Br_3[SeO_3]_2$ and $Tb_5O_4Cl_3[SeO_3]_2$

The two phases $M_5O_4X_3[SeO_3]_2$ corresponding to M = Gd, X = Br and M = Tb, X = Cl are isostructural. In their monoclinic unit cell, there are three crystallographic different M^{3+} sites. M1 (*2b*, site symmetry: 2/m) has an eightfold coordination. Four O2 belonging to two $[SeO_3]^{2-}$ groups and four oxide anions $(O3)^{2-}$ are making up a square prismatic coordination polyhedra. The distortion of the bond lengths and angles within the $[(M1)O_8]$ polyhedra (fig. 5.3.2.a) are mainly caused by polyhedral interconnections. Each polyhedron shares two edges O2–O2 (d(O2–O2) = 259 pm for both the Gd and Tb compound) with two $[SeO_3]^{2-}$ pyramids which are jammed in the notches between them. These edges are by far the shortest within the polyhedron and the corresponding opposite bond angles are reduced to values from 72.8° to 62.5° (Gd) and from 73.8° to 62.1° (Tb). The related O2–Se–O2 angles are also reduced to values from the average of 101° (as given by *Fischer* and *Zemann* [108]) to values as small as

95.9° (Gd) and 96.5° (Tb), whereas the remaining two angles of the $[SeO_3]^{2-}$ pyramid are extended to about 97.3° (Gd) and 97.4° (Tb). Another such an example is found in $Li_2Cu_3(SeO_3)(SeO_4)_2$ where the smallest O–Se–O angle is only 90.7° [109]. The M2 atoms are surrounded by six oxygen atoms (four oxide ions and two O2 as monodentate ligands of $[SeO_3]^{2-}$ groups) and one chloride anion forming a capped trigonal prismatic coordination sphere. The site symmetry *m* occupied by M2 atoms (4i) is absolutely reflected here with the symmetry plane constructed by M2 and X2. The $(M3)^{3+}$ cations reside in a distorted square antiprismatic coordination built up by two oxide ions, three $[SeO_3]^{2-}$ groups (monodentately connected to $[(M3)O_5X_3]$ polyhedra through the oxygen atoms O2 (2×) and O1 (1×)) and three chloride anions (fig. 5.3.2.a). The single crystallographic selenium atom has the well-known one-sided threefold coordination with classical bond lengths and angles (d(Se–O) = 165 – 174 pm, 3×; ∢(O–Se–O) = 96 – 97°, 3×; displacement of Se^{4+} from the O–O–O plane: 86 pm in $Tb_5O_4Cl_3[SeO_3]_2$ and 85 pm in $Gd_5O_4Br_3[SeO_3]_2$). Due to the lone pair of electrons (designed by *E*) at the Se atoms, its coordination ψ^1-polyhedra can be described as a tetrahedron $[SeO_3E]^{2-}$. Equally significant, five terminal M^{3+} along with one edge-spanning M^{3+} cations complete the cationic neighbourhood of the $[SeO_3]^{2-}$ groups in both compounds (fig. 5.3.2.b).

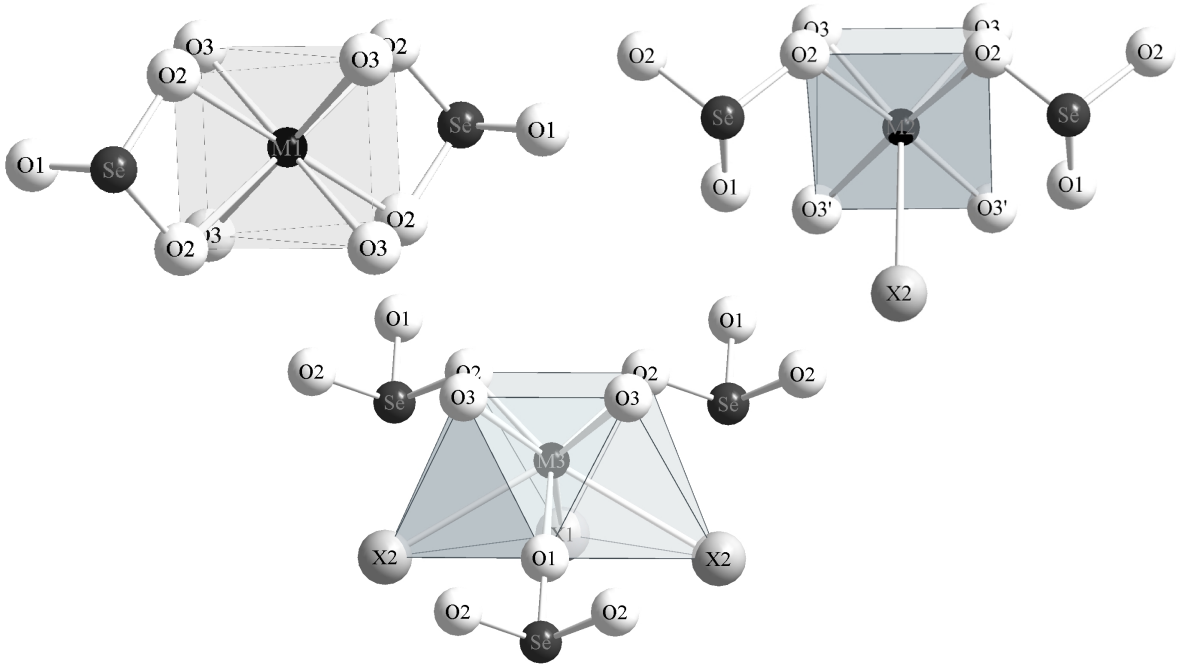

Fig. 5.3.2.a: Square prismatic, capped trigonal prismatic and distorted square antiprismatic coordination of oxygen and halide particles around M^{3+} cations $M_5O_4X_3[SeO_3]_2$ (M = Gd, X = Br; M = Tb, X = Cl)

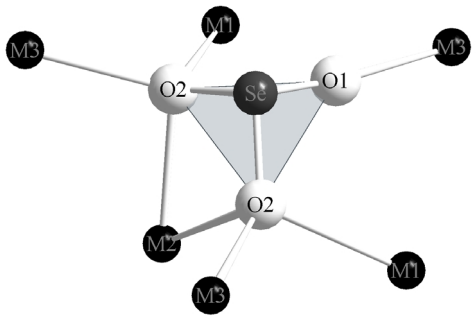

Fig. 5.3.2.b: Coordination sphere about the trigonal pyramidal $[SeO_3]^{2-}$ anion consisting of six cations (five terminal and one edge-spanning M^{3+})

There are two symmetrically independent X-sites in both compounds. The $(X1)^-$ anions located at the special site (*2c*; 0, 0, ½; site symmetry: 2/m) of the space group C2/m are linear coordinated by two M^{3+} cations with M–X–M-bond angles of 180°, whereas $(X2)^-$ is one-sided trigonal coordinated by three M^{3+} and its coordination figure shows two different bond angles of 79.8° (2×) and 125.3 (1×) for Tb and 76.3 (2×) and 119.7 (1×) for Gd (fig. 5.3.2.c). The M–O-bond lengths between 222 and 265 pm for Gd–O bonds or 219 and 261 pm for Tb–O bonds correlate well with those in the ternary compounds $M_2O[SeO_3]_2$ (M = Gd, Tb) (paragraph 4.3). In the same way, values in the range of 301 – 318 pm for Gd–Br bonds and 283 – 307 pm for Tb–Cl bonds compare satisfactorily with related ones in the tetragonal GdOBr and TbOCl (d(Gd–Br) = 319 and 320 pm, d(Tb–Cl) = 307 and 310 pm, PbFCl-type structure) [107] for example.

The crystal structure of $M_5O_4X_3[SeO_3]_2$ is layered and built up of corrugated lanthanide-oxygen sheets $^2_\infty\{[O_4M_5]^{7+}\}$, formed by *edge*- and *vertex*-shared $[OM_4]^{10+}$ tetrahedra (d(O3–Gd) = 227 – 234 pm and d(O3–Tb) = 225 – 233 pm, 4× each), spreading out parallel to (001). Furthermore, the structure is highly related to the "*lone-pair*" channel structures of $M_2O[SeO_3]_2$ (see [97] and paragraph 4.2) and $M_3O_2Cl[SeO_3]_2$ (see [110] and paragraph 5.1.2), where single ($^1_\infty\{[OM_2]^{4+}\}$) and double chains ($^1_\infty\{[O_2M_3]^{5+}\}$) of *trans*-edge connected $[OM_4]^{10+}$ tetrahedra are present. As an extension of this kind of connectivity, the double chains ($^1_\infty\{[O_2M_3]^{5+}\}$) of the $M_3O_2Cl[SeO_3]_2$-type structure are further condensed via common vertices to form the above-mentioned $^2_\infty\{[O_4M_5]^{7+}\}$ layers (fig. 5.3.2.d). As previously observed in the $M_4O_3Cl_2[SeO_3]_2$-type structure (see paragraph 4.2.2) the cohesion of the network is ensured by $[SeO_3]^{2-}$ and halide (Cl^- or Br^- anions) which are positioned at both sides of the $^2_\infty\{[O_4M_5]^{7+}\}$ layers in 2:3-molar ratio thus allowing charge compensation and the three-dimensional interconnection (fig. 5.3.2.e). Interestingly such an arrangement provides

again a further example of selenates(IV) of the rare-earth elements in which interaction between the lone pairs *E* and the large chloride or bromide anions is observed. The distances *E*–X (X = Cl or Br) of 347 pm and 351 pm, respectively, for $Tb_5O_4Cl_3[SeO_3]_2$ and $Gd_5O_4Br_3[SeO_3]_2$ appear to be more or less comparable to the corresponding ones (333 pm) in the structures of $MCl[SeO_3]$ (M = Nd, Er, Ho) [36]. Once again, the triangular faces of the $[OM_4]^{10+}$ tetrahedra forming layers are not parallelly orientated to the O–O–O face of the $[SeO_3]^{2-}$ groups, thus it becomes clear that the face-to-face relationship between oxocentered tetrahedra and $[SeO_3]^{2-}$ entities as stated by *Krivovichev* in the crystal structures of $Cu_9O_2Cl_6[SeO_3]_4$ and $Cu_5O_2Cl_2[SeO_3]_2$ may only occur when $[OM_4]$ tetrahedra share just vertices while forming chains or layers [38, 39]. In addition, following the topological properties of tetrahedra in polyions studied by *Wells* [111 – 113] and *Krivovichev* [114], we ought to mention that all $[(O3)M_4]$ tetrahedral units in $M_5O_4X_3[SeO_3]_2$ are topologically equivalent for having the same arrangement of shared elements: three edges and one vertex sharing each when forming the $^{2}_{\infty}\{[O_4M_5]^{7+}\}$ sheets (fig. 5.3.2.d). The $^{2}_{\infty}\{[O_4M_5]^{7+}\}$ homometallic layer is topologically exactly the same as the $^{2}_{\infty}\{[O_4Bi_2Cu_3]^{4+}\}$ heterometallic one in the structure of $A_2[Bi_2Cu_3O_4](AsO_4)_2 \cdot 2H_2O$ (A = Na, K) [115], thus both can be considered as related crystal structures with identical cationic layers. If one denotes within layers the metal bridging corners and bridging edges by $M_{b\text{-}c}$ and $M_{b\text{-}e}$, respectively, the $(M1)_{b\text{-}e}$ metals atoms have eight M···M metal-metal contacts against ten for $(M2)_{b\text{-}c}$ and only five for $(M3)_{b\text{-}e}$. Therefore, the $(M1)_{b\text{-}e}$ and $(M2)_{b\text{-}c}$ atoms are secured to the layers more firmly than the $(M3)_{b\text{-}e}$ ones. Shortening of the O–$(M2)_{b\text{-}c}$ and O–$(M3)_{b\text{-}e}$ distances leads to the shortening of $(M2)_{b\text{-}c}$–$(M3)_{b\text{-}e}$ (363 pm) and $(M2)_{b\text{-}c}$–$(M2)_{b\text{-}c}$ (357 pm) contacts and hence causes the $(M2)_{b\text{-}c}$–$(M3)_{b\text{-}e}$ and $(M2)_{b\text{-}c}$–$(M2)_{b\text{-}c}$ repulsion. These repulsive forces are compensated by an increase of the $(M1)_{b\text{-}e}$–$(M2)_{b\text{-}c}$ (382 pm) and $(M1)_{b\text{-}e}$–$(M3)_{b\text{-}e}$ (394 pm) distances leading to an increase of the $(M2)_{b\text{-}c}$–O–$(M1)_{b\text{-}e}$ (112°) and $(M2)_{b\text{-}c}$–O–$(M3)_{b\text{-}e}$ (117°) valence angles. In the above description, we have used the rule by *Wells* (1970) [111 – 113] stating that if an edge is shared between to polyhedra, its vertices are not counted as shared vertices between these polyhedra. However, it was convenient for us to consider the M2 atoms in the polyion $^{2}_{\infty}\{[O_4M_5]^{7+}\}$ as bridging vertex-atoms by the fact that they relate different $^{1}_{\infty}\{[O_2M_3]^{5+}\}$ slabs only via corners (fig. 5.3.2.d).

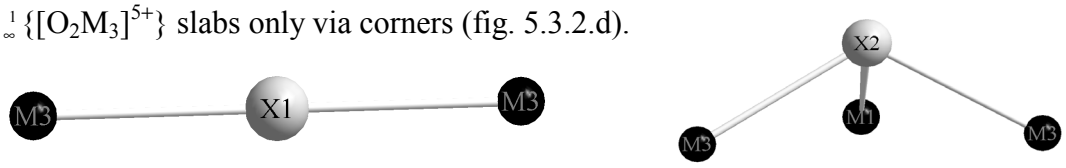

Fig. 5.3.2.c: Coordination spheres about the X^- anions in $M_5O_4X_3[SeO_3]_2$

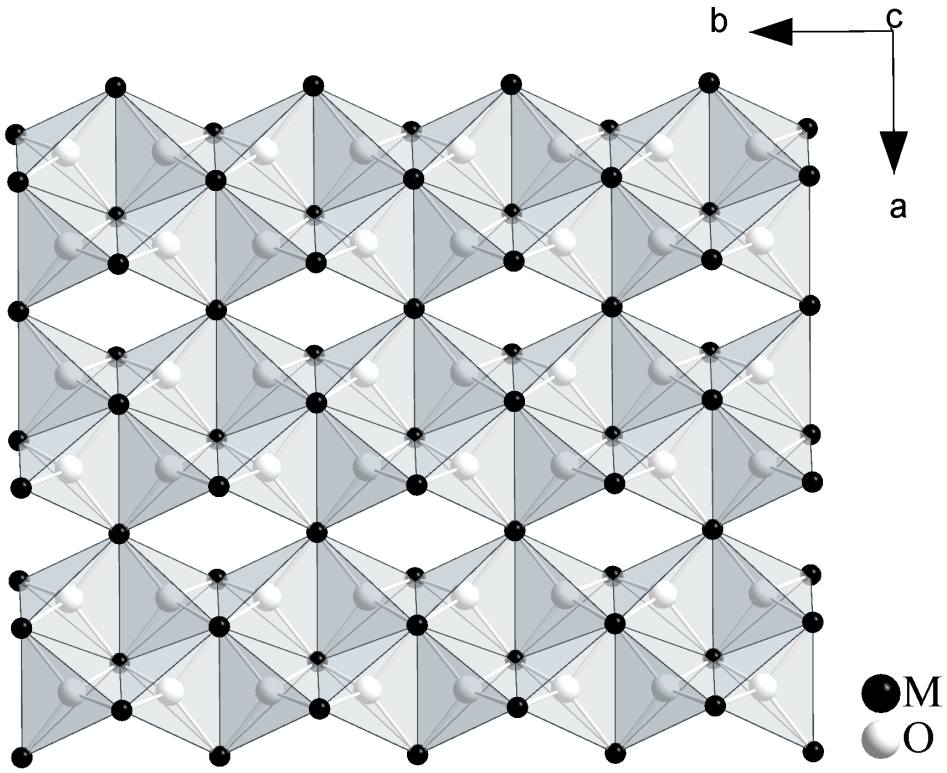

Fig. 5.3.2.d: The connectivity among $^{1}_{\infty}\{[O_2M_3]^{5+}\}$ double chains in (001) projection leading to the $^{2}_{\infty}\{[O_4M_5]^{7+}\}$ sheets in the crystal structure of $M_5O_4X_3[SeO_3]_2$

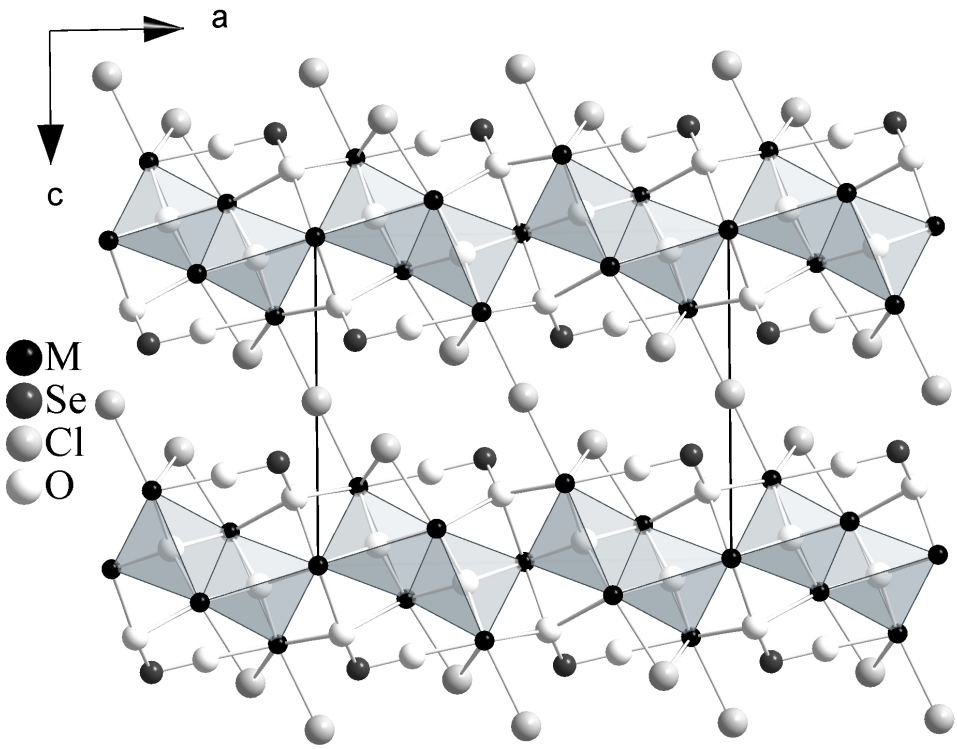

Fig. 5.3.2.e: The whole crystal structure of $M_5O_4X_3[SeO_3]_2$ viewed down (010) where the $^{2}_{\infty}\{[O_4M_5]^{7+}\}$ layers and the three-dimensional framework are emphasized

5.3.3 Structural data for $Gd_5O_4Br_3[SeO_3]_2$ and $Tb_5O_4Cl_3[SeO_3]_2$

Table 5.3.3.a: Crystallographic data for $Gd_5O_4Br_3[SeO_3]_2$ and $Tb_5O_4Cl_3[SeO_3]_2$

Formula		Gd	Tb
Crystal system and space group		monoclinic, C2/m (No. 12)	
Formula unit per unit cell (Z)		2	
Unit cell parameters:	a =	1243.70(10) pm	1229.13(4) pm
	b =	549.91(4) pm	546.17(4) pm
	c =	1005.29(9) pm	978.79(7) pm
	β =	91.869(3) °	90.485(6) °
Calculated density (D_x / g · cm^3)		6.495	6.161
Molar volume (V_m / cm^3 · mol^{-1})		198.524	197.871
Diffractometer, radiation		κ-CCD (Fa. Nonius); Mo-K_α: λ = 71.07 pm	
$2\theta_{max.}$		54.9	55.0
Index range	$\pm h_{max} / \pm k_{max} / \pm l_{max}$ =	16 / 6 / 13	15 / 7 / 12
F(000)		1146	1048
Absorption coefficients (μ)		37.85	32.75
Absorption correction		Numerical, after crystal shape optimization with the program X-SHAPE [53]	
Other data corrections		background, polarization, *Lorentz* factors	
Collected reflections		5914	6679
Unique reflections		870	836
R_{int} / R_σ		0.075 / 0.045	0.091 / 0.052
Reflections with $\lvert F_o\rvert \geq 4\sigma\lvert F_o\rvert$		734	735
Structure solution and refinement		Program system SHELX-97 [58]	
Scattering factors		International Tables, Vol. C [85]	
R_1 / R_1 with $\lvert F_o\rvert \geq 4\sigma\lvert F_o\rvert$		0.051 / 0.039	0.036 / 0.031
wR_2 / Goodness of fit (GooF)		0.137 / 1.011	0.078 / 1.06
Extinction (g)		0.00149(13)	0.00294(18)
Residual electron density	max.	5.53	1.53
(ρ / e$^-$ 10^6 pm)	min.	–1.93	–1.58

Table 5.3.3.b: Atomic coordinates for $Gd_5O_4Br_3[SeO_3]_2$ and $Tb_5O_4Cl_3[SeO_3]_2$

Atoms	Wyckoff Position	x / a	y / b	z / c
Gd1	2b	1/2	0	0
Gd2	4i	0.20861(6)	0	0.39703(9)
Gd3	4i	0.10770(6)	0	0.73244(9)
Se	4i	0.4150(1)	0	0.8062(2)
Br1	2c	0	0	0
Br2	4i	0.3189(2)	0	0.1343(2)
O1	4i	0.2860(9)	0	0.7589(7)
O2	8j	0.4536(7)	0.2351(6)	0.7021(8)
O3	8j	0.1460(5)	0.2467(6)	0.5584(7)
Tb1	2b	1/2	0	0
Tb2	4i	0.21283(4)	0	0.10593(5)
Tb3	4i	0.09915(4)	0	0.76280(5)
Se	4i	0.40565(8)	0	0.6836(1)
Cl1	2c	0	0	1/2
Cl2	4i	0.3337(2)	0	0.3538(3)
O1	4i	0.2743(6)	0	0.7211(8)
O2	8j	0.0562(4)	0.2625(9)	0.2079(5)
O3	8j	0.3563(4)	0.2546(9)	0.0588(5)

Table 5.3.3.c: Anisotropic thermal displacement parameters[b)] (U_{ij}/pm^2) for $Gd_5O_4Br_3[SeO_3]_2$ and $Tb_5O_4Cl_3[SeO_3]_2$

Atoms	U_{11}	U_{22}	U_{33}	U_{23}	U_{13}	U_{12}
Gd1	128(5)	117(5)	134(6)	0	5(3)	0
Gd2	132(6)	100(6)	121(7)	0	3(4)	0
Gd3	125(5)	115(5)	136(5)	0	7(3)	0
Se	121(8)	119(8)	136(10)	0	–7(6)	0
Br1	364(15)	203(13)	174(15)	0	101(11)	0
Br2	244(10)	255(10)	156(11)	0	12(7)	0
O1	85(36)	104(38)	164(47)	24(27)	13(31)	1(25)
O2	199(44)	110(38)	212(46)	62(33)	72(33)	–23(29)
O3	193(39)	565(40)	250(39)	0	52(41)	0
Tb1	133(3)	154(4)	232(9)	0	–4(3	0
Tb2	141(3)	161(3)	241(3)	0	–8(2)	0
Tb3	136(3)	163(3)	241(3)	0	–11(2)	0
Se	138(5)	176(6)	237(5)	0	6(4)	0
Cl1	428(23)	271(22)	338(21)	0	–83(18)	0
Cl2	305(14)	425(18)	260(13)	0	–23(11)	0
O1	175(37)	709(71)	446(51)	0	106(36)	0
O2	277(26)	162(28)	251(24)	8(21)	8(21)	–25(21)
O3	145(23)	131(28)	286(27)	–29(17)	–36(23)	13(17)

[b)] defined as temperature factor according to: $\exp[-2\pi^2(a^{*2}h^2U_{11} + b^{*2}k^2U_{22} + c^{*2}l^2U_{33} + 2b^*c^*klU_{23} + 2a^*c^*hlU_{13} + 2a^*b^*hkU_{12})]$

Table 5.3.3.d: Selected internuclear distances (d/pm) and angles (∢/deg) in $Gd_5O_4Br_3[SeO_3]_2$ and $Tb_5O_4Br_3[SeO_3]_2$

Gd		Tb	
	d / pm		d / pm
Gd1 – O3	234.8 (4×)	Tb1 – O3	232.4 (4×)
– O2	249.2 (4×)	– O2	250.6 (4×)
Gd2 – O3	227.2 (2×)	Tb2 – O3	225.7 (2×)
– O3′	231.5 (2×)	– O3′	229.6 (2×)
– O2	265.6 (2×)	– O2	260.6 (2×)
– Br2	301.5 (1×)	– Cl2	283.4 (1×)
Gd3 – O1	222.4 (1×)	Tb3 – O1	219.5 (1×)
– O3	227.7 (2×)	– O3	226.5 (2×)
– O2	241.8 (2×)	– O2	240.7 (2×)
– Br1	304.4 (1×)	– Cl1	283.7 (1×)
– Br2	317.9 (2×)	– Cl2	307.5 (2×)
Se – O1	165.9 (1×)	Se – O1	165.9 (1×)
– O2	174.1 (2×)	– O2	173.8 (2×)
	∢ / grd		∢ / grd
Gd2 – O3 – Gd2	102.5	Tb2 – O3 – Tb2	102.6
Gd2 – O3 – Gd1	106.3	Tb2 – O3 – Tb1	105.9
Gd2 – O3 – Gd3	106.8	Tb2 – O3 – Tb3	106.6
Gd3 – O3 – Gd1	112.2	Tb3 – O3 – Tb1	111.5
Gd3 – O3 – Gd2	113.1	Tb3 – O3 – Tb2	112.6
Gd2 – O3 – Gd1	117.1	Tb2 – O3 – Tb1	117.4
O2 – Se – O2	95.7 (1×)	O2 – Se – O2	96.6 (1×)
O1 – Se – O2	96.4 (2×)	O1 – Se – O2	97.1 (2×)

Table 5.3.3.e: Motifs of mutual adjunction in $Gd_5O_4Br_3[SeO_3]_2$ and $Tb_5O_4Br_3[SeO_3]_2$

	X1	X2	O1	O2	O3	CN
M1	0 / 0	0 / 0	0 / 0	4 / 1	4 / 1	8
M2	0 / 0	1 / 1	0 / 0	2 / 1	4 / 2	7
M3	1 / 2	2 / 2	1 / 1	2 / 1	2 / 1	8
Se	0 / 0	0 / 0	1 / 1	2 / 1	0 / 0	3
CN	2	3	2	4	4	

5.4 Structure of $M_9O_8Br_3[SeO_3]_4$ (M = La, Pr) and $M_9O_8Cl_3[SeO_3]_4$ (M = Pr, Nd, Sm, Gd)

5.4.1 Synthesis methods

Samples were prepared by solid-state reaction between M_2O_3, MOX, MX_3 and SeO_2 (M = La, Nd, Sm and Gd; X = Cl or Br). Additional powder of metallic praseodymium was added in the case of the mixed-valence compound Pr_6O_{11}. MOX samples such like PrOX were synthesized as described in paragraph 5.1.1. The starting materials could be weighed in stoichiometric proportions according to the following reactions:

$$7\ M_2O_3 + 3\ MOX + MX_3 + 8\ SeO_2 \longrightarrow 2\ M_9O_8X_3[SeO_3]_4 \qquad (12)$$

$$21\ Pr_6O_{11} + 33\ PrOX + PrX_3 + 88\ SeO_2 + 18\ Pr \longrightarrow 22\ Pr_9O_8X_3[SeO_3]_4 \qquad (13)$$

The best synthesis conditions typically were 850°C for seven days in evacuated sealed silica tubes followed by slow cooling (0.1°C/min) until 400°C, finally the furnace was turned off and allowed to reach the room temperature soon. Upon washing for dissolving the excess of CsCl or CsBr which were used as flux, fine-shaped single crystals could be obtain as green thin platelets for the praseodymium, yellowish green ones for the neodymium and colourless ones for the remainder elements compounds stated above. For checking the purity of our single crystals, we compared the theoretical powder X-ray diffractogram (negative intenities) with the experimental one (positive intensities) in the case of $Pr_9O_8Cl_3[SeO_3]_4$. From diagram 5.4.1.a, it is clear that no unknown phases are present in our single-crystalline sample. Crystallographic data obtained from X-ray measurement data, final atomic parameters and selected bond distances and angles as well as the motifs of the mutual adjunction are outlined in paragraph 5.4.3.

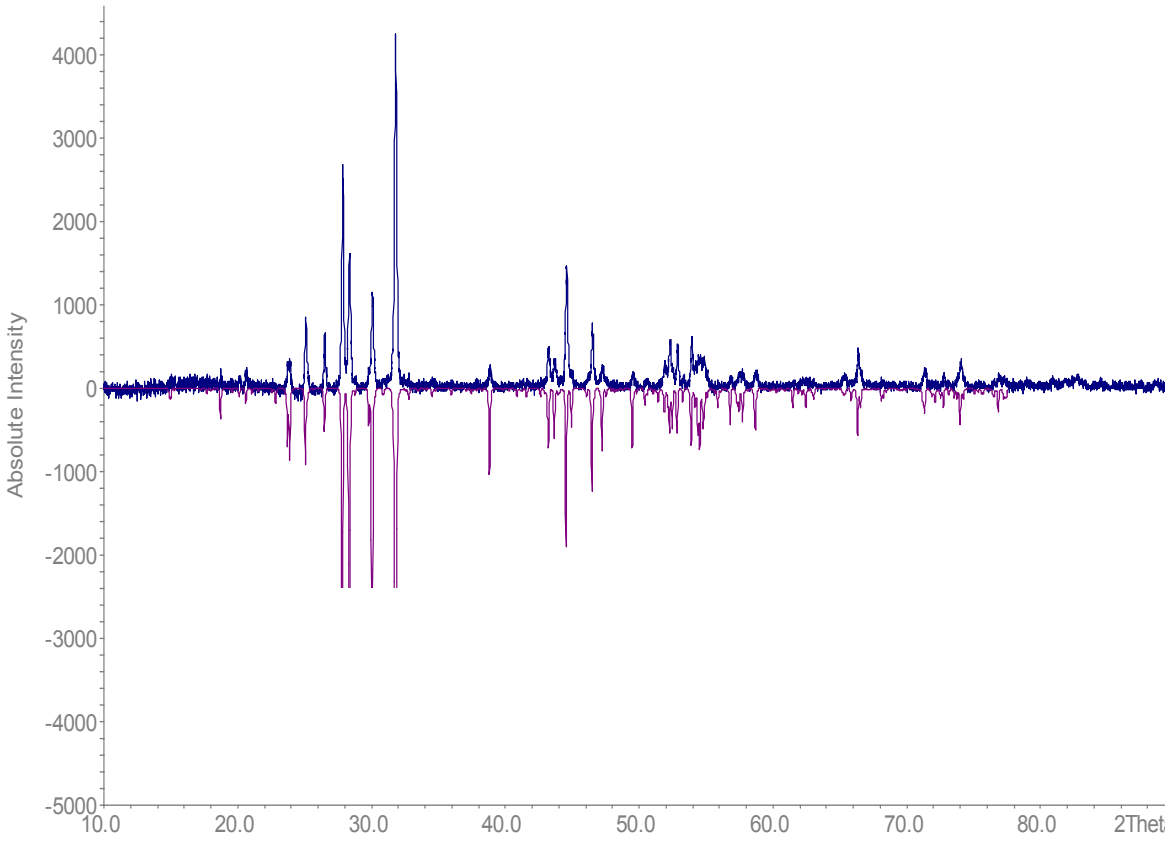

Diagram 5.4.1.a: Comparison of the measured powder X-ray diffractogram of $Pr_9O_8Cl_3[SeO_3]_4$ (*above*) with the theoretical one (*below*)

5.4.2 Structure description of $M_9O_8Br_3[SeO_3]_4$ (M = La, Pr) and $M_9O_8Cl_3[SeO_3]_4$ (M = Pr, Nd, Sm, Gd)

The five compounds of the formula $M_9O_8X_3[SeO_3]_4$ (La, Pr, Nd, Sm, Gd) are all isostructural and crystallize in the $P\bar{1}$ space group of the triclinic crystal system. Their structures are highly related to the $M_4O_3Cl_2[SeO_3]_2$ (M = Er, Yb) and $M_5O_4X_3[SeO_3]_2$ (M = Gd, Tb) type arrangements (X = Cl or Br). Investigated in this work (paragraph 5.2 and 5.3) these were found to build up metal-oxygen layers described as $^2_\infty\{([O_3M_4]^{6+})_2\}$ and $^2_\infty\{[O_4M_5]^{7+}\}$, respectively. The $^2_\infty\{[O_8M_9]^{11+}\}$ ones in the present case are also formed by oxocentered tetrahedra $[OM_4]^{10+}$ connected via edges and vertices similar to the connectivity found in the former compounds. The layers are further sandwiched by $[SeO_3]^{2-}$ groups and interleaved by

halide anions which in both cases (Cl^- or Br^-) fuse adjacent layers through M–X–M bonds (fig. 5.4.2.a), therefore being the second closest relationship among the three series of compounds that appears. Those similarities are shown best only by the close agreement of the crystal framework structures but not by the unit cell constants or the crystal system, despite the common space group $P\bar{1}$ is adopted by both series $M_4O_3Cl_2[SeO_3]_2$ and $M_9O_8X_3[SeO_3]_4$ of compounds.

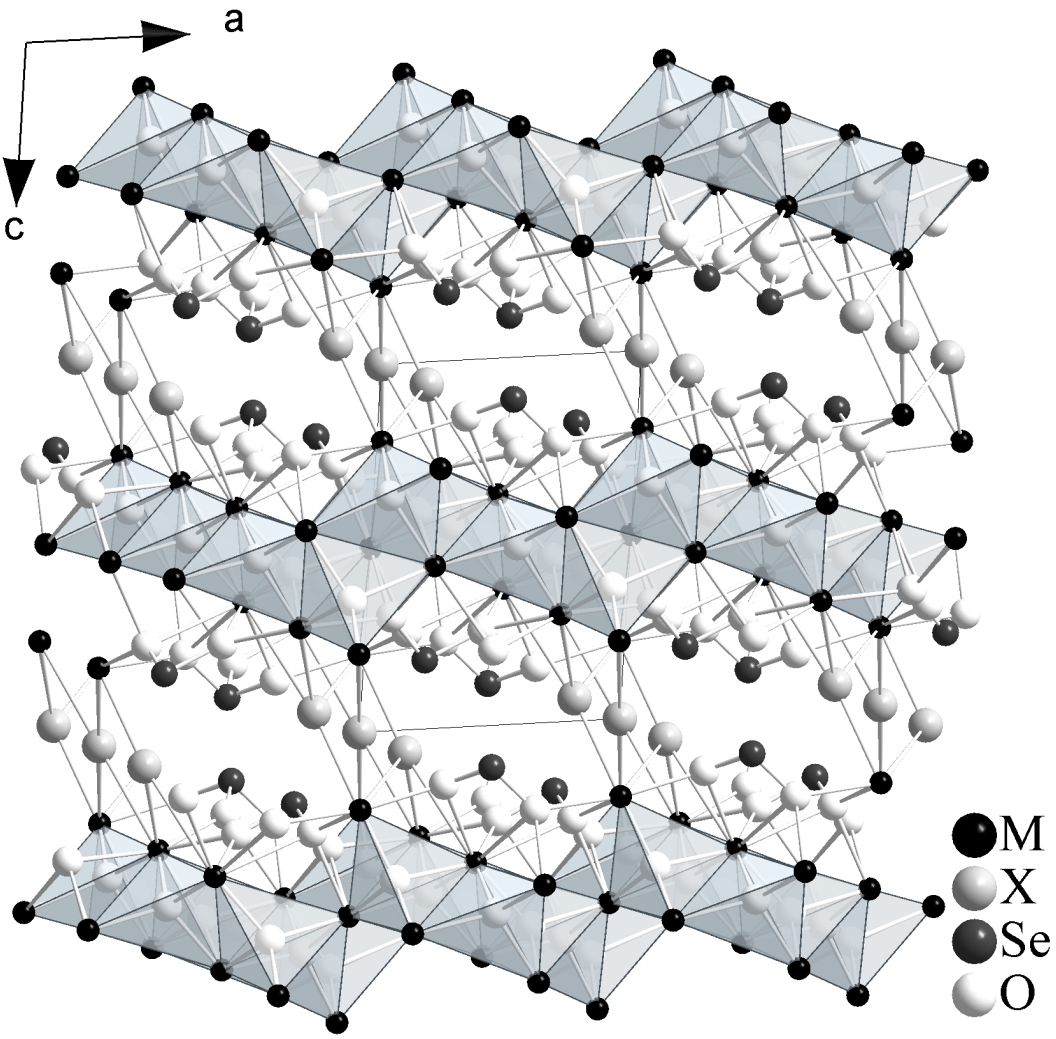

Fig. 5.4.2.a: Crystal structure of $M_9O_8X_3[SeO_3]_4$ where $^2_\infty\{[O_8M_9]^{11+}\}$ layers of fused $[OM_4]^{10+}$ tetrahedra are emphasized

Within the $^2_\infty\{[O_8M_9]^{11+}\}$ layers, one out of the four nonequivalent tetrahedral $[OM_4]^{10+}$ units involved has four edges (but no vertex) in common with neighbouring ones, whereas three edges and one vertex each are shared by the three others (fig. 5.4.2.b). These edges and corners as shared resemble the ones in the $^2_\infty\{[O_4M_5]^{7+}\}$ and $^2_\infty\{([O_3M_4]^{6+})_2\}$ layers (paragraph 5.2.3 and 5.2.2) as well. In the five investigated compounds, the non-shared edges exhibit

M···M metal-metal contacts in $[OM_4]$ tetrahedra within layers which have values ranging between 378.8 and 399.6 pm against 355.4 and 364.3 pm for the metal-metal contacts of shared edges, thus reflecting the distortion of the tetrahedra. The average O–M-bond lengths deminishes from lanthanum (247 pm) through neodymium (240.5 pm) up to 235.5 pm for gadolinium. This trend is also followed by the unit cell constants (see table 5.4.3.a) and obviously due the lanthanide contraction.

Taking all metal-metal contacts up to 400 pm into account and the quotation of the paragraph 5.3.2, $(M1)_{b\text{-}c}$, $(M2)_{b\text{-}c}$ and $(M5)_{b\text{-}c}$ have ten, respectively, eight metals contacts within the layers while $(M3)_{b\text{-}c}$ and $(M4)_{b\text{-}e}$ have only six and five ones. This reveals strong connectivity on the one hand and the more or less weak engagement on the other hand of the M^{3+} cations in the sheets. The M–O–M-bond angles in which both M–M contacts represent non-shared edges of the $[OM_4]^{10+}$ tetrahedra are ranging from 112 to 123°. This values deviate relatively strong from the corresponding ones (103 – 105°) in which M–M contacts represent sharing edges of the tetrahedral units. These deviations are indeed dictated by the topology of tetrahedral linkage and reflect once more the distortion of the tetrahedra within the layers. This geometrical topology is remarkably similar to the one shown in the $M_5O_4X_3[SeO_3]_2$-type structure (paragraph 5.3.2) by the way.

Further key features in this structure are the interaction between the free electron pairs at the selenium atoms and halide anions which bridge different layers. Distances like d(Se–Br) (but non-bonding) of 346 – 375 pm and 367 – 398 pm in $M_9O_8Br_3[SeO_3]_4$ (M = La resp. Pr) and d(Se–Cl) of 321 – 370 pm 319 – 368 pm, 318 – 366 pm and 316 – 365 pm in $M_9O_8Cl_3[SeO_3]_4$ (M = Pr, Nd, Sm, Gd resp.) occur. The high values in the case of the bromides may be attributed to the large ionic radiis of Br^- compared to Cl^-. Nevertheless this provides large voids for the free *non*-binding electron pairs ("*lone pairs*") of the Se^{4+} cations between layers. The cationic environment of $[(Se1)O_3]^{2-}$ consists of three terminal and two edge-spanning M^{3+} cations each whereas four terminal against two edge-spanning M^{3+} are observed around $[(Se2)O_3]^{2-}$ (fig. 5.4.2.c). There are five crystallographically different M^{3+} cations in the structure. While $(M1)^{3+}$ at the special position 0, ½, ½ (*1g*, site symmetry: $\bar{1}$, center of inversion) and $(M2)^{3+}$ are square prismatically coordinated by O^{2-} anions only, the vicinity of $(M3)^{3+}$ and $(M4)^{3+}$ exhibits square antiprisms of O^{2-} and X^- anions, whereas the $(M5)^{3+}$ environment can be looked at as a capped square prismatic ones. The shortest edges of the $[MO_8]$ polyhedra (O9–O10 = 254 pm, 2×, for $[(M1)O_8]$ and O6–O7 = 244.6 pm, 1×, for $[(M2)O_8]$; all as mean values) are due to the bidentate effect of the complex anions $[SeO_3]^{2-}$

that are grafted onto the coordination sphere through O6, O7, O9 and O10. Consequently those polyhedra are more or less strongly distorted (fig. 5.4.2.d).

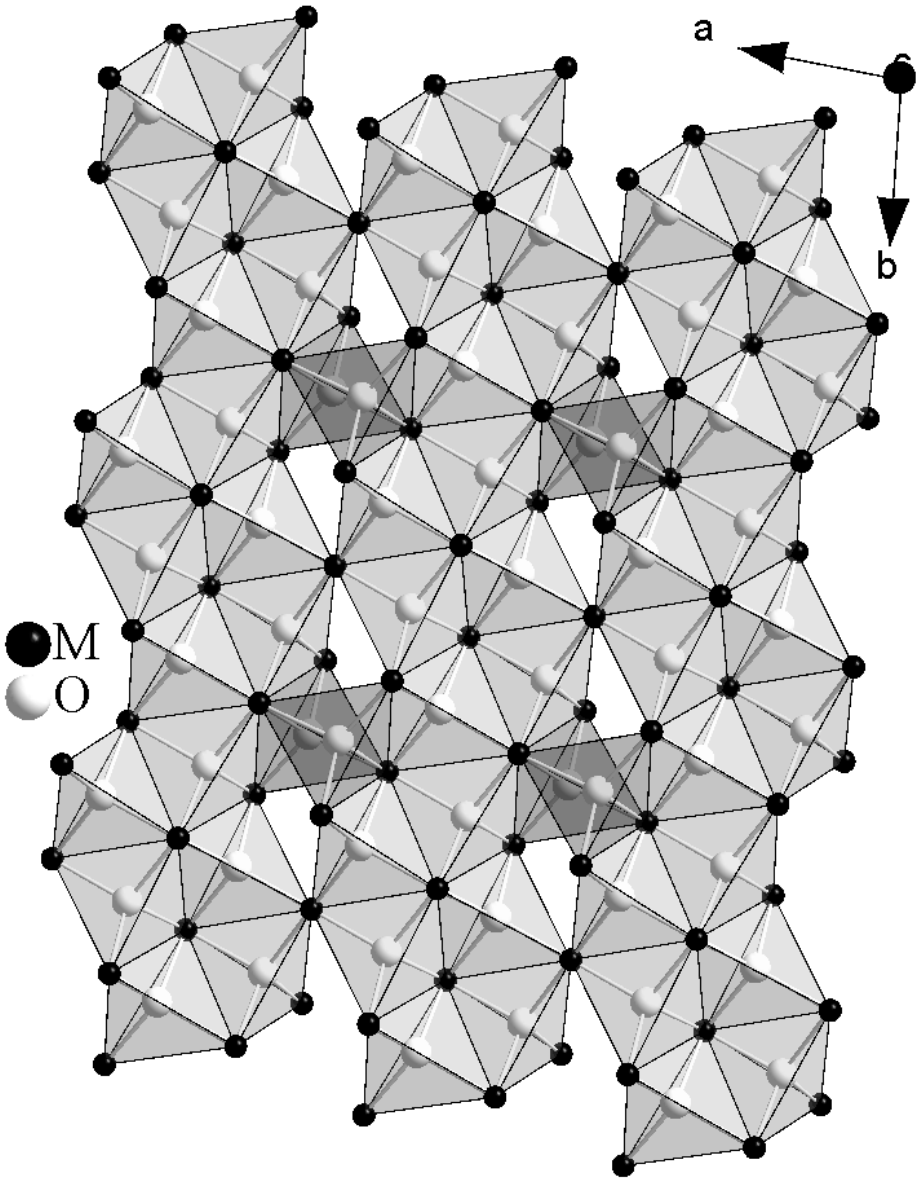

Fig. 5.4.2.b: Crystal structure of $M_9O_8X_3[SeO_3]_4$ viewed down (001) showing the connectivity among the cationic $[OM_4]^{10+}$ tetrahedra

Two short edges (O5–O6) and (O8–O10) are also detectable in the $[(M5)O_8X]$ polyhedra for the same reason, but the irregularities around $[(M3)O_6X_2]$ and $[(M4)O_5X_3]$ can be rather attributed to two different types of ligands than to the monodentate coordination of $[SeO_3]^{2-}$ complex anions. The coordination figures are thoroughly shown in figure 5.4.2.d. If all $[(M2)O_8]$ polyhedra are connected, it appears that parallel anionic zigzag chains are running along [100] within the framework structure formed by edges-sharing of $[(M2)O_8]$ polyhedra

(O3–O3 = 284.2 pm and O4–O4 = 289.6 pm) and described like $^{1}_{\infty}\{[(M2)_2O_{14}]^{22-}\}$ (fig. 5.4.2.e). The $[(M1)O_8]$ polyhedra are located between adjacent $^{1}_{\infty}\{[(M2)_2O_{14}]^{22-}\}$ strands and combine them through two opposite edges (O2–O9 = 279.5 pm; 2×) into a two-dimensional anionic layer like $^{2}_{\infty}\{[(M2)_{4/2}(M1)_{2/2}O_{18}]^{23-}\}$ extending parallel to (001) (see fig. 5.4.2.f).

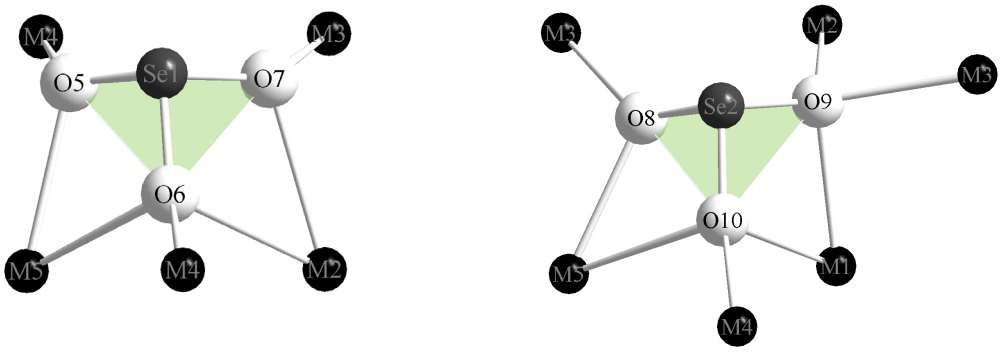

Fig. 5.4.2.c: Vicinity of M^{3+} cations about the two different ψ^1-tetrahedral $[SeO_3]^{2-}$ groups

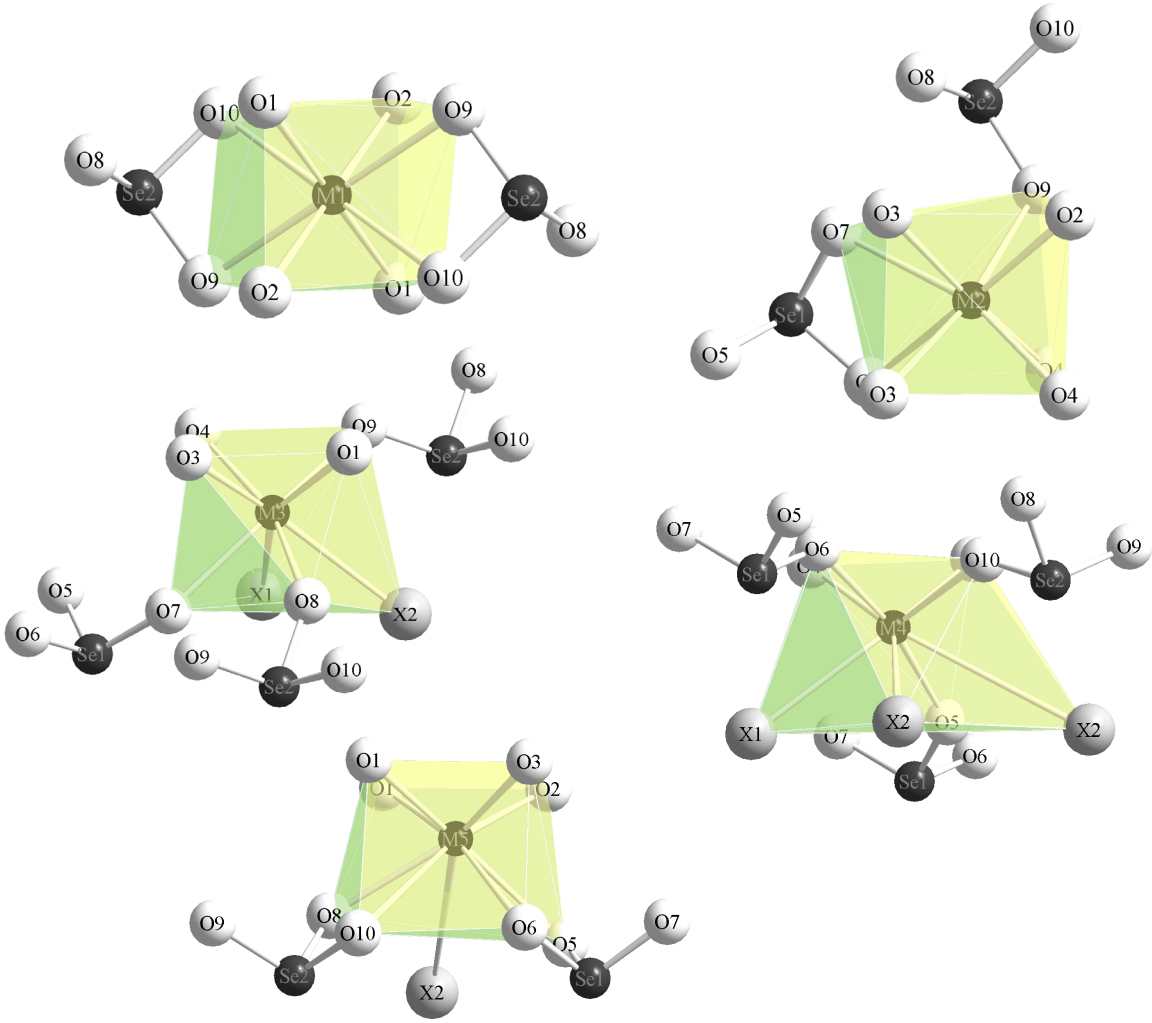

Fig. 5.4.2.d: Coordination of oxide (O^{2-}), halide (X^-) and $[SeO_3]^{2-}$ anions about the five crystallographically different M^{3+} cations in $M_9O_8X_3[SeO_3]_4$

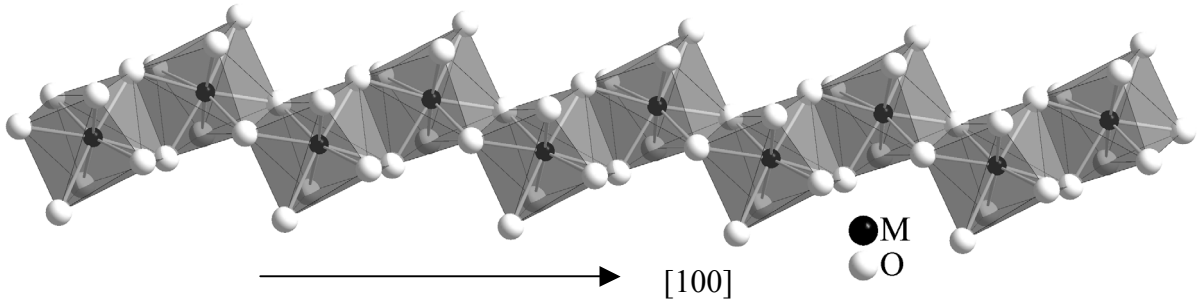

Fig. 5.4.2.e: The infinite $^{1}_{\infty}\{[(M2)_2O_{14}]^{22-}\}$ chain running along the [100] direction in the crystal structure of $M_9O_8X_3[SeO_3]_4$

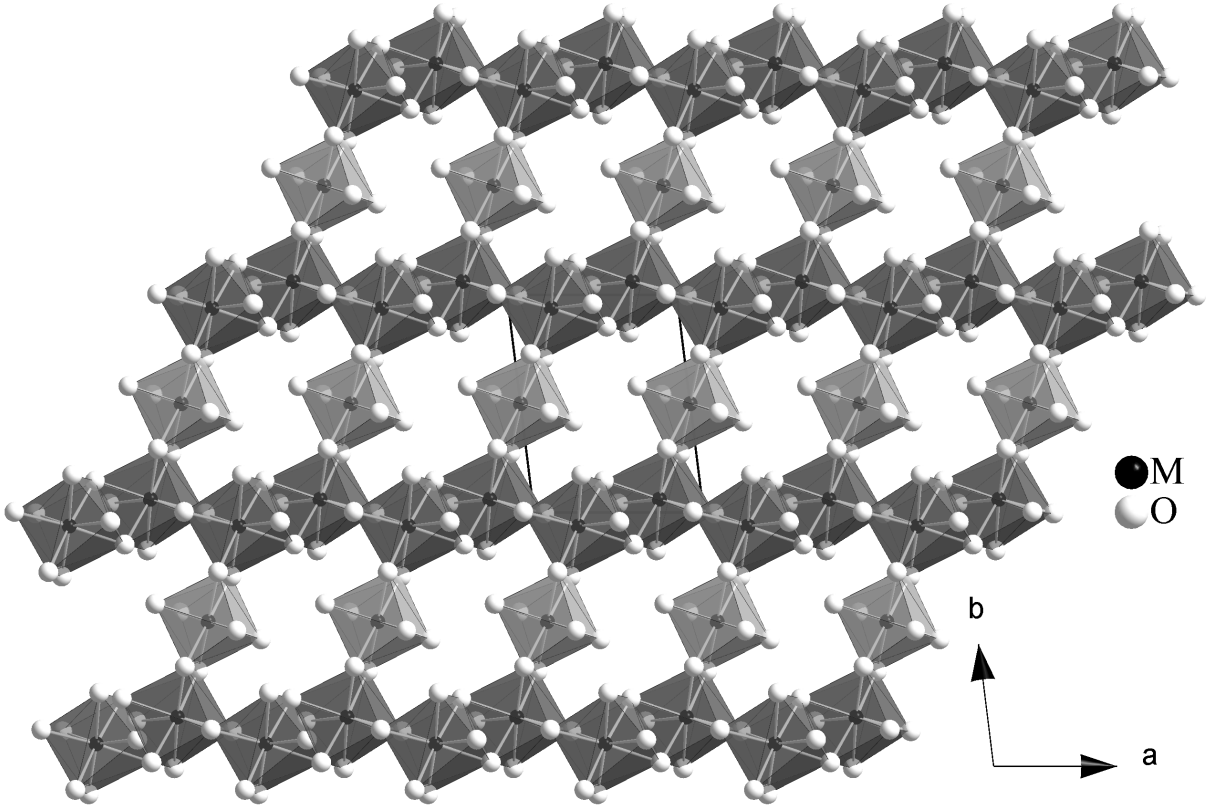

Fig. 5.4.2.f: (001) projection of the $^{2}_{\infty}\{[(M2)_{4/2}(M1)_{2/2}O_{18}]^{23-}\}$ layers in the crystal structure of $M_9O_8X_3[SeO_3]_4$ (M1: medium grey, M2: dark grey polyhedra)

5.4.3 Structural data for $M_9O_8Br_3[SeO_3]_4$ (M = La, Pr) and $M_9O_8Cl_3[SeO_3]_4$ (M = Pr, Nd, Sm, Gd)

Table 5.4.3.a: Crystallographic data for $M_9O_8Br_3[SeO_3]_4$ (M = La, Pr)

M		La	Pr
Crystal system and space group		triclinic, $P\bar{1}$ (No. 2)	
Formula unit per unit cell (Z)		1	
Unit cell parameters:	a / pm =	711.72(3)	700.35(4)
	b / pm =	919.56(4)	906.09(6)
	c / pm =	996.58(5)	985.91(7)
	α / ° =	99.658(2)	99.623(3)
	β / ° =	94.938)2)	95.076(3)
	γ / ° =	95.840(2)	95.874(3)
Calculated density (D_x / g · cm^3)		5.553	5.835
Molar volume (V_m / cm^3 · mol^{-1})		345.342(4)	341.123(1)
Diffractometer, radiation		κ-CCD (Fa. Nonius); Mo-K_α: λ = 71.07 pm	
$2\theta_{max.}$		55.1	
Index range:	$\pm h_{max}$ / $\pm k_{max}$ / $\pm l_{max}$ =	9 / 11 / 12	
F(000)		914	932
Absorption coefficients (μ / mm^{-1})		25.28	28.55
Absorption correction		Numerical, after crystal shape optimization with the program X-SHAPE [53]	
Other data corrections		background, polarization, *Lorentz* factors	
Collected reflections		19846	19357
Unique reflections		2913	2782
R_{int} / R_σ		0.129 / 0.070	0.107 / 0.054
Reflections with $\|F_o\| \geq 4\sigma\|F_o\|$		2060	2143
Structure solution and refinement		Program system SHELX-97 [58]	
Scattering factors		International Tables, Vol. C [85]	
R_1 / R_1 with $\|F_o\| \geq 4\sigma\|F_o\|$		0.101 / 0.064	0.095 / 0.072
wR_2 / Goodness of fit (GooF)		0.139 / 1.104	0.198 / 1.136
Extinction (g)		0.0052(7)	0.0042(5)
Residual electron density (ρ / e$^-$ 10^6 pm)		max. 1.95 ; min. –2.72	max. 7.75 ; min. –3.95

Table 5.4.3.b: Crystallographic data for $M_9O_8Cl_3[SeO_3]_4$ (M = Pr, Nd, Sm, Gd)

M		Pr	Nd	Sm	Gd
Crystal system and space group		triclinic, $P\bar{1}$ (No. 2)			
Formula unit per unit cell (Z)		1			
Unit cell parameters:	a / pm =	700.12(1)	696.30(2)	688.70(1)	680.17(5)
	b / pm =	901.63(2)	896.80(3)	888.79(2)	882.86(7)
	c / pm =	966.88(2)	963.87(4)	959.09(2)	960.18(8)
	α / ° =	99.787(1)	99.528(2)	98.647(1)	97.241(6)
	β / ° =	94.979(1)	95.176(2)	95.419(1)	95.539(6)
	γ / ° =	95.901(1)	95.893(2)	96.031(1)	96.265(6)
Calculated density (D_x / g · cm^3)		5.612	5.773	6.066	6.341
Molar volume (V_m / cm^3 · mol^{-1})		343.210	341.352	340.924	340.301
Diffractometer, radiation		κ-CCD (Fa. Nonius); Mo-K_α: λ = 71.07 pm			
$2\theta_{max.}$		55.0	54.8	54.9	54.9
Index range: $\pm h_{max}$ / $\pm k_{max}$ / $\pm l_{max}$ =		9 / 11 / 12	9 / 11 / 12	8 / 11 / 12	8 / 11 / 12
F(000)		878.0	887	905	923
Absorption coefficients (μ / mm^{-1})		24.58	26.14	29.42	32.89
Absorption correction		Numerical, after crystal shape optimization with the program X-SHAPE [53]			
Other data corrections		background, polarization, *Lorentz* factors			
Collected reflections		20169	21619	19168	17564
Unique reflections		2730	2667	2612	2579
R_{int} / R_σ		0.044 / 0.021	0.098 / 0.056	0.066 / 0.036	0.049 / 0.030
Reflections with $\|F_o\| \geq 4\sigma\|F_o\|$		2612	1946	2191	2223
Structure solution and refinement		Program system SHELX-97 [58]			
Scattering factors		International Tables, Vol. C [85]			
R_1 / R_1 with $\|F_o\| \geq 4\sigma\|F_o\|$		0.019 / 0.021	0.069 / 0.040	0.046 / 0.034	0.040 / 0.031
wR_2 / Goodness of fit (GooF)		0.057 / 1.039	0.095 / 1.029	0.103 / 1.151	0.067 / 1.04
Extinction (g)		0.0153(2)	0.00195(4)	0.00105(5)	0.0012(7)
Residual electron density	max.	1.12	2.55	1.73	2.35,
(ρ / e$^-$ 10^6 pm)	min.	–1.36	–2.09	–3.56	–2.26

Table 5.4.3.c: Atomic coordinates for $M_9O_8X_3[SeO_3]_2$ (M = La, Pr, Nd, Sm, Gd)

Atoms	Wyckoff Position	x / a	y / b	z / c
La1	1g	0	1/2	1/2
La2	2i	0.2582(1)	0.1865(1)	0.2922(1)
La3	2i	0.5163(2)	0.3802(1)	0.6334(1)
La4	2i	0.2517(2)	0.9395(1)	0.5606(1)
La5	2i	0.0221(2)	0.7518(1)	0.2088(1)
Br1	1a	0	0	0
Br2	2i	0.2045(3)	0.4155(2)	0.0812(2)
Se1	2i	0.2359(3)	0.6546(2)	0.8030(2)
Se2	2i	0.4633(3)	0.1370(2)	0.8812(2)
O1	2i	0.2962(4)	0.4172(3)	0.4486(3)
O2	2i	0.1744(4)	0.7010(3)	0.4034(3)
O3	2i	0.4409(4)	0.1454(3)	0.4861(3)
O4	2i	0.0690(4)	0.9877(3)	0.3548(3)
O5	2i	0.3491(4)	0.7473(4)	0.1497(3)
O6	2i	0.2963(4)	0.1837(3)	0.7643(3)
O7	2i	0.5061(5)	0.0314(3)	0.1896(3)
O8	2i	0.5536(4)	0.3427(3)	0.2597(4)
O8	2i	0.9038(4)	0.2654(3)	0.3033(3)
O10	2i	0.1656(4)	0.4670(3)	0.7407(3)
Pr1	1g	0	1/2	1/2
Pr2	2i	0.2561(1)	0.1874(1)	0.2944(1)
Pr3	2i	0.5168(2)	0.3796(1)	0.6313(1)
Pr4	2i	0.2524(1)	0.9393(1)	0.5601(1)
Pr5	2i	0.02020(2)	0.7529(1)	0.2121(1)
Br1	1a	0	0	0
Br2	2i	0.2032(4)	0.4116(3)	0.789(2)
Se1	2i	0.4661(3)	0.1361(2)	0.8828(2)
Se2	2i	0.2389(3)	0.6556(3)	0.8039(2)
O1	2i	0.2962(4)	0.4172(3)	0.4486(3)
O2	2i	0.1744(4)	0.7010(3)	0.4034(3)

Table 5.4.3.c: continued

Atoms	Wyckoff Position	x / a	y / b	z / c
O3	2i	0.4409(4)	0.1454(3)	0.4861(3)
O4	2i	0.0690(4)	0.9877(3)	0.3548(3)
O5	2i	0.3491(4)	0.7473(4)	0.1497(3)
O6	2i	0.2963(4)	0.1837(3)	0.7643(3)
O7	2i	0.5061(5)	0.0314(3)	0.1896(3)
O8	2i	0.5536(4)	0.3427(3)	0.2597(4)
O9	2i	0.9038(4)	0.2654(3)	0.3033(3)
O10	2i	0.1656(4)	0.4670(3)	0.7407(3)
Pr1	1g	0	1/2	1/2
Pr2	2i	0.74741(3)	0.05930(2)	0.44000(2)
Pr3	2i	0.25454(3)	0.18814(2)	0.28753(2)
Pr4	2i	0.02467(3)	0.75309(2)	0.20382(2)
Pr5	2i	0.48251(3)	0.61945(2)	0.36518(2)
Cl1	2a	0	0	0
Cl2	2i	0.8192(2)	0.5991(1)	0.9206(1)
Se1	2i	0.46147(6)	0.14330(4)	0.88946(4)
Se2	2i	0.76399(6)	0.34676(4)	0.18933(4)
O1	2i	0.2962(4)	0.4172(3)	0.4486(3)
O2	2i	0.1744(4)	0.7010(3)	0.4034(3)
O3	2i	0.4409(4)	0.1454(3)	0.4861(3)
O4	2i	0.0690(4)	0.9877(3)	0.3548(3)
O5	2i	0.3491(4)	0.7473(4)	0.1497(3)
O6	2i	0.2963(4)	0.1837(3)	0.7643(3)
O7	2i	0.5061(5)	0.0314(3)	0.1896(3)
O8	2i	0.5536(4)	0.3427(3)	0.2597(4)
O8	2i	0.9038(4)	0.2654(3)	0.3033(3)
O10	2i	0.1656(4)	0.4670(3)	0.7407(3)
Nd1	1g	0	1/2	1/2
Nd2	2i	0.25492(8)	0.18984(6)	0.28854(6)
Nd3	2i	0.51781(9)	0.37978(6)	0.63387(7)

Table 5.4.3.c: continued

Atoms	Wyckoff Position	x / a	y / b	z / c
Nd4	2i	0.25232(8)	0.94067(6)	0.55950(7)
Nd5	2i	0.02366(8)	0.75527(6)	0.20542(7)
Cl1	1a	0	0	0
Cl2	2i	0.1798(5)	0.3980(4)	0.0778(3)
Se1	2i	0.2364(2)	0.6524(1)	0.8112(1)
Se2	2i	0.4639(2)	0.1423(1)	0.8888(1)
O1	2i	0.0684(10)	0.9885(8)	0.3550(8)
O2	2i	0.4387(10)	0.1453(8)	0.4867(8)
O3	2i	0.1749(10)	0.7018(8)	0.4058(8)
O4	2i	0.2976(10)	0.4176(8)	0.4482(8)
O5	2i	0.1644(11)	0.4658(8)	0.7404(8)
O6	2i	0.0964(11)	0.7341(8)	0.6953(8)
O7	2i	0.2966(11)	0.1839(9)	0.7632(9)
O8	2i	0.6524(11)	0.2534(9)	0.8482(8)
O9	2i	0.4466(10)	0.6445(8)	0.7406(9)
O10	2i	0.4978(12)	0.9772(8)	0.8095(9)
Sm1	1g	0	1/2	1/2
Sm2	2i	0.25257(7)	0.19318(5)	0.29048(5)
Sm3	2i	0.52058(7)	0.37723(7)	0.63045(5)
Sm4	2i	0.25294(6)	0.94017(5)	0.55848(5)
Sm5	2i	0.02171(7)	0.76133(5)	0.20883(6)
Cl1	1a	0	0	0
Cl2	2i	0.8230(4)	0.6114(3)	0.9297(3)
Se1	2i	0.4699(1)	0.1404(1)	0.8866(1)
Se2	2i	0.2384(1)	0.6483(1)	0.8108(41
O1	2i	0.0681(9)	0.9921(7)	0.3563(8)
O2	2i	0.4404(9)	0.1458(7)	0.4865(7)
O3	2i	0.1735(9)	0.7034(7)	0.4071(8)
O4	2i	0.2952(9)	0.4182(7)	0.4494(7)
O5	2i	0.0972(9)	0.7337(7)	0.6959(8)

Table 5.4.3.c: continued

Atoms	Wyckoff Position	x / a	y / b	z / c
O6	2i	0.1590(9)	0.4622(7)	0.7387(8)
O7	2i	0.2980(9)	0.1799(8)	0.7629(8)
O8	2i	0.6574(10)	0.2567(8)	0.8458(8)
O9	2i	0.5043(11)	0.9651(8)	0.8051(9)
O10	2i	0.4512(9)	0.6489(8)	0.7378(9)
Gd1	1g	0	1/2	1/2
Gd2	2i	0.74897(6)	0.06160(5)	0.44347(5)
Gd3	2i	0.25312(6)	0.19747(5)	0.29341(4)
Gd4	2i	0.02009(6)	0.77052(5)	0.21208(5)
Gd5	2i	0.47758(6)	0.62716(5)	0.37274(5)
Cl1	1a	0	0	0
Cl2	2i	0.1789(5)	0.3798(5)	0.0636(4)
Se1	2i	0.4815(1)	0.1367(1)	0.88485(9)
Se2	2i	0.7648(1)	0.3564(1)	0.18831(9)
O1	2i	0.2978(8)	0.4192(7)	0.4489(7)
O2	2i	0.1717(9)	0.7067(6)	0.4095(6)
O3	2i	0.4399(8)	0.1451(6)	0.4865(6)
O4	2i	0.0616(9)	0.9957(7)	0.3587(7)
O5	2i	0.3360(11)	0.7413(12)	0.1549(8)
O6	2i	0.3048(10)	0.1740(10)	0.7647(8)
O7	2i	0.5004(12)	0.0425(11)	0.2045(9)
O8	2i	0.5486(11)	0.3578(12)	0.2611(9)
O9	2i	0.9077(10)	0.2730(10)	0.3063(7)
O10	2i	0.1611(12)	0.4573(10)	0.7360(8)

Table 5.4.3.d: Anisotropic thermal displacement parameters[b] (U_{ij}/pm^2) for $M_9O_8X_3[SeO_3]_2$ (M = La, Pr, Nd, Sm, Gd)

Atoms	U_{11}	U_{22}	U_{33}	U_{23}	U_{13}	U_{12}
La1	134(7)	120(7)	165(8)	43(6)	22(6)	26(5)
La2	122(5)	109(5)	175(6)	37(4)	6(4)	20(4)
La3	139(5)	125(5)	169(5)	34(4)	11(4)	24(4)
La4	118(5)	116(5)	176(5)	26(4)	–1(4)	20(4)
La5	133(5)	136(5)	171(6)	31(4)	–4(4)	19(4)
Br1	400(18)	229(15)	267(16)	28(13)	–73(13)	–12(13)
Br2	325(11)	250(11)	210(10)	46(8)	–8(8)	33(9)
Se1	129(9)	158(9)	200(10)	41(7)	–17(7)	14(7)
Se2	153(9)	177(9)	160(9)	18(8)	21(7)	22(7)
O1	112(60)	160(64)	283(75)	96(57)	22(53)	33(49)
O2	152(64)	202(67)	210(71)	115(57)	–45(53)	–44(51)
O3	205(69)	107(60)	251(74)	–50(54)	90(56)	–77(51)
O4	106(61)	198(67)	249(72)	131(56)	–46(51)	36(50)
O5	87(57)	282(74)	206(67)	98(57)	44(49)	108(52)
O6	211(69)	164(65)	203(70)	67(55)	–46(54)	39(53)
O7	191(65)	49(56)	239(70)	–19(50)	2(53)	17(47)
O8	264(76)	237(75)	296(80)	67(63)	39(61)	–44(59)
O9	268(76)	215(72)	359(85)	83(63)	151(64)	74(59)
O10	241(76)	353(84)	245(78)	71(65)	25(60)	55(63)

Table 5.4.3.d: continued

Atoms	U_{11}	U_{22}	U_{33}	U_{23}	U_{13}	U_{12}
Pr1	123(7)	120(7)	165(8)	43(6)	22(6)	26(5)
Pr2	143(5)	109(5)	175(6)	37(4)	6(4)	20(4)
Pr3	146(5)	125(5)	169(5)	34(4)	11(4)	24(4)
Pr4	137(5)	116(5)	176(5)	26(4)	–1(4)	20(4)
Pr5	147(5)	136(5)	171(6)	31(4)	–4(4)	19(4)
Br1	390(17)	295(16)	274(17)	28(13)	–73(13)	–12(13)
Br2	378(12)	298(11)	265(12)	46(8)	–8(8)	33(9)
Se1	129(9)	158(9)	200(10)	41(7)	–17(7)	14(7)
Se2	153(9)	177(9)	160(9)	18(8)	21(7)	22(7)
O1	112(60)	160(64)	283(75)	96(57)	22(53)	33(49)
O2	152(64)	202(67)	210(71)	115(57)	–45(53)	–44(51)
O3	205(69)	107(60)	251(74)	–50(54)	90(56)	–77(51)
O4	106(61)	198(67)	249(72)	131(56)	–46(51)	36(50)
O5	87(57)	282(74)	206(67)	98(57)	44(49)	108(52)
O6	211(69)	164(65)	203(70)	67(55)	–46(54)	39(53)
O7	191(65)	49(56)	239(70)	–19(50)	2(53)	17(47)
O8	264(76)	237(75)	296(80)	67(63)	39(61)	–44(59)
O9	268(76)	215(72)	359(85)	83(63)	151(64)	74(59)
O10	241(76)	353(84)	245(78)	71(65)	25(60)	55(63)
Pr1	68(2)	76(2)	88(2)	16(1)	8(1)	12(1)
Pr2	76(1)	74(1)	88(1)	15(1)	3(1)	4(1)
Pr3	77(1)	73(1)	91(1)	17(1)	3(1)	4(1)
Pr4	77(1)	96(1)	92(1)	22(1)	–2(1)	6(1)
Pr5	80(1)	76(1)	91(1)	19(1)	3(1)	11(1)
Cl1	391(10)	232(8)	190(8)	36(6)	22(7)	–28(7)
Cl2	234(6)	226(5)	170(5)	66(4)	18(4)	12(4)
Se1	98(2)	114(2)	87(2)	17(1)	17(2)	19(1)
Se2	85(2)	106(2)	94(2)	10(2)	–3(1)	9(1)
O1	118(14)	78(13)	112(14)	18(11)	8(11)	31(11)

Table 5.4.3.d: continued

Atoms	U_{11}	U_{22}	U_{33}	U_{23}	U_{13}	U_{12}
O2	100(13)	93(13)	107(14)	20(11)	3(11)	25(10)
O3	99(14)	89(13)	86(14)	11(11)	–4(11)	12(10)
O4	94(14)	103(12)	124(15)	21(11)	–3(11)	3(10)
O5	119(14)	281(17)	228(17)	89(13)	17(12)	–50(12)
O6	107(14)	178(14)	154(15)	34(12)	–14(12)	19(11)
O7	276(17)	146(15)	220(16)	23(12)	9(14)	110(13)
O8	107(14)	151(14)	357(19)	26(13)	88(13)	–8(11)
O9	115(14)	130(13)	138(15)	35(11)	25(11)	38(11)
O10	160(15)	112(13)	159(15)	29(11)	19(12)	–3(11)
Nd1	68(2)	76(2)	88(2)	16(1)	8(1)	12(1)
Nd2	76(1)	74(1)	88(1)	15(1)	3(1)	4(1)
Nd3	77(1)	73(1)	91(1)	17(1)	3(1)	4(1)
Nd4	77(1)	96(1)	92(1)	22(1)	–2(1)	6(1)
Nd5	80(1)	76(1)	91(1)	19(1)	3(1)	11(1)
Cl1	391(10)	232(8)	190(8)	36(6)	22(7)	–28(7)
Cl2	234(6)	226(5)	170(5)	66(4)	18(4)	12(4)
Se1	98(2)	114(2)	87(2)	17(1)	17(2)	19(1)
Se2	85(2)	106(2)	94(2)	10(2)	–3(1)	9(1)
O1	118(14)	78(13)	112(14)	18(11)	8(11)	31(11)
O2	100(13)	93(13)	107(14)	20(11)	3(11)	25(10)
O3	99(14)	89(13)	86(14)	11(11)	–4(11)	12(10)
O4	94(14)	103(12)	124(15)	21(11)	–3(11)	3(10)
O5	119(14)	281(17)	228(17)	89(13)	17(12)	–50(12)
O6	107(14)	178(14)	154(15)	34(12)	–14(12)	19(11)
O7	276(17)	146(15)	220(16)	23(12)	9(14)	110(13)
O8	107(14)	151(14)	357(19)	26(13)	88(13)	–8(11)
O9	115(14)	130(13)	138(15)	35(11)	25(11)	38(11)
O10	160(15)	112(13)	159(15)	29(11)	19(12)	–3(11)

Table 5.4.3.c: continued

Atoms	U_{11}	U_{22}	U_{33}	U_{23}	U_{13}	U_{12}
Sm1	68(2)	76(2)	88(2)	16(1)	8(1)	12(1)
Sm2	76(1)	74(1)	88(1)	15(1)	3(1)	4(1)
Sm3	77(1)	73(1)	91(1)	17(1)	3(1)	4(1)
Sm4	77(1)	96(1)	92(1)	22(1)	–2(1)	6(1)
Sm5	80(1)	76(1)	91(1)	19(1)	3(1)	11(1)
Cl1	391(10)	232(8)	190(8)	36(6)	22(7)	–28(7)
Cl2	234(6)	226(5)	170(5)	66(4)	18(4)	12(4)
Se1	98(2)	114(2)	87(2)	17(1)	17(2)	19(1)
Se2	85(2)	106(2)	94(2)	10(2)	–3(1)	9(1)
O1	118(14)	78(13)	112(14)	18(11)	8(11)	31(11)
O2	100(13)	93(13)	107(14)	20(11)	3(11)	25(10)
O3	99(14)	89(13)	86(14)	11(11)	–4(11)	12(10)
O4	134(30)	115(29)	332(38)	27(23)	–27(27)	11(24)
O5	189(38)	892(70)	260(42)	63(43)	49(32)	–262(41)
O6	83(30)	596(51)	247(38)	119(35)	–59(27)	–4(31)
O7	477(53)	439(51)	514(57)	41(43)	67(43)	124(42)
O8	201(40)	807(69)	600(62)	242(52)	163(40)	–6(42)
O9	231(34)	151(30)	230(34)	70(26)	85(27)	23(26)
O10	720(62)	203(38)	264(41)	47(31)	–89(40)	37(38)
Gd1	85(3)	96(3)	131(3)	14(2)	12(2)	23(2)
Gd2	93(2)	96(2)	215(3)	31(2)	20(2)	16(2)
Gd3	111(2)	97(2)	165(2)	12(2)	19(2)	24(2)
Gd4	139(2)	203(2)	177(2)	85(2)	23(2)	42(2)
Gd5	106(2)	112(2)	175(2)	26(2)	19(2)	19(2)
Cl1	1964(91)	705(41)	640(41)	455(35)	493(50)	106(48)
Cl2	409(17)	919(27)	424(18)	422(19)	132(14)	85(18)
Se1	220(5)	319(5)	128(5)	3(4)	33(4)	144(4)
Se2	124(4)	248(5)	136(4)	30(3)	–4(3)	–20(3)

Table 5.4.3.d: continued

Atoms	U_{11}	U_{22}	U_{33}	U_{23}	U_{13}	U_{12}
O1	72(26)	106(27)	206(32)	–4(23)	–8(23)	81(22)
O2	129(28)	99(27)	202(32)	48(23)	41(24)	59(23)
O3	109(28)	83(27)	196(32)	27(23)	3(23)	12(22)
O4	134(30)	115(29)	332(38)	27(23)	–27(27)	11(24)
O5	189(38)	892(70)	260(42)	63(43)	49(32)	–262(41)
O6	83(30)	596(51)	247(38)	119(35)	–59(27)	–4(31)
O7	477(53)	439(51)	514(57)	41(43)	67(43)	124(42)
O8	201(40)	807(69)	600(62)	242(52)	163(40)	–6(42)
O9	231(34)	151(30)	230(34)	70(26)	85(27)	23(26)
O10	720(62)	203(38)	264(41)	47(31)	–89(40)	37(38)

[b] defined as temperature factor according to: $\exp[-2\pi^2(a^{*2}h^2U_{11} + b^{*2}k^2U_{22} + c^{*2}l^2U_{33} + 2b^*c^*klU_{23} + 2a^*c^*hlU_{13} + 2a^*b^*hkU_{12})]$

Table 5.4.3.e: Selected internuclear distances (d/pm) and angles (∢/deg) in $M_9O_8X_3[SeO_3]_2$ (M = La, Pr, Nd, Sm, Gd)

		$M_9O_8Br_3[SeO_3]_2$		$M_9O_8Cl_3[SeO_3]_2$			
		La	Pr	Pr	Nd	Sm	Gd
M1 – O1	(2×)	240.0	235.9	234.0	233.8	230.0	229.6
– O2	(2×)	248.1	246.3	244.2	242.4	239.2	236.2
– O10	(2×)	260.0	258.4	258.1	256.5	252.8	251.1
– O9	(2×)	262.2	259.3	258.6	256.9	256.7	253.6
M2 – O2		241.9	238.8	239.2	231.8	235.0	231.3
– O3		242.1	239.7	240.1	234.1	235.1	232.3
– O4		243.8	240.7	240.1	237.4	235.3	233.2
– O3′		248.4	242.0	240.8	240.0	237.5	235.9
– O4′		258.4	257.6	257.0	262.2	252.8	245.1
– O9		273.8	267.3	265.8	266.0	261.4	261.5
– O6		274.5	271.3	266.1	274.4	264.0	266.5
– O7		276.3	274.9	278.8	287.9	276.2	269.1
M3 – O3		236.7	232.7	232.2	231.5	228.5	227.0
– O4		238.3	232.8	233.6	232.0	229.7	227.9
– O1		239.9	234.7	234.1	232.6	229.9	228.0
– O8		252.3	246.5	245.4	244.7	241.3	239.8
– O7		256.5	254.4	251.8	248.8	245.4	243.2
– O9		266.0	259.1	263.1	261.7	257.0	252.1
– X2		324.8	320.0	305.5	302.5	297.2	292.8
– X1		339.5	336.6	327.1	327.2	327.9	333.3
M4 – O2		231.0	224.3	225.9	226.1	223.7	223.4
– O4		238.5	232.0	233.2	231.0	228.3	226.0
– O5		238.9	235.2	237.8	236.5	233.5	230.2
– O6		245.7	240.5	240.7	238.3	234.7	234.0
– O10		250.3	242.7	243.8	241.9	237.7	237.6
– X2		323.8	319.4	301.8	300.1	294.4	293.8

Table 5.4.3.e: continued

	$M_9O_8Br_3[SeO_3]_2$		$M_9O_8Cl_3[SeO_3]_2$			
	La	Pr	Pr	Nd	Sm	Gd
– X1	334.7	331.4	322.2	319.7	313.4	305.2
– X2′	387.5	386.6	381.7	375.4	383.7	386.9
M5 – O3	237.4	233.3	233.4	237.5	228.2	226.0
– O1	239.9	235.1	236.1	237.6	231.5	229.0
– O2	243.2	238.0	238.8	237.6	233.8	231.2
– O1′	245.9	243.5	242.3	241.3	237.1	232.9
– O5	271.2	265.3	264.4	255.3	259.0	258.3
– O8	280.8	276.9	269.2	264.0	261.0	259.7
– O6	282.5	277.4	276.4	265.4	274.1	272.2
– O10	291.2	285.1	287.8	278.7	291.5	289.6
– X2	346.5	347.4	350.1	360.6	3662.6	373.4
O1 – M3	238.9	224.3	234.0	231.0	228.3	228.0
– M5	239.9	238.0	234.1	232.6	228.5	229.0
– M1	242.1	240.7	236.1	237.6	235.0	229.6
– M5′	258.4	246.3	242.3	255.3	252.8	232.9
O2 – M4	236.7	232.7	225.9	231.5	228.2	223.4
– M5	237.4	233.3	238.8	231.8	229.7	231.2
– M2	241.9	239.7	240.1	237.6	235.3	231.4
– M1	248.4	242.0	244.2	241.3	237.5	236.2
O3 – M5	231.0	232.0	233.4	226.1	223.7	226.0
– M3	243.2	234.7	233.6	237.4	233.8	227.0
– M2	243.8	238.8	240.1	237.5	235.1	232.3
– M2′	248.1	257.6	240.8	242.4	239.2	235.9
O4 – M4	238.3	232.8	233.2	232.0	229.9	226.0
– M3	239.9	235.1	233.2	233.8	230.0	228.0
– M2	240.0	235.9	239.2	234.1	231.5	233.2
– M2′	245.9	243.5	257.0	240.0	237.1	245.1

Table 5.4.3.e: continued

	$M_9O_8Br_3[SeO_3]_2$		$M_9O_8Cl_3[SeO_3]_2$			
	La	Pr	Pr	Nd	Sm	Gd
Se1 – O5	167.0	166.7	167.7	166.9	168.1	165.8
– O6	170.6	167.9	167.9	170.4	168.6	167.3
– O7	172.8	169.9	171.1	171.9	169.7	172.5
Se2 – O8	168.8	167.3	167.5	167.9	168.3	168.9
– O9	169.0	173.2	170.4	168.0	170.5	171.0
– O10	171.7	173.7	171.6	171.7	171.5	171.3
	∢ / grd	∢ / grd	∢ / grd	∢ / grd		∢ / grd
M5 – O1 – M5′	99.8	98.6	99.8	98.6	99.0	99.9
M3 – O1 – M5	104.4	103.4	103.2	102.4	101.8	104.3
M1 – O1 – M5	105.3	105.6	105.7	103.5	103.1	105.9
M3 – O1 – M1	110.9	106.8	107.6	112.7	110.6	113.8
M3 – O1 – M1	113.9	113.0	111.7	118.5	112.7	114.9
M5 – O1 – M1	117.5	113.5	119.2	121.8	120.5	119.9
M5 – O2 – M2	102.6	102.1	103.1	104.4	102.8	103.9
M4 – O2 – M2	104.5	104.5	105.6	106.1	105.3	104.1
M5 – O2 – M1	105.6	105.4	106.4	107.5	107.2	104.3
M4 – O2 – M5	110.4	110.5	107.6	113.2	116.0	111.3
M4 – O2 – M1	112.1	113.2	111.3	114.3	117.4	115.0
M2 – O2 – M1	116.4	115.7	114.6	117.6	121.9	117.9
M3 – O3 – M2	103.7	102.6	104.5	105.1	102.5	103.8
M5 – O3 – M2	104.3	104.6	105.0	106.5	104.1	104.1
M5 – O3 – M3	106.5	106.7	106.3	108.8	104.9	105.6
M2 – O3 – M2′	105.6	110.6	110.5	110.3	111.5	106.3
M3 – O3 – M2	111.2	115.3	112.7	110.9	114.6	115.2
M5 – O3 – M2	113.8	119.5	120.9	114.3	116.7	122.4
M4 – O4 – M2	103.1	103.5	101.1	105.2	101.7	102.7
M3 – O4 – M2	104.3	104.5	103.6	106.9	102.8	103.3

Table 5.4.3.e: continued

	$M_9O_8Br_3[SeO_3]_2$		$M_9O_8Cl_3[SeO_3]_2$			
	La	Pr	Pr	Nd	Sm	Gd
M2 – O4 – M2′	105.0	104.8	111.0	111.5	104.7	105.1
M3 – O4 – M2′	111.7	112.1	118.2	113.3	111.9	114.1
M4 – O4 – M3	114.4	114.3	119.5	115.7	113.5	117.4
O6 – Se1 – O7	93.4	94.1	94.7	93.5	95.4	93.4
O5 – Se1 – O6	97.5	99.2	98.7	97.6	96.3	96.9
O5 – Se1 – O7	100.5	104.1	103.3	101.9	103.9	107.8
O8 – Se2 – O10	91.7	92.5	91.9	92.9	93.7	90.5
O9 – Se2 – O10	96.9	97.5	94.1	99.1	97.9	96.3
O8 – Se2 – O9	103.0	101.6	102.0	103.2	101.9	102.2

Table 5.4.3.f: Motifs of mutual adjunction in $M_9O_8X_3[SeO_3]_2$ (M = La, Pr, Nd, Sm, Gd)

	X1	X2	O1	O2	O3	O4	O5	O6	O7	O8	O9	O10	CN
M1	0 / 0	0 / 0	2 / 1	2 / 1	0 / 0	0 / 0	0 / 0	0 / 0	0 / 0	0 / 0	2 / 1	2 / 1	8
M2	0 / 0	0 / 0	0 / 0	1 / 1	2 / 2	2 / 2	0 / 0	1 / 0	1 / 1	0 / 0	1 / 1	0 / 0	8
M3	1 / 2	1 / 1	1 / 1	0 / 0	1 / 1	1 / 1	0 / 0	0 / 0	1 / 1	1 / 1	1 / 1	0 / 0	8
M4	1 / 2	1+1/1	0 / 0	1 / 1	0 / 0	1 / 1	1 / 1	1 / 1	0 / 0	0 / 0	0 / 0	1 / 1	7+1
M5	0 / 0	0+1/1	2 / 2	1 / 1	1 / 1	0 / 0	1 / 1	1 / 0	0 / 0	1 / 1	0 / 0	1 / 0	8+1
Se1	0 / 0	0 / 0	0 / 0	0 / 0	0 / 0	0 / 0	1 / 1	1 / 1	1 / 1	0 / 0	0 / 0	0 / 0	3
Se2	0 / 0	0 / 0	0 / 0	0 / 0	0 / 0	0 / 0	0 / 0	0 / 0	0 / 0	1 / 1	1 / 1	1 / 1	3
CN	4	3	4	4	4	4	3	2	3	3	4	3	

6 An alkali metal oxoselenate(IV) of a trivalent rare-earth element: $Li_3Lu_5[SeO_3]_9$

Although the number of known mixed-metal compounds containing Se(IV) is large, only few alkali metal lanthanide oxoselenates(IV) were investigated until now. Research has being focussed especially on mixed transition metal or on alkali transition metal selenates(IV) [40 – 45] instead. During our attempt to prepare $Lu_2[SeO_3]_3$ using LiBr as fluxing agent, certain percentages of $Li_3Lu_5[SeO_3]_9$ were also detectable as by-product. Additionally to this new compound, the only other oxidic phases with alkali metal, rare-earth element and Se(IV) so far characterized are the two non-isostructural sodium selenites $NaY[SeO_3]_2$ and $NaLa[SeO_3]_2$ [46].

6.1 Synthesis of $Li_3Lu_5[SeO_3]_9$

Colourless platelet-shaped single crystals of $Li_3Lu_5[SeO_3]_9$ were obtained as by-product during an experiment to synthesize $Lu_2[SeO_3]_3$ by reacting Lu_2O_3 and SeO_2 in 1:3 molar ratio with an excess of LiBr like flux in an evacuated sealed silica ampoule at 830°C for seven days. The cooling process was the same as in paragraph 3.1. Upon opening the silica tube, suitable air and water stable single crystals of $Li_3Lu_5[SeO_3]_9$ were recovered from the sample under microscope. Preliminary X-ray investigations were done by oscillation and *Weissenberg* photography, followed by a κ-CCD measurement. Crystal data and additional information about the refinement can be taken from the table in paragraph 6.3 which also contains the final structural parameters, selected interatomic bond lengths and angles as well as the motifs of mutual adjunction.

6.2 Structure description of $Li_3Lu_5[SeO_3]_9$

The crystal structure of $Li_3Lu_5[SeO_3]_9$ exhibits five crystallographically different Lu^{3+} cations in eight-and sevenfold coordination. $(Lu1)^{3+}$ and $(Lu2)^{3+}$ are surrounded by six complex $[SeO_3]^{2-}$ anions which coordinated the central cations fourfold in mono- and twofold in bidentate manner, a distorted square prismatic or antiprismatic coordination sphere results in those cases. On the other hand, six $[SeO_3]^{2-}$ groups (five mono- against one bidentate grafts for the coordination number of seven as expected for the small Lu^{3+} radiis) are

observed about $(Lu3)^{3+}$, $(Lu4)^{3+}$ and $(Lu5)^{3+}$ each. Their coordination polyhedra can actually be regarded as a distorted capped trigonal prism (fig. 6.2.a) in all cases. The Lu–O-bond lengths between 218 and 255 pm are entirely consistent with those in the ternary $Lu_2[SeO_3]_3$ compound (paragraph 3.5).

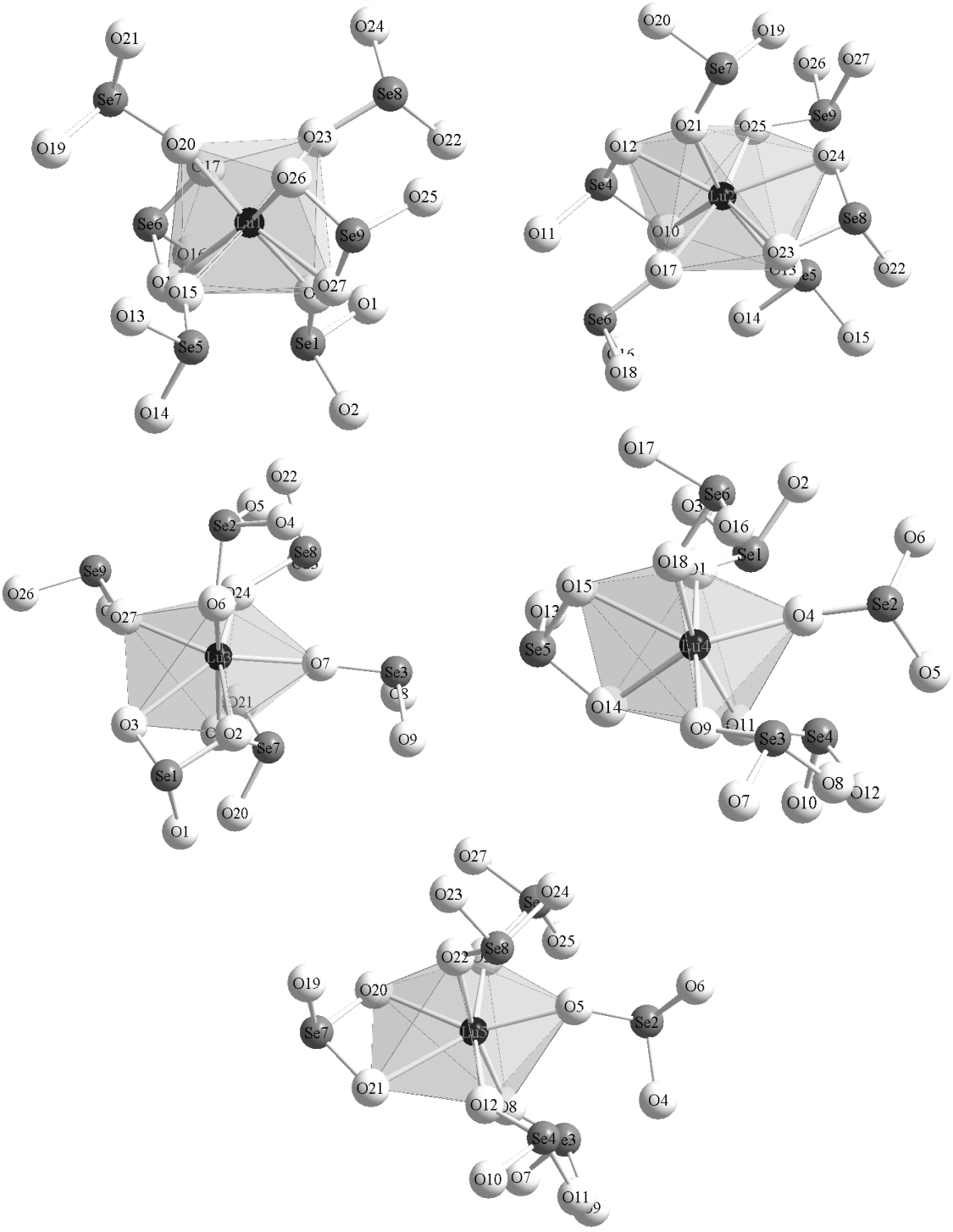

Fig. 6.2.a: Coordination of six $[SeO_3]^{2-}$ anions about the five crystallographically different Lu^{3+} cations in $Li_3Lu_5[SeO_3]_9$

Among the three Li^+ cation sites, two are trigonal-bipyramidally coordinated similar to the lithium coordination in the crystal structure of Li_4SeO_5 [116] (CN = 5) while the remaining one shows a distorted trigonal antiprismatic coordination (CN = 6). The $[(Li2)O_5]$ polyhedra presents a more or less regular bipyramid as compared to the $[(Li1)O_5]$ unit. The irregularity of the latter is due to the short O6–O25 contact of the same $[(Se4)O_3]^{2-}$ group which is edge-attached to this polyhedra. The $[(Li1)O_5]$ (resp. $[(Li2)O_5]$) polyhedra are connected via common edges (O2–O2 resp. O16–O16) to centrosymmetric dimers, which are perfectly repeated in the unit cell according to the 2_1 screw axis of the $P2_1/n$ space group. The structure can then be looked at as formed by isolated anionic groups described like $[(Li1)_2O_8]^{14-}$, $[(Li2)_2O_8]^{14-}$ and $[(Li3)O_6]^{11-}$ (fig. 6.2.b). Within the $[(Li2)_2O_8]^{14-}$ dimers, the two apical oxygen atoms are residing at the same side of the equatorial plane and both belong to the same $[(Se4)O_3]^{2-}$ groups, therefore further connectivity among $[(Li2)O_5]$ polyhedra occurs through two O10–Se4–O11 contacts. Four other $[SeO_3]^{2-}$ groups are attached to the $[(Li2)_2O_8]^{14-}$ dimer only by vertices leading to an isolated complex $[(Li2)_2(SeO_3)_6]^{10-}$ in the structure. In the same way, six $[SeO_3]^{2-}$ groups are grafted onto the $[(Li1)_2O_8]^{14-}$ dimer also leading to such a $[(Li1)_2(SeO_3)_6]^{10-}$ complex, but none of these $[SeO_3]^{2-}$ units fuse the two $[(Li1)O_5]$ bipyramids among themselves as observed for the $[(Li2)O_5]$ polyhedra. The six oxygen atoms of the $[(Li3)O_6]$ polyhedron belong to four selenate groups, two of them being attached in a chelating manner whereas the remainder are only monodentate ligands. Those complex anions are shown in figure 6.2.b and the complete structure of $Li_3Lu_5[SeO_3]_9$ in figure 6.2.c. The $[(Li1)_2O_8]^{14-}$, $[(Li2)_2O_8]^{14-}$ and $[(Li3)O_6]^{11-}$ in the unit cell are shifted by ½ in the [001] direction, so that the whole structure can be described as hexagonal closest packing with a stacking mode of the sequence …A B A′ B A… along the length of the b-axis (capital letters denote $[(Li1)_2O_8]^{14-}$ and $[(Li2)_2O_8]^{14-}$ layers and small letters the $[(Li3)O_6]^{11-}$ ones; fig. 6.2.c). The Li–O-bond lengths (191 – 223 pm) are ranging normally between the typical Li–O distances for tetrahedral (196.3 pm) and octahedral (212.5 pm) Li^+ coordination [117], and are also not far away from those in the hexagonal lithium peroxide Li_2O_2 where Li–O distances between 196 and 214 pm [118] emerge. However, the contacts Li1–O7 (263.8 pm), Li3–O15 (245.3 pm) and Li3–O3 (249.3 pm) are slightly elongated, but comply well with other Li–O-bond lengths in phases containing Li^+ and $[SeO_3]^{2-}$ ions [119, 120]. We ought to mention that in a comprehensive paper on the crystal chemistry of lithium by *Wanger* [120] no case of Li^+ in trigonal prismatic or antiprismatic oxygen coordination is reported except for the $[LiO_6]$ polyhedra in $Li_5Mn^{II}_4Mn^{III}[SeO_3]_8$ [119] were trigonal

prismatic coordination with Li–O distances ranging from 205.7 to 288.0 pm occurs. Thus, the assumed trigonal antiprism of the [(Li3)O_6] polyhedra in $Li_3Lu_5[SeO_3]_9$ complies rather well with the corresponding [LiO_6] ones in $Li_5Mn^{II}_4Mn^{III}[SeO_3]_8$. The cationic environment of the nine crystallographically different trigonal non-planar $[SeO_3]^{2-}$ groups consist of either terminal or edges-spanning Li^+ / Lu^{3+} ions and is represented in figure 6.2.d. Their shape, bond lengths and angles are similar to those quoted in the literature for related compounds.

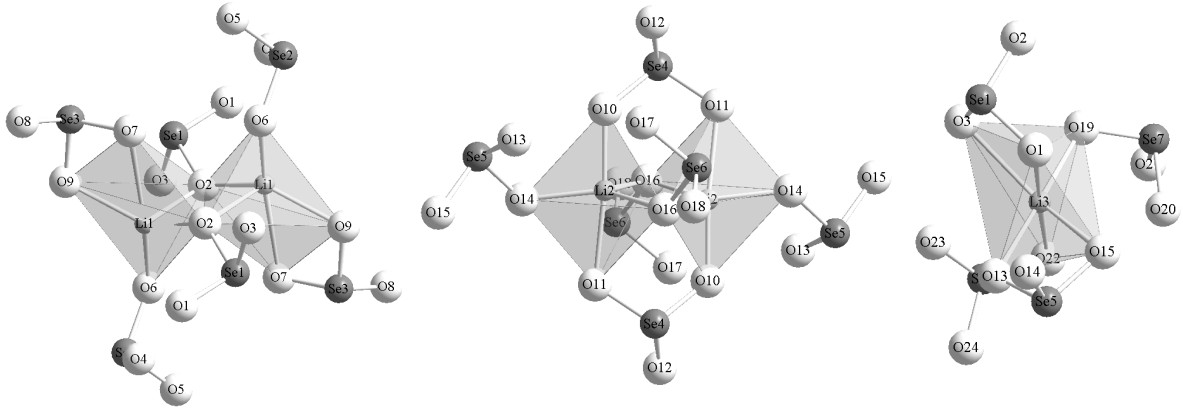

Fig. 6.2.b: $[(Li1)_2(SeO_3)_6]^{10-}$, $[(Li2)_2(SeO_3)_6]^{10-}$ and $[(Li3)(SeO_3)_4]^{5-}$ complex anions in the crystal structure of $Li_3Lu_5[SeO_3]_9$

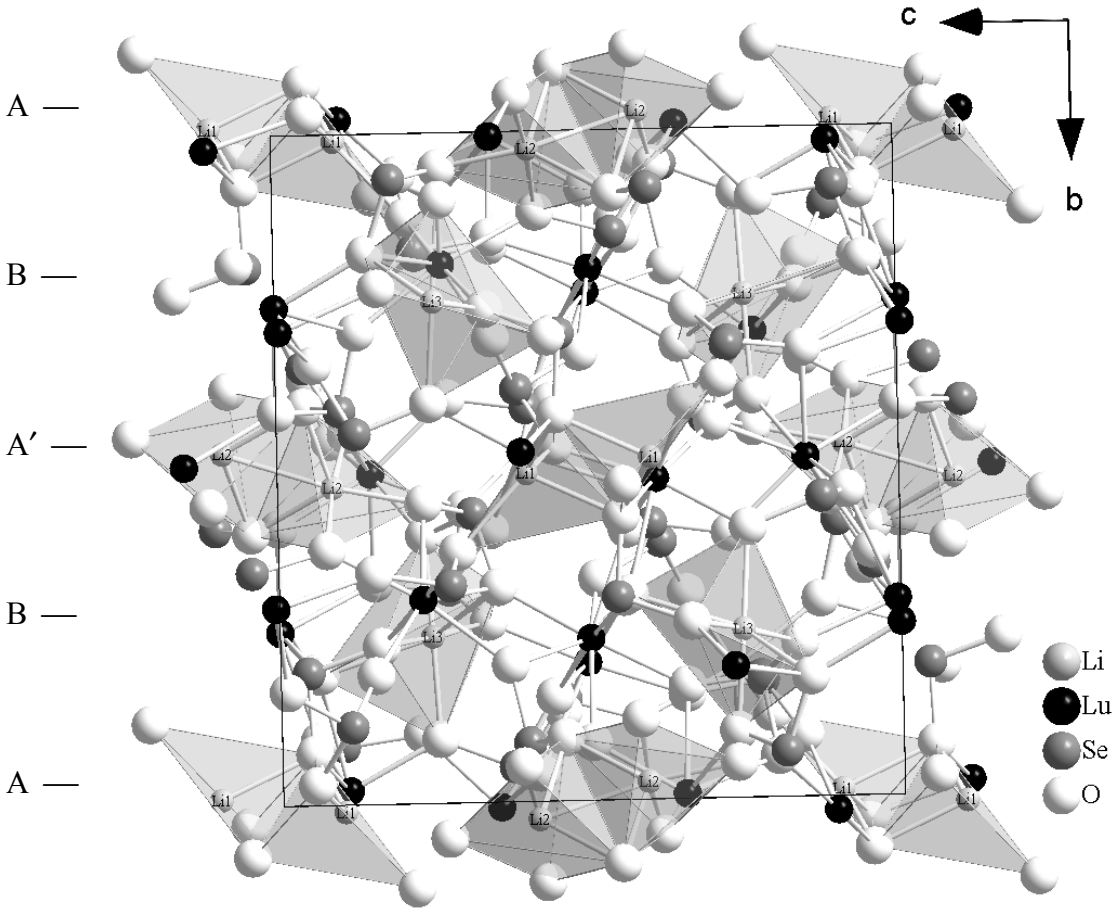

Fig. 6.2.c: Crystal structure of $Li_3Lu_5[SeO_3]_9$ as viewed at a (100) projection

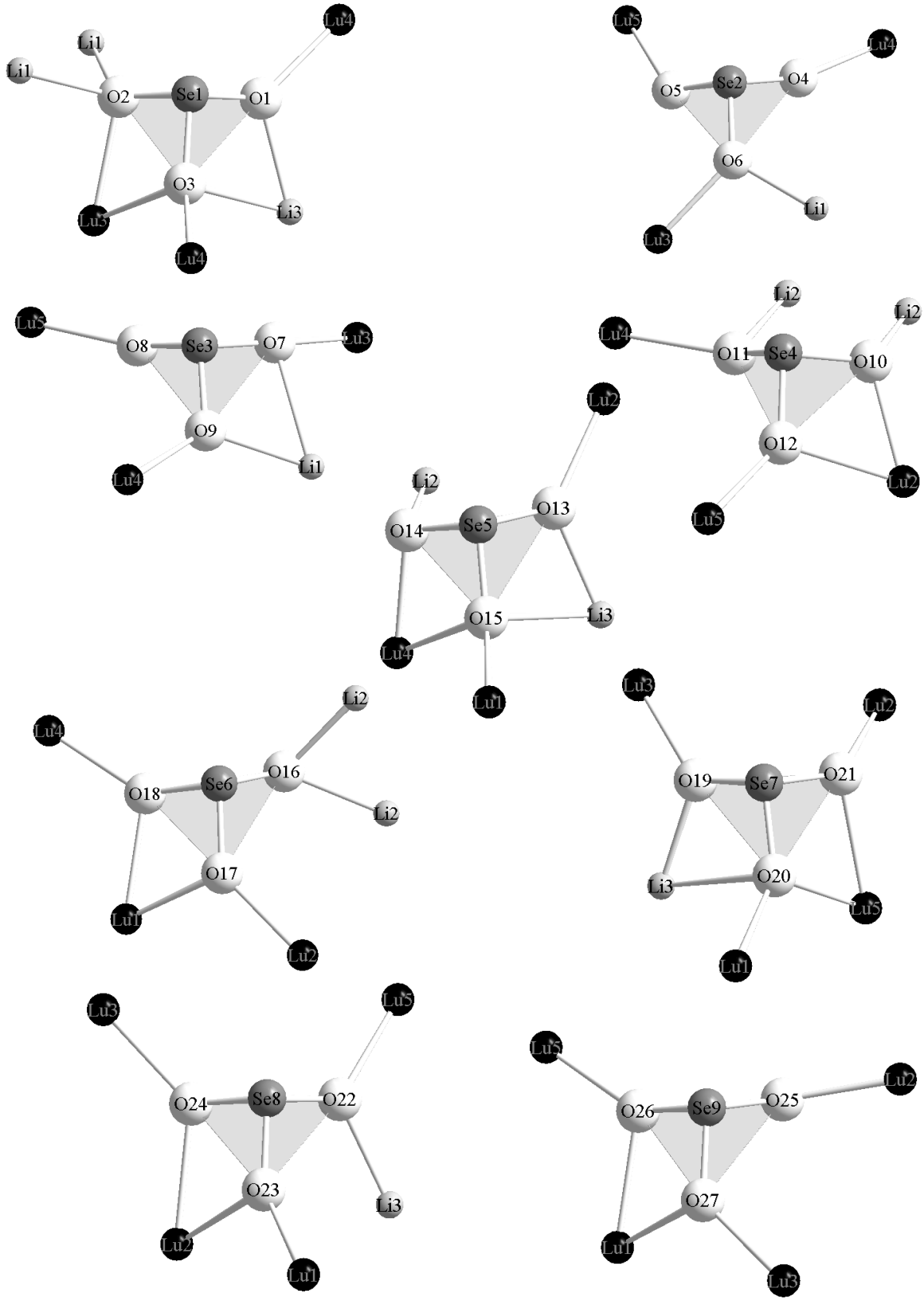

Fig. 6.2.d: Coordination of Li^{+} and Lu^{3+} about the nine crystallographically different $[SeO_3]^{2-}$ units in $Li_3Lu_5[SeO_3]_9$

6.3 Structural data for $Li_3Lu_5[SeO_3]_9$

Table 6.3.a: Crystallographic data for $Li_3Lu_5[SeO_3]_9$ and their determination

Formula		$Li_3Lu_5[SeO_3]_9$
Crystal system and space group		monoclinic, $P2_1/n$ (No. 14)
Formula unit per unit cell (Z)		4
Unit cell parameters:	a =	1393.85(9) pm
	b =	1394.51(9) pm
	c =	1409.48(9) pm
	β =	113.006(8) °
Calculated density (D_x / g · cm^3)		5.369
Molar volume (V_m / cm^3 · mol^{-1})		379.714
Diffractometer, radiation		κ-CCD (Fa. Nonius); Mo-K_α: λ = 71.07 pm
$2\theta_{max.}$		60.1
Index range	$\pm h_{max} = \pm k_{max} = \pm l_{max}$ =	19
F(000)		3544.0
Absorption coefficient (μ)		32.50 mm^{-1}
Absorption correction		Numerical, after crystal shape optimization with
Other data corrections		the program X-SHAPE [53]
		background, polarization, *Lorentz* factors
Collected reflections		76352
Unique reflections		7386
R_{int} / R_σ		0.086 / 0.039
Reflections with $\|F_o\| \geq 4\sigma\|F_o\|$		6381
Structure solution and refinement		Program system SHELX-97 [58]
Scattering factors		International Tables, Vol. C [85]
R_1 / R_1 with $\|F_o\| \geq 4\sigma\|F_o\|$		0.045 / 0.034
wR_2 / Goodness of fit (GooF)		0.066 / 1.126
Extinction (g)		0.00019(2)
Residual electron density (ρ / e$^-$ · 10^6 pm)		max. 1.56
		min. –2.03

Table 6.3.b: Atomic coordinates for $Li_3Lu_5[SeO_3]_9$

Atoms	Wyckoff position	x / a	y / b	z / c
Lu1	4e	0.18092(2)	0.25821(2)	0.00020(2)
Lu2	4e	0.28426(2)	0.49261(2)	0.14954(2)
Lu3	4e	0.34236(2)	0.02113(2)	0.10770(2)
Lu4	4e	0.18788(2)	0.19633(2)	0.73111(2)
Lu5	4e	0.39861(2)	0.20615(2)	0.49394(2)
Se1	4e	0.45619(5)	0.19705(5)	0.04472(5)
Se2	4e	0.30031(5)	0.38474(5)	0.61360(5)
Se3	4e	0.45315(5)	0.17599(5)	0.77509(5)
Se4	4e	0.12836(5)	0.15261(5)	0.45665(5)
Se5	4e	0.04621(5)	0.06891(5)	0.81218(5)
Se6	4e	0.28671(5)	0.41266(5)	0.89869(5)
Se7	4e	0.48687(5)	0.05245(5)	0.37467(5)
Se8	4e	0.22024(5)	0.31813(5)	0.27266(5)
Se9	4e	0.08807(5)	0.08755(5)	0.09920(5)
O1	4e	0.0324(4)	0.2645(4)	0.6625(4)
O2	4e	0.4718(4)	0.0763(4)	0.0517(4)
O3	4e	0.3420(4)	0.1928(4)	0.0633(4)
O4	4e	0.2323(6)	0.3081(4)	0.6530(6)
O5	4e	0.3076(5)	0.3309(4)	0.5112(4)
O6	4e	0.2104(4)	0.4705(4)	0.5551(4)
O7	4e	0.0420(4)	0.4059(4)	0.3407(4)
O8	4e	0.4376(4)	0.1570(4)	0.6526(4)
O9	4e	0.3467(4)	0.1259(4)	0.7880(4)
O10	4e	0.0795(4)	0.0524(4)	0.3885(4)
O11	4e	0.1451(4)	0.1204(4)	0.5775(4)
O12	4e	0.2480(4)	0.1333(4)	0.4526(4)
O13	4e	0.4252(4)	0.3998(4)	0.2341(4)
O14	4e	0.1111(4)	0.0527(4)	0.7338(4)
O15	4e	0.0973(4)	0.1793(4)	0.8520(4)

Table 6.3.b: continued

Atoms	Wyckoff position	x / a	y / b	z / c
O16	4e	0.4150(4)	0.4055(4)	0.9561(4)
O17	4e	0.2466(4)	0.4134(4)	0.0000(4)
O18	4e	0.2464(4)	0.2955(4)	0.8694(4)
O19	4e	0.4271(4)	0.0961(4)	0.2549(4)
O20	4e	0.0307(4)	0.3437(4)	0.9399(4)
O21	4e	0.3872(4)	0.0428(4)	0.4149(4)
O22	4e	0.3390(4)	0.2694(4)	0.3353(4)
O23	4e	0.2217(4)	0.3304(4)	0.1532(4)
O24	4e	0.2373(4)	0.4384(4)	0.2990(4)
O25	4e	0.1460(4)	0.1042(4)	0.2255(4)
O26	4e	0.0414(4)	0.1978(4)	0.0541(4)
O27	4e	0.1888(4)	0.0965(4)	0.0599(8)
Li1	4e	0.4049(12)	0.0106(10)	0.9001(11)
Li2	4e	0.0211(10)	0.0266(10)	0.5883(11)
Li3	4e	0.4297(12)	0.2485(10)	0.2453(12)

Table 6.3.c: Anisotropic thermal displacement parameters[b] (U_{ij}/pm^2) for $Li_3Lu_5[SeO_3]_9$

	U_{11}	U_{22}	U_{33}	U_{23}	U_{13}	U_{12}
Lu1	84(1)	107(1)	93(1)	–4(1)	32(1)	2(1)
Lu2	92(1)	108(1)	97(1)	–4(1)	36(1)	9(1)
Lu3	95(1)	129(1)	100(1)	7(1)	41(1)	11(1)
Lu4	96(1)	113(1)	96(1)	–2(1)	40(1)	0(1)
Lu5	92(1)	124(1)	103(1)	0(1)	44(1)	–10(1)
Se1	111(3)	115(3)	131(3)	–4(2)	60(3)	–13(2)
Se2	147(3)	113(3)	124(3)	8(2)	40(3)	13(3)
Se3	105(3)	125(3)	129(3)	20(3)	41(2)	14(3)
Se4	105(3)	112(3)	129(3)	–7(2)	53(3)	6(3)
Se5	130(3)	119(3)	128(3)	2(2)	58(3)	–22(3)
Se6	147(3)	124(3)	109(3)	–3(2)	60(3)	–17(3)
Se7	123(3)	107(3)	122(3)	–16(2)	55(2)	–8(2)
Se8	108(3)	113(3)	109(3)	5(2)	61(2)	–2(2)
Se9	117(3)	124(3)	135(3)	24(2)	60(3)	–3(3)
O1	161(24)	233(28)	143(25)	64(21)	45(20)	74(21)
O2	165(24)	121(23)	182(25)	–41(19)	80(20)	–40(19)
O3	89(22)	192(26)	206(26)	72(20)	67(19)	54(19)
O4	661(50)	193(36)	700(50)	216(34)	528(43)	53(33)
O5	436(36)	344(34)	185(28)	60(24)	186(26)	151(28)
O6	168(24)	175(26)	132(24)	32(19)	43(20)	94(20)
O7	221(27)	299(32)	235(28)	–112(24)	64(23)	–159(24)
O8	275(30)	297(32)	189(27)	45(24)	73(23)	25(25)
O9	94(22)	133(28)	221(26)	17(21)	90(20)	27(20)
O10	109(22)	215(26)	143(24)	–15(20)	77(19)	6(20)
O11	256(27)	218(27)	143(25)	–19(21)	132(21)	–21(22)
O12	90(22)	184(25)	202(26)	–56(20)	46(20)	–59(20)
O13	82(22)	227(28)	256(28)	101(22)	51(20)	29(20)
O14	120(22)	176(25)	153(24)	–17(20)	67(19)	–9(20)
O15	208(25)	162(25)	100(23)	–21(19)	55(20)	–65(20)

Table 6.3.c: continued

	U_{11}	U_{22}	U_{33}	U_{23}	U_{13}	U_{12}
O16	147(24)	223(27)	231(27)	–38(22)	89(21)	–43(21)
O17	173(24)	198(25)	114(23)	–19(19)	116(19)	–22(20)
O18	192(25)	162(25)	192(26)	–61(20)	131(21)	–56(20)
O19	202(25)	210(27)	100(23)	–13(20)	30(20)	–30(21)
O20	73(21)	123(23)	164(24)	56(19)	45(18)	31(18)
O21	138(23)	213(26)	118(24)	–46(20)	51(19)	–38(20)
O22	158(23)	171(25)	108(23)	66(19)	60(19)	77(19)
O23	190(24)	166(25)	88(22)	12(19)	56(19)	–11(20)
O24	155(24)	139(24)	189(25)	0(20)	110(20)	–7(20)
O25	328(31)	227(29)	154(26)	26(22)	123(23)	66(24)
O26	143(24)	153(25)	193(26)	86(20)	71(20)	90(20)
O27	163(24)	219(27)	223(27)	81(22)	137(21)	68(21)
Li1	357(81)	262(74)	301(77)	82(59)	195(66)	133(62)
Li2	106(56)	268(72)	271(72)	14(55)	28(52)	72(52)
Li3	371(80)	182(68)	458(90)	–105(61)	322(72)	–106(60)

[b] defined as temperature factor according to: $\exp[-2\pi^2(a^{*2}h^2U_{11} + b^{*2}k^2U_{22} + c^{*2}l^2U_{33} + 2b^*c^*klU_{23} + 2a^*c^*hlU_{13} + 2a^*b^*hkU_{12})]$

Table 6.3.d: Selected internuclear distances (d/pm) and angles (∢/deg) in $Li_3Lu_5[SeO_3]_9$

$Li_3Lu_5[SeO_3]_9$							
	d / pm		d / pm		d / pm		d / pm
Lu1 – O15	223.8	Lu2 – O17	225.2	Lu3 – O7	218.9	Lu4 – O4	213.5
– O23	224.8	– O13	226.4	– O19	220.8	– O1	221.3
– O3	225.9	– O25	226.5	– O6	223.3	– O9	226.3
– O20	226.6	– O21	230.9	– O27	223.9	– O18	226.6
– O17	234.9	– O10	232.0	– O24	233.1	– O11	227.1
– O27	239.6	– O12	237.0	– O2	236.3	– O14	227.8
– O18	240.7	– O23	243.2	– O3	247.4	– O15	249.7
– O26	249.8	– O24	255.3				
Lu5 – O8	219.5	Li1 – O2	199.3	Li2 – O10	190.9	Li3 – O13	211.5
– O12	219.6	– O6	202.2	– O14	197.5	– O19	213.1
– O5	222.2	– O2′	217.2	– O16	209.8	– O22	213.2
– O22	224.0	– O9	217.7	– O16′	211.5	– O1	217.9
– O26	227.0	– O7	263.8	– O11	222.0	– O15	244.7
– O20	235.6					– O3	249.5
– O21	251.3						
Se1 – O1	167.1	Se2 – O4	166.2	Se3 – O7	167.3	Se4 – O10	168.2
– O2	169.6	– O5	166.5	– O8	167.5	– O11	168.7
– O3	171.2	– O6	169.5	– O9	171.3	– O12	171.2
Se5 – O13	167.2	Se6 – O16	165.3	Se7 – O19	167.8	Se8 – O22	168.5
– O14	169.4	– O17	172.4	– O20	169.6	– O23	170.0
– O15	169.7	– O18	172.5	– O21	169.9	– O24	171.4
Se9 – O25	165.9						
– O26	169.3						
– O27	170.3						

Table 6.3.d: continued

	∢ / grd		∢ / grd		∢ / grd
O2 – Se1 – O3	93.6	O5 – Se2 – O6	100.4	O7 – Se3 – O9	98.5
O1 – Se1 – O3	97.5	O4 – Se2 – O6	101.9	O7 – Se3 – O8	103.4
O1 – Se1 – O2	104.1	O4 – Se2 – O5	103.6	O8 – Se3 – O9	106.1
O10 – Se4 – O12	91.9	O14 – Se5 – O15	94.3	O18 – Se6 – O17	91.3
O10 – Se4 – O11	102.8	O13 – Se5 – O15	99.6	O16 – Se6 – O17	103.5
O11 – Se4 – O12	103.9	O13 – Se5 – O14	105.3	O16 – Se6 – O18	104.4
O20 – Se7 – O21	93.2	O23 – Se8 – O24	93.5	O26 – Se9 – O27	93.2
O19 – Se7 – O20	99.7	O22 – Se8 – O23	99.8	O25 – Se9 – O27	102.8
O19 – Se7 – O21	102.4	O22 – Se8 – O24	104.9	O25 – Se9 – O26	103.3

Table 6.3.e: Motifs of mutual adjunction in $Li_3Lu_5[SeO_3]_9$

	O1	O2	O3	O4	O5	O6	O7	O8	O9	O10	O11	O12	O13	O14
Lu1	0 / 0	0 / 0	1 / 1	0 / 0	0 / 0	0 / 0	0 / 0	0 / 0	0 / 0	0 / 0	0 / 0	0 / 0	0 / 0	0 / 0
Lu2	0 / 0	0 / 0	0 / 0	0 / 0	0 / 0	0 / 0	0 / 0	0 / 0	0 / 0	1 / 1	0 / 0	1 / 1	1 / 1	0 / 0
Lu3	0 / 0	1 / 1	1 / 1	0 / 0	0 / 0	1 / 1	1 / 1	0 / 0	0 / 0	0 / 0	0 / 0	0 / 0	0 / 0	0 / 0
Lu4	1 / 1	0 / 0	0 / 0	1 / 1	0 / 0	0 / 0	0 / 0	0 / 0	1 / 1	0 / 0	1 / 1	0 / 0	0 / 0	1 / 1
Lu5	0 / 0	0 / 0	0 / 0	0 / 0	1 / 1	0 / 0	0 / 0	1 / 1	0 / 0	0 / 0	1 / 1	1 / 1	0 / 0	0 / 0
Se1	1 / 1	1 / 1	1 / 1	0 / 0	0 / 0	0 / 0	0 / 0	0 / 0	0 / 0	0 / 0	0 / 0	0 / 0	0 / 0	0 / 0
Se2	0 / 0	0 / 0	0 / 0	1 / 1	1 / 1	1 / 1	0 / 0	0 / 0	0 / 0	0 / 0	0 / 0	0 / 0	0 / 0	0 / 0
Se3	0 / 0	0 / 0	0 / 0	0 / 0	0 / 0	0 / 0	1 / 1	1 / 1	1 / 1	0 / 0	0 / 0	0 / 0	0 / 0	0 / 0
Se4	0 / 0	0 / 0	0 / 0	0 / 0	0 / 0	0 / 0	0 / 0	0 / 0	0 / 0	1 / 1	1 / 1	1 / 1	0 / 0	0 / 0
Se5	0 / 0	0 / 0	0 / 0	0 / 0	0 / 0	0 / 0	0 / 0	0 / 0	0 / 0	0 / 0	0 / 0	0 / 0	1 / 1	1 / 1
Se6	0 / 0	0 / 0	0 / 0	0 / 0	0 / 0	0 / 0	0 / 0	0 / 0	0 / 0	0 / 0	0 / 0	0 / 0	0 / 0	0 / 0
Se7	0 / 0	0 / 0	0 / 0	0 / 0	0 / 0	0 / 0	0 / 0	0 / 0	0 / 0	0 / 0	0 / 0	0 / 0	0 / 0	0 / 0
Se8	0 / 0	0 / 0	0 / 0	0 / 0	0 / 0	0 / 0	0 / 0	0 / 0	0 / 0	0 / 0	0 / 0	0 / 0	0 / 0	0 / 0
Se9	0 / 0	0 / 0	0 / 0	0 / 0	0 / 0	0 / 0	0 / 0	0 / 0	0 / 0	0 / 0	0 / 0	0 / 0	0 / 0	0 / 0
Li1	0 / 0	2 / 2	0 / 0	0 / 0	0 / 0	1 / 1	0 / 0	0 / 0	1 / 1	0 / 0	0 / 0	0 / 0	0 / 0	0 / 0
Li2	0 / 0	0 / 0	0 / 0	0 / 0	0 / 0	0 / 0	0 / 0	0 / 0	0 / 0	1 / 1	1 / 1	0 / 0	0 / 0	1 / 1
Li3	1 / 1	0 / 0	1 / 0	0 / 0	0 / 0	0 / 0	0 / 0	0 / 0	0 / 0	1 / 0	0 / 0	0 / 0	1 / 1	0 / 0
CN	3	4	3	2	2	3	2	2	3	3	3	3	3	3

Table 6.3 e: continued

	O15	O16	O17	O18	O19	O20	O21	O22	O23	O24	O25	O26	O27	CN
Lu1	1 / 1	0 / 0	1 / 1	1 / 1	0 / 0	1 / 1	0 / 0	0 / 0	1 / 1	0 / 0	0 / 0	1 / 1	1 / 1	8
Lu2	0 / 0	0 / 0	1 / 1	0 / 0	0 / 0	0 / 0	1 / 1	0 / 0	1 / 1	1 / 1	1 / 1	0 / 0	0 / 0	8
Lu3	0 / 0	0 / 0	0 / 0	0 / 0	1 / 1	0 / 0	0 / 0	0 / 0	0 / 0	1 / 1	0 / 0	0 / 0	1 / 1	7
Lu4	1 / 1	0 / 0	0 / 0	1 / 1	0 / 0	0 / 0	0 / 0	0 / 0	0 / 0	0 / 0	0 / 0	0 / 0	0 / 0	7
Lu5	0 / 0	0 / 0	0 / 0	0 / 0	0 / 0	1 / 1	1 / 1	1 / 1	0 / 0	0 / 0	0 / 0	1 / 1	0 / 0	7
Se1	0 / 0	0 / 0	0 / 0	0 / 0	0 / 0	0 / 0	0 / 0	0 / 0	0 / 0	0 / 0	0 / 0	0 / 0	0 / 0	3
Se2	0 / 0	0 / 0	0 / 0	0 / 0	0 / 0	0 / 0	0 / 0	0 / 0	0 / 0	0 / 0	0 / 0	0 / 0	0 / 0	3
Se3	0 / 0	0 / 0	0 / 0	0 / 0	0 / 0	0 / 0	0 / 0	0 / 0	0 / 0	0 / 0	0 / 0	0 / 0	0 / 0	3
Se4	0 / 0	0 / 0	0 / 0	0 / 0	0 / 0	0 / 0	0 / 0	0 / 0	0 / 0	0 / 0	0 / 0	0 / 0	0 / 0	3

Table 6.3 e: continued

	O15	O16	O17	O18	O19	O20	O21	O22	O23	O24	O25	O26	O27	CN
Se5	1 / 1	0 / 0	0 / 0	0 / 0	0 / 0	0 / 0	0 / 0	0 / 0	0 / 0	0 / 0	0 / 0	0 / 0	0 / 0	3
Se6	0 / 0	1 / 1	1 / 1	1 / 1	0 / 0	0 / 0	0 / 0	0 / 0	0 / 0	0 / 0	0 / 0	0 / 0	0 / 0	3
Se7	0 / 0	0 / 0	0 / 0	0 / 0	1 / 1	1 / 1	1 / 1	0 / 0	0 / 0	0 / 0	0 / 0	0 / 0	0 / 0	3
Se8	0 / 0	0 / 0	0 / 0	0 / 0	0 / 0	0 / 0	0 / 0	1 / 1	1 / 1	1 / 1	0 / 0	0 / 0	0 / 0	3
Se9	0 / 0	0 / 0	0 / 0	0 / 0	0 / 0	0 / 0	0 / 0	0 / 0	0 / 0	0 / 0	1 / 1	1 / 1	1 / 1	3
Li1	0 / 0	0 / 0	0 / 0	0 / 0	0 / 0	0 / 0	0 / 0	0 / 0	0 / 0	0 / 0	0 / 0	0 / 0	0 / 0	5
Li2	0 / 0	2 / 2	0 / 0	0 / 0	0 / 0	0 / 0	0 / 0	0 / 0	0 / 0	0 / 0	0 / 0	0 / 0	0 / 0	5
Li3	1 / 0	0 / 0	0 / 0	0 / 0	1 / 1	0 / 0	0 / 0	1 / 1	0 / 0	0 / 0	0 / 0	0 / 0	0 / 0	6
CN	3	3	3	3	3	3	3	3	3	3	2	3	3	

7 An alkali metal halide oxoselenate(IV) of a trivalent rare-earth element: $CsTmCl_2[SeO_3]$

7.1 Synthesis of $CsTmCl_2[SeO_3]$

$CsTmCl_2[SeO_3]$ was prepared by solid-state reaction of stoichiometric quantities of Tm_2O_3, $TmCl_3$, SeO_2 and CsCl according to the following reaction scheme.

$$2\ Tm_2O_3 + TmCl_3 + 6\ SeO_2 + CsCl \longrightarrow 3\ CsTmCl_2[SeO_3] + Tm_2[SeO_3]_3 \quad (14)$$

The solid components of the starting materials were heated together at 830°C for seven days in evacuated sealed silica tubes. After this period, the furnace was cooled down slowly with about 0.1°C/min to 400°C and then switched off. Two different major phases were observed, one of which consisted of colourless needle-shaped crystals of $Tm_2[SeO_3]_3$ (paragraph 3.5), and the other of colourless flat ones of $CsTmCl_2[SeO_3]$, both stable in air and water. Data collection parameters are listed in table 6.3.a in agreement with the centrosymmetric space group $P2_1/n$. Positional and anisotropic thermal displacement parameters obtained in the final full-matrix least-squares refinement, selected bond distances and angles for $CsTmCl_2[SeO_3]$ are summarized in paragraph 6.3.

7.2 Structure description of $CsTmCl_2[SeO_3]$

The structure of $CsTmCl_2[SeO_3]$ is illustrated in figure 7.2.a. There are eight different unique atoms in the unit cell, all of which occupy the same general Wyckoff position (4e). The thulium cations have seven nearest neighbours (five oxygen, d(Tm–O) = 225 – 240 pm and two chlorine atoms, d(Tm–Cl) = 261 pm) in an approximate pentagonal bipyramid $[TmO_5Cl_2]$ with both chloride anions occupying the apical positions. Five oxygen atoms (one O1, two O2 and two O3) serve to fuse the $[TmO_5Cl_2]$ polyhedra with four nearby oxoselenate(VI) groups via edge and corner sharing (fig. 7.2.b, *left*). The cesium cation is ninefold coordinated in the shape of a tricapped trigonal prism. The caps are consisting only of the three oxygen atoms of one single selenate group located approximately normal to a rectangular face of the prism (fig. 7.2.b, *right*). This coordination sphere is smaller compared to that one observed in, for example, $CsTe_2O_6$ (CN = 18) [121], and this can be explained by the fact that six large Cl^- anions are involved. The effective coordination number (ECoN) obtained from MAPLE [62]

for the Cs^+ cation in this compound is no more than 6.98, suggesting that O3 and O2 belong in actual fact only to its second coordination sphere (d(Cs–O = 382.9 and 407.4 pm, respectively).

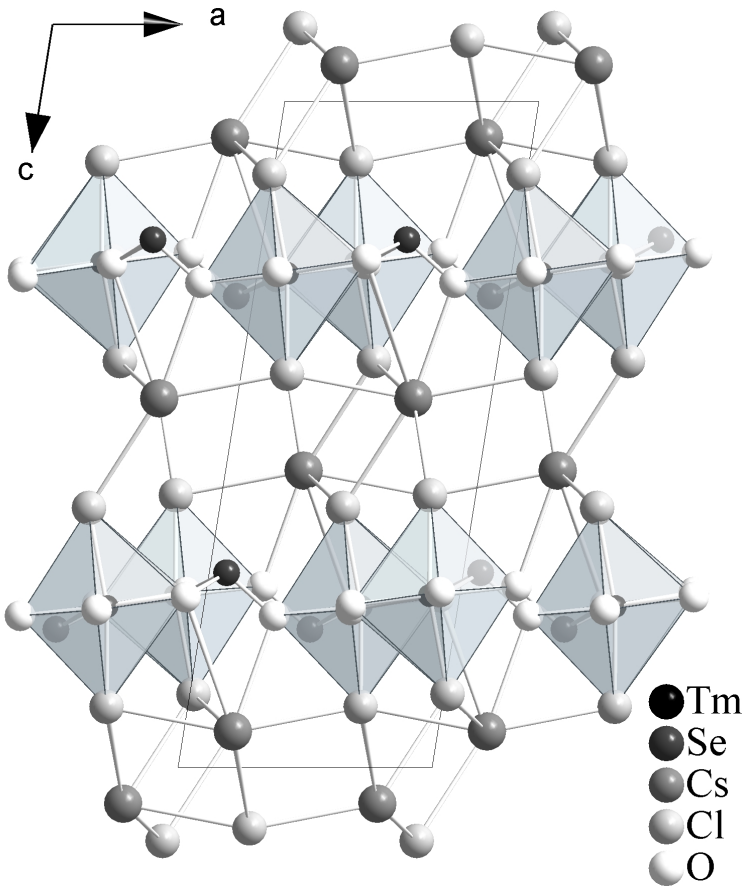

Fig. 7.2.a: Packing diagram of $CsTmCl_2[SeO_3]$ viewed down [010] in a $[TmO_5Cl_2]$ polyhedra representation

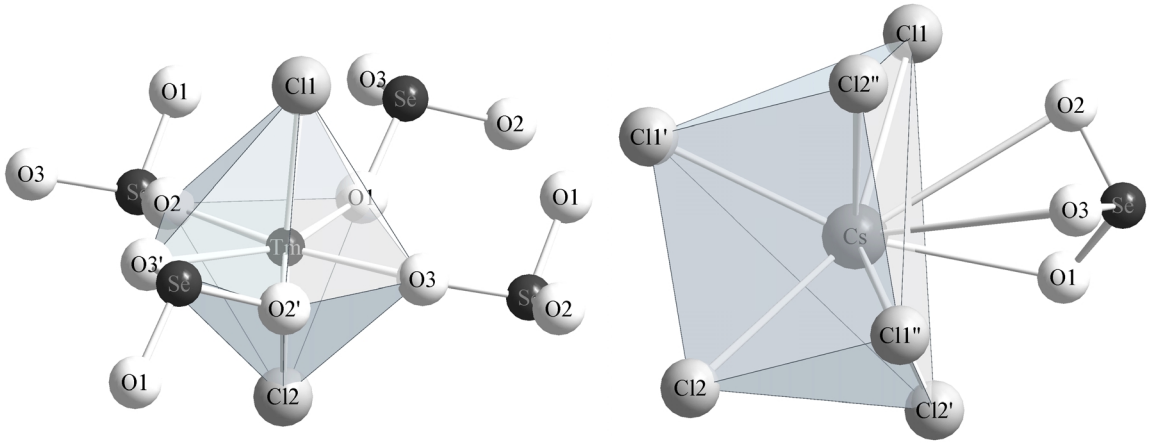

Fig. 7.2.b: Pentagonal bipyramid of oxygen and chlorine about Tm^{3+} showing four attached $[SeO_3]^{2-}$ groups (*left*), and distorted tricapped trigonal prismatic coordination of oxygen and chlorine about Cs^+ (*right*) in $CsTmCl_2[SeO_3]$

The $[SeO_3]^{2-}$ groups adopt their usual ψ^1-tetrahedral geometry (d(Se–O) = 166 – 172 pm), with the Se^{4+} lone-pair electrons presumably occupying the fourth tetrahedral vertex. The O–Se–O bond angles show a few particular distortions (values of 90° for the O2–Se–O3 angle versus 104° for the O1–Se–O2 and O1–Se–O3 ones), but are well within the range observed for others oxoselenates(IV) described in this work. Furthermore, five cations (three Tm^{3+} terminal, one Tm^{3+} and one Cs^+ edge-spanning each) complete the coordination sphere about the trigonal pyramidal $[Se(O1)(O2)(O3)]^{2-}$ anion (fig. 7.2.c) and the distance between the central cation of the pyramid (Se^{4+}) and the plane containing O1, O2, O3 is about 80 pm.

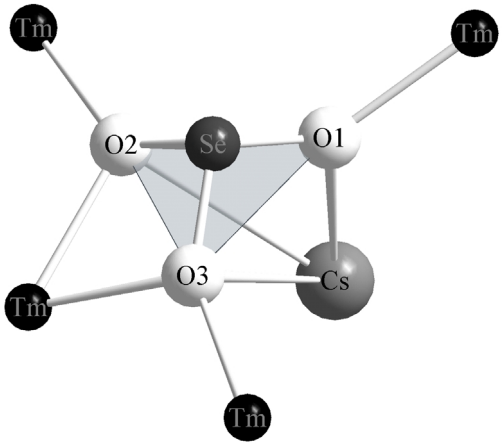

Fig. 7.2.c: Coordination sphere about the trigonal pyramidal $[SeO_3]^{2-}$ anion consisting of five cations (four Tm^{3+} and one Cs^+)

The main structural feature in $CsTmCl_2[SeO_3]$ emphasizes either chains or layers which contain $[TmO_5Cl_2]$ polyhedra and all selenium atoms, interleaved with cesium layers. The packing of these polyhedral building units can be visualized in terms of parallel infinite anionic zigzag strands $^1_\infty\{[TmO^e_{4/2}O^t_{1/1}Cl^t_{2/1}]^{5-}\}$ ($\equiv {}^1_\infty\{[TmO_3Cl_2]^{5-}\}$) propagating parallel to the [010] direction (fig. 7.2.d). The $[SeO_3]^{2-}$ groups are grafted onto the $[TmO_5Cl_2]$ polyhedra linking different $^1_\infty\{[TmO_3Cl_2]^{5-}\}$ strands via one edge (O2–O3) and one vertex (O1) to form layers parallel to the (001) plane such that a two-dimensional network described as $^2_\infty\{[TmCl_2(SeO_3)_{2/2}]\}^-$ formed by complex chains is observed (fig. 7.2.e). The layers built up by the pentagonal bipyramids $[TmO_5Cl_2]^{9+}$ and the $[SeO_3E]^{2-}$ tetrahedra exhibit remarkable similarities with the one formed by the bicapped trigonal prisms $[MO_8]$ (M = Nd, Sm) and analogous $[SeO_3E]^{2-}$ groups in the crystal structures of $Nd[HSeO_3][SeO_3] \cdot 2H_2O$ [11] and $Sm[HSeO_3[[SeO_3] \cdot 2H_2O$ [12]. These edges and corners shared with the $[SeO_3]^{2-}$ groups were previously observed in $CuLa_2[SeO_3]_4$ and $NaLa[SeO_3]_2$ as well, with the difference that

only half of the selenium atoms in the latter are located within the sheets [48, 52]. Very recently similar sheets described like $^{2}_{\infty}\{[GdCl(SeO_3)_2\}^{2-}$ were observed in the crystal structure of $CuGdCl[SeO_3]_2$ [48]. The O2 and O3 atoms that fuse $[SeO_3E]^{2-}$ groups with the $[TmO_5Cl_2]$ polyhedra via an edge are at a distance of 238 and 240 pm, respectively, apart from the Tm^{3+} cations, whereas O1 that bridges the two groups via a vertex is only 227 pm away, indicating a strong association between the parallel chains along [001]. Half of the selenium atoms in $CsTmCl_2[SeO_3]$ have their lone-pair electrons oriented above the anionic layer and the other half below it for centrosymmetric reasons. The position of the Cs^+ cations when connecting neighbouring layers along the *c* direction is essentially the same as that one of Na^+ in $NaLa[SeO_3]_2$. Within $^{2}_{\infty}\{[TmCl_2(SeO_3)_{2/2}]\}^{-}$ layers, if one removes all cations and the anions that are not in the plane of the sheet (Cl^- anions), the topological structure of the layer may be described in terms of the sheet anion-topology as stated by *Burns et al.* [122, 123]. The anions in the plane of the sheet separated by less than 304 pm and practically part of the same coordination polyhedra are joined by lines and the projection of the sheet anion-topology gives a two-dimensional tiling of space reflecting the packing of anions within the plane of the sheet. This projection is shown in figure 7.2.f. It consists of pentagons, rectangles and triangles. In the sheet, the pentagons are occupied by thulium cations, the triangles enclose selenium and the rectangles are unfilled.

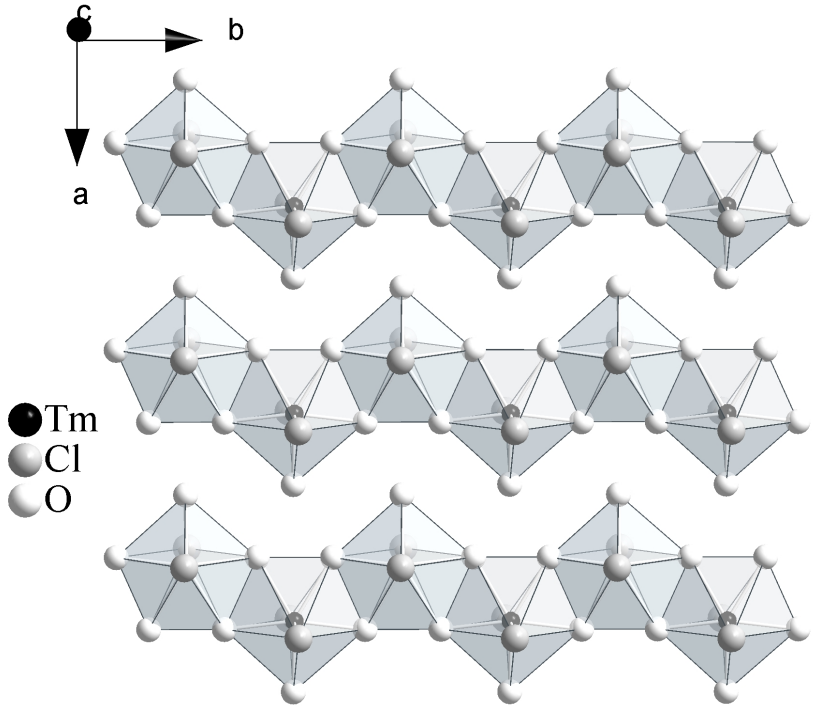

Fig. 7.2.d: Structure of $CsTmCl_2[SeO_3]$ viewed along [001] (only the parallel strands $^{1}_{\infty}\{[TmO_3Cl_2]^{5-}\}$ are represented)

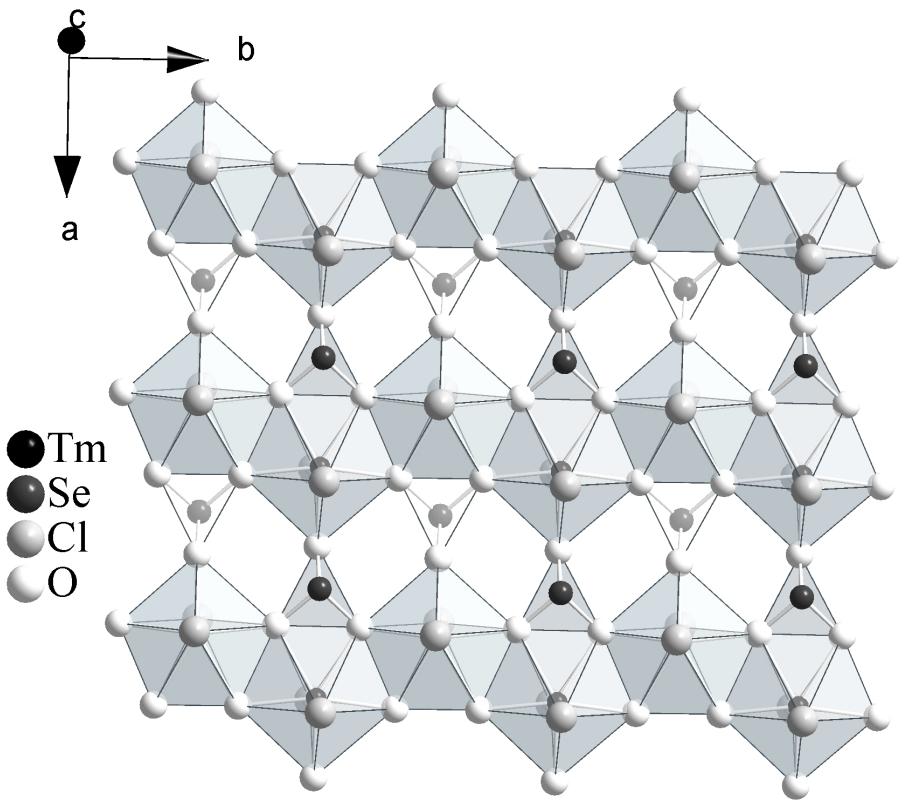

Fig. 7.2.e: Structure of $CsTmCl_2[SeO_3]$ viewed along [001] (the $^{2}_{\infty}\{[TmCl_2(SeO_3)_{2/2}]\}^{-}$ layer is represented)

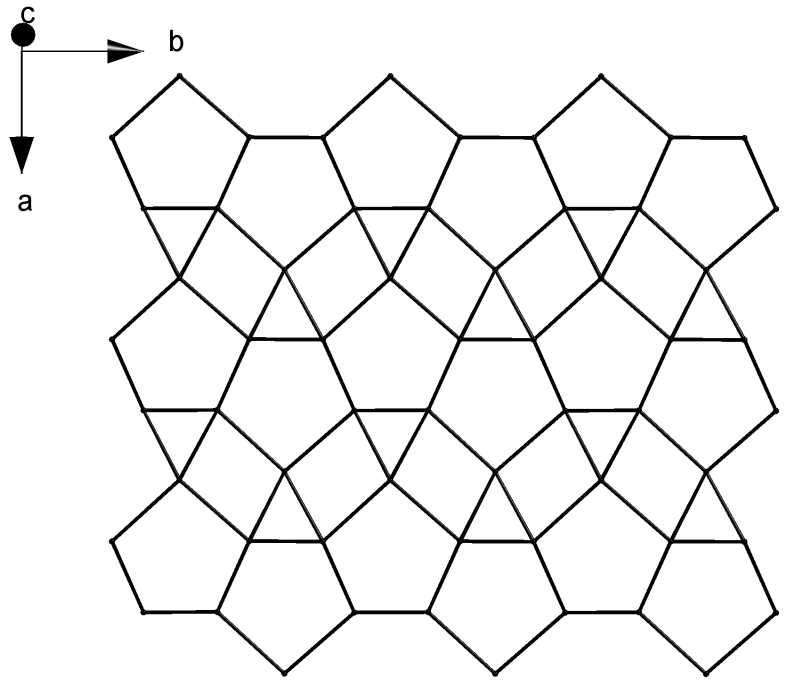

Fig. 7.2.f: The anion-topology of the $^{2}_{\infty}\{[TmCl_2(SeO_3)_{2/2}]\}^{-}$ sheet in the structure of $CsTmCl_2[SeO_3]$

7.3 Structural data for $CsTmCl_2[SeO_3]$

Table 7.3.a: Crystallographic data for $CsTmCl_2[SeO_3]$ and their determination

Formula		$CsTmCl_2[SeO_3]$
Crystal system and space group		monoclinic, $P2_1/n$ (No. 14)
Formula unit per unit cell (Z)		4
Unit cell parameters:	a =	658.92(5) pm
	b =	689.26(6) pm
	c =	1752.5(1) pm
	β =	99.093(7) °
Calculated density (D_x / g · cm^3)		4.223
Molar volume (V_m / cm^3 · mol^{-1})		118.32
Diffractometer, radiation		κ-CCD (Fa. Nonius); Mo-K_α: λ = 71.07 pm
$2\theta_{max.}$		60.1
Index range:	$\pm h_{max}$ / $\pm k_{max}$ / $\pm l_{max}$ =	9 / 9 / 24
F(000)		864
Absorption coefficient (μ)		21.09 mm^{-1}
Absorption correction		Numerical, after crystal shape optimization with the program X-SHAPE [53]
Other data corrections		background, polarization, *Lorentz* factors
Collected reflections		18536
Unique reflections		2309
R_{int} / R_σ		0.055 / 0.028
Reflections with $\|F_o\| \geq 4\sigma\|F_o\|$		2176
Structure solution and refinement		Program system SHELX-97 [58]
Scattering factors		International Tables, Vol. C [85]
R_1 / R_1 with $\|F_o\| \geq 4\sigma\|F_o\|$		0.035 / 0.032
wR_2 / Goodness of fit (GooF)		0.081 / 1.090
Extinction (g)		0.0023(2)
Residual electron density (ρ / e$^-$ · 10^6 pm)		max.: 2.20
		min.: –2.22

Table 7.3.b: Atomic coordinates for $CsTmCl_2[SeO_3]$

Atom	Wyckoff Position	x / a	y / b	z / c
Cs	4e	0.19304(8)	0.20950(8)	0.94572(3)
Tm	4e	0.11872(3)	0.32123(3)	0.25820(1)
Cl1	4e	0.4854(3)	0.1895(3)	0.6101(1)
Cl2	4e	0.1802(3)	0.3386(3)	0.4089(1)
Se	4e	0.06818(8)	0.18288(8)	0.70761(3)
O1	4e	0.2818(6)	0.1733(6)	0.7722(3)
O2	4e	0.4194(6)	0.4958(6)	0.2366(3)
O3	4e	0.4219(6)	0.1455(6)	0.2443(3)

Table 7.3.c: Anisotropic thermal displacement parameters[b)] (U_{ij}/pm^2) for $CsTmCl_2[SeO_3]$

Atom	U_{11}	U_{22}	U_{33}	U_{23}	U_{13}	U_{12}
Cs	285(2)	688(4)	393(3)	103(2)	120(2)	84(2)
Tm	112(1)	108(1)	299(2)	–4(1)	41(1)	0(1)
Cl1	386(9)	466(10)	288(8)	13(7)	53(7)	–44(8)
Cl2	254(8)	680(13)	313(8)	–75(8)	44(6)	–33(8)
Se	120(2)	157(3)	262(3)	5(2)	54(2)	0(2)
O1	92(17)	253(22)	333(23)	–11(16)	43(15)	–2(14)
O2	168(18)	124(18)	455(26)	26(17)	72(17)	42(15)
O3	141(17)	88(17)	604(29)	20(16)	101(18)	3(15)

[b)] defined as temperature factor according to: $\exp[-2\pi^2(a^{*2}h^2U_{11} + b^{*2}k^2U_{22} + c^{*2}l^2U_{33} + 2b^*c^*klU_{23} + 2a^*c^*hlU_{13} + 2a^*b^*hkU_{12})]$

Table 7.3.d: Selected interatomic distances (d/pm) and angles (∢/deg) for $CsTmCl_2[SeO_3]$

$CsTmCl_2[SeO_3]$					
	d / pm		d / pm		d / pm
Cs – O1	319.6	Tm – O1	227.2	Se – O1	166.2
Cs – O3	382.9	Tm – O2	226.1	Se – O2	170.1
Cs – O2	*407.7*	Tm – O2′	239.9	Se – O3	171.4
Cs – Cl1	345.0	Tm – O3	225.1		∢ / grd
Cs – Cl1′	359.5	Tm – O3′	238.1	O1 – Se – O2	103.5
Cs – Cl1″	385.0	Tm – Cl1	260.6	O1 – Se – O3	103.8
Cs – Cl2	335.5	Tm – Cl2	261.1	O2 – Se – O3	90.2
Cs – Cl2′	338.9				
Cs – Cl2″	361.3				

Table 7.3.e: Motifs of mutual adjunction in $CsTmCl_2[SeO_3]$

	Cl1	Cl2	O1	O2	O3	CN
Cs	3 / 3	3 / 3	1 / 1	0+1 / 0	1 / 1	8+1
Tm	1 / 1	1 / 1	1 / 1	2 / 2	2 / 2	7
Se	0 / 0	0 / 0	1 / 1	1 / 1	1 / 1	3
CN	4	4	3	3	4	

8 An alkali metal oxyhalide oxoselenate(IV) of a trivalent rare-earth element: $CsEu_4O_3Cl_3[SeO_3]_2$

8.1 Synthesis of $CsEu_4O_3Cl_3[SeO_3]_2$

Our attempt to synthesize $Eu_4O_3Cl_2[SeO_3]_2$ isostructural with $M_4O_3Cl_2[SeO_3]_2$ (M = Er, Yb) using the same stoichiometric mixture and reaction conditions as stated in paragraph 5.2 failed and the reaction product was identified to be colourless, platelet-shaped single crystals of $CsEu_4O_3Cl_3[SeO_3]_2$ instead of $Eu_4O_3Cl_2[SeO_3]_2$. A compilation of the crystal data, technical details of the data collection and the structure refinement, at long last selected internuclear distances and angles for this new *quasi*-quinary phase are given in paragraph 8.3.

8.2 Structure description of $CsEu_4O_3Cl_3[SeO_3]_2$

$CsEu_4O_3Cl_3[SeO_3]_2$ forms a complicated framework structure as illustrated in figure 8.2.a. It can be geometrically described to consist of two differently charged slabs $^{2}_{\infty}\{[(Cs)_{1/1}(Cl1,3)^{e}_{6/3}(Cl2)^{e}_{2/2}]\}^{2-}$ and $^{2}_{\infty}\{[O_3Eu_4]\}^{6+}$ alternatingly arranged approximately normal to the (001) plane. The anionic sheets are combined by face-linkage of $[CsCl_8]$ polyhedra to one-dimensional zigzag chains propagating along [100] and described as $^{1}_{\infty}\{[(Cs)_{1/1}(Cl1,3)^{e}_{6/3}(Cl2)^{t}_{2/1}]\}^{3-}$. Further interconnection takes place by common edges (Cl2–Cl2) to form the above-mentioned layers (fig. 8.2.b). The cationic ones are formed by oxocentered tetrahedra $[OEu_4]^{10+}$ which are joined by four common edges each to form the infinite planar $^{2}_{\infty}\{[O_3Eu_4]\}^{6+}$ slabs (fig. 8.2.c). By this arrangement scheme, *Wells* concept of topological equivalent polyhedra is respected for all $[OEu_4]$ units. Within the layers, any pair of tetrahedra represents a $[O_2Eu_6]$ dimer, a strip of the layer is the $(OEu_{4/2})_n$ chain similar to the $^{1}_{\infty}\{[OM_{4/2}]^{4+}\}$ single strands described in paragraph 4.3 for the $M_2O[SO_3]_2$-type compounds, and a strip two tetrahedra in width is the $(O_2Eu_3)_n$ (n is an integer) double chain as the $^{1}_{\infty}\{[O_2M_3]^{5+}\}$ ones observed in the $M_3O_2Cl[SeO_3]_2$-type structures in paragraph 5.1.5. Thus, $^{1}_{\infty}\{[OM_2]^{4+}\}$ and $^{1}_{\infty}\{[O_2M_3]^{5+}\}$ chains can easily be outlined in the $^{2}_{\infty}\{[O_3Eu_4]\}^{6+}$ sheets. The linkage of the O^{2-} centered $(Eu^{3+})_4$ tetrahedra through edges deminishes bond angles $\sphericalangle$(Eu–O–Eu) which are opposite to the shared edge to values ranged between 103 and 108° thus leading to short M···M contacts for all M^{3+} cations under consideration. These

diminitions are compensated by an increase of the bond angles opposite to non-shared edges to values between 113 and 120°. This structural geometry of fused oxocentered tetrahedra has been observed throughout this whole work.

As depicted in figure 8.2.a, different layers are packed together by $[(Eu4)Cl_4O_4]$ polyhedra (four Eu4–Cl bonds with d(Eu4–Cl) ranging from 274 to 300 pm on one side and four Eu4–O bonds with d(Eu4–O) ranged between 244 and 248 pm on the other of the square antiprism about $(Eu4)^{3+}$) to a framework arrangement. An important feature of the structure is the occurrence of bicapped cuboctahedral empty cavities with the characteristic distances $d_{□\text{-}Eu4}$ = 394.4 pm, $d_{□\text{-}Cs}$ = 378.3 pm, $d_{□\text{-}Cl3}$ = 308.7 pm, $d_{□\text{-}Cl1}$ = 317.3 pm and $d_{□\text{-}Cl2}$ = 352.8 pm (where □ denotes the cavity center). This particular site presented in figure 8.2.d is built from eight chloride anions making up a cube which is capped by four cesium and two apical europium cations. Interestingly in this structure, the $[SeO_3]^{2-}$ units are positioned at both sides of the $^{2}_{\infty}\{[O_3Eu_4]\}^{6+}$ layers such that the non-binding electron pairs at the Se^{4+} cations are orientated toward small channels between the two different adjacent layers. In addition, the distances of the selenium to opposite chloride ions within tunnels (≈ 350 pm) are comparable to the corresponding ones observed for the simple chloride oxoselenates(IV) presented in the paragraphs 5.2, 5.3 and 5.4 and ref. [36]. The oxygen atoms of the $[(Eu4)Cl_4O_4]$ units belong only to oxoselenate groups and are together with $(Eu4)^{3+}$ cations not involved in the formation of the $^{2}_{\infty}\{[O_3Eu_4]\}^{6+}$ sheets. This makes an important difference to all the other oxyhalide oxoselenates(IV) investigated in the course of this work where all lanthanide cations are part of the strands or layers of condensed oxocentered tetrahedra. The position of the $[SeO_3]^{2-}$ groups at both sides of the $^{2}_{\infty}\{[O_3Eu_4]\}^{6+}$ layers in the present compound agrees well with similar situations exhibited in others oxyhalide oxoselenates(IV) described in this dissertation (paragraphs 5.2, 5.3 and 5.5).

In the centrosymetric unit cell of $CsEu_4O_3Cl_3[SeO_3]_2$, the two different $[SeO_3]^{2-}$ groups are in their typical one-sided pyramidal coordination of three oxygen atoms around Se^{4+} with mean Se–O-bond lengths varying from 164 to 175 pm and bond angles ∢(O–Se–Se) from 97 to 99°. Both are more or less regular and all their oxygen atoms are further connected to three Eu^{3+} each, so that three Eu^{3+} cations which are terminal and three other ones being edge-spanning complete their cationic environment (fig. 8.2.e). Consequently, a coordination number of four results for all oxygen atoms in this compound. The three symmetrically independent Eu^{3+} cations are eight- and ninefold coordinated. The square prismatic $[(Eu1)O_8]$ cube (d(Eu1–O) = 223 – 267 pm) shows two short intrapolyhedral distances (O5–O6 = 259

pm and O4–O7 = 260 pm) and two rather small angles (O6–Eu1–O5 = 59.0° and O4–Eu1–O7 = 58.8°) caused by the edge-linkage with two adjacent $[SeO_3]^{2-}$ groups. The distorted capped square antiprisms $[(Eu2)O_9]$ and $[(Eu3)O_9]$ are very similar with Eu–O-bond lengths ranging from 227 to 313 pm. Polyhedral distortions can again be explained by the presence of further common edges and vertices with neighbouring $[SeO_3]^{2-}$ groups. Four chloride and four oxygen particles best positioned in the shape of a square antiprism complete the anionic vicinity of $(Eu4)^{3+}$ cations as mentioned before. The single Cs^+ cation type is coordinated by eight Cl^- anions just making up an irregular square prism or *pseudo*-cube. The Cs–Cl distances (341 – 409 pm) within the $[CsCl_8]$ polyhedron comply well with the analogous ones in $CsTmCl_2[SeO_3]$ [124] and are not far from the value of 356.4 pm (8×) observed in the cubic CsCl [125]. Those coordination polyhedra are depicted in figure 7.2.f.

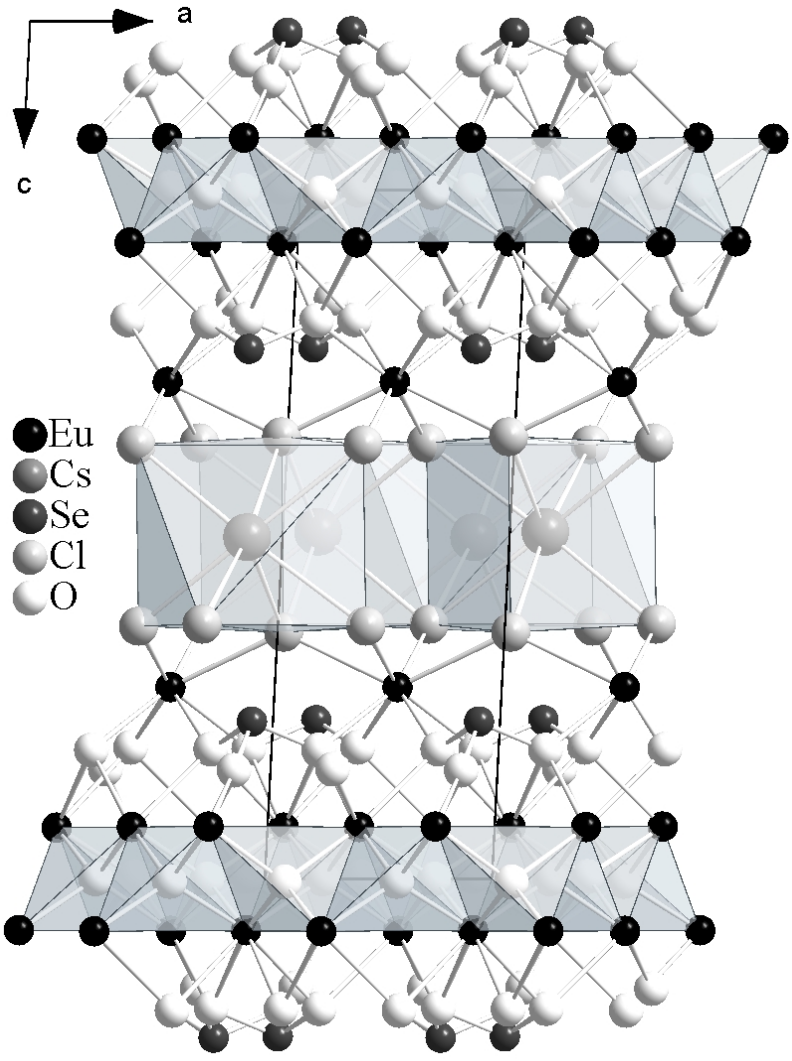

Fig. 8.2.a: Crystal structure of $CsEu_4O_3Cl_3[SeO_3]_2$ viewed onto (010) with layers of condensed oxocentered tetrahedra $[OEu_4]$ and $[CsCl_8]$ polyhedra

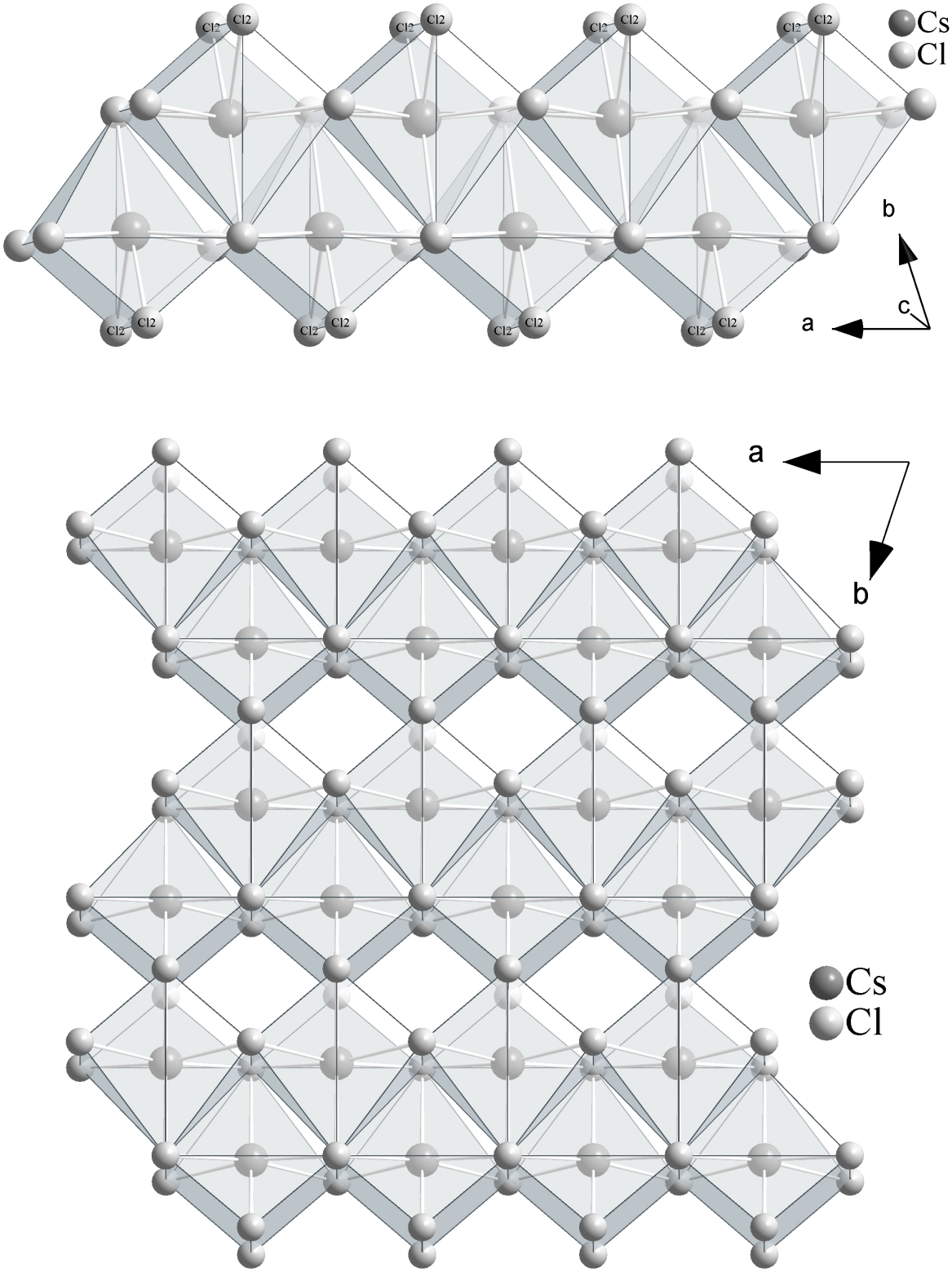

Fig. 8.2.b: $^{1}_{\infty}\{[(Cs)_{1/1}(Cl1,3)^{e}_{6/3}(Cl2)^{t}_{2/1}]\}^{3-}$ zigzag chains along [100] (*above*) and the corresponding $^{2}_{\infty}\{[(Cs)_{1/1}(Cl1,3)^{e}_{6/3}(Cl2)^{e}_{2/2}]\}^{2-}$ layers viewed at (001) (*below*) consisting of condensed [$CsCl_8$] *pseudo*-cubes

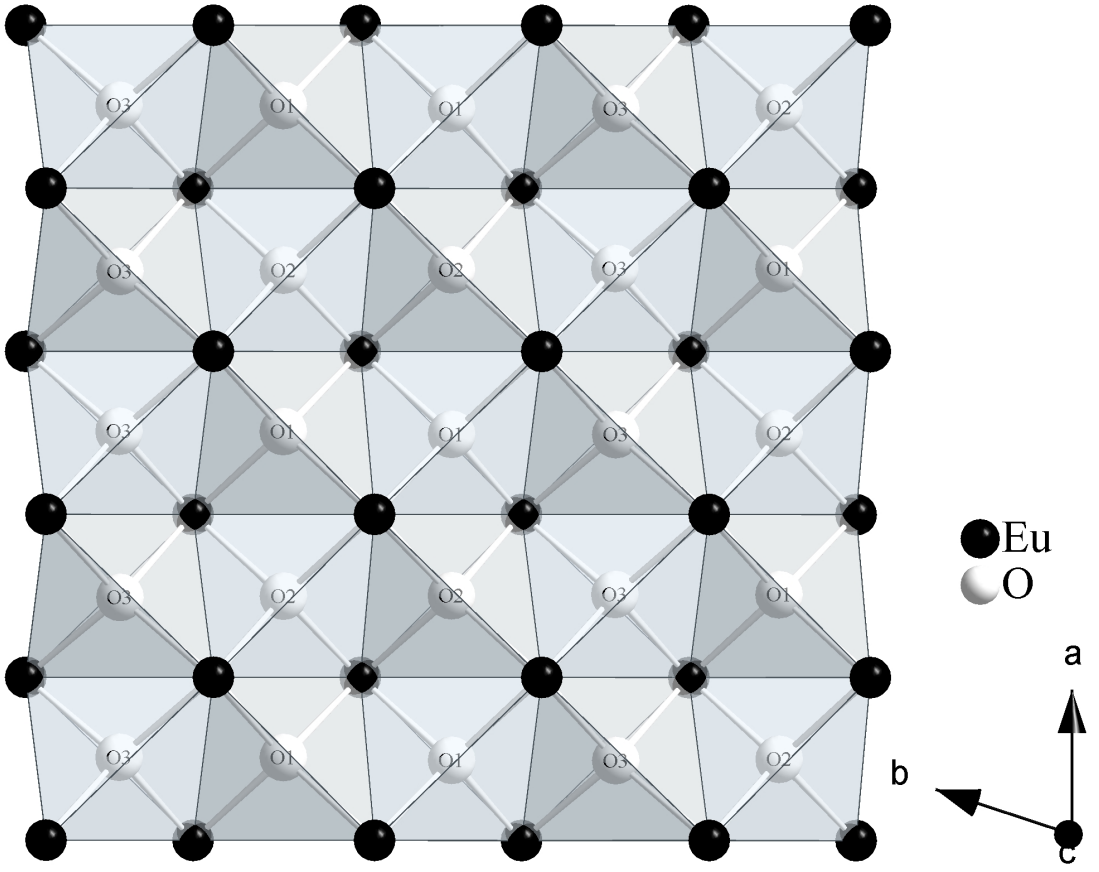

Fig. 8.2.c: Connectivity among the $[OEu_4]^{10+}$ tetrahedra leading to *quasi*-planar $^{2}_{\infty}\{[O_3Eu_{3+1}]\}^{6+}$ sheets as (001) projection

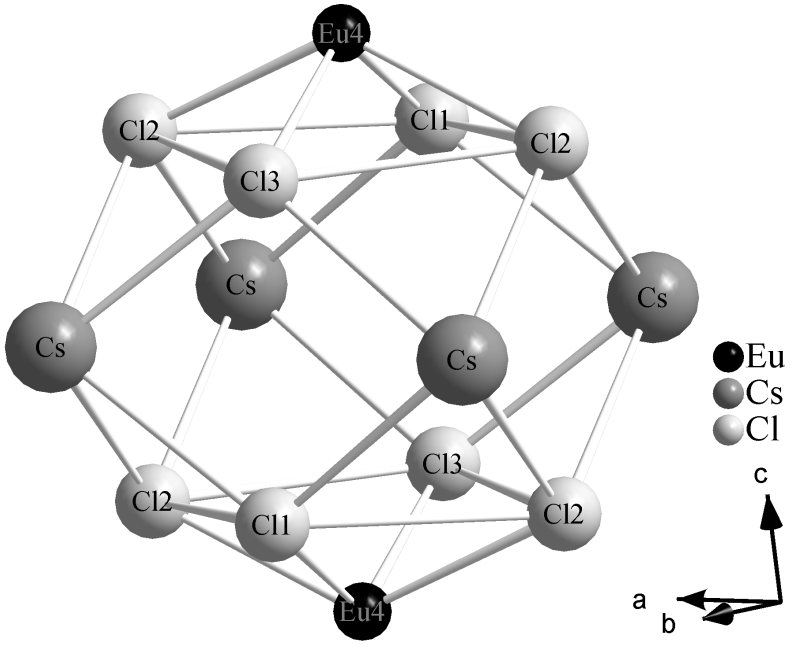

Fig. 8.2.d: Part of the structure of $CsEu_4O_3Cl_3[SeO_3]_2$ showing an empty cavity with the shape of a bicapped cuboctahedron

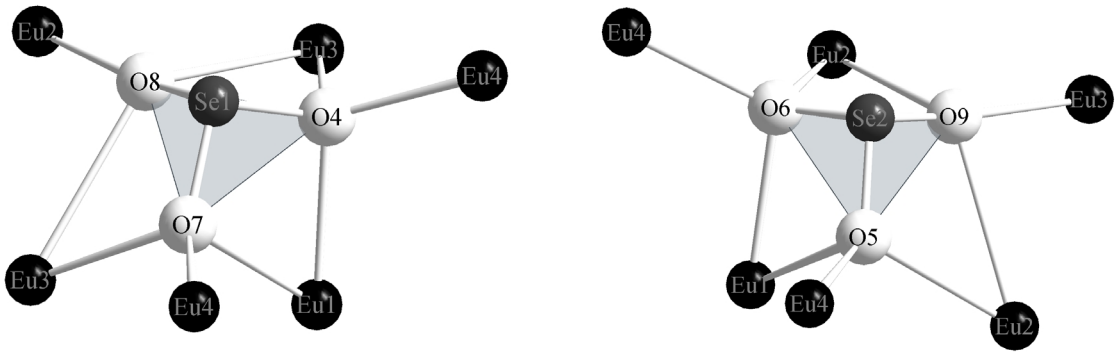

Fig. 8.2.e: Coordination of Eu^{3+} cations about the two crystallographically different $[SeO_3]^{2-}$ groups in $CsEu_4O_3Cl_3[SeO_3]_2$

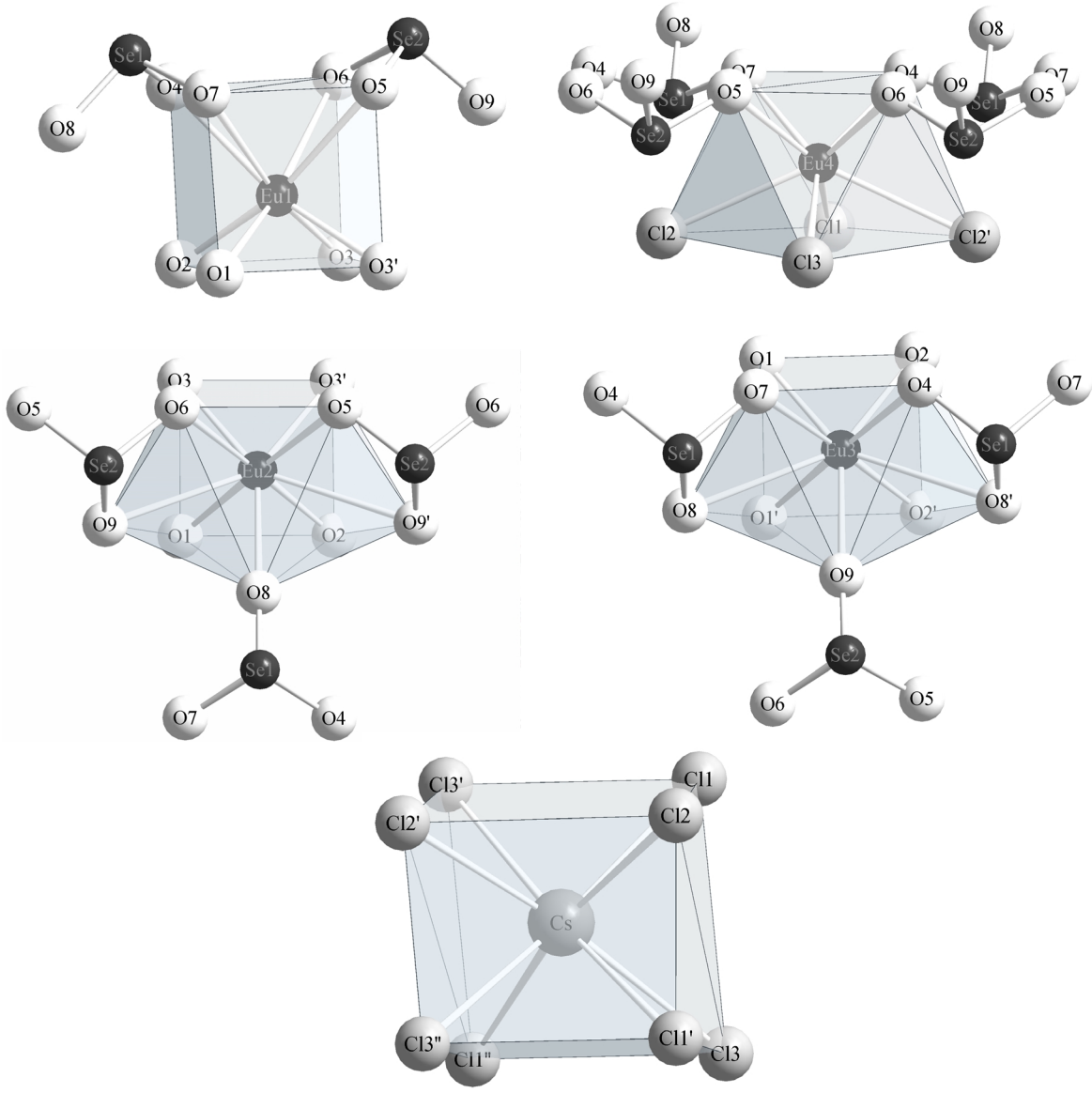

Fig. 8.2.f: Coordination polyhedra about the Eu^{3+} and Cs^{+} cations in the crystal structure of $CsEu_4O_3Cl_3[SeO_3]_2$

8.3 Structural data for $CsEu_4O_3Cl_3[SeO_3]_2$

Table 8.3.a: Crystallographic data for $CsEu_4O_3Cl_3[SeO_3]_2$

Formula		$CsEu_4O_3Cl_3[SeO_3]_2$
Crystal system and space group		triclinic, $P\bar{1}$ (No. 2)
Formula unit per unit cell (Z)		2
Unit cell parameters:	a / pm =	545.09(2)
	b / pm =	879.99(3)
	c / pm =	1597.44(7)
	α / ° =	81.036(2)
	β / ° =	89.992(2)
	γ / ° =	71.926(2)
Calculated density (D_x / g · cm^3)		5.310
Molar volume (V_m / cm^3 · mol^{-1})		216.405
Diffractometer, radiation		κ-CCD (Fa. Nonius); Mo-K_α: λ = 71.07 pm
$2\theta_{max.}$		55.1
Index range	$\pm h_{max}$ / $\pm k_{max}$ / $\pm l_{max}$ =	7 / 11 / 20
F(000)		996
Absorption coefficient (μ / mm^{-1})		25.36
Absorption correction		Numerical, after crystal shape optimization with the program X-SHAPE [53]
Other data corrections		background, polarization, *Lorentz* factors
Collected reflections		24069
Unique reflections		3170
R_{int} / R_σ		0.175 / 0.094
Reflections with $\|F_o\| \geq 4\sigma\|F_o\|$		2155
Structure solution and refinement		Program system SHELX-97 [58]
Scattering factors		International Tables, Vol. C [85]
R_1 / R_1 with $\|F_o\| \geq 4\sigma\|F_o\|$		0.122 / 0.081
wR_2 / Goodness of fit (GooF)		0.207 / 1.058
Extinction (g)		0.00081(3)
Residual electron density (ρ / e$^-$ 10^6 pm)		max. 5.56; min. −3.50

Table 8.3.b: Atomic coordinates for $CsEu_4O_3Cl_3[SeO_3]_2$

Atoms	Wyckoff Position	x / a	y / b	z / c
Eu1	2i	0.9287(2)	0.1433(1)	0.07451(7)
Eu2	2i	0.5975(2)	0.8057(1)	0.07529(8)
Eu3	2i	0.2600(2)	0.4805(1)	0.07608(8)
Eu4	2i	0.4594(2)	0.0804(1)	0.27837(7)
Cs	2i	0.8439(3)	0.3122(2)	0.5038(1)
Se1	2i	0.8099(4)	0.3784(3)	0.2306(2)
Se2	2i	0.0926(4)	0.8139(3)	0.2285(2)
Cl1	2i	0.3345(12)	0.3300(8)	0.3698(5)
Cl2	2i	0.9732(12)	0.0528(7)	0.3580(4)
Cl3	2i	0.6131(12)	0.7706(8)	0.3670(5)
O1	2i	0.4192(27)	0.6700(16)	0.9961(9)
O2	2i	0.9144(27)	0.6697(16)	0.9959(9)
O3	2i	0.2544(29)	0.0009(16)	0.0001(9)
O4	2i	0.1005(30)	0.2752(22)	0.1892(11)
O5	2i	0.7931(30)	0.9373(19)	0.1873(11)
O6	2i	0.2683(28)	0.9383(19)	0.1885(11)
O7	2i	0.6211(30)	0.2783(21)	0.1910(11)
O8	2i	0.7270(58)	0.5445(25)	0.1593(14)
O9	2i	0.1604(56)	0.6913(25)	0.1578(15)

Table 8.3.c: Anisotropic thermal displacement parameters[a)] (U_{ij}/pm^2) for $CsEu_4O_3Cl_3[SeO_3]_2$

	U_{11}	U_{22}	U_{33}	U_{23}	U_{13}	U_{12}
Eu1	168(6)	100(5)	354(8)	–49(5)	12(5)	–38(4)
Eu2	1684(6)	103(5)	353(8)	–57(5)	14(5)	–39(4)
Eu3	201(6)	93(5)	348(7)	–63(5)	20(5)	–42(4)
Eu4	202(6)	144(6)	395(8)	–71(5)	14(5)	–57(4)
Cs	316(9)	315(9)	494(11)	–87(8)	19(7)	–113(7)
Se1	249(12)	97(10)	337(14)	–37(9)	8(9)	–31(9)
Se2	274(12)	143(11)	326(14)	–76(10)	7(10)	–56(9)
Cl1	286(32)	380(36)	514(43)	–231(31)	68(28)	–106(27)
Cl2	364(34)	181(27)	385(39)	–64(24)	38(26)	–89(24)
Cl3	314(34)	283(33)	555(46)	96(30)	3(29)	–102(27)
O1	217(80)	50(66)	186(83)	–54(57)	7(60)	111(58)
O2	205(79)	58(66)	273(89)	9(59)	30(62)	–59(59)
O3	319(87)	20(64)	305(95)	–53(58)	75(66)	–51(60)
O4	276(90)	465(113)	307(101)	–182(81)	74(70)	–162(80)
O5	243(89)	185(84)	494(114)	121(75)	–122(74)	–9(68)
O6	166(79)	223(84)	354(98)	7(69)	99(64)	11(64)
O7	264(90)	339(99)	363(105)	–110(78)	14(72)	–117(75)
O8	1870(277)	181(107)	422(143)	129(95)	66(154)	–54(139)
O9	1777(268)	177(104)	536(151)	–286(101)	145(155)	–7(134)

[a)] defined as temperature factor according to: $\exp[-2\pi^2(a^{*2}h^2U_{11} + b^{*2}k^2U_{22} + c^{*2}l^2U_{33} + 2b^*c^*klU_{23} + 2a^*c^*hlU_{13} + 2a^*b^*hkU_{12})]$

Table 8.3.d: Selected internuclear distances (d/pm) and angles (∢/deg) in $CsEu_4O_3Cl_3[SeO_3]_2$

$CsEu_4O_3Cl_3[SeO_3]_2$							
	d / pm		d / pm		d / pm		d / pm
Eu1 – O2	223.6	Eu2 – O1	227.1	Eu3 – O1	227.6	Eu4 – O4	273.8
– O1	224.9	– O2	228.3	– O2	228.6	– O7	274.3
– O3	228.6	– O3	228.3	– O2′	231.4	– O6	244.1
– O3′	229.8	– O3′	229.2	– O1′	232.4	– O5	244.2
– O5	262.4	– O8	236.9	– O9	236.2	– Cl1	246.5
– O6	262.6	– O5	266.3	– O7	268.5	– Cl3	248.3
– O4	263.1	– O6	268.7	– O4	269.1	– Cl2	300.0
– O7	267.1	– O9	308.2	– O8	310.9	– Cl2′	300.1
		– O9′	313.7	– O8′	312.1		
Cs – Cl3	341.3	Se1 – O8	164.6	Se2 – O9	164.4		
– Cl3′	342.6	– O7	172.3	– O5	171.9		
– Cl2	343.4	– O4	174.9	– O6	172.0		
– Cl1	345.1						
– Cl1′	345.7	O1 – Eu1	224.9	O2 – Eu1	223.6	O3 – Eu2	228.3
– Cl2	346.3	– Eu2	227.1	– Eu2	228.3	– Eu1	228.6
– Cl1″	387.4	– Eu3	227.6	– Eu3	228.6	– Eu2′	229.2
– Cl3″	409.0	– Eu3′	232.4	– Eu3′	231.4	– Eu1′	229.8
		∢ / grd				∢ / grd	
O7 – Se1 – O4		97.2		O6 – Se2 – O5		97.8	
O8 – Se1 – O7		98.6		O9 – Se2 – O6		97.9	
O8 – Se1 – O4		98.7		O5 – Se2 – O5		98.9	

Table 8.3.d: Continued

	∢ / grd		∢ / grd		∢ / grd
Eu3 – O1 – Eu3′	104.1	Eu3 – O2 – Eu3′	104.4	Eu2 – O3 – Eu1	103.7
Eu1 – O1 – Eu3	105.3	Eu1 – O1 – Eu2	105.7	Eu2 – O1 – Eu1′	104.1
Eu1 – O1 – Eu2	106.0	Eu1 – O1 – Eu3	106.0	Eu1 – O1 – Eu1′	105.4
Eu2 – O1 – Eu3	107.7	Eu2 – O1 – Eu3′	106.9	Eu2 – O1 – Eu2′	108.4
Eu2 – O1 – Eu3′	113.8	Eu2 – O1 – Eu3	113.6	Eu1 – O1 – Eu1′	117.9
Eu1 – O1 – Eu3	120.3	Eu1 – O1 – Eu3	120.5	Eu1 – O1 – Eu2′	117.9

Table 8.3.e: Motifs of mutual adjunction in $CsEu_4O_3Cl_3[SeO_3]_2$

	Cl1	Cl2	Cl3	O1	O2	O3	O4	O5	O6	O7	O8	O9	CN
Eu1	0 / 0	0 / 0	0 / 0	1 / 1	1 / 1	2 / 2	1 / 1	1 / 1	1 / 1	1 / 1	0 / 0	0 / 0	8
Eu2	0 / 0	0 / 0	0 / 0	1 / 1	1 / 1	2 / 2	0 / 0	1 / 1	1 / 1	0 / 0	1 / 1	2 / 0	9
Eu3	0 / 0	0 / 0	0 / 0	2 / 2	2 / 2	0 / 0	1 / 1	0 / 0	0 / 0	1 / 1	1 / 0	1 / 1	9
Eu4	1 / 1	2 / 2	1 / 1	0 / 0	0 / 0	0 / 0	1 / 1	1 / 1	1 / 1	1 / 1	0 / 0	0 / 0	8
Cs	3 / 3	2 / 2	3 / 3	0 / 0	0 / 0	0 / 0	0 / 0	0 / 0	0 / 0	0 / 0	0 / 0	0 / 0	8
Se1	0 / 0	0 / 0	0 / 0	0 / 0	0 / 0	0 / 0	1 / 1	0 / 0	0 / 0	1 / 1	1 / 1	0 / 0	3
Se2	0 / 0	0 / 0	0 / 0	0 / 0	0 / 0	0 / 0	0 / 0	1 / 1	1 / 1	0 / 0	0 / 0	1 / 1	3
CN	4	4	4	4	4	4	4	4	4	4	2	2	

9 Summary and outlook

9.1 Results

This work was initially intended to investigate how far the existence range of the oxoselenates(IV) $M_2[SeO_3]_3$ can be extended to small and heavy lanthanides, and to synthesise rare-earth oxoselenates(IV) containing O^{2-} centered $[M^{3+}]_4$ tetrahedra units as well as to determine the influence of halide anions (Cl^-, Br^-) on the structure of lanthanides oxide oxoselenates(IV).

The first part could be successfully done. It could be shown that under suitable reaction condition, oxoselenates(IV) of the type $M_2[SeO_3]_3$, M = Sc, Y, La – Lu, could be obtained with all M^{3+} cations. While $Sc_2[SeO_3]_3$ adopts a new structure type, $Ce_2[SeO_3]_3$ is isostructural with $La_2[SeO_3]_3$, $Pr_2[SeO_3]_3$ with $Nd_2[SeO_3]_3$ and the remaining Y, Sm until Lu with the published $Er_2[SeO_3]_3$. Also, during attempts to synthesize $Lu_2[SeO_3]_3$, a new $Li_3Lu_5[SeO_3]_9$ was obtained and its structure elucidated.

The second class of compounds, ($M_2O[SeO_3]_2$), shows an existence range limited to the elements M = Sm – Tm with the same reaction conditions, although experiments at other conditions (temperature, composition of the educt mixture, flux) are still to be done.

For the rare-earth oxyhalide oxoselenates(IV), four new structure types of either smaller or heavier rare-earth elements were synthesized and characterized, namely $M_3O_2Cl[SeO_3]_2$ (M = Tb, Dy, Er), $M_4O_3Cl_2[SeO_3]_2$ (M = Er, Yb), $M_5O_4X_3[SeO_3]_2$ (M = Gd, Tb) and finally $M_9O_8X_3[SeO_3]_4$ (M = La, Pr with X = Br and M = Pr, Nd, Sm, Gd with X = Cl). The first class crystallizes with the same formula in two different structure types depending only upon the cationic radius of the rare-earth element, whereas all compounds belonging to the same groups of the remaining three are isostructural. As we can see, their existence range is so limited that even by varying the conditions of preparation, very little could be found out about the four series of compounds. However many other measurements which could lead to analogues structures are still to be carried out. Two side products $CsTmCl_2[SeO_3]$ and $CsEu_4O_3Cl_3[SeO_3]_2$ were detected and structurally characterized during the course of this dissertation. Remarkably enough, our presumption at the beginning of this work that halide anions X^- (X = Cl, Br) could given isotypical oxyhalide oxoselenates(IV) of the trivalent lanthanides seem to be fully confirmed and both are crystallographically identical in a given structure type. Nevertheless, experiments to try and synthesize similar compounds with the remaining halides still to be done. Those experiments and results are among the first in the

chemistry of rare-earth oxide and oxyhalide oxoselenate(IV). The work on such structures were taken up later on and have not been so extensively explored.

9.1.1 Oxoselenates(IV) of trivalent lanthanide

9.1.1.1 The hexagonal $Sc_2[SeO_3]_3$

The scandium oxoselenate(IV), $Sc_2[SeO_3]_3$, crystallizes in the hexagonal system, space group $P6_3/m$ and contains only a single crystallographically Sc^{3+} cation in sixfold coordination. The trigonal antiprismatic polyhedra $[ScO_6]^{9-}$ share common face (O1, O1, O1) to form $[Sc_2O_9]^{12-}$-dimer which are linked by eight vertices of the isolated ψ^1-tetrahedral $[SeO_3]^{2-}$ anions to a three dimensional framework structure. The *non*-binding electron pair at the Se^{4+} are located within hexagonal channels propagating along the [001] direction. If one regards the complex $[SeO_3]^{2-}$ anions as dianionic spheres (Z^{2-}), the crystal structure of $Sc_2[SeO_3]_3$ ($\equiv Sc_2Z_3$) represents a cation-deficient NiAs-type (hexagonal, $P6_3/mmc$) arrangement with 1/3 of the cations missing in an ordered fashion.

hexagonal, $P6_3/m$ (No. 176), Z = 2	lattice constants		
	a / pm	c / pm	c/a
$Sc_2[SeO_3]_3$	814.28(5)	764.56(4)	0.939

9.1.1.2 The orthorhombic $Ce_2[SeO_3]_3$

The crystal structure of $Ce_2[SeO_3]_3$ exhibits a single Ce^{3+} cation and two different $[SeO_3]^{2-}$ groups. Four O-monodentate $[SeO_3]^{2-}$ and three O-chelating $[SeO_3]^{2-}$ groups for a coordination number ten are observed about the Ce^{3+} ion. The polyhedral connectivity in $Ce_2[SeO_3]_3$ results in infinite sheets of triangular-face-sharing (O1, O2 and O3) and edge-sharing (O3 and O4) CeO_{10} groups arrayed normal to [001]. The $[(Se1)O_3]^{2-}$ are closely related to these layers whereas $[(Se2)O_3]^{2-}$ groups serve to fuse them into a three-dimensional structure. Viewed down [010], the structure of $Ce_2[SeO_3]_3$ appears to be infinite channels of approximatly 354 pm (2×), 431 pm (2×) and 558 pm (2×) in whose spaces for *non*-binding electron pairs at the Se^{4+} cations are found.

orthorhombic, Pnma (No. 62), Z = 4	lattice constants		
	a / pm	b / pm	c / pm
$Ce_2[SeO_3]_3$	839.23(3)	1421.12(4)	704.58(2)

9.1.1.3 The monoclinic $Pr_2[SeO_3]_3$

The monoclinic $Pr_2[SeO_3]_3$ distinguishes six different rare-earth cations occupying the same *Wyckoff* position and are nine and ten times surrounded by oxygen in a various coordination shape. All coordination polyhedra deviate significantly from their ideal shape. The structure can be termed as layers of $[PrO_9]$ and $[PrO_{10}]$ polyhedra which are linked by either faces or edges leading to rectangular channels along [101]. The $[(Se5)O_3]^{2-}$, $[(Se7)O_3]^{2-}$ and $[(Se9)O_3]^{2-}$ groups are located between layers, and ensure stabilization as well as the three-dimensional framework structure of the compound. The remaining six $[SeO_3]^{2-}$ groups are situated approximately within the layers such that their free electron pairs are pointed toward the channels.

monoclinic, $P2_1/n$ (No. 14), Z = 12	lattice constants			
	a / pm	b / pm	c / pm	β / grd
$Pr_2[SeO_3]_3$	1683.36(2)	705.06(1)	2166.37(3)	102.061(1)

9.1.1.4 The triclinic $M_2[SeO_3]_3$ (M = Y, Sm – Lu)

Since oxoselenates(IV) of the heavier rare-earth element crystallize in two different systems: orthorhombic (La, Ce) and monoclinic (Nd, Pr), they are isostructural with smaller lanthanide (Sm – Lu) as well as Yttrium and crystallize in the published $Er_2[SeO_3]_3$ type structure. With these results we have shown that compounds with the formula $M_2[SeO_3]_3$ exist for the all the rare-earth elements. Both crystallographically independent M^{3+} cations adopt a coordination number of seven and eight, but eight and nine for the light Sm^{3+} cations in the form of pentagonal bipyramidal units on the one hand and a very distorted figure on the other. The linkage of the M^{3+} polyhedra and the $[SeO_3]^{2-}$ groups leads to rectangular channels running

parallel to [011] for $Sm_2[SeO_3]_3$ and along [01 $\bar{1}$] for Y, Eu – Lu providing enough space to incorporate the lone pairs at the selenium atoms.

$M_2[SeO_3]_3$	lattice constants					
triclinic, P $\bar{1}$ (No. 2), Z = 2	a / pm	b / pm	c / pm	α / grd	β / grd	γ / grd
$Y_2[SeO_3]_3$	699.34(5)	802.48(6)	898.82(8)	71.332(3)	69.916(3)	65.770(4)
$Sm_2[SeO_3]_3$	698.60(1)	789.60(2)	910.34(2)	96.693(1)	104.639(1)	115.867(1)
$Eu_2[SeO_3]_3$	712.64(4)	812.85(4)	911.52(6)	71.372(2)	70.075(2)	65.652(2)
$Gd_2[SeO_3]_3$	710.52(5)	810.87(7)	906.73(8)	71.364(4)	70.168(4)	65.747(4)
$Tb_2[SeO_3]_3$	706.20(3)	806.29(4)	904.06(5)	71.476(2)	70.084(2)	65.896(2)
$Dy_2[SeO_3]_3$	703.08(1)	804.10(2)	900.96(2)	71.383(1)	70.095(1)	65.903(1)
$Ho_2[SeO_3]_3$	700.79(3)	802.04(4)	897.69(4)	71.370(2)	70.098(2)	65.935(2)
[a] *$Er_2[SeO_3]_3$*	*698.2(1)*	*800.6(1)*	*895.0(1)*	*71.38(1)*	*70.13(1)*	*65.87(1)*
$Tm_2[SeO_3]_3$	694.61(3)	796.58(4)	891.96(5)	71.480(2)	70.223(2)	65.964(2)
$Yb_2[SeO_3]_3$	691.79(1)	793.93(1)	890.01(2)	71.455(1)	70.293(1)	65.038(1)
$Lu_2[SeO_3]_3$	690.22(2)	793.41(2)	887.26(2)	71.413(1)	70.235(1)	65.985(1)

[a] *Data from wickleder et al. [19]*

9.1.2 Oxide Oxoselenates(IV) of trivalent lanthanides: $M_2O[SeO_3]_2$ (M = Sm – Tm)

It was difficult to produce the oxide oxoselenates(IV) of this structure type in high yield and a structure determination only for the smaller lanthanides was possible. They crystallize tetragonally and exhibit M^{3+} cations in square antiprismatic coordination of eight oxygen atoms each. Six of the latter belong to six different isolated ψ^1-tetrahedral $[SeO_3]^{2-}$ anions whereas the remaining two are not bonded to selenium at all. Their coordination sphere actually consists of four M^{3+} cations arranged as a tetrahedron. These $[OM_4]^{10+}$ tetrahedra form infinite one-dimensional $^1_\infty\{[OM_{4/2}]^{4+}\}$ chains along [001] by sharing *trans*-oriented edges which are packed such that a central strand is quadratically surrounded in (001) projection by four chains at a distance of $a/\sqrt{2}$ and another square of four more of them at a factor of $\sqrt{2}$ (≡ the value of a) further apart and rotated by 45°. Charge balance and three-dimensional interconnection of this particular rod-packing occurs via discrete trigonal

$[SeO_3]^{2-}$ pyramids so that the whole structure gets strongly influenced by the stereochemical lone pair activity of these groups. Interestingly, the $\bar{4}$ symmetry of the $^{1}_{\infty}\{[OM_{4/2}]^{4+}\}$ chains is perfectly repeated by the "lone pair" channels of the *non*-binding electrons at the Se^{4+} cations.

$M_2O[SeO_3]_2$	Lattice constants		
tetragonal, $P4_2/ncm$ (No. 138), Z = 4	a / pm	c / pm	c/a
$Sm_2O[SeO_3]_2$	1075.07(15)	526.35(7)	0.490
$Eu_2O[SeO_3]_2$	1074.05(7)	525.77(3)	0.490
$Gd_2O[SeO_3]_2$	1068.73(6)	525.03(2)	0.491
$Tb_2O[SeO_3]_2$	1064.57(8)	521.56(4)	0.490
$Dy_2O[SeO_3]_2$	1060.07(4)	520.00(2)	0.490
$Ho_2O[SeO_3]_2$	1055.70(3)	518.80(1)	0.491
$Er_2O[SeO_3]_2$	1052.20(6)	517.35(2)	0.491
$Tm_2O[SeO_3]_2$	1048.87(5)	514.25(4)	0.490

9.1.3 Oxyhalide Oxoselenates(IV) of trivalent lanthanides

9.1.3.1 Compounds of the formula $M_3O_2Cl[SeO_3]_2$ (M = Tb, Dy, Er)

Two structure types of rare-earth oxyhalide oxoselenates(IV) with the formula $M_3O_2Cl[SeO_3]_2$ can be differentiated in the course of this work: $M_3O_2Cl[SeO_3]_2$ (orthorhombic, Pnma; M = Tb, Dy) and $Er_3O_2Cl[SeO_3]_2$ (monoclinic, C2/c). Both contains $[OM_4]$-tetrahedra that convened over common edges to form $^{1}_{\infty}\{[(M1)_{3/3}(M2)_{2/1}O_{4/2}]^{5+}\}$ (≡ $^{1}_{\infty}\{[O_2M_3]^{5+}\}$) double chains. These strands arrange themselves such that a central one is quadratically surrounded: in (100) projection for M = Tb, Dy and in (001) projection for Er by four chains at the same distance. This occurs via $[SeO_3]^{2-}$ pyramids leading to hexagonal channel between four cationic chains. The structure differ only in the stacking sequence when viewed down the (010) plane. Whereas in the orthorhombic compounds consecutive $^{1}_{\infty}\{[O_2M_3]^{5+}\}$ strands are stacked without displacement, the corresponding ones in $Er_3O_2Cl[SeO_3]_2$ are shifted from each other along [001] direction. The $(M1)^{3+}$ (M = Tb, Dy)

and $(Er1)^{3+}$ cations are eightfold coordinated in the shape of a bicapped trigonal prism while $(M2)^{3+}$ (M = Tb, Dy) exhibit a distorted square antiprism for a coordination number 8 against only seven for $(Er2)^{3+}$.

$M_3O_2Cl[SeO_3]_2$			$Er_3O_2Cl[SeO_3]_2$
orthorhombic, Pnma (No. 62), Z = 4			monoclinic, C2/c (No. 15), Z = 4
	Tb	Dy	a = 1498.23(6)
a / pm	535.16(4)	533.81(2)	b = 1102.03(5)
b / pm	1530.51(9)	1521.04(7)	c = 547.95(3)
c / pm	1081.72(7)	1076.56(4)	β = 105.515

9.1.3.2 Compounds of the formula $M_4O_3Cl_2[SeO_3]_2$ (M = Er, Yb)

The triclinic crystal structure of $M_4O_3Cl_2[SeO_3]_2$ is based on the two-dimensional layers $^{2}_{\infty}\{([O_3M_4]^{6+})_2\}$ running parallel to (011) which are composed of $[O_6M_{12}]^{24+}$ units formed by oxocentered tetrahedra linked by edges. Further connectivity of the $[O_6M_{12}]^{24+}$ groups occurs via two trans-edges and four vertices of the $[OM_4]$-tetrahedra to the above sheets. Within layers, each $[OM_4]$ tetrahedra share either two edges and one vertex or three edges and one vertex with neighbouring ones. The chloride anions are located between the layers and link them into a three-dimensional framework. The pyramidal $[SeO_3]^{2-}$ and Cl^- reveal a peculiar bonding scheme with their lone pair that interact between layers. The six crystallographically different M^{3+} are distorted square antiprisms or prisms and capped trigonal prisms coordinated to oxygen and chloride.

$M_4O_3Cl_2[SeO_3]_2$	lattice constants					
triclinic, $P\bar{1}$ (No. 2), Z = 2	a / pm	b / pm	c / pm	α / grd	β / grd	γ / grd
$Er_4O_3Cl_2[SeO_3]_2$	861.64(2)	1170.56(3)	1208.42(3)	67.666(1)	77.833(1)	85.270(1)
$Yb_4O_3Cl_2[SeO_3]_2$	853.88(1)	1145.90(2)	1195.47(2)	68.132(1)	78.113(1)	85.747(1)

9.1.3.3 Structure of $Gd_5O_4Br_3[SeO_3]_2$ and $Tb_5O_4Cl_3[SeO_3]_2$

$Gd_5O_4Br_3[SeO_3]_2$ and $Tb_5O_4Cl_3[SeO_3]_2$ are isostructural and contain three different crystallographically M^{3+} cations in seven- and eightfold coordination of O^{2-} and X^- anions. Their crystal structure consists of layers built up of corrugated metal-oxygen sheets $^2_\infty\{[O_4M_5]^{7+}\}$, formed by *edge*- and *vertex*-shared $[OM_4]^{10+}$-tetrahedra, spreading parallel (001). These layers are bordered by ψ^1-tetrahedral $[SeO_3]^{2-}$ groups and chloride anions in a 2:3-molar ratio both of which are responsible for charge compensation and three-dimensional interconnection. The structure is highly related to the "lone pair" channel structures of $M_2O[SeO_3]_2$ and $M_3O_2Cl[SeO_3]_2$, where single ($^1_\infty\{[OM_2]^{4+}\}$) and double chains ($^1_\infty\{[O_2M_3]^{5+}\}$) of *trans*-edge connected $[OM_4]^{10+}$-tetrahedra are present. As an extension of this kind of connectivity, the $^1_\infty\{[O_2M_3]^{5+}\}$ double chains of the $M_3O_2Cl[SeO_3]_2$ structure are further condensed via common vertices to form the above-mentioned $^2_\infty\{[O_4M_5]^{7+}\}$ layers.

$M_5O_4X_3[SeO_3]_2$	lattice constants			
monoclinic, C2/m (No. 12), Z = 2	a / pm	b / pm	c / pm	β / grd
$Gd_5O_4Br_3[SeO_3]_2$	1243.70(10)	549.91(4)	1005.29(9)	91.869(3)
$Tb_5O_4Cl_3[SeO_3]_2$	1229.13(4)	546.17(4)	978.79(7)	90.485(6)

9.1.3.4 Structure of $M_9O_8Br_3[SeO_3]_4$ (M = La, Pr) and $M_9O_8Cl_3[SeO_3]_4$ (M = Pr, Nd, Sm, Gd)

This novel class ofcompounds contains a network of *edge*-sharing $[OM_4]$-tetrahedra forming two-dimensional cationic layers best described as $^2_\infty\{[O_8M_9]^{11+}\}$ which spread parallel to (001). As previously observed in $M_4O_3Cl_2[SeO_3]_2$ and $M_5O_4X_3[SeO_3]_2$ with $^2_\infty\{([O_3M_4]^{6+})_2\}$ and $^2_\infty\{[O_5M_4]^{7+}\}$ layers, respectively, the above-mentioned sheets are sandwiched between ψ^1-tetrahedral $[SeO_3]^{2-}$ groups and halide anions leading to the three-dimensional linkage of the structure. The distances of the selenium atoms to opposite halide anions are important for providing large voids for the free *non*-binding electron pairs ("*lone pair*") of the Se^{4+} cations between different layers. Within the $^2_\infty\{[O_8M_9]^{11+}\}$ layers, one of the four tetrahedral $[OM_4]$ units involved has four edges in common with neighbouring ones whereas only three edges are shared by the three others. Five crystallographically different M^{3+} cations are present in

this structure. While $(M1)^{3+}$ and $(M2)^{3+}$ are square prismatically coordinated by eight oxygen, $(M3)^{3+}$ and $(M4)^{3+}$ are square antiprismatically surrounded by oxygen and halide. Finally, the $(M5)^{3+}$ environment can be looked at as a capped square prismatic ones.

$M_9O_8X_3[SeO_3]_4$	lattice constants					
triclinic, $P\bar{1}$ (No. 2), Z = 1	a / pm	b / pm	c / pm	α / grd	β / grd	γ / grd
$La_9O_8Br_3[SeO_3]_4$	711.72(3)	919.56(4)	996.58(5)	99.856(2)	94.938(2)	95.840(2)
$Pr_9O_8Br_3[SeO_3]_4$	700.35(4)	906.09(6)	985.91(7)	99.623(3)	95.076(3)	95.874(3)
$Pr_9O_8Cl_3[SeO_3]_4$	700.12(1)	901.63(2)	966.88(2)	99.787(1)	94.979(1)	95.901(1)
$Nd_9O_8Cl_3[SeO_3]_4$	696.30(2)	896.80(3)	963.87(3)	99.528(2)	95.176(2)	95.893(2)
$Sm_9O_8Cl_3[SeO_3]_4$	688.70(1)	888.79(2)	959.09(2)	98.674(1)	95.419(1)	96.031(1)
$Gd_9O_8Cl_3[SeO_3]_4$	680.17(5)	882.86(7)	960.18(8)	97.241(6)	95.539(6)	96.265(6)

9.1.4 The alkali metal oxoselenate(IV) of trivalent lanthanide: $Li_3Lu_5[SeO_3]_9$

While attempting to synthesize $Lu_2[SeO_3]_3$, $Li_3Lu_5[SeO_3]_9$ was obtained by the reaction of the educt with LiBr which served as flux. Its structure can be termed as a sequence of isolated $[(Li1)_2O_8]^{14-}$, $[(Li2)_2O_8]^{14-}$ and $[(Li3)O_6]^{11-}$ anions between which $[SeO_3]^{2-}$ groups and Lu^{3+} cations are arranged. According to literature, the trigonal antiprism coordination about Li3 seem to be novel in the chemistry of lithium. The small Lu^{3+} cations exhibit a coordination number eight and seven in the shape of irregular square prism or antiprisms and capped trigonal prisms. Finally, Se^{4+} adopt the classical one-sided trigonal pyramidal $[SeO_3]^{2-}$-unit with the fourth vertex of the pyramid occupied by the free electron pairs "*lone pair*" of the Se^{4+} cations.

monoclinic, $P2_1/n$ (No. 14), Z = 4	lattice constants			
	a / pm	b / pm	c / pm	β / grd
$Li_3Lu_5[SeO_3]_9$	1393.85(5)	1394.51(2)	1409.48(2)	113.006(1)

9.1.5 The alkali metal halide oxoselenate(IV) of trivalent lanthanide: $CsTmCl_2[SeO_3]$

$CsTmCl_2[SeO_3]$ crystal structure is characterized by layers parallel to (001) consisting of parallel zigzag strands $^{1}_{\infty}\{[TmO^{e}_{4/2}O^{t}_{1/1}Cl^{t}_{2/1}]^{5-}\}$ ($\equiv {}^{1}_{\infty}\{[TmO_3Cl_2]^{5-}\}$) with both chloride anions occupying apical positions in the pentagonal bipyramid $[TmO_5Cl_2]$. Four of the five equatorial oxygen atoms are utilized to share *trans*-edges, whereas one remains terminal and is syndiotactically ordered along the chain direction [010]. Within layers these different chains are held together by Se^{4+} cations via both an edge and a vertex of a trigonal $[SeO_3]^{2-}$ pyramid to $^{2}_{\infty}\{[TmCl_2(SeO_3)_{2/2}]\}^{-}$ layers. The Cs^{+} coordination sphere can be described as a (2+1)-capped trigonal prism with all three oxygen atoms in the triangular face of a single $[SeO_3]^{2-}$ anion. The crystal structure is strongly influenced by the stereochemical lone pair effect at the Se^{4+} cations reflected by the formation of discrete ψ^1-tetrahedral $[SeO_3E]^{2-}$ groups (E = non-binding electron pair).

monoclinic, $P2_1/n$ (No. 14), Z = 4	lattice constants			
	a / pm	b / pm	c / pm	β / grd
$CsTmCl_2[SeO_3]$	658.92(5)	689.26(6)	1752.5(1)	99.093(7)

9.1.6 The alkali metal oxide halide oxoselenate(IV) of trivalent lanthanide: $CsEu_4O_3Cl_3[SeO_3]_2$

In the triclinic caesium europium oxide oxoselenates(IV), the heavy alkaline cation have a coordination number of eight built up of chlorides in the shape of a square prism. The $[CsCl_8]$ polyhedron share two faces and one edge to $^{2}_{\infty}\{[(Cs)_{1/1}(Cl1,3)^{e}_{6/3}(Cl2)^{e}_{2/2}]\}^{2-}$ sheets in the (001) plane while the linkage of the $[OEu_4]$-tetrahedra occurs via four common edges to $^{2}_{\infty}\{[O_3Eu_4]\}^{6+}$ thick layers. The compound contains prismatic bipyramidal empty cavities built up of eight chlorides making a square prism capped by four caesium and two europium. All Eu^{3+} are not involved in the $^{2}_{\infty}\{[O_3Eu_4]\}^{6+}$ layers as in other oxyhalide oxoselenates(IV) synthesized in this work. The three-dimensional framework suggests itself by linkage of different layers over $[(Eu4)O_4Cl_4]$ polyhedron. The Eu^{3+} cations are eight- and ninefold coordinated in a shape of a square prisms, square antiprisms and capped square antiprisms.

triclinic, $P\bar{1}$ (No. 2), Z = 2	lattice constants					
	a / pm	b / pm	c / pm	α / grd	β / grd	γ / grd
$CsEu_4O_3Cl_3[SeO_3]_2$	545.09(2)	879.99(3)	1597.44(7)	81.036(2)	89.992(2)	71.926(2)

9.2 Outlook

The structure chemistry of the binary systems M_2O_3 – SeO_2 at under 800°C has been hardly investigated, leading us to two new structure types $M_2[SeO_3]_3$ and $M_2O[SeO_3]_2$. While the former could be obtained in large quantities for all rare-earth elements, the latter was gained only in small quantities from samarium to thulium. A method for the selective preparation of large quantities would therefore be desirable. Our main concern is the synthesis and structure analysis of a representative with the heaviest Yb and Lu on the one hand and with the light M (M = La – Nd) atoms on the other. Furhter investigations should be made in order to try to solve other formulas type such as single crystals of $M_2O_2[SeO_3]$ and $M_2Se_4O_{11}$ which were observed by means of phase diagrams but no crystallographic data are available hitherto. Possible physical or chemical properties of these compounds will be of interest to us in the near future.

Concerning oxyhalide oxoselenates(IV) of the trivalent lanthanides, they were almost unelucidated so far, hence their structural determinations presented in this dissertation could lay the first foundation in this field. Crystals being obtained in small quantity and for a limited number of rare-earth elements, the search for an effective method of synthesis leading to fill the gaps in the presumably different structure types and single crystals of high quality are to be taken into account in the future. Hydrothermal synthesis could be an alternative. If large single crystals are present, their characteristics could be determined by physical measurements.

The area of the mixed metals oxoselenates(IV) is not widely explored. However, little research has been carried out for mixed transition metal oxoselenates(IV). This is not true regarding compounds with both d- and f-elements or with alkali metal and f-elements. The combination of magnetic activities of d- and f-metals in the same oxoselenates(IV) compounds are of fundamental interest in solid-state chemistry and materials science, and are also potential for useful physical properties. To date very little is known about such materials, therefore experiments for the preparation of oxoselenates(IV) with both transition metals and lanthanoids should be given more attention.

10 Zusammenfassung und Ausblick

10.1 Ergebnisse

Die Zielsetzung der vorliegenden Arbeit war einerseits zu prüfen, in wie weit der Existenzbereich der Selten-Erd-Metall(III)-Oxoselenate(IV) $M_2[SeO_3]_3$ (M = Sc, Y, La; Ce – Lu) hin zu den kleineren und schwereren Lanthaniden erweitert werden kann und andererseits sollten basische Selten-Erd-Metall(III)-Oxoselenate(IV) mit O^{2-}-zentrierten $(M^{3+})_4$-Tetraedereinheiten synthetisiert und deren Existenzbereich bestimmt werden. Außerdem wurde der Einfluß von Halogenid-Anionen (Cl^- und Br^-) auf die Kristallstruktur der Lanthanid(III)-Oxid-Oxoselenate(IV) untersucht.

Der erste Teil konnte erfolgreich abgeschlossen werden. Es wurde gezeigt, dass bei entsprechenden Reaktionsbedingungen Oxoselenate(IV) vom Typ $M_2[SeO_3]_3$ (M = Sc, Y, La; Ce – Lu mit sämtlichen M^{3+}-Kationen erhalten werden können. Während $La_2[SeO_3]3$ und $Ce_2[SeO_3]_3$, $Pr_2[SeO_3]_3$ und $Nd_2[SeO_3]_3$ principiell die selbe Kristallstruktur ausbilden, liegt für $Sc_2[SeO_3]_3$ ein neuer Strukturtyp zugrunde. Die verbleibenden Selten-Erd-Elemente Y und Sm bis Lu bilden isostrukturelle $M_2[SeO_3]_3$-Phasen zum literaturbekannten $Er_2[SeO_3]_3$. Zusätzlich wurde bei Versuchen zur Darstellung von $Lu_2[SeO_3]_3$ ein neues Lithium-Selten-Erd-Metall(III)-Oxoselenat(IV) $Li_3Lu_5[SeO_3]_9$ synthetisiert und dessen Kristallstruktur aufgeklärt.

Der Existenzbereich der zweiten in dieser Arbeit aufgeführten Verbindungsklasse $M_2O[SeO_3]_2$ ist innerhalb der untersuchten Reaktionsbedingungen auf die Elemente M = Sm – Tm beschränkt. Deshalb sollten künftig noch weitere Darstellungsversuche bei verschiedenen Reaktionsbedingungen (Temperatur, Zusammensetzung der Eduktmischung, Flußmittel) eventuell sogar unter Hochdruck-Einfluß durchgeführt werden.

Vier neue Strukturtypen $M_3O_2Cl[SeO_3]_2$ (M = Tb, Dy, Er), $M_4O_3Cl_2[SeO_3]_2$ (M = Er, Yb), $M_5O_4X_3[SeO_3]_2$ (M = Gd, X = Br; Tb, X = Cl) und $M_9O_8X_3[SeO_3]_4$ (M = La, Pr mit X = Br und M = Nd, Sm, Gd mit X = Cl), die entweder nur mit den schwereren oder nur mit den leichteren Selten-Erd-Elementen vorkommen, wurden im Gebiet der Selten-Erd-Metall(III)-Oxid-Halogenid-Oxoselenate(IV) synthetisiert und charakterisiert. Der erste Verbindungstyp kristallisiert, trotz gleicher Summenformel, in Abhängigkeit vom M^{3+} Kationenradius der Selten-Erd-Elemente in zwei verschiedenen Kristallstrukturen, während die restlichen drei Verbindungstypen mit gleicher Summenformel auch gleiche Kristallstrukturen ausbilden. Die Existenzbereiche dieser vier Verbindungsklassen sind sehr klein, jedoch trugen auch

Änderungen innerhalb der Synthesebedingungen nur wenig zu deren Erweiterung bei. Allerdings sind noch viele Versuche zur Darstellung analoger Strukturen denkbar. Zusätzlich wurden im Rahmen dieser Dissertation zwei Caesiumhaltige Nebenprodukte, $CsTmCl_2[SeO_3]$ und $CsEu_4O_3Cl_3[SeO_3]$ entdeckt und strukturell charakterisiert. Die durchgeführten Untersuchungen an Selten-Erd-Metall(III)-Oxid-Halogenid-Oxoselenaten(IV) verifizieren die anfängliche Annahme, dass die Halogenid-Anionen X^- (X = Cl, Br) kristallographisch äquivalent sind und isotype Oxid-Halogenid-Oxoselenate der dreiwertigen Lanthanide ausbilden. Trotzdem sollten, um weitere Aussagen machen zu können, auch Versuche zur Darstellung ähnlicher Verbindungen mit den noch verbleibenden Halogeniden durchgeführt werden. Es wurde erst verhältnismäßig spät mit Arbeiten über die Selten-Erd-Metall(III)-Oxid-Halogenid-Oxoselenate(IV) begonnen, deshalb gehören die vorliegenden Experimente und Ergebnisse zu den ersten auf diesem Gebiet der Chemie.

10.1.1 Oxoselenate(IV) der dreiwertigen Selten-Erd-Elemente

10.1.1.1 Das hexagonale $Sc_2[SeO_3]_3$

Scandium-Oxoselenat(IV) $Sc_2[SeO_3]_3$ kristallisiert hexagonal in der Raumgruppe $P6_3/m$ mit nur einem kristallographisch nicht unterscheidbaren sechsfach koordinierten Sc^{3+}-Kation. Trigonale $[ScO_6]^{9-}$-Antiprismen verknüpfen über gemeinsame Flächen (O1,O1,O1) zu $[Sc_2O_9]^{12-}$-Doppeln, die über acht Ecken durch die isolierten ψ^1-tetraedrischen $[SeO_3]^{2-}$-Anionen zu einer dreidimensionalen Gerüststruktur verbunden sind. Die nicht-bindenden Elektronenpaare "lone-pair" der $[SeO_3]^{2-}$-Einheiten befinden sich in sechseckigen Kanälen, die parallel [001] verlaufen. Wird das komplexe $[SeO_3]^{2-}$-Anion durch ein kugelsymmetrisches, zweifach negativ geladenes Anion (Z^{2-}) ersetzt, so kann die Kristallstruktur von $Sc_2[SeO_3]_3$ (≡ Sc_2Z_3) als kationendefekte NiAs-Struktur, in der ein Drittel der kationischen Gitterplätze in geordneter Art und Weise unbesetzt bleiben, beschrieben werden.

hexagonal, $P6_3/m$ (No. 176), Z = 2	Gitterkonstanten		
	a / pm	c / pm	c/a
$Sc_2[SeO_3]_3$	814,28(5)	764,56(4)	0,939

10.1.1.2 Das orthorhombische $Ce_2[SeO_3]_3$

Die Kristallstruktur von $Ce_2[SeO_3]_3$ im $La_2[SeO_3]_3$-Typ enthält ein kristallographisch nicht unterscheidbares Ce^{3+}-Kation und zwei kristallographisch unterschiedliche $[SeO_3]^{2-}$-Einheiten. Vier O^{2-}-Anionen von vier monodental koordinierenden und sechs Sauerstoff-Teilchen von drei bidentalen, chelatartig angreifenden $[SeO_3]^{2-}$-Baueinheiten bilden mit einer Koordinationszahl von zehn die anionische Umgebung der Ce^{3+}-Kationen. Durch Verknüpfung der $[CeO_{10}]$-Polyeder über Dreiecksflächen (O1,O2,O3) und Kanten (O3 – O4) bilden sich Schichten, die senkrecht zu [001] angeordnet sind. Die $[(Se1)O_3]^{2-}$-Anionen sind am Aufbau dieser Schichten beteiligt, während die $[(Se2)O_3]^{2-}$-Einheiten die Struktur dreidimensional verknüpfen. Ein Blick entlang [010] auf die Kristallstruktur von $Ce_2[SeO_3]_3$ zeigt unendliche Kanäle von ungefähr 354 pm (2×), 431 pm (2×) und 558 pm (2×) Ausdehnung, in denen genügend Platz zur Aufnahme der nicht-bindenden Elektronenpaare an den $[SeO_3]^{2-}$-Gruppen bleibt.

orthorhombisch, Pnma (No. 62), Z = 4	Gitterkonstanten		
	a / pm	b / pm	c / pm
$Ce_2[SeO_3]_3$	839,23(3)	1421,12(4)	704,58(2)

10.1.1.3 Das monokline $Pr_2[SeO_3]_3$

Im monoklinen $Pr_2[SeO_3]_3$ ($Nd_2[SeO_3]_3$-Typ) werden sechs kristallographisch unterschiedliche Selten-Erd-Kationen beobachtet. Sie besetzen alle die gleiche *Wyckoff-Lage* und sind von neun bzw. zehn Sauerstoffatomen in unterschiedlichen Koordinationsfiguren umgeben. Alle Koordinationspolyeder weichen deutlich von ihrer Idealform ab. Die Kristallstruktur kann durch Schichten aus $[PrO_9]$- und $[PrO_{10}]$-Polyedern, die entweder über Flächen oder Kanten verknüpft sind, beschrieben werden. Dies führt zu viereckigen Kanälen, die entlang [101] verlaufen. Die $[(Se5)O_3]^{2-}$-, $[(Se7)O_3]^{2-}$- und $[(Se9)O_3]^{2-}$-Einheiten befinden sich zwischen dies Schichten. Sie dienen zur Ausbildung einer dreidimensionalen Gerüststruktur und geben somit der Verbindung Stabilität. Die verbleibenden sechs $[SeO_3]^{2-}$-Einheiten liegen fast vollständig innerhalb der Schichten vor, so dass ihr freies Elektronenpaar in Richtung Kanal angeordnet ist.

monoklin, $P2_1/n$ (No. 14), Z = 12	Gitterkonstanten			
	a / pm	b / pm	c / pm	β / grd
$Pr_2[SeO_3]_3$	1683,36(2)	705,06(1)	2166,37(3)	102,061(1)

10.1.1.4 Das trikline $M_2[SeO_3]_3$ (M = Y, Sm – Lu)

Während die Oxoselenate(IV) der leichteren Selten-Erd-Elemente in zwei unterschiedlichen Kristallsystemen kristallisieren, orthorhombisch (M = La, Ce) und monoklin (M = Pr, Nd), bilden sie sowohl mit den kleineren Lanthanoiden als auch mit Yttrium den selben Strukturtyp aus und kristallisieren wie das literaturbekannte $Er_2[SeO_3]_3$. Es wurde also gezeigt, dass Verbindungen des Formeltyps $M_2[SeO_3]_3$ für *alle* Selten-Erd-Elemente (außer Promethium) existieren. Die beiden kristallographisch unterschiedlichen M^{3+}-Kationen weisen Koordinationszahlen von sieben und acht auf, was einerseits pentagonal bipyramidale Koordinationsfiguren und andererseits stark verzerrte Koordinationsplyeder ergibt. Für die großen Sm^{3+}-Kationen erhöhen sich die Koordinationszahlen auf acht und neun. Durch Verknüpfung der M^{3+}-Polyeder mit den $[SeO_3]^{2-}$-Einheiten bilden sich im Falle von $Sm_2[SeO_3]_3$ parallel [011] und für M = Y und Eu – Lu parallel $[01\bar{1}]$ rechteckige Kanäle aus. Diese bieten ausreichend Platz für die einsamen Elektronenpaare am Selenatom.

$M_2[SeO_3]_3$	Gitterkonstanten					
triklin, $P\bar{1}$ (No. 2), $Z = 2$	a / pm	b / pm	c / pm	α / grd	β / grd	γ / grd
$Y_2[SeO_3]_3$	699,34(5)	802,48(6)	898,82(8)	71,332(3)	69,916(3)	65,770(4)
$Sm_2[SeO_3]_3$	698,60(1)	789,60(2)	910,34(2)	96,693(1)	104,639(1)	115,867(1)
$Eu_2[SeO_3]_3$	712,64(4)	812,85(4)	911,52(6)	71,372(2)	70,075(2)	65,652(2)
$Gd_2[SeO_3]_3$	710,52(5)	810,87(7)	906,73(8)	71,364(4)	70,168(4)	65,747(4)
$Tb_2[SeO_3]_3$	706,20(3)	806,29(4)	904,06(5)	71,476(2)	70,084(2)	65,896(2)
$Dy_2[SeO_3]_3$	703,08(1)	804,10(2)	900,96(2)	71,383(1)	70,095(1)	65,903(1)
$Ho_2[SeO_3]_3$	700,79(3)	802,04(4)	897,69(4)	71,370(2)	70,098(2)	65,935(2)
[a] *$Er_2[SeO_3]_3$*	*698,2(1)*	*800,6(1)*	*895,0(1)*	*71,38(1)*	*70,13(1)*	*65,87(1)*
$Tm_2[SeO_3]_3$	694,61(3)	796,58(4)	891,96(5)	71,480(2)	70,223(2)	65.964(2)
$Yb_2[SeO_3]_3$	691,79(1)	793,93(1)	890,01(2)	71,455(1)	70,293(1)	65,038(1)
$Lu_2[SeO_3]_3$	690,22(2)	793,41(2)	887,26(2)	71,413(1)	70,235(1)	65,985(1)

[a] *Daten von wickleder et al. [19]*

10.1.2 Oxid-Oxoselenate(IV) der dreiwertigen Selten-Erd-Elemente: $M_2O[SeO_3]_2$ (M = Sm – Lu)

Die Oxid-Oxoselenate(IV) in diesem Strukturtyp ($M_2O[SeO_3]_2$) sind nur schwer in großer Ausbeute zu erhalten und konnten nur für die kleineren Lanthanoide erfolgreich nachgewiesen werden. In der tetragonalen Kristallstruktur für den Formeltyp $M_2O[SeO_3]_2$ (M = Sm – Lu) sind die M^{3+}-Kationen quadratisch antiprismatisch von acht Sauerstoffatomen umgeben, von denen sechs zu sechs verschiedenen, isolierten, ψ^1-tetraedrischen $[SeO_3]^{2-}$-Einheiten gehören, während die verbleibenden zwei *nicht* an Selen gebunden sind. Deren koordinativ wirksame Umgebung besteht aus vier tetraedrisch angeordneten M^{3+}-Kationen. Die $[OM_4]^{10+}$-Tetraeder verknüpfen über *trans*-ständige Kanten zu eindimensionalen $^1_\infty\{[OM_{4/2}]^{4+}\}$-Ketten. Diese sind so gepackt, dass ein Zentralstrang in der Projektionsebene (001) von vier benachbarten quadratisch in einem Abstand von $a/\sqrt{2}$ umgeben ist. Das Packungsmotiv wird durch ein weiteres Quadrat aus vier Strängen mit Abstand $\sqrt{2}$ (≡ Betrag von a), das im Vergleich zum Ersten um 45° gedreht vorliegt, vervollständigt. Ladungsausgleich und dreidimensionale Verknüpfung dieser besonderen Stabpackung erfolgt

durch diskrete trigonale $[SeO_3]^{2-}$-Pyramiden, so dass die Struktur stark durch die stereochemisch aktiven "lone-pairs" dieser Gruppen beeinflußt wird. Um so bemerkenswerter ist es, dass sich die $\bar{4}$-Symmetrie der $^{1}_{\infty}\{[OM_{4/2}]^{4+}\}$-Ketten bei den "lone-pair"-Kanälen, die sich aus den nicht-bindenden Elektronenpaaren der Se^{4+}-Kationen bilden, exakt wiederholt.

$M_2O[SeO_3]_2$	Gitterkonstanten		
tetragonal, $P4_2/ncm$ (No. 138), Z = 4	a / pm	c / pm	c/a
$Sm_2O[SeO_3]_2$	1075,07(9)	526,35(5)	0,490
$Eu_2O[SeO_3]_2$	1074,05(7)	525,77(3)	0,490
$Gd_2O[SeO_3]_2$	1068,73(6)	525,03(2)	0,491
$Tb_2O[SeO_3]_2$	1064,57(8)	521,56(4)	0,490
$Dy_2O[SeO_3]_2$	1060,07(4)	520,00(2)	0,490
$Ho_2O[SeO_3]_2$	1055,70(3)	518,80(1)	0,491
$Er_2O[SeO_3]_2$	1052,20(6)	517,35(2)	0,491
$Tm_2O[SeO_3]_2$	1048,87(5)	514,25(4)	0,490

10.1.3 Oxidhalogenid-Oxoselenate(IV) der dreiwertigen Selten-Erd-Elemente

10.1.3.1 Verbindungen des Formeltyps $M_3O_2Cl[SeO_3]_2$ (M = Tb, Dy, Er)

Im Verlauf dieser Arbeit konnten von den Selten-Erd-Metall(III)-Oxidchlorid-Oxoselenaten(IV) der Summenformel $M_3O_2Cl[SeO_3]_2$ zwei unterschiedliche Strukturtypen $M_3O_2Cl[SeO_3]_2$ (orthorhombisch, Pnma; M = Tb, Dy) und $Er_3O_2Cl[SeO_3]_2$ (monoklin, C2/c) synthetisiert werden. Beide enthalten $[OM_4]^{10+}$-Tetraeder, die über gemeinsame Ecken zu Doppelketten $^{1}_{\infty}\{[(M1)_{3/3}(M2)_{2/1}O_{4/2}]^{5+}\}$ ($\equiv$ $^{1}_{\infty}\{[O_2M_3]^{5+}\}$) verbunden sind. Diese Stränge ordnen sich so an, daß in der Projektionsebene (100) für M = Tb, Dy bzw. (001) für M = Er ein Zentralstrang äquidistant von vier weiteren in Form eines Quadrats umgeben ist. Die weitere Verknüpfung der Stränge erfolgt durch $[SeO_3]^{2-}$-Pyramiden. Dies führt zu hexagonalen Kanälen zwischen jeweils vier kationischen Ketten. Beim Blick auf die (010)-Ebene unterscheiden sich die beiden Strukturen lediglich durch die Stapelungsreihenfolge.

Während in den orthorhombisch kristallisierenden Verbindungen aufeinanderfolgende Stränge deckungsgleich gestapelt sind, verschieben sich die entsprechenden Doppelketen in $Er_3O_2Cl[SeO_3]_2$ entlang [001] gegeneinander. Die $(M1)^{3+}$-(M = Tb, Dy) und $(Er1)^{3+}$-Kationen sind achtfach in Form eines zweifach überkappten trigonalen Prismas koordiniert, wohingegen $(M2)^{3+}$ (M = Tb, Dy) mit einer Koordinationszahl von acht ein quadratisches Prisma als Koordinationfigur aufweist, während $(Er2)^{3+}$ nur eine Koordinationszahl von sieben zukommt.

$M_3O_2Cl[SeO_3]_2$			$Er_3O_2Cl[SeO_3]_2$
orthorhombisch, Pnma (No. 62), Z = 4			monoklin, C2/c (No. 15), Z = 4
	Tb	Dy	a = 1498,23(6) pm
a / pm	535,16(4)	533,81(2)	b = 1102,03(5) pm
b / pm	1530,51(9)	1521,04(7)	c = 547,95(3) pm
c / pm	1081,72(7)	1076,56(4)	β = 105,515 °

10.1.3.2 Verbindungen des Formeltyps $M_4O_3Cl_2[SeO_3]_2$ (M = Er, Yb)

Die trikline Kristallstruktur für den Formeltyp $M_4O_3Cl_2[SeO_3]_2$ basiert auf parallel zu (011) liegenden, zweidimensionalen $^{2}_{\infty}\{([O_3M_4]^{6+})_2\}$-Schichten. Diese sind aus $[O_6M_{12}]^{24+}$-Einheiten aufgebaut, die ihrerseits aus kantenverknüpften, sauerstoffzentrierten $(M^{3+})_4$-Tetraedern entstehen. Der Zusammenschluß zu Schichten erfolgt durch eine Verkettung der $[O_6M_{12}]^{24+}$-Gruppen über *trans*-ständige Kanten und vier Ecken. Jedes $[OM_4]^{10+}$-Tetraeder teilt so innerhalb der Schichten entweder *zwei* Kanten und *eine* Ecke oder *drei* Kanten und *eine* Ecke mit seinen Nachbarn. Zwischen den Schichten befinden sich die Chlorid-Anionen, die zur Ausbildung eines dreidimensionalen Netzwerkes dienen. Durch die einsamen Elektronenpaare der Cl^{-}-Anionen und pyramidalen der $[SeO_3]^{2-}$-Baueinheiten die zwischen den Schichten wechselwirken, zeigen diese Verbindungen ein einzigartiges Bindungsschema. Die sechs kristallographisch unterschiedlichen M^{3+}-Kationen sind verzerrt quadratisch-antiprismatisch oder -prismatisch bzw. einfach-überkappt trigonal-prismatisch von Sauerstoff und Chlor umgeben.

$M_4O_3Cl_2[SeO_3]_2$	Gitterkonstanten					
triklin, $P\bar{1}$ (No. 2), $Z = 2$	a / pm	b / pm	c / pm	α / grd	β / grd	γ / grd
$Er_4O_3Cl_2[SeO_3]_2$	861,64(2)	1170,56(3)	1208,42(3)	67,666(1)	77,833(1)	85,270(1)
$Yb_4O_3Cl_2[SeO_3]_2$	853,88(1)	1145,90(2)	1195,47(2)	68,132(1)	78,113(1)	85,747(1)

10.1.3.3 Die Kristallstrukturen von $Gd_5O_4Br_3[SeO_3]_2$ und $Tb_5O_4Cl_3[SeO_3]_2$

$Gd_5O_4Br_3[SeO_3]_2$ und $Tb_5O_4Cl_3[SeO_3]_2$ kristallisieren im gleichen Strukturtyp. Die drei kristallographisch unterschiedlichen M^{3+}-Kationen sind sieben- bzw. achtfach von O^{2-}- und X^--Anionen umgeben. Parallel (001) liegende Schichten aus gewellten $^2_\infty\{[O_4M_5]^{7+}\}$-Metall-Sauerstoff-Ebenen, die aus kanten- und eckenverknüpften $[OM_4]^{10+}$-Tetraedern aufgebaut sind, erzeugen diese Kristallstruktur. Solche Schichten sind von ψ^1-tetraedrischen $[SeO_3]^{2-}$-Einheiten und Halogenid-Anionen, die sowohl zur dreidimensionalen Verknüpfung als auch zum Ladungsausgleich dienen, im Verhältnis 2:3 eingerahmt. Die Struktur ist eng mit den "lone-pair"-Kanalstrukturen der Formeltypen $M_2O[SeO_3]_2$ und $M_3O_2Cl[SeO_3]_2$ verwandt, in denen Einzel- ($^1_\infty\{[OM_2]^{4+}\}$) und Doppelketten ($^1_\infty\{[O_2M_3]^{5+}\}$) aus *trans*-kantenverknüpften $[OM_4]^{10+}$-Tetraedern vorherrschen. Als eine Art Erweiterung dieses Verknüpfungstyps sind die Doppel-Ketten ($^1_\infty\{[O_2M_3]^{5+}\}$) aus der Kristallstruktur von $M_3O_2Cl[SeO_3]_2$ über gemeinsame Ecken zu den oben erwähnten $^2_\infty\{[O_4M_5]^{7+}\}$-Schichten weiter verbunden.

$M_5O_4X_3[SeO_3]_2$	Gitterkonstanten			
monoklin, C2/m (No. 12), $Z = 2$	a / pm	b / pm	c / pm	β / grd
$Gd_5O_4Br_3[SeO_3]_2$	1243,70(9)	549,91(4)	1005,29(8)	91,869(7)
$Tb_5O_4Cl_3[SeO_3]_2$	1229,13(4)	546,17(4)	978,79(7)	90,485(6)

10.1.3.4 Die Kristallstrukturen von $M_9O_8Br_3[SeO_3]_4$ (M = La, Pr) und $M_9O_8Cl_3[SeO_3]_4$ (M = Pr, Nd, Sm, Gd)

Diese neue Verbindungsklasse enthält ein Netzwerk aus kantenverknüpften $[OM_4]^{10+}$-Tetraedern, die parallel zu (001) zweidimensionale, kationische Schichten der Zusammensetzung $^{2}_{\infty}\{[O_8M_9]^{11+}\}$ ausbilden. Wie schon in den Kristallstrukturen von $M_4O_3Cl_2[SeO_3]_2$ und $M_5O_4X_3[SeO_3]_2$ mit $^{2}_{\infty}\{([O_3M_4]^{6+})_2\}$- bzw. $^{2}_{\infty}\{[O_4M_5]^{7+}\}$-Schichten, sind zwischen die Schichten ψ^1-tetraedrische $[SeO_3]^{2-}$-Einheiten und Halogenid-Anionen eingeschoben, wodurch eine dreidimensionale Vernetzung der Struktur erreicht wird. Die Selenatome und ihre gegenüberliegenden Halogenid-Anionen sind durch beträchtliche Abstände voneinander getrennt. Es entstehen dadurch hinreichend große Lücken, um die freien, *nicht*-bindenden Elektronenpaare ("*lone pairs*") der Se^{4+}-Kationen unterschiedlicher Schichten aufzunehmen. Innerhalb der $^{2}_{\infty}\{[O_8M_9]^{11+}\}$-Ebenen teilt eines von vier $[OM_4]^{10+}$-Tetraedern vier Kanten mit seinen Nachbarn, während die anderen drei nur jeweils über drei Kanten kondensiert sind. Die Kristallstruktur enthält fünf kristallographisch unterschiedliche M^{3+}-Kationen, von denen $(M1)^{3+}$ und $(M2)^{3+}$ quadratisch-prismatisch von acht Sauerstoffatomen koordiniert werden, während sich $(M3)^{3+}$ und $(M4)^{3+}$ quadratisch-antiprismatisch mit Sauerstoff und Halogen umgeben. Die Koordinationsumgebung von $(M5)^{3+}$ kann schließlich als einfach überkapptes quadratisches Prisma (CN = 9) beschrieben werden.

$M_9O_8X_3[SeO_3]_4$	Gitterkonstanten					
triklin, $P\bar{1}$ (No. 2), Z = 1	a / pm	b / pm	c / pm	α / grd	β / grd	γ / grd
$La_9O_8Br_3[SeO_3]_4$	711,72(3)	919,56(4)	996,58(5)	99,856(2)	94,938(2)	95,840(2)
$Pr_9O_8Br_3[SeO_3]_4$	700,35(4)	906,09(6)	985,91(7)	99,623(3)	95,076(3)	95,874(3)
$Pr_9O_8Cl_3[SeO_3]_4$	700,12(1)	901,63(2)	966,88(2)	99,787(1)	94,979(1)	95,901(1)
$Nd_9O_8Cl_3[SeO_3]_4$	696,30(2)	896,80(3)	963,87(3)	99,528(2)	95,176(2)	95,893(2)
$Sm_9O_8Cl_3[SeO_3]_4$	688,70(1)	888,79(2)	959,09(2)	98,674(1)	95,419(1)	96,031(1)
$Gd_9O_8Cl_3[SeO_3]_4$	680,17(5)	882,86(7)	960,18(8)	97,241(6)	95,539(6)	96,265(6)

10.1.4 Alkalimetall-Oxoselenate(IV) der dreiwertigen Selten-Erd-Element: $Li_3Lu_5[SeO_3]_9$

Beim Versuch zur Darstellung von $Lu_2[SeO_3]_3$ entstand gelegentlich $Li_3Lu_5[SeO_3]_9$ durch Reaktion der Edukte mit dem als Flussmittel beigemengten LiBr. Die Kristallstruktur kann als Ansammlung isolierter $[(Li1)_2O_8]^{14-}$-, $[(Li2)_2O_8]^{14-}$-, $[(Li3)O_6]^{11-}$-Anionen zwischen denen $[SeO_3]^{2-}$-Einheiten und Lu^{3+}-Kationen eingelagert sind, beschrieben werden. Laut Literatur scheint die trigonal-antiprismatische Umgebung für $(Li3)^+$ eine Neuheit auf dem Gebiet der Lithium-Oxochemie zu sein. Die kleinen Lu^{3+}-Kationen sind entweder achtfach in Form von verzerrten quadratischen Prismen oder Antiprismen bzw. siebenfach als einfach überkappte trigonale Prismen koordiniert. Die Koordinationsfigur um Selen entspricht der klassischen, einseitig pyramidalen $[SeO_3]^{2-}$-Einheit, in der die vierte Ecke eines ψ^1-Tetraeders durch das freie Elektronenpaar des Se^{4+}-Kations besetzt ist.

monoklin, $P2_1/n$ (No. 14), Z = 4	Gitterkonstanten			
	a / pm	b / pm	c / pm	β / grd
$Li_3Lu_5[SeO_3]_9$	1393,85(5)	1394,51(2)	1409,48(2)	113,006(1)

10.1.5 Alkalimetall-Halogenid-Oxoselenate(IV) der dreiwertigen Selten-Erd-Element: $CsTmCl_2[SeO_3]$

Die Kristallstruktur von $CsTmCl_2[SeO_3]$, die der Verwendung von CsCl als flussmittel ihren Ursprung verdankt, wird durch parallel zu (001) liegende Schichten aufgebaut. Diese bestehen aus gleichgerichteten "Zick-Zack"-Ketten $^1_\infty\{[TmO_{4/2}O_{1/1}Cl_{2/1}]^{5-}\}$ Strängen (≡ $^1_\infty\{[TmO_3Cl_2]^{5-}\}$), in denen die apikalen Positionen der pentagonalen Bipyramiden $[TmO_5Cl_2]$ durch die beiden Cl^--Anionen besetzt sind. Vier der fünf äquatorialen Sauerstoffatome tragen zur *trans*-Kantenverknüpfung der Polyeder bei, während ein terminales syndiotaktisch entlang der Kettenfortpflanzungsrichtung [010] angeordnet ist. Innerhalb der Schichten werden je zwei Stränge durch Se^{4+}-Kationen, sowohl über eine Kante als auch über eine Ecke der trigonalen $[SeO_3]^{2-}$-Pyramide zu $^2_\infty\{[TmCl_2(SeO_3)_{2/2}]^-\}$-Schichten verbunden. Die Koordinationsfigur um Cs^+ kann als (2+*1*)-fach überkapptes trigonales Prisma betrachtet werden, in dem drei Sauerstoffatome einer Ebene die Dreiecksgrundfläche eines

einzelnen $[SeO_3]^{2-}$-Anions bilden. Der stereochemisch wirksame "lone-pair"-Effekt am Se^{4+}-Kation beeinflußt die Kristallstruktur maßgeblich, was sich durch die Ausbildung diskreter ψ^1-tetraedrischer $[SeO_3E]^{2-}$-Einheiten (*E* = *nicht*-bindendes Elektronenpaar) wieder spiegelt.

monoklin, $P2_1/n$ (No. 14), Z = 4	Gitterkonstanten			
	a / pm	b / pm	c / pm	β / grd
$CsTmCl_2[SeO_3]$	658,92(5)	689,26(6)	1752,5(1)	99,093(7)

10.1.6 Alkalimetall-Oxidhalogenid-Oxoselenate(IV) der dreiwertigen Selten-Erd-Element: $CsEu_4O_3Cl_3[SeO_3]_2$

Im triklin kristallisierenden Cäsium-Europium(III)-Oxidchlorid-Oxoselenat(IV) bilden acht Chlorid-Anionen in Form eines quadratischen Prismas die Koordinationsumgebung der schweren Alkalimetall-Kationen. Die $[CsCl_8]$-Polyeder teilen sich jeweils zwei Flächen und eine Kante, was zu in der (001)-Ebene liegenden $^2_\infty\{[(Cs)_{1/1}(Cl1,3)_{6/3}(Cl2)_{2/2}]\}^{2-}$-Schichten führt, während die $[OEu_4]^{10+}$-Tetraeder durch Verknüpfung über gemeinsame Kanten "dicke" $^2_\infty\{[O_3Eu_4]\}^{6+}$-Schichten bilden. Die Verbindung enthält leere, doppelt-überkappt Kuboktaedrische Hohlräume, die aus acht Chlorid-Anionen in Form eines quadratischen Prismas (Würfels), das durch vier Cäsium- und zwei Europium-Kationen überkappt ist, aufgebaut werden. Anders as in allen anderen Oxidhalogenid-Oxoselenaten(IV) sind nicht alle M-Kationen direkt am Aufbau der $^2_\infty\{[O_3Eu_4]\}^{6+}$-Schichten beteiligt. Die Verknüpfung der unterschiedlichen Schichten durch $[(Eu4)O_4Cl_4]$ Polyeder ergibt schließlich ein dreidimensionales Netzwerk. Die vier kristallographisch unterschiedlichen Eu^{3+}-Kationen sind quadratisch-antiprismatisch oder -prismatisch bzw. verzerrt einfach-überkappt quadratisch-prismatisch von Sauerstoff und Chlor umgeben.

triklin, $P\bar{1}$ (No. 2), Z = 2	Gitterkonstanten					
	a / pm	b / pm	c / pm	α / grd	β / grd	γ / grd
$CsEu_4O_3Cl_3[SeO_3]_2$	545,09(2)	879,99(3)	1597,44(7)	81,036(2)	89,992(2)	71,926(2)

10.2 Ausblick

Die Strukturchemie der binären Systeme M_2O_3 – SeO_2 (M = Sc, Y, La; Ce – Lu) wurde bei Temperaturen unterhalb 800°C genauestens untersucht. Dies führte zu zwei neuen Strukturtypen für die Zusammensetzungen $M_2[SeO_3]_3$ und $M_2O[SeO_3]_2$. Während Vertreter des ersten für alle Selten-Erd-Elemente (außer Promethium) in großer Ausbeute erhalten werden konnten, fielen beim zweiten nur Verbindungen Samarium bis Thulium in geringen Mengen an. Deshalb wäre die Entwicklung einer gezielten Darstellungsmethode für große Substanzmengen dieser Verbindungen wünschenswert. Das Hauptaugenmerk sollte jedoch auf die Synthese und Strukturbestimmung eines Stellvertreters der kleinen Kationen Yb^{3+} bzw. Lu^{3+} einerseits und der großen M^{3+}-Kationen (M = La – Nd) andererseits, gelegt werden. Weitere Untersuchungen zur Aufklärung der Strukturen von $M_2O_2[SeO_3]$-und $M_2Se_4O_{11}$-Phasen anhand von Einkristalldaten sind notwendig. Diese konnten mit Hilfe von Phasendiagrammen zwar beobachtet werden, aber es sind bisher noch keine kristallographischen Daten zugänglich. Im nächster Zeit werden auch physikalische und chemische Eigenschaften dieser Verbindungen wichtig sein.

Die Oxidhalogenid-Oxoselenate(IV) der dreiwertigen Selten-Erd-Elemente waren bis jetzt fast vollständig unerforscht. Daher bildet die in dieser Arbeit vorgelegte sammlung an Kristallstrukturaufkärungen den Grundstock für weitere Arbeiten auf diesem Gebiet. Kristalle wurden oft nur in geringer Ausbeute und für eine beschränkte Anzahl an Selten-Erd-Elementen gefunden. Die Suche nach effektiven Synthesemethoden, die zur Auffüllung der Lücken innerhalb der vermutlich unterschiedlichen Strukturtypen und hoher Einkristallausbeute führt, sollte fortgesetzt werden. Hydrothermalsynthesen könnten hierbei eine gute Alternative bieten. Sollten auf diese Weise sehr große Kristalle entstehen, könnten auch deren physikalische Eigenschaften gemessen werden.

Das Gebiet der gemischt-metallischen Oxoselenate(IV) ist noch längst nicht ausreichend erforscht. Jedoch sind einige Arbeiten über gemischte Übergangsmetall-Oxoselenate(IV) bekannt, diese spiegeln aber nicht die Gegebenheiten für Verbindungen mit Mischungen aus d- und f-Elementen bzw. Alkalimetallen und f-Elementen wider. Gerade die Kombination der magnetischen Eigenschaften von d- und f-Metallen in den selben Oxoselenaten(IV) sind innerhalb der Festkörperchemie und Materialwissenschaft sicher von großem Interesse. Außerdem verfügen sie über ein großes Potential an nützlichen physikalischen Anwendungsmöglichkeiten. Bis heute ist nur wenig über solche Materialien bekannt, deshalb finden Experimente mit Oxoselenaten(IV), die sowohl Übergangsmetalle als auch Lanthanoide enthalten, immer mehr Beachtung.

11 References

[1] J. J. Berzelius: *Acad. Handl. Stockholm* **39** (1818) 13.

[2] L. Niinistö, M. Leskela: *Handbook on the Physics and Chemistry of Rare Earths*, (K. A. Gschneidner, Jr. and L. Eyring, Eds.), *Elsevier*, Amsterdam/New York, 1987, pp. 91 – 320.

[3] E. Giesbrecht, G. Vicentini, L. Barbieri: *An. Acad. Bras. Cienc*. **40** (1968) 453.

[4] G. S. Savchenko, I. V. Tananaev, A. N. Volodina: *Inorg. Mater*. **4** (1968) 965.

[5] E. Immonen, M. Koskenlina, L. Niinisto, T. Pakkanen: *Finn. Chem. Lett*. **3** (1976) 67.

[6] M. de Pedro, R. Enjalbert, A. Castro, J. C. Trombe, J. Galy: *J. Solid State Chem*. **108** (1994) 87.

[7] M. Koskenlina, J. Valkonen: *Acta Chem. Scand*. **A 31** (1977) 457.

[8] L. D. Iskhakova, S. M. Ovanisyan, V. K. Trunov: *Zh. Strukt. Khim*. **32** (1991) 30.

[9] R. Morris, W. T. A. Harrison, G. D. Stucky, A. K. Cheethan: *Acta Crystallogr*. **C 48** (1992) 1182.

[10] A. Castro, R. Enjalbert, M. de Pedro, J. C. Trombe: *J. Solid State Chem*. **112** (1994) 418.

[11] M. Koskenlina, I. Mutikainen, M. Leskelä, L. Niinisto: *Acta Crystallogr*. **C 50** (1994) 1384.

[12] W. T. A. Harrison, Z. Zhang: *Eur. J. Solid State Inorg. Chem*. **34** (1997) 599.

[13] M. Stancheva, R. Petrova: J. Macicek, *Acta Crystallogr*. **C 54** (1998) 699.

[14] J. Valkonen: *Acta Crystallogr*. **B 34** (1978) 3064.

[15] J. Valkonen, M. Leskelä: *Acta Crystallogr*. **B 34** (1978) 1957.

[16] M. S. Wickleder: *Z. Anorg. Allg. Chem*. **626** (2000) 547.

[17] W. T. A. Harrison: *Acta Crystallogr*. **C 56** (2000) 627.

[18] I. Krügermann, M. S Wickleder: *Z. Anorg. Allg. Chem*. **628** (2002) 2197.

[19] I. Krügermann, M. S Wickleder: *J. Solid State Chem*. **167** (2002) 113.
I. Krügermann: *Dissertation*, Univ. Köln (2002).

[20] M. Zhang-Preße: *Dissertation*, Univ. Dresden (2001).

[21] H. Oppermann, M. Zhang-Preße, P. Schmidt: *Z. Naturforsch*. **57 b** (2002) 868.

[22] M. Zhang-Preße, H. Oppermann: *Z. Naturforsch*. **57 b** (2002) 621.

[23] H. Oppermann, M. Zhang-Preße, St. Weck, S. Liebig: *Z. Anorg. Allg. Chem*. **628** (2002) 81.

[24] H. Oppermann, M. Zhang-Preße: *Z. Naturforsch*. **56 b** (2001) 917.

[25] G. G. Gospodinov, M. G. Stancheva: *J. Therm. Anal.* **67** (2002) 643.

[26] G. G. Gospodinov, M. G. Stancheva: *Monatsh. Chem.* **132** (2001) 1036.

[27] G. G. Gospodinov, M. G. Stancheva: *Monatsh. Chem* **130** (1999) 725.

[28] G. G. Gospodinov, M. G. Stancheva: *J. Therm. Anal.* **Vol. 48** (1997) 1351.

[29] M. de Pedro, I. Rasines, A. Castro: *J. Mat. Sci. Lett*. **12** (1993) 1637.

[30] M. de Pedro, J. C. Trombe, A. Castro: *J. Mat. Sci. Lett*. **14** (1995) 994.

[31] G. Giester: *Z. Kristallogr*. **211** (1996) 603.

[32] P. G. Jones, G. M. Sheldrick, E. Schwarzmann, A. Vielmäder: *Z. Naturforsch*. **38 b** (1983) 10.

[33] F. A. Weber, Th. Schleid: *Z. Anorg. Allg. Chem.* **626** (2000) 1285.

[34] M. S. Wickleder, I. Göhausen: *Z. Anorg. Allg. Chem*. **626** (2000) 1725.

[35] P. S. Berdonosov, S. Yu. Stefanovitch V. A. Dolgikh: *J. Solid State Chem*. **149** (2000) 236.

[36] M. S. Wickleder: *Z. Naturforsch*. **57 b** (2002) 1414.

[37] H. Oppermann, H. Dao Quoc, M. Zhang-Preße, P. Schmidt, B. A. Popovkin, P. S. Berdonosov, V. A. Dolgikh: *Z. Anorg. Allg. Chem*. **628** (2002) 891.

[38] S. V. Krivovichev, S. K. Filatov, T. F. Semenova, I. V. Rozhdestvenskaya: *Z. Kristallogr*. **213** (1998) 645.

[39] S. V. Krinovichev, R. R. Shuvalov, T. F. Semenova, S. K. Filatov: *Z. Kristallogr*. **214** (1999) 135.

[40] J. Reim, K. Griesar, W. Haase, B. Krebs: *J. Chem. Soc. Dalton Trans*. **1995** (1995) 2649.

[41] D. P. Goldberg, A. Caneschi, C. D. Delfs, R. Sessoli, S. J. Lippard: *J. Amer. Chem. Soc*. **117** (1995) 5789.

[42] H. Effenberger: *J. Solid State Chem*. **70** (1987) 303.

[43] H. Effenberger: *J. Solid State Chem*. **73** (1988) 118.

[44] H. Effenberger: *Acta Crystallogr*. **C 44** (1988) 800.

[45] H. Effenberger: *Acta Chem. Scand*. **50** (1996) 967.

[46] R. E. Morris, J. A. Hriljac, A. K. Cheetham: *Acta Crystallogr*. **C 46** (1990) 2013.

[47] W. T. A. Harrison, Z. Zhang: *J. Solid State Chem*. **133** (1997) 572.

[48] M. S. Wickleder: unpublished work.

[49] P. S. Halasyamani, K. R. Poeppelmeier: *Chem. Mater*. **10** (1998) 2753.

[50] I. -C. Khoo, F. Simoni, C. Umeton: In *Novel Optical Materials and Applications*, Eds;

John Wiley & Sons: New York (1997), pp. 175 – 204.

[51] S. R. Marder, J. E. Sohn, G. D. Stucky: In *Materials for Nonlinear Optics*, Eds; ACS Symposium **Ser. 455**, *Am. Chem. Soc*: Washington, DC (1991), pp. 2 – 30.

[52] W. Herrendorf: *Programm HABITUS*, Gießen (1995).

[53] Fa. Stoe & Cie GmbH: *Programm X.SHAPE, Version 1.06*, Darmstadt (1999).

[54] G. M. Sheldrick: *Programm SHELXS-86*, Göttingen (1986).

[55] W. Massa: *Kristallstrukturbestimung*, 2. Auflage, Teubner-Verlag, Stuttgart (1996).

[56] G. M. Sheldrick: *Programm SHELX-86*, Cambridge, U. K. (1976).

[57] G. M. Sheldrick: *Programm SHELXL-93*, Göttingen (1993).

[58] G. M. Sheldrick: *Programm System SHELX-97*, Göttingen (1997).

[59] Fa. Stoe & Cie GmbH: *Programm WinXPOW, Version 1.04,* Darmstadt (1998).

[60] Fa. Stoe & Cie GmbH: *Programm X-RED, Version 1.19,* Darmstadt (1999).

[61] Fa. Stoe & Cie GmbH: *Programm X-STEP 32 (Version 2.14, 1997)* and *X-STEP 32 (Version 1.05f, 2000),* Darmstadt.

[62] R. Hübenthal, R. Hoppe: *Programm MAPLE 4.0*, Gießen (1995).

[63] Fa. CRYSTAL IMPACT: *Programm Diamond, Version 2.1c*, Bonn (1999).

[64] E. Griesbrecht, M. Perrier, W. W. Wendlandt: *Anais Acad. Bras. Cienc*. **34** (1962) 37.

[65] E. Griesbrecht, I. Giolito: *Anais Acad. Bras. Cienc*. **39** (1967) 233.

[66] I. A. Maier, Yu. L. Suponitskii, M. Kh. Karapet'yants: *Izv. Vyssh. Uchebn. Zaved. Khim. Khim. Tekhnol*. **14** (1971) 3.

[67] M. A. Nabar, S. V. Paralkar: *Thermochim. Acta* **17** (1976) 239.

[68] M. A. Nabar, S. V. Paralkar: *Thermochim. Acta* **15** (1976) 390.

[69] B. Hájek, N. Novotna, J. Hradilová: *J. Less-Common Met*. **66** (1979) 121.

[70] G. S. Savchenko, I. V. Tananaev, A. N. Volodina: *Inorg. Mater*. **4** (1968) 1097.

[71] O. Rademacher, H. Göbel, H. Oppermann: *Z. Kristallogr. NCS* **215** (2000) 339.

[72] A. F. Holleman, E. Wiberg: *Lehrbuch der Anorganischen Chemie*, 101. Auflage, Walter-de-Gruyter-Verlag, Berlin, New York (1995).

[73] J. Valkonen, L. Niinistö, B. Eriksson, L. O. Larsson, U. Skoglund: *Acta Chem. Scand. Ser*. **A 29** (1975) 866.

[74] J. Valkonen, M. Leskelä: *Acta Crystallogr*. **B 34** (1978) 1323.

[75] J. Valkonen: *Acta Crystallogr*. **B 34** (1978) 1957.

[76] J. Valkonen, L. Niinistö: *Acta Crystallogr*. **B 34** (1978) 266.

[77] R. G. Sizora, A. A. Voronkov, N. V. Belov: *Sov. Phys. Dokl*. **19** (1975) 472.

[78] R. E. Morris, M. P. Attfield, A. K. Cheetham: *Acta Crystallogr*. **C 50** (1994) 473.

[79] F. A. Cotton, D. A. Ucko: *Inorg. Chim. Acta* **1** (1972) 161.

[80] B. Charlot, E. Parthé: *Acta Crystallogr*. **B 34** (1978) 645.

[81] G. Aminoff: *Z. Kristallogr.* **58** (1923) 203.
W. F. de Jong: *Physica* **5** (1925) 194.

[82] M. S. Wickleder: *Z. Anorg. Allg. Chem*. **626** (2000) 1468.

[83] Th. Schleid, F. Lissner: *Z. Anorg. Allg. Chem*. **615** (1992) 19.

[84] W. H. Bragg, W. L. Bragg: *Nature (London)* **105** (1920) 646.
W. H. Bragg: *J. Chem. Soc.* **121** (1922) 2766.

[85] Th. Hahn, A. J. C. Wilson (eds.), *International Tables for Crystallography*, 3rd Edition, Kluwer Academic Publishers, Dordrecht, Boston, London (1992).

[86] T. Grundmeier, W. Urland: *Z. Anorg. Allg. Chem*. **621** (1995) 1977.
T. Grundmeier, W. Urland: *Z. Anorg. Allg. Chem*. **623** (1997) 1744.

[87] R. D. Shannon, C. T. Prewitt: *Acta Crystallogr*. **B 25** (1969) 925.

[88] F. C. Hawthorne, T. S. Ercit L. A. Groat: *Acta Crystallogr*. **C 42** (1986) 1285.

[89] F. C. Hawthorne, L. A. Groat and T. S. Ercit: *Acta Crystallogr*. **C 43** (1987) 2044.

[90] A. Castro, M. de Pedro, J. Rasines: *J. Therm. Anal* **40** (1993) 1109.

[91] G. G. Gospodinov, M. G. Stancheva: *Monatsh. Chem.* **133** (2002) 1381.

[92] R. Rajagopal, V. R. Ajgaonkar: *Monatsh. Chem***. 133** (2002) 1387.

[93] L. Niinistö, J. Valkonen, P. Ylinen: *Inorg. Nucl. Chem. Lett.* **16** (1980) 13.

[94] S. Karvinen, K. Lumme, L. Niinistö: *J. Therm. Anal.* **32** (1987) 919.

[95] M. Wildner: *J. Solid State Chem*. **113** (1994) 252.

[96] H. Effenberger, F. Pertlik: *Monatsh. Chem***. 117** (1986) 887.

[97] J. Wontcheu, Th. Schleid: *Z. Anorg. Allg. Chem*. **628** (2002) 1941.

[98] A. Pabst: *Amer. Mineral.* **59** (1974) 353.

[99] D. Knobloch, F. Pertlik, J. Zemann: *N. Jahrb. Mineral. Monatsh.* **1980** (1980) 230.

[100] H. Effenberger, H. Langhof: *Acta Crystallogr.* **C 40** (1984) 1299.

[101] K.-F. Hesse, B. Simons: *Z. Kristallogr.* **161** (1982) 289.

[102] P. Millet, B. Bastide, V. Pashchenko, S. Gnatchenko, V. Gapon, Y. Ksari, A. Stepanov: *J. Mater. Chem*. **11** (2001) 1152.

[103] R. Berrigan, B. M. Gatehouse: *Acta Crystallogr.*. **C 52** (1996**)** 496.

[104] P. Caro, J. Derouet, P. Brun: *Bull. Soc. Chim. France* **8** (1972**)** 3023.

[105] G. Haueseler, F. Matthes: *J. Less-Common Met.* **9** (1965) 133.

[106] W. W. Wendlandt: *J. Inorg. Nucl. Chem*. **9** (1959) 136.

[107] D. H. Templeton, C. H. Dauben: *J. Am. Cem. Soc*. **75** (1953) 6069.

[108] R. Fischer, J. Zemann: *Handbook of Geochemistry* II-3, 34-A; Springer, Berlin Heidelberg, New York (1974).

[109] G. Giester: *Monatsh. Chem***. 120** (1989) 661.

[110] J. Wontcheu, Th. Schleid: *Z. Kristallogr*. **Suppl. 19** (2002) 138.

[111] A. F. Wells: *Models in Structural Inorganic Chemistry*, Oxford University Press, Oxford, U. K. (1970).

[112] A. F. Wells: *Structural Inorganic Chemistry, Clarendon Press*, Oxford U. K (1984a) p. 198.

[113] A. F. Wells: *Philos. Trans. Royal Soc. London* **319** (1986) 291.

[114] S. V. Krivovichev, S. K. Filatov, T. F. Semenova: *Z. Kristallogr*. **212** (1997) 411.

[115] H. Effenberger, R. Miletich: *Z. Kristallogr.* **210** (1995) 421.

[116] H. Haas, M. Jansen: *Z. Anorg. Allg. Chem*. **626** (2000) 1174.

[117] H. Föppl: *Z. Anorg. Allg. Chem*. **291** (1957) 12.

[118] H. Föppl: *Z. Anorg. Allg. Chem*. **291** (1957) 13.

[119] M. Wildner: *J. Solid State Chem*. **103** (1993) 341.

[120] M. Wanger, T. Armbruster: *Eur. J. Mineral*. **3** (1991) 387.

[121] F. A. Weber, S. F. Meier, Th. Schleid: *Z. Kristallogr*. **Suppl. 18** (2001) 149.

[122] P. C. Burns, M. L. Miller, R. C. Ewing: *Can. Mineral*. **34** (1996) 845.

[123] P. C. Burns: *Rev. Mineral*. **38** (1999) 23.

[124] J. Wontcheu, Th. Schleid: *J. Solid State Chem*. **171** (2003) 429.

[125] M. Blackman, I. H. Khan: *Proc. Phys. Soc*. **77** (1961) 471.

Curriculum Vitae

Name Wontcheu
Surname Joseph
Date of birth 28th April 1967
Place of birth Bafang (Haut-Nkam)
Citizenship Cameroonian Adresse: Kernerstr. 43, 71672 Marbach (Neckar)

Education

1974-1980 Primary school Ecole Notre Dame de Banka; CEPE (Certificat d'Etudes Primaire Elémentaire in June 1980)

1980-1984 Collège Saint Paul de Bafang; BEPC (Brevet d'Etude du Premier Cycle du Second Dégré in June 1984)

1985-1990 Lycée de Nkol-Eton, Yaounde Cameroon; Baccalauréat in June 1990

Universities backgrounds

1990–1994 University of Yaounde I, Camreoon, Bachelor's in Chemistry in June 1994

1994–1996 University of Yaounde I, Cameroon, Master's in Chemistry, Speciality: Materials Sciences, June 1996

1996–1998 University of Yaounde I, Cameroon, First Year Doctorate Degree (DEA), Speciality: Materials Sciences, June 1998

1998–2000 Doctorate research and Graduate assistant at the department of Inorganic Chemistry, University of Yaounde I, Cameroon

From September 2000 to date: Ph. D. programme, Institut für Anorganische Chemie, Universität Stuttgart (Germany), Speciality: Solid-State Chemistry, Supervisor: Prof. Dr. Thomas Schleid. Research Topic: Oxoselenates(IV) of the Trivalent Rare-Earth Elements and Some Derivatives

Languages Writing and Speaking

1 French, very good
2 English, good
3 German, good
4 My mother language: Fè-Fè